GRI-94/0167

T. F. Hentz

GRI

Topical Report

Geology of a Stratigraphically Complex Natural Gas Play: Canyon Sandstones, Val Verde Basin, Southwest Texas

Prepared by:
The University of Texas at Austin
Austin, Texas

Gas Research Institute

Drilling and Completion Group
July 1994

GEOLOGY OF A STRATIGRAPHICALLY COMPLEX NATURAL GAS PLAY: CANYON SANDSTONES, VAL VERDE BASIN, SOUTHWEST TEXAS

TOPICAL REPORT

(January 1993 – October 1993)

Prepared by

Stephen E. Laubach, Sigrid J. Clift, H. Scott Hamlin,
Shirley P. Dutton, Tucker F. Hentz, Hwanjo Baek, and Barbara A. Marin

Bureau of Economic Geology
W. L. Fisher, Director
The University of Texas at Austin
Austin, Texas 78713-7508

for

GAS RESEARCH INSTITUTE
Contract No. 5082-211-0708
John Hansen, Project Manager

July 1994

DISCLAIMER

LEGAL NOTICE This work was prepared by the Bureau of Economic Geology as an account of work sponsored by the Gas Research Institute (GRI). GRI, nor members of GRI, nor any person acting on behalf of either:

a. Makes any warranty or representation, expressed or implied, with respect to the accuracy, completeness, or usefulness of the information contained in this report, or that the use of any apparatus, method, or process disclosed in this report may not infringe privately owned rights; or

b. Assumes any liability with respect to the use of, or for damages resulting from the use of, any information, apparatus, method, or process disclosed in this report.

50272-101

REPORT DOCUMENTATION PAGE	1. REPORT NO. GRI-94/0167	2.	3. Recipient's Accession No.

4. Title and Subtitle
Geology of a Stratigraphically Complex Natural Gas Play: Canyon Sandstones, Val Verde Basin, Southwest Texas

5. Report Date July 1994

6.

7. Author(s) S. E. Laubach, S. J. Clift, H. S. Hamlin, S. P. Dutton, T. F. Hentz, H. Baek, B. A. Marin

8. Performing Organization Rept. No.

9. Performing Organization Name and Address
Bureau of Economic Geology
The University of Texas at Austin
University Station, Box X
Austin, TX 78713-7508

10. Project/Task/Work Unit No.

11. Contract(C) or Grant(G) No.
(C) 5082-211-0708
(G)

12. Sponsoring Organization Name and Address
Gas Research Institute
8600 West Bryn Mawr Avenue
Chicago, IL 60631

Project Manager:
John Hansen

13. Type of Report & Period Covered
Topical January 1993 - October 1993

14.

15. Supplementary Notes
Topical report on geologic controls of production behavior of low-permeability, gas-bearing Canyon Sandstones, including stratigraphy, diagenesis, and structure (natural fractures).

16. Abstract (Limit: 200 words)

This report examines the influence of stratigraphy, diagenesis, natural fractures, and in situ stress on low-permeability, gas-bearing sandstone reservoirs of the Paleozoic Ozona and Sonora Canyon Sandstones of the Val Verde Basin, Texas. The main stratigraphic controls on distribution and quality of Canyon Sandstone reservoirs are submarine fan depositional patterns. These patterns are revealed in regional facies and maximum sandstone maps. Siderite cement is key to good within-sandstone reservoir quality. Natural fractures are widespread in both Ozona and Sonora Canyon sandstones. They could be future targets for advanced drilling methods, and they need to be taken into account in hydraulic fracture treatment design and reservoir management.

17. Document Analysis a. Descriptors

a. Texas, Val Verde Basin, Canyon Sandstone, Ozona, Sonora, tight gas sandstones, stratigraphy, depositional systems, submarine fans, sandstone diagenesis, reservoir quality, natural fractures, hydraulic fracture treatment, horizontal drilling, fracture toughness tests

b. Identifiers/Open-Ended Terms

b. stratigraphy of Sonora and Ozona Canyon Sandstones, influence of depositional environment on reservoir development, innovative mapping methods for submarine fan reservoirs, petrography of Canyon Sandstone, core study of Paleozoic sandstone, diagenetic history of tight gas sandstone, Val Verde Basin, natural fractures, fracture toughness testing of variably cemented sandstone, recognition of reactivation of natural fractures

18. Availability Statement	19. Security Class (This Report)	21. No. of Pages
Release unlimited	Unclassified	136
	20. Security Class (This Page) Unclassified	22. Price

RESEARCH SUMMARY

Title	Geology of a stratigraphically complex natural gas play: Canyon sandstones, Val Verde Basin, southwest Texas
Contractor	Bureau of Economic Geology, The University of Texas at Austin, GRI Contract No. 5082-211-0708, titled "Geologic analysis of primary and secondary tight gas sands objectives"
Principal Investigator	Stephen E. Laubach
Report Period	January 1993–October 1993
Objectives	The primary objective of this report is increased understanding of a key complex gas reservoir system—the Canyon sandstones of the Val Verde Basin, Texas. A secondary objective is to describe new stratigraphic, diagenetic, and structural geologic tools that will be widely applicable to other geologically complex reservoirs. This study aims to develop a model of the Canyon's physical geologic framework, which is necessary to understand the distribution and reservoir behavior of the gas resource. Using this geologic framework, Canyon operators can target areas where new wells, recompletions, or additional analyses will be most beneficial, thus reducing risk and costs while increasing the success of their exploration and development programs. Such knowledge is also necessary for effective, efficient application of new technologies for resource extraction.
Technical Perspective	Canyon sandstones have yielded almost 2.2 trillion cubic feet (Tcf) of gas and—in existing wells—contain estimated additional reserves of 2 Tcf. Operator interest and activity are at an all-time high, and continued drilling will undoubtedly lead to significant reserve growth. Average recovery per completion is a modest 0.7 billion cubic ft (Bcf), but the range is broad (up to 5 Bcf/well), and average drilling density is still relatively low. Low well density and the geologic complexity in the play documented by our study and recognized by operators suggest that opportunities exist for increasing Canyon productivity by taking advantage of better understanding of reservoir attributes. Geological heterogeneity is the main cause of low productivity from Canyon sandstones. Most Canyon reservoirs occur within a crosscutting mosaic of lenticular channel and lobe facies of submarine-fan depositional systems. In the pervasively gas-saturated Canyon trends, the challenge for geologists is to understand and predict the distribution of high-deliverability compartments within the reservoir mosaic. Our study shows that the occurrence and nature of Canyon sweet spots are controlled by (1) depositional processes that control sandstone distribution and initial reservoir properties, (2) postdepositional diagenetic modifications that preserve or destroy reservoir quality, and (3) structural activity leading to the development of natural fractures and permeable pathways.

Results

Geologic controls on Canyon reservoir quality were established, distribution of reservoir sandstone facies was mapped at regional and local scales, compositional and diagenetic influences on petrophysical properties were determined, and characteristics of natural fracture systems were documented.

Ozona and Sonora Canyon gas producing trends contain thick (up to 1,000 ft) stacks of sandstone, which are vertically compartmentalized by shale. Individual sandstone beds are only inches to a few feet thick between shale interbeds. Ozona and Sonora sandstones are widespread, extending across large parts of Crockett and Sutton Counties, but individual sandstone bodies rarely extend more than a few miles. This stratigraphic complexity results from deposition in a series of small, laterally coalescing submarine fans. Reservoir quality in thick-bedded but lenticular, fan-channel sandstones is generally better than it is in thin-bedded but more sheet-like fan-lobe sandstones. Techniques were developed to distinguish and map these two components of Canyon submarine fans, and their influence on reservoir quality was documented using production data.

Within individual Canyon sandstone bodies, reservoir quality is further compartmentalized by compositional and diagenetic variations. Clay laminations and matrix are abundant in many zones, and postdepositional compaction and cementation have reduced reservoir quality in clean sandstone layers. Diagenetic studies show, however, that the presence of siderite cement is the key to good within-sandstone reservoir quality in many Sonora Canyon sandstones. Our studies show what factors control siderite genesis, but it is currently not possible to predict the exact location of siderite-controlled sweet spots. This result points to an area of well log analysis or development that could aid Canyon operations: tools for siderite cement recognition. Nevertheless, a subtle relationship to depositional facies was documented, suggesting that predictive capabilities could be developed.

Natural fractures are widespread in both Sonora and Ozona Canyon sandstones. For the most part these fractures as seen in core are short (less than 10 inches tall) and this, as well as the closely spaced interbeds in Canyon turbidites that will tend to create vertical permeability barriers and baffles, suggests that successful horizontal drilling to exploit these fractures will be challenging and possibly ineffective. On the other hand, large fractures may exist elsewhere in the Canyon; their identification and exploitation are potential areas of future Canyon activity. Natural fractures can also promote permeability anisotropy and hydraulic fracture tortuosity, and awareness of their existence and character can help guide reservoir stimulation and management decisions.

As part of our study of the role of diagenesis and natural fractures, we tested certain rock properties. We have used laboratory tests to document fracture toughness of Sonora and Ozona sandstones—values average 1.77 ± 0.46 $MN/m^{1.5}$ to 1.72 ± 0.60 $MN/m^{1.5}$. By developing criteria for recognizing reactivation of natural fractures and by documenting reactivation in Canyon core, this study shows that fracture reactivation and possibly the growth of multiple fracture strands near the wellbore is likely in rocks with fracture toughness values within the range reported for other tight gas sandstones. These results can be taken into account in fracture treatment design.

Technical Approach

The approach of this study was to use available subsurface data—geophysical well logs and limited core—to map regional and field-scale Canyon sandstone distribution, interpret and characterize depositional systems and facies, investigate how the diagenetic history of the sandstones has modified reservoir porosity and permeability and other rock properties, and document the occurrence and attributes of natural fractures in Canyon cores. As part of the study of the effects of diagenesis and natural fractures, a laboratory study was carried out that characterized the fracture toughness of Canyon Sandstones.

Implications

Heterogeneous, tight reservoirs, such as those in Canyon sandstones, require sophisticated geologic characterization techniques to identify favorable areas. Innovative characterization techniques were successfully applied, and a good basic understanding of controls on Canyon reservoir properties was achieved. When results of this research are combined with experiences of Canyon operators, both the potential and the technical challenges of the Canyon gas play become apparent. Research findings presented here have value as a starting position for the more focused analyses that operators perform when designing exploration and development programs. Finally, now that the basic geologic controls on Canyon reservoir quality are understood, a next step would be to develop techniques for predicting or detecting specific effects of cement distribution and natural fractures at regional and local scales.

CONTENTS

Figures

Tables

Canyon Sandstone Gas Play: A Target for Reserve Growth

H. S. Hamlin

Canyon sandstones form a low-permeability, geologically complex gas play in the Val Verde Basin of southwest Texas (fig. 1). Canyon gas reservoirs, at depths between about 2,500 and 8,500 ft, have yielded almost 2.2 trillion cubic ft (Tcf) of gas and have estimated additional reserves in existing wells of 2 Tcf (Hugman and others, 1993). Continued play development will probably increase this number. Canyon reservoirs account for a significant portion of domestic tight gas production, reserves, and new completions (fig. 2). Low well density and geologic complexity suggest that opportunities abound for increasing Canyon productivity through an improved understanding of reservoir characteristics. Within the limits of the data available to us, the research results presented in this report provide that improved understanding of Canyon reservoir geology (table 1). A relative dearth of published geologic descriptions of Canyon sandstones and the current high level of industry interest were important motivations for this study.

The majority of low-permeability gas production in the greater Permian Basin area comes from Canyon sandstone reservoirs in the Val Verde Basin (Dutton and others, 1993). The total extent of Canyon producing trends spans 3,800 mi² (National Petroleum Council, 1980). Our study focuses on the two most prolific parts of the Canyon: the Ozona Canyon trend in Crockett County and the Sonora Canyon trend in Sutton County. Excellent potential for reserve growth beyond existing estimates lies in infill and extension drilling in the main producing trends and in new-field discoveries in the southern and western parts of the basin. Historically, the number of Canyon completions tripled between 1975 and 1991, and one quarter of all new domestic tight gas completions (exclusive of the Appalachian basins) in 1991 were Canyon wells (fig. 2) (Hugman and others, 1993). Average recovery per completion is a modest 0.7 billion cubic ft (Bcf), but average drilling density is still relatively low (1.25 wells/mi²).

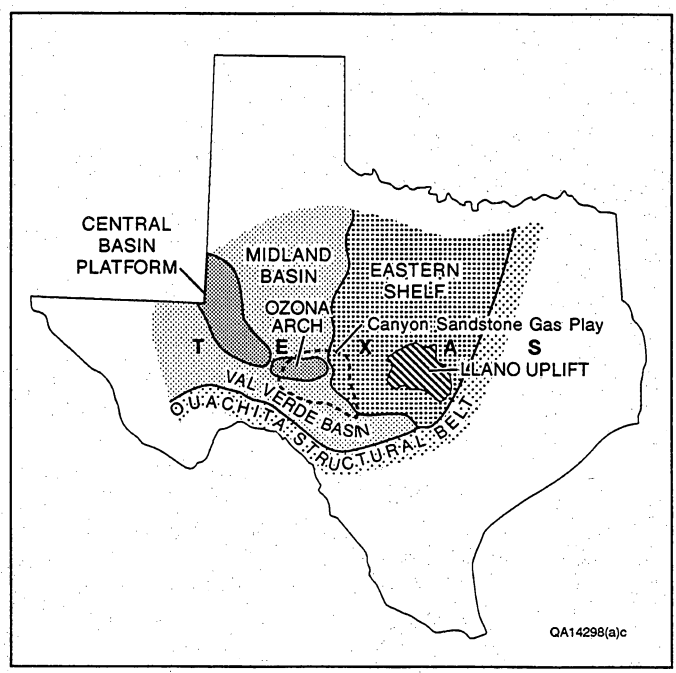

Figure 1. Map of Texas showing principal Late Pennsylvanian-Early Permian tectonic elements and Canyon Sandstone gas play.

Geological heterogeneity is the main cause of low productivity from Canyon sandstone reservoirs. Geological heterogeneity is manifested by irregularly shaped permeability compartments and internal baffles and barriers to vertical and lateral flow. In the pervasively gas-saturated Canyon trends, the challenge for geologists is to understand and predict the distribution of "sweet spots" or high-deliverability compartments within the complex reservoir mosaic. Our study shows that the occurrence and nature of Canyon sweet spots are controlled by (1) depositional processes that control sandstone distribution and initial (pre-diagenesis) reservoir properties, (2) postdepositional diagenetic modifications that preserve or destroy reservoir quality, and (3) compaction and tectonic activity leading to the development of natural fractures and permeable pathways. Although based primarily on well logs supplemented with limited core data, the research described in this report nevertheless achieved these important objectives:

- identified regional sandstone fairways to guide exploration and development
- interpreted and characterized depositional systems and facies and documented their control on productivity
- showed how the diagenetic history of the sandstones has modified reservoir porosity and permeability and other rock properties

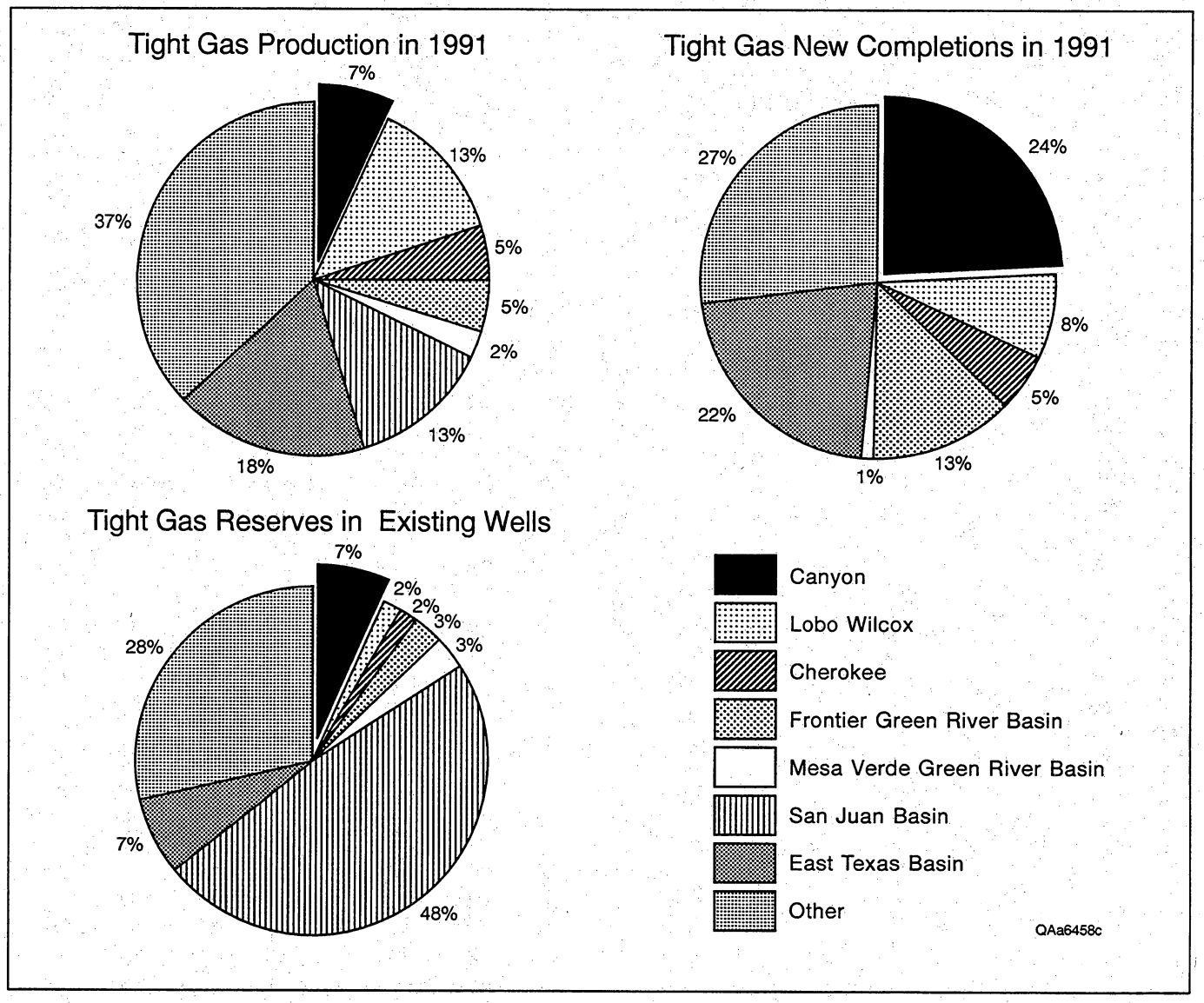

Figure 2. Relative proportions of tight-gas production, new completions, and reserves in formations in non-Appalachian, continental U.S. basins.

- found potential targets for future exploitation by documenting the occurrence and attributes of natural fractures in Canyon cores.
- identified growth of multiple fracture strands and near-wellbore tortuosity as potential influences on reservoir response to hydraulic fracture treatment.

Although the influences of depositional environment, diagenesis, and natural fractures on Canyon reservoir quality can be documented, no technologies yet exist for failsafe identification of sweet spots. Our research shows that, with the fundamental knowledge summarized in this report as a base and using comprehensive sets of core and seismic data, significant future advances in the development of such technologies are possible.

Benefits of Canyon Research

Canyon operators are well aware of the problems and challenges involved in developing the Canyon gas resource. In a telephone survey conducted as part of our study, Canyon operators cite several lines of evidence that indicate that reservoirs are heterogeneous and are composed of small permeability compartments: (1) interstratification of water-saturated and gas-saturated sandstones, (2) multiple pay zones having different pressures, (3) low productivity from thick pay zones, and (4) variable drainage areas. Although operators agree that the economic future of Canyon gas development is bright—reserves are high, drilling costs are relatively low,

Table 1. Summary of research objectives, techniques, and results presented in this report.

Challenge	Approach	Benefit
Document regional sandstone distribution	Sandstone maps and cross sections; well data appendices	Provided context for exploration and development
Characterize reservoir facies	Interpretation of core and well logs; facies mapping	Identified and characterized prospective reservoir facies; predicted some reservoir properties
Explain field-scale production patterns	Comparison of sandstone and facies maps with initial well potentials	Identified stratigraphic controls on productivity; provided starting point for designing development programs and for application of advanced technologies
Document postdepositional modification of reservoir properties	Petrographic analysis of sandstone composition, diagenesis, and porosity distribution	Identified important controls on porosity, such as siderite in the Sonora, further research needed to develop predictive capabilities
Determine if natural fractures are present and ascertain whether they could affect development	Studies of core and borehole-imaging logs, laboratory testing of mechanical properties	Identified that natural fractures are widespread and may control gas flow locally; reservoir stimulation may be detrimentally attected by fractures; potential exists to improve fracture flow by acid stimulation

significant infill potential remains—the operators also recognize that better methods for understanding the controls on permeability distribution, water saturation, and relative pay contribution would reduce uncertainty and increase the success of their development programs.

At a well attended Canyon sandstone workshop, where the results of this research were presented, participants completed a questionnaire that provided additional information about Canyon operators and the challenges they face. The high attendance at the workshop (over 350 geologists, engineers, and managers) attests to the level of interest in the Canyon play and to the importance of geologic studies to Canyon operators, who indicated on the questionnaire that they make extensive use of geological knowledge to reduce risk in development decisions. Workshop participants responded that they found the information presented useful to their work and suggested areas where additional research is most needed:

- extension of the regional framework beyond the limits of the Ozona and the Sonora
- more rigorous analysis of production data
- closer look at hard-to-document controls such as natural fractures and diagenesis
- incorporation of seismic data into both regional and field-scale work.

A major benefit of regional geologic reservoir characterization is the low cost involved in application; drilling and completion costs are not increased. According to Canyon operators, an average Canyon gas well must produce 0.3 Bcf in order to pay for drilling and completion costs. Since average cumulative recovery per well is 0.7 Bcf, net profit averages 0.4 Bcf. Well productivity varies widely, however, and net per-well profit reaches 5 Bcf locally. Insights from regional studies aimed at identifying prospective areas and from field-scale studies aimed at understanding local controls on reservoir quality can be used to strategically locate wells for increasing average per-well production without significantly increasing per-well costs.

Objectives of Study

Canyon sandstones were studied as part of the Tight Gas Sands project, a research program supported by the Gas Research Institute (GRI) that focuses on low-permeability sandstones. The geologic research presented here is one aspect of this broader, multidisciplinary program designed to increase knowledge about—and ultimate recovery of—unconventional gas resources through integration of geology, log analysis, reservoir engineering, and hydraulic fracture modeling. The goal

of the geologic studies described here is development of insights, methods, and technology that can be applied to the Canyon and to other tight gas sandstones to enable greater recovery of gas in place in low-permeability reservoirs.

Much of the data used in this study is derived from two cooperative wells (fig. 3, Appendix A). Cooperative wells are gas wells in which operating companies allowed GRI contractors to collect data necessary for formation evaluation and hydraulic-fracture-treatment design. Data acquisition and analysis reports for these wells have been published elsewhere (CER Corporation, 1991a, 1991b; Miller and others, 1991; NSI Technologies, Inc., 1991a–1991d; Hamlin and others, 1992b). Industry core donations were an additional important source of data; these donated cores are archived at the Core Research Center of the Bureau of Economic Geology.

The objective of the geologic study of the Canyon Sandstone formation is to develop a complete description of the physical characteristics of the reservoir sandstones, which is necessary to understand the distribution and reservoir behavior of the tight gas resource and test and apply new technologies for resource extraction. Geologic studies can explain the physical characteristics of Canyon sandstones and provide information necessary for accurate formation evaluation, reservoir modeling, and fracture analysis. Geologic characteristics that are critical to an understanding of Canyon sandstones, or any other tight gas sandstone, are

- depositional systems and the distribution of reservoir facies,
- diagenetic history of the formation and mineralogic composition of the reservoir
- structural history and setting of the basin and its contained reservoirs.

Within the limits of available data, research results presented in this report provide a comprehensive description of the basic geological properties of Canyon Sandstone reservoirs.

Methods and Data

This geologic study focused on (1) Sonora Canyon sandstones, which extend across western Sutton, northern Edwards, southwestern Schleicher, and eastern Crockett Counties and (2) Ozona Canyon sandstones, which extend across southern Crockett, northern Val Verde, and northeastern Terrell Counties. Lower Canyon sandstones in the south and undifferentiated "Wolfcamp" sandstones in the west are not discussed in this report. The location of the GRI cooperative wells directed our initial focus on the Sonora Canyon in Sutton County. Well logs from about 1,600 wells and 480 ft of Sonora Canyon core from the two cooperative wells (fig. 3) were our main data sources. An additional 870 ft of Sonora and Ozona core from several older wells (fig. 3) provided supplementary data, especially for natural fracture analysis.

Stratigraphic correlations were made using gamma-ray logs supplemented locally with acoustic, SP, and resistivity logs. Macroscopic and microscopic core descriptions provided data for calibrating logs for lithology and depositional environment interpretations. Core-to-log depth matching was done by comparing downhole gamma-ray logs to core gamma-ray scans. Gamma-ray logs also formed the main data base for sandstone thickness calculations, although SP, resistivity, neutron, and acoustic logs provided additional lithologic information. The cut-off for measuring net sandstone was approximately half way between the maximum and minimum gamma-ray responses in the Canyon interval being measured. A universal cut-off based on API units was not used because of variabilities in log quality and measurement conditions. Formation tops and sandstone measurements from well logs used on regional cross sections (fig. 3) are tabulated in Appendix B.

The thickest individual sandstone (maximum sandstone) in each correlation unit was mapped on the theory that thick-bedded sandstones are generally more permeable than are thin-bedded sandstones. Furthermore, the distribution of the thickest sandstones typically defines the framework of a depositional system, particularly one in which lenticular channel-fill sandstones form a key component. For this study individual maximum sandstones do not contain shale interbeds greater than 5 ft thick. Because thick Canyon sandstones are generally not continuous between wells, our maximum sandstone maps delineate thickness patterns in a stack of sandstone bodies but not the continuity of individual bodies.

Composition of Canyon sandstones were determined by standard thin-section petrography and scanning electron microscopy (SEM) with an energy dispersive X-ray spectrometer (EDX). Point counts (200 points) of thin sections from representative samples from available cores were used to determine mineral composition and porosity. Matrix-free sandstones were sampled preferentially because they are likely to represent the best reservoirs. Grain size and sorting were determined by grain-size point counts (50 points).

Natural fractures in all available Canyon core (both oriented and unoriented) were mapped and described. Oriented core and borehole-imaging geophysical logs provided information on fracture orientation. Petrographic and SEM analyses were used to characterize fracture-filling minerals. Laboratory studies of rock mechanics parameters and the morphology of induced and natural fractures were carried out in order to better

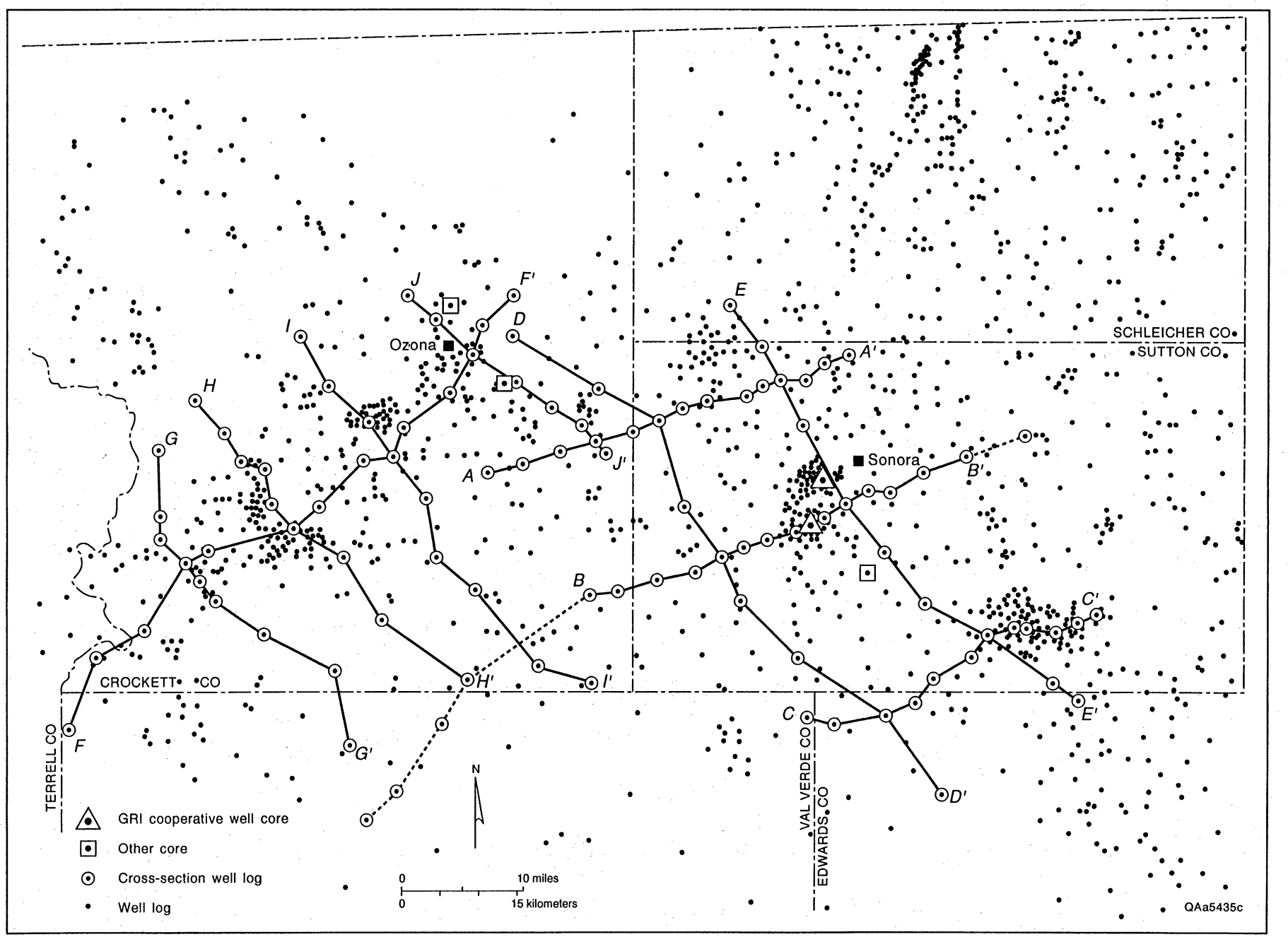

Figure 3. Index map of subsurface data used in Canyon sandstones study. Regional Val Verde Basin cross section (fig. 4) is an extended version of B–B′ (dashed lines). Data from GRI cooperative wells and cross section wells are listed in Appendices A and B.

understand the impact of diagenesis on parameters affecting procedures such as drilling and hydraulic fracturing and to understand the conditions under which natural fractures could be reactivated. Methods used in these studies are described in a later section.

Geologic Setting

The Val Verde Basin is a northwest-trending foreland basin within the Permian Basin region, which also encompasses the Midland and Delaware Basins and adjacent uplifts (Sanders and others, 1983; Hills and Galley, 1988). The basin forms an asymmetric trough; its deepest part (foredeep) is adjacent to the Ouachita structural belt in the south (fig. 1). The Val Verde Basin is one of a series of foreland basins that formed along the southern margin of the North American plate as a result of tectonic loading and other processes associated with plate collision and suturing during Ouachita orogenesis (Wuellner and others, 1986; Meckel and others, 1992). Cambrian- to Cretaceous-aged sedimentary fill in the foredeep reaches 28,000 ft, most of which is Pennsylvanian and Permian (Desmoinesian to Leonardian) (fig. 4). The basin is bounded on the north and east by shelf-like positive structural features: Central Basin Platform, Ozona Arch, and Eastern Shelf (fig. 1).

Val Verde Basin stratigraphy records the evolution of a basin whose shape and fill evolved under the influence of a nearby active tectonic belt. Lower and middle Paleozoic shallow-marine carbonates and clastics fill the Tobosa Basin, which was located on the southern passive margin of the North American craton and was ancestral to the Permian Basin (Hills and Galley, 1988). The Val Verde Basin became distinct during Late Mississippian time, when the Tobosa Basin began to separate into several basins and uplifts. Following widespread carbonate deposition in the middle Pennsylvanian (lower Desmoinesian Strawn Group), the Val Verde foredeep began to subside rapidly, creating a deep trough in the south adjacent to a shallow shelf in the north (fig. 5). Northward-prograding clastic wedges, derived from rising Ouachita highlands to the south, filled the southern part of the basin during the late Desmoinesian to Virgilian (Lehtonen, 1987). During this same time (late Desmoinesian to Virgilian), a thin black shale condensed section was deposited in the northern and eastern parts of the deep Val Verde Basin, and carbonates accumulated on flanking shelves. Beginning in the Early Permian (Wolfcampian to early Leonardian), deposition of clastic slope wedges prograded the southern margin of the Eastern Shelf southwestward. On the basin floor the distal parts of these northeastwardly derived slope wedges merged and interfingered with a continuing influx of Ouachita sediments from the south. As tectonic activity decreased in the Late Permian, carbonate sedimentation spread across the basin. Cretaceous carbonate rocks unconformably overlie Permian clastics and extend to the surface of the Val Verde Basin. Well, seismic, and vitrinite reflectance data suggest that, in the southern part of the basin, thousands of feet of Permian rocks were eroded before deposition of the Cretaceous (Sanders and others, 1983).

Regional distribution of Canyon sandstones and gas production in the Val Verde Basin is controlled by the depositional and tectonic history outlined above. The thin (100 to 400 ft) black shale that drapes Strawn carbonates throughout the northern part of the basin is probably the source for gas in overlying Canyon reservoirs (National Petroleum Council, 1980). Lower Canyon sandstones, which include the Epps and Ray sandstones, are part of the upper Desmoinesian-Virgilian, northward-prograding wedges that fill the deepest part of the basin but that also have experienced the greatest amount of uplift and erosion (figs. 4 and 6). Lower Canyon sandstones are currently productive only along their distal margins in the north, where they onlap the lower slope of the Eastern Shelf (fig. 7). The fact that thick lower Canyon sandstones in the south have yielded little gas may be attributable to postdepositional uplift, erosional truncation, and meteoric flushing (National Petroleum Council, 1980). Meteoric flushing refers to deep, downward circulation of relatively fresh ground water, which is driven by gravitational forces associated with uplift and topographic relief. As has recently been shown in the San Juan Basin (Kaiser and others, 1991), this process can affect movement of gas and water on a basinwide scale. Alternatively, the current scarcity of lower Canyon gas reservoirs may simply reflect insufficient exploration and development.

Sonora Canyon sandstones lie basinward of the southwest margin of the Eastern Shelf (fig. 6), extending down the slope and onto the adjacent basin floor. The Sonora Canyon also displays onlap relative to underlying Strawn carbonates (fig. 4), but depositional patterns indicate that Sonora sandstones were southward prograding and derived sediment from source areas to the northeast. To the southwest, Sonora sandstones grade into basinal shales, and because they are nowhere in direct contact with the pre-Cretaceous unconformity (fig. 4), they may have been somewhat protected from meteoric flushing. To the northeast Sonora sandstones thin and pinch out near the margin of the Eastern Shelf. The Sonora interval is the most prolific of the several Canyon gas-bearing intervals in the Val Verde Basin and is productive throughout its extent (fig. 7).

The Ozona Canyon interval is more tabular relative to wedge-shaped geometries displayed by underlying intervals and apparently records the last major clastic depositional episode filling the Val Verde Basin. The Ozona interval seems to occupy a basin floor position

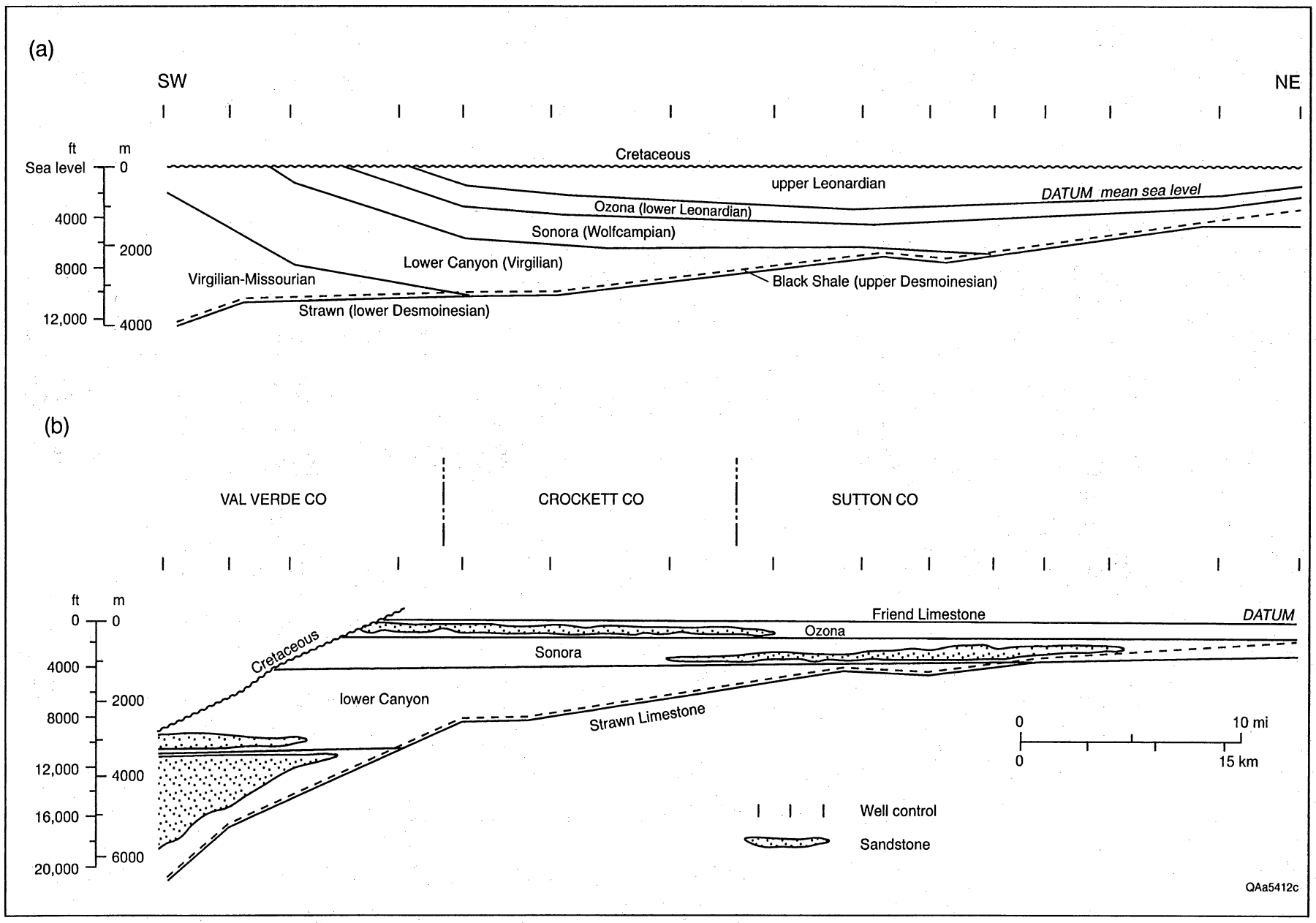

Figure 4. Regional cross section extending from the southwest margin of the Eastern Shelf into the deep Val Verde Basin (see figure 3 for location of section line) and showing (a) structural and (b) stratigraphic configurations of the major Canyon sandstone intervals.

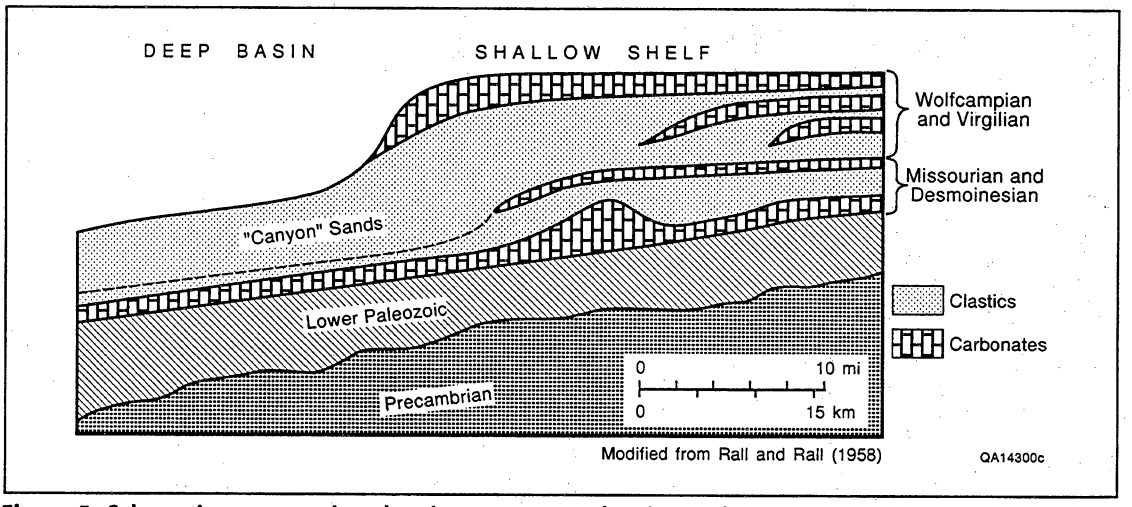

Figure 5. Schematic cross section showing Late Pennsylvanian-Early Permian depositional topography, northeastern Val Verde Basin. Modified from Rall and Rall (1958).

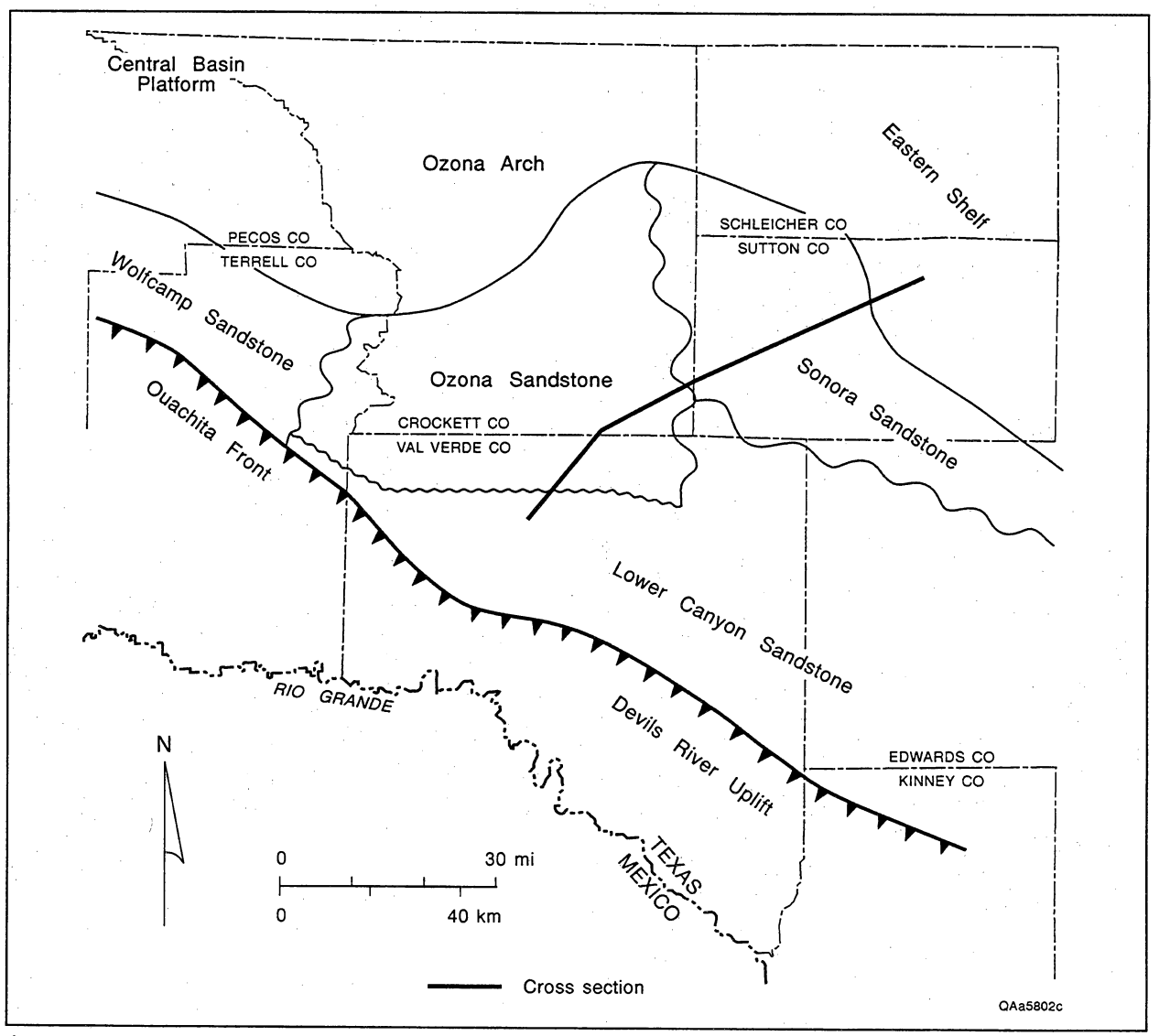

Figure 6. Map view of Canyon sandstone intervals in the Val Verde Basin. Overlap and interfingering exist along the boundaries between some intervals. Vertical separations between intervals are shown in figure 4. Line of cross section in figure 4 is also shown.

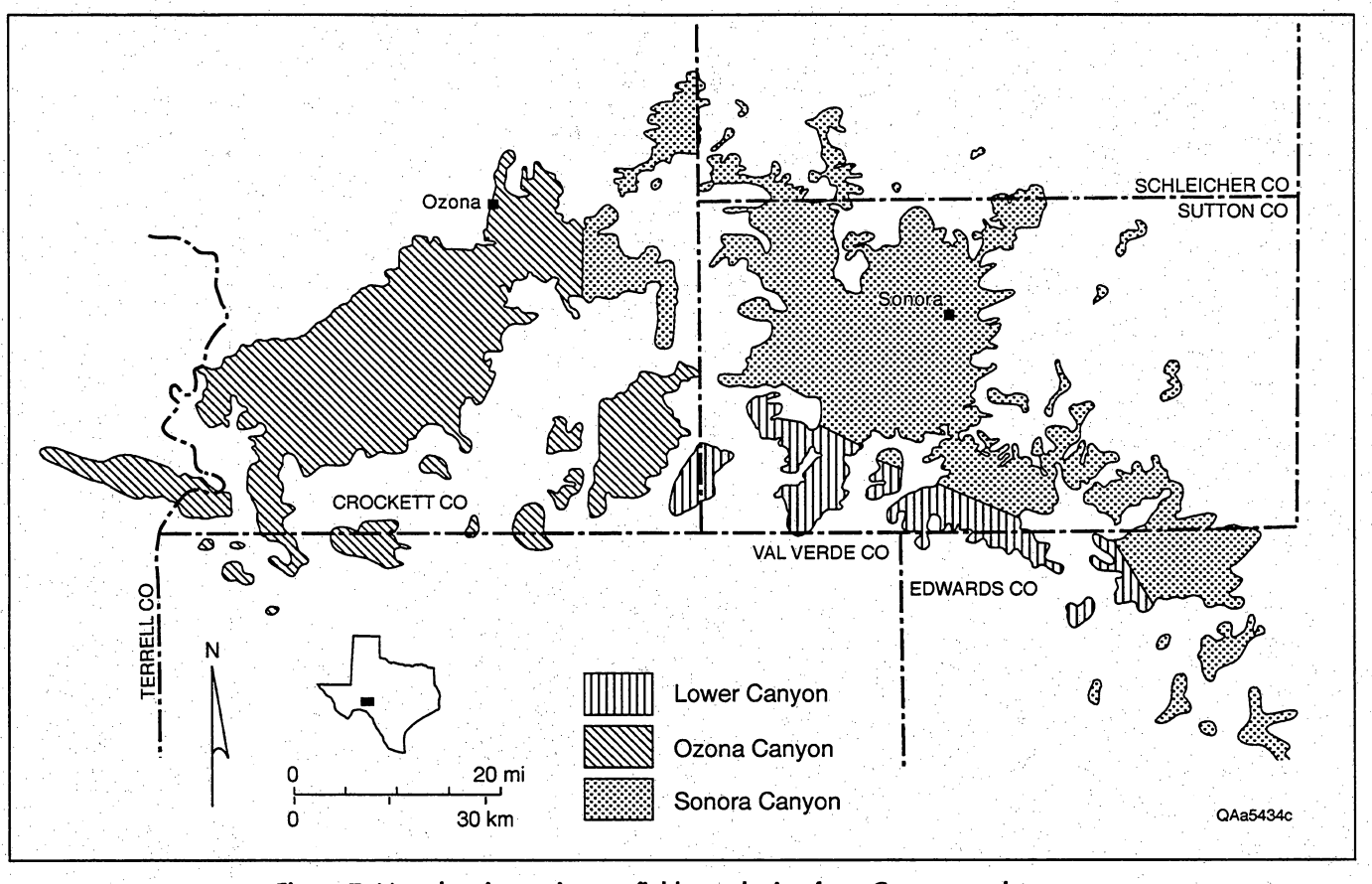

Figure 7. Map showing major gas fields producing from Canyon sandstones.

but lies in a much shallower basin than existed during deposition of older Canyon intervals. Sediment sources for Ozona sandstones were mainly to the south and west, and these sandstones probably extended farther south prior to erosional truncation (figs. 4 and 6). Along the southern margins of the Ozona Arch and Central Basin Platform, Ozona sandstones grade into shelf limestones and shales. Despite erosional truncation and exposure to meteoric flushing, Ozona sandstones contain gas reservoirs that are nearly as prolific as are Sonora reservoirs.

Reservoir Engineering and Production Data

Early summaries of petrophysical properties and production characteristics of Canyon sandstones are described in a study by the National Petroleum Council (1980), and more recent compilations are in reports based on data from the GRI cooperative wells (Appendix A). Canyon reservoir porosity ranges from 1 to 15 percent, averaging 7.4 percent in the Sonora and 6.9 percent in the Ozona (table 2). Log porosities in the best reservoir zones reach 14 percent, although net pay porosity cut-

Table 2. Canyon Sandstone production data, reservoir properties, and engineering parameters.

	Sonora	Ozona
Producing completions in 1992	2,362	1,702
Cumulative production through 1992 (Bcf)	1,401	893
Net pay thickness (ft)	25–720	15–300
Porosity, range/average (%)	2–15/7.4	1–12/6.9
Permeability, range (md)	0.001–0.4	0.001–0.1
Water saturation (%)	>20	>20
Reservoir temperature, range (°F)	125–185	100–175
Reservoir pressure, range (psi)	500–3,000	500–3,000
Reservoir depth, range (ft)	2,500–8,500	2,500–7,000
Post-frac initial potential, average CAOF (Mcf/d)	3,300	2,300
Recovery per completion, average (Bcf)	0.73	0.73

off is typically 5 percent. Restored state (net overburden pressure) core permeabilities in Sonora sandstones range from 0.001 to 0.03 md in the GRI cooperative wells. Basinwide average permeabilities are slightly higher (table 2), and thin beds having permeabilities around 1 md have been reported (Trabelsi, 1994). Because of low permeabilities, large net pay thicknesses are commonly necessary for economic completions. Water saturations in Canyon reservoirs commonly exceed 20 percent, and water production is a problem locally. Formation water resistivity averages 0.088 W·m at 75RF (80,000 ppm total dissolved solids), the cementation exponent is 2.07, and the saturation exponent is 2.09 (Hamlin and others, 1992b).

Canyon reservoirs typically have low temperatures and pressures. Reservoir temperatures range from 100° to 185°F, and reservoir pressures are 300 to 3,500 psi. Since depths to Canyon reservoirs range from 2,500 to 8,500 ft, pressure gradients range from 0.15 to 0.45 psi/ft. Low temperatures and pressures are generally attributed to uplift and meteoric flushing that occurred prior to deposition of Cretaceous carbonates (National Petroleum Council, 1980). At that time natural gas may have been lost from the system through breached seals, diffusion, and solution in circulating ground water. Uplift can also promote formation of natural fractures by reducing lateral loads on rocks.

In situ stress measurements in the GRI cooperative wells indicate stress gradients of 0.61 to 0.65 psi/ft in sandstone and 0.73 to 0.83 psi/ft in shale (Miller and others, 1991). A stress profile from the lower part of the Sonora Canyon is shown in figure 8. Maximum horizontal compressive stress was determined by several methods to be oriented approximately north-northeast (Miller and others, 1991). Because of low reservoir permeabilities, hydraulic fracture treatments are universal and typically consist of 50,000 to 70,000 gallons of gel and 100,000 to 120,000 pounds of sand. One of the GRI cooperative

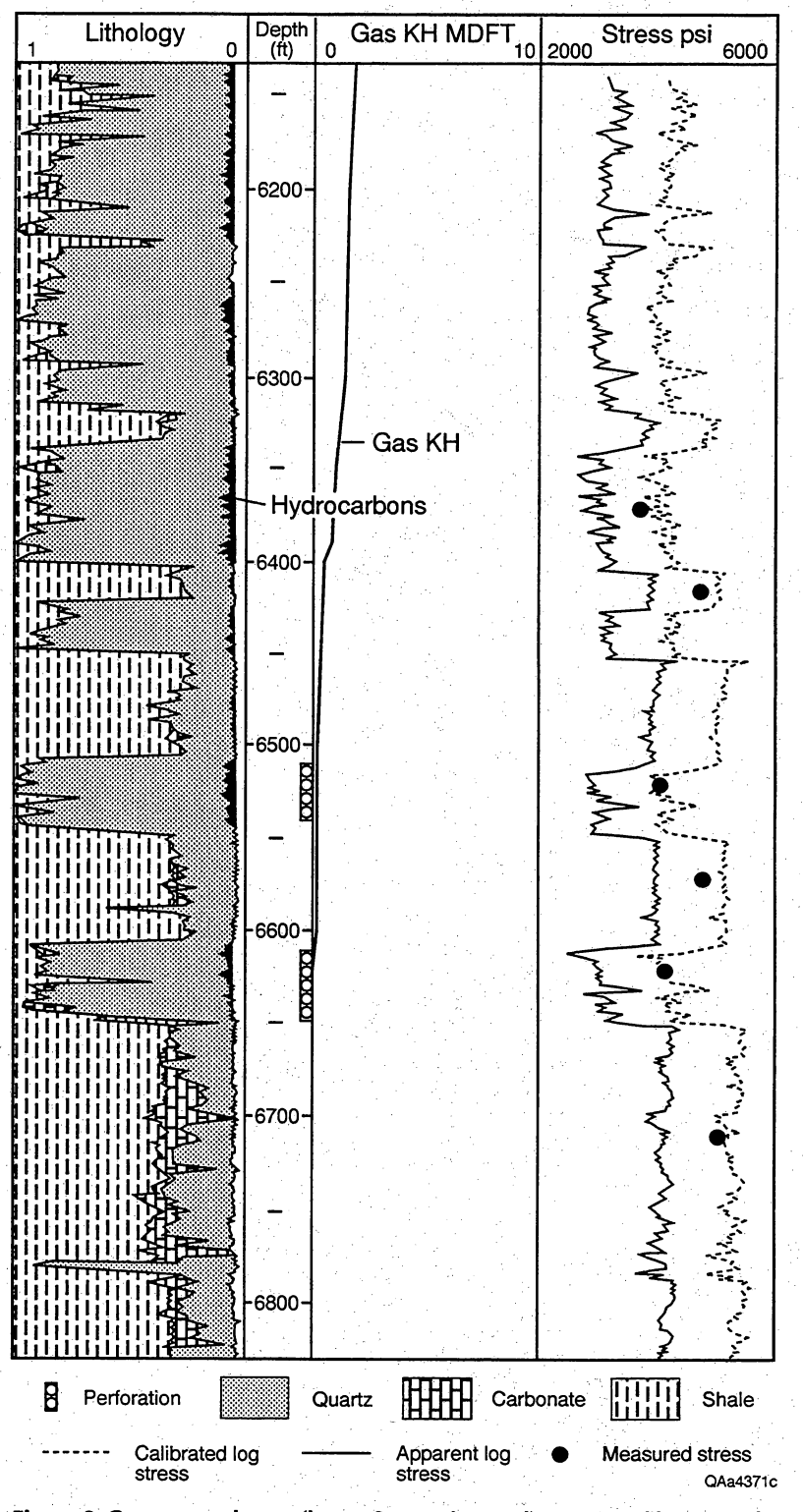

Figure 8. Canyon sandstone (lower Sonora interval) stress profile, example from Phillips Ward C No. 11, GRI cooperative well (W. Whitehead, personal communication, 1992).

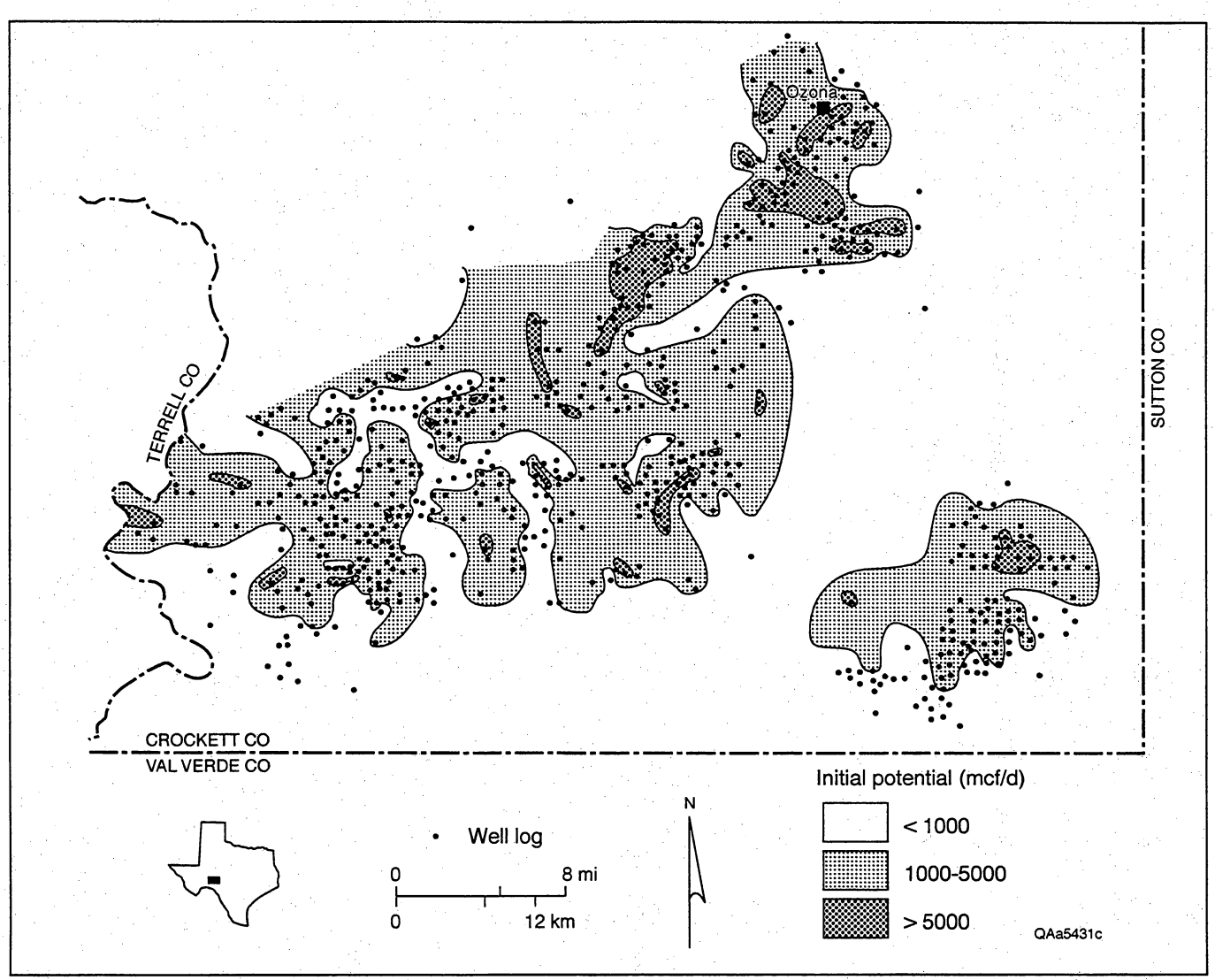

Figure 9. Map showing initial open-flow potentials (after fracture stimulation) for Ozona Canyon gas wells.

wells improved production by hydraulic fracture stimulation from 40 Mcf/d to 339 Mcf/d. Canyon operators report production improvements of 3 to 10 times after fracture stimulation.

The availability of a large data base of completion information from wells in Crockett County permitted us to make a more detailed characterization of initial productivity and completion practices in Ozona sandstone reservoirs. The median initial open-flow potential (after fracture stimulation) for 725 Ozona wells is 1,600 Mcf/d, but the range spans several orders of magnitude (<100 to >10,000 Mcf/d). Although many of the low-productivity wells are located around the margins of the main Ozona trend, where net sandstone content is low, large well-to-well productivity variations exist in the heart of the trend (fig. 9). Statistical analysis revealed that initial well productivity in the Ozona is unrelated to size of fracture stimulation treatment, completion date (year), reservoir depth, pressure, or temperature. Aside from certain variations in completion practices, which can only be assessed qualitatively, the process of elimination leaves responsible for well productivity variability only geologic properties that are intrinsic to the reservoir sandstones: reservoir size, internal complexity, and quality. Productivity variations as high as 5,000 to 10,000 Mcf/D between wells located a few thousand feet apart (fig. 9) constrain the size of reservoir compartments in the Ozona. Detailed mapping confirms that many Ozona and Sonora sandstones are discontinuous at this same scale. Furthermore, sandstone continuity is only the first order of reservoir heterogeneity; permeable baffles and barriers within individual sandstones are created by sedimentary, diagenetic, and structural processes.

Ozona Canyon Stratigraphy

H. S. Hamlin, S. J. Clift

The Ozona Canyon interval is composed of several sandstone dominated zones separated by thick shales (fig. 10). Each sandstone zone typically contains several hundred feet of interbedded sandstones and shales, both having bed thicknesses mostly less than 20 ft. These sandstone zones are relatively continuous across the Ozona trend, although individual sandstones are discontinuous. The Ozona interval thickens to the northwest from less than 1,000 ft in northwest Edwards County to 1,500 ft in central Crockett County (fig. 11). The interval thickens more abruptly in southwest Crockett, where it partly interfingers with and partly overlies a thick Wolfcamp sandstone interval that is gas productive to the west in Terrell County (Horton, 1977). To the south in northern Val Verde County, the Ozona interval is erosionally truncated (figs. 4 and 11). For this study the upper and lower boundaries of the Ozona are defined by thin, regionally continuous limestones (fig. 10). The Ozona interval dips gently (20 to 50 ft/mi) to the northwest across most of Crockett County, but dips steepen to 100 to 300 ft/mi in the south near the pre-Cretaceous unconformity (fig. 12).

Sedimentary structures observed in core, sandstone geometries and distribution patterns, and regional paleogeographic context indicate that Ozona sandstones formed in submarine fan depositional systems (Mitchell, 1975; Berg, 1986; Lehtonen, 1987). Thinly interlaminated sandstone/shale sequences display sedimentary structures consistent with deposition from gravity-driven density flows (turbidity currents). Unconfined turbidity currents deposited the thin sandstones that form the broad lobes of the submarine fan, whereas thicker sandstones, having lenticular geometries and upward-fining vertical profiles, formed where turbidity currents were confined to channels on the fan surface (fig. 13). Thus, the shapes and internal stratification of Ozona sandstones are inherited from the submarine fan depositional environment.

The Ozona sandstones occupy a basin floor position adjacent and parallel to the south-facing slope of the Ozona Arch. Determining source areas and directions of transport for Ozona depositional systems is challenging because the southern part of the Ozona interval was removed during postdepositional uplift and erosion. Furthermore, sandstone distribution patterns, a complicated superposition of sandstone geometries and orientations, in the extant Ozona suggest multiple directions of sediment input. In order to unravel some of this complexity and characterize individual reservoir sandstone facies, each of the four major Ozona sandstone-bearing zones is described separately.

Ozona Producing Trend

The main Ozona producing trend is approximately 73 mi long and 28 mi wide across central Crockett County and extends into eastern Terrell and northwestern Val Verde Counties (fig. 7). The main Ozona trend coincides with the regional distribution of Ozona sandstone, although a separate Ozona sandstone is productive in Adams-Baggett field in southeast Crockett County. Depths to Ozona reservoirs range from about 6,000 to 7,500 ft in the main trend and about 4,000 to 5,500 ft in Adams-Baggett field. Although interwell variability in productivity is high, wells in the northeast part of the trend have, on average, greater flow potentials than do wells in the southwest or southeast (fig. 9). The south part of the trend experienced greatest uplift and erosion during the formation of the pre-Cretaceous unconformity and may have lost some of its gas resource at that time. Pervasive loss of porosity by silica cementation is another potential reason for poor reservoir quality locally in the south (National Petroleum Council, 1980).

Total sandstone content of the Ozona trend reaches 640 ft in southwest Crockett County, but net sandstone thickness and geographic distribution vary considerably among the Ozona zones. Stratigraphic cross sections (figs. 14 through 18) and net sandstone maps (figs. 19 through 22) illustrate these variations. Additionally, maps of the thickest individual sandstones in each zone (maximum sandstone) emphasize the distribution of the most prospective reservoirs (figs. 23 through 26). In the Ozona trend, the thickest sandstones are generally the most productive. Finally, maps showing prominent vertical trends in grain size and sandstone abundance (log facies maps, see figs. 27 through 30), when used in conjunction with net sandstone and maximum sandstone maps, are a powerful tool for reconstructing the sandstone framework architecture of Ozona depositional systems.

Regional Sandstone Distribution

Zone 1 is the uppermost Ozona zone, within which sandstones are most abundant in the lower third (figs. 14 through 18). The upper part of zone 1 is dominated by shales and thin limestones. Zone 1 sandstones grade into

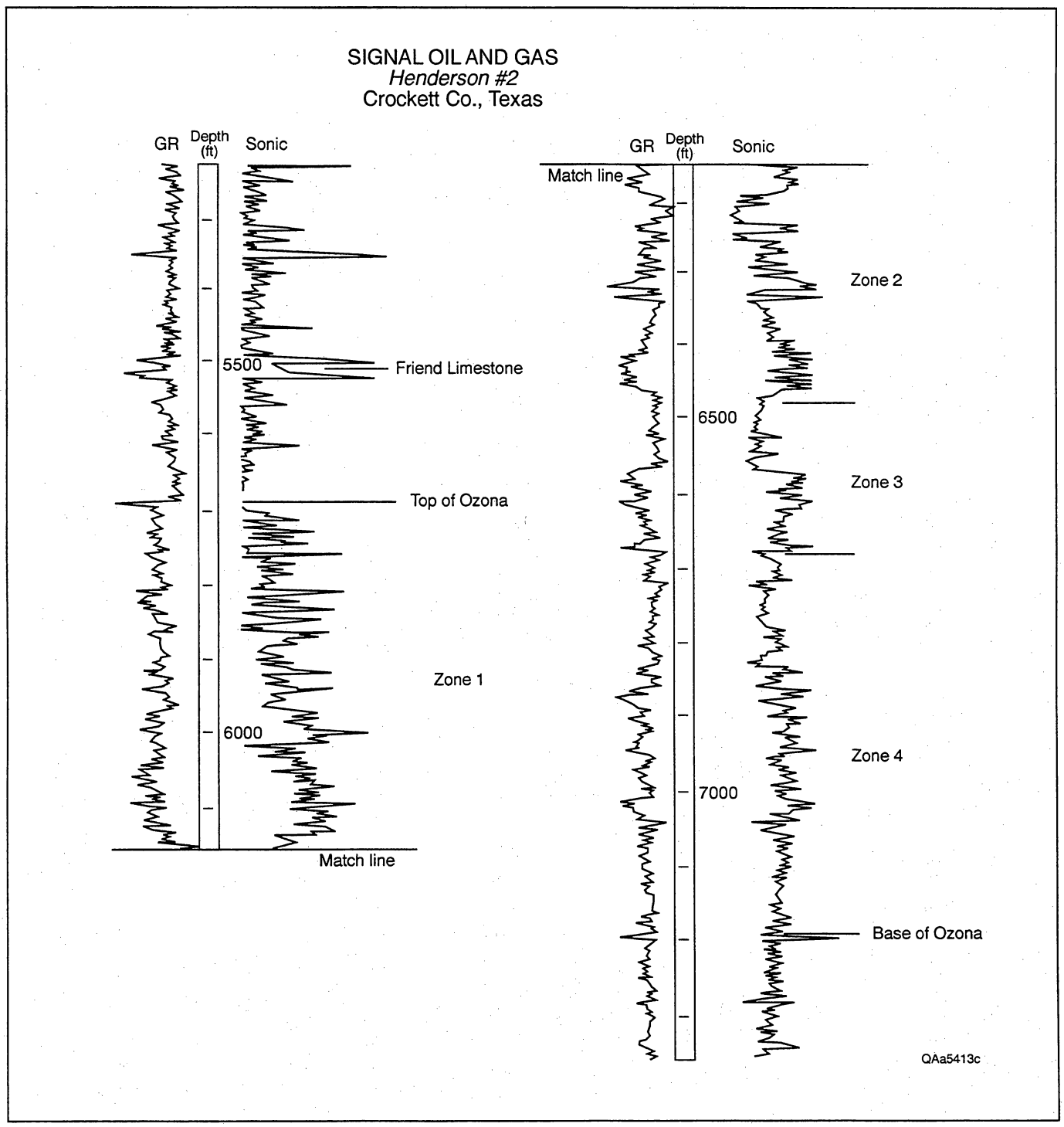

Figure 10. Gamma-ray and sonic logs from a typical Ozona well showing the four main sandstone zones.

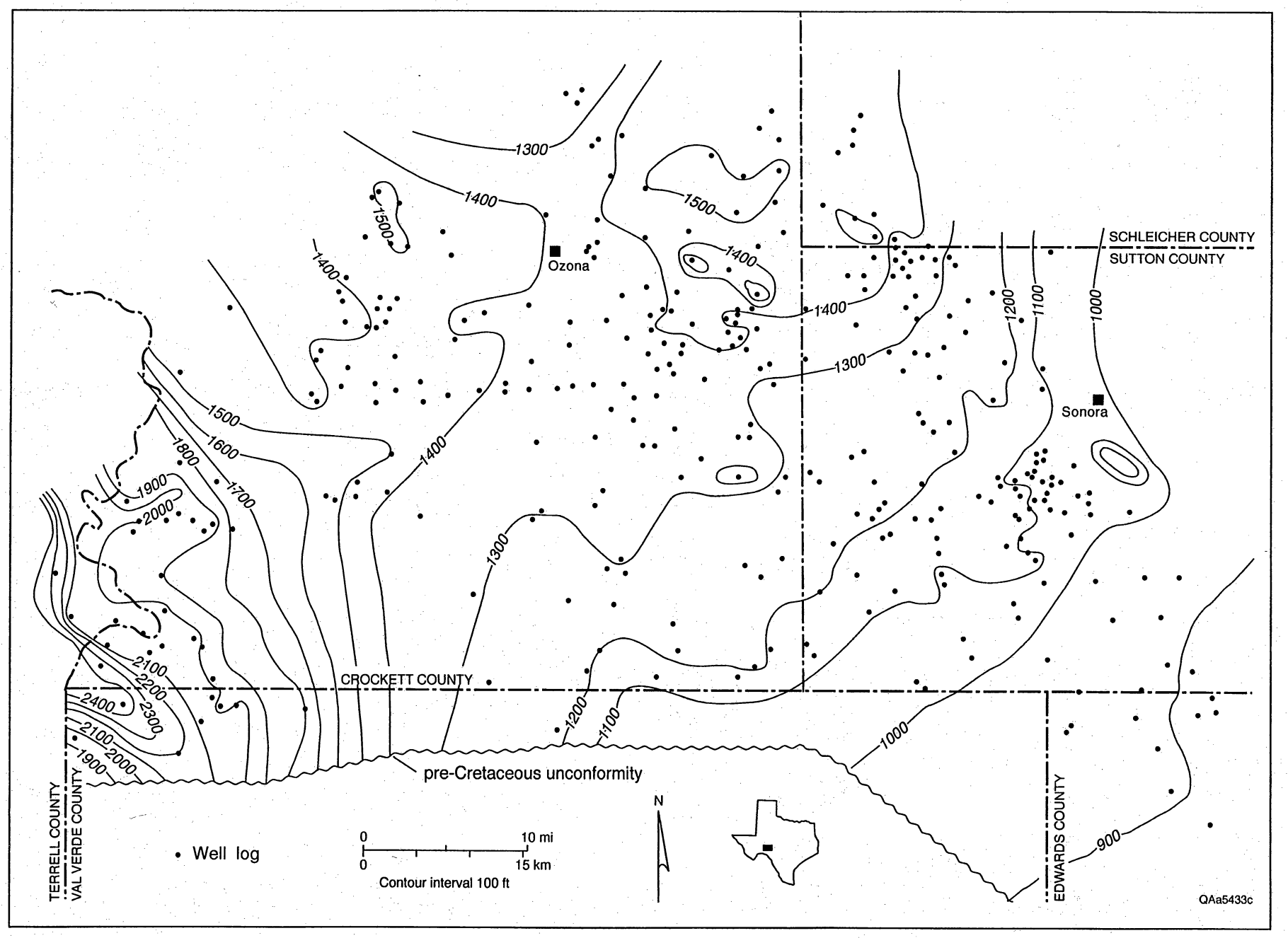

Figure 11. Isopach map of Ozona Canyon interval.

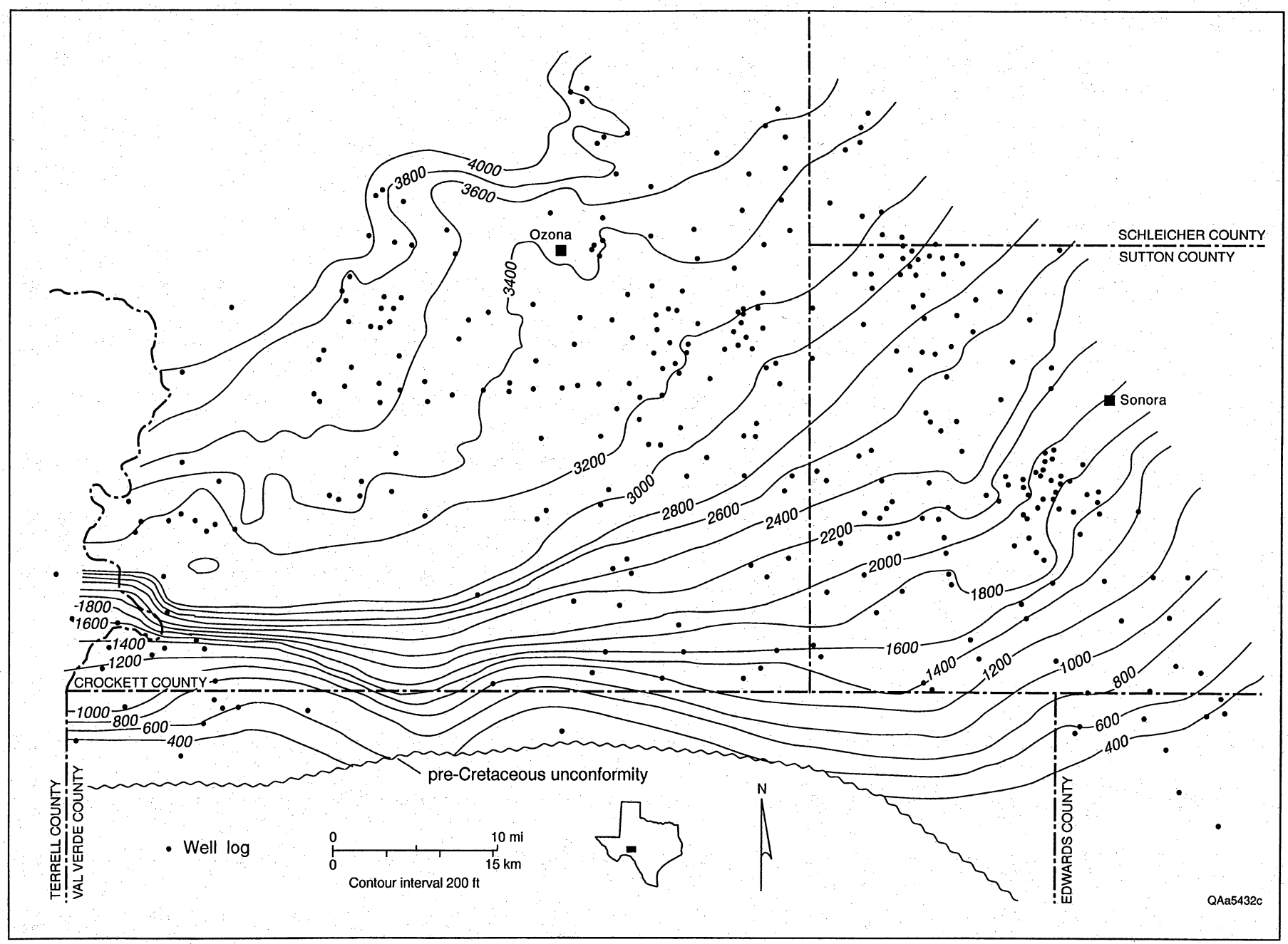

Figure 12. Structure map contoured on the top of the Ozona Canyon interval.

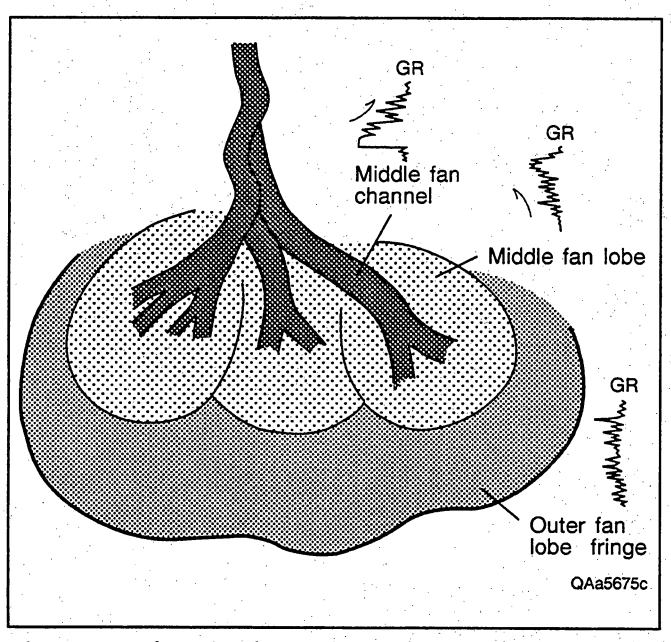

Figure 13. Submarine fan model showing typical gamma-ray log responses caused by Canyon fan channel and lobe facies. Model simplified from illustrations and descriptions in Shanmugam and Moiola (1988).

shale to the southwest and northeast and into limestone to the southeast. Net sandstone in zone 1 reaches 60 to 150 ft in several isolated depocenters, which are enclosed in a broader belt containing thinner sandstone (fig. 19). Thicker sandstones in zone 1 generally display upward-fining log patterns (fig. 27) and form narrow belts and pods (fig. 23).

Thick individual sandstone bodies displaying upward-fining trends probably represent submarine fan channel deposits, whereas thinner sandstone bodies displaying upward-coarsening trends were deposited by prograding fan lobes (Tyler and Gholston, 1988). The fan channel and lobe facies grade into an enclosing body of thin-bedded sandstones in thick shales that form a distal fan lobe fringe (figs. 27 and 13).

Zone 1 sandstones contribute to gas production primarily in the areas where individual sandstone bodies are greater than 20 ft thick (fig. 23). At the north end of the zone 1 maximum-sandstone trend, a small area having maximum single sandstone thicknesses ranging from 40 to 85 ft supports a group of wells in which initial potentials exceeded 5,000 Mcf/d (compare figs. 23 and 9). In this productive area, several channel-fill deposits are superposed and laterally coalesced, creating an unusually extensive high-quality pay zone.

Zone 2 is composed of upper and lower sandstone units, which are most distinct in the central part of the main Ozona trend (figs. 14 through 18). Although not mapped separately, the lower sandstone unit is thickest in the southwest, whereas the upper unit is best developed in the northeast. A separate sandstone unit within zone 2 is located to the southeast in the Adams-Baggett field (fig. 20). Zone 2 sandstones extend southward to the pre-Cretaceous uniformity in Val Verde County and westward into Terrell County. Along the main Ozona trend, thick sandstones displaying upward-fining log patterns are flanked to the southeast by thinner, upward-coarsening sandstones (fig. 28). In the southeast corner of Crockett County, however, thick sandstones in the Adams-Baggett area display primarily upward-coarsening log patterns (compare figs. 20 and 28). Zone 2 in the Adams-Baggett area is composed largely of a single sandstone reaching 160 ft in thickness, whereas along the main Ozona trend, zone 2 includes several sandstones having individual thicknesses mostly less than 60 ft (fig. 24).

Zone 2 contains many of the most productive reservoirs in the Ozona interval. High initial potentials (>5,000 Mcf/d, see fig. 9) are most common in the northeastern part of the main trend, where most of the Ozona gas wells are perforated either in zones 1 and 2 or in zone 2 alone. In the upper part of zone 2, upward-fining channel sandstones having individual thickness 40 to 100 ft are the most prospective targets. Sandstones in the lower part of zone 2 are productive in the southwestern part of the Ozona trend, but because most wells there are perforated in several different zones, the relative contribution of zone 2 sandstones to gas production in the southwest could not be determined.

Zone 3 sandstones are generally located in the lower part of the zone to the northeast but thicken to fill the entire zone in the south and southwest (figs. 14 through 18). Zone 3 sandstones extend along the main Ozona trend and out of the study area to the south and west, displaying complicated lobate and belt-like geometries (fig. 21). These complex sandstone geometries are highlighted on the log-facies map, where northwest-oriented upward-fining trends are prominent (fig. 29). The thickest individual sandstones in zone 3 lie mainly in a narrow belt along the axis of the Ozona trend (fig. 25).

Unlike the other Ozona zones, sandstone development in zone 4 does not coincide with the main Ozona trend. Zone 4 sandstones are apparently thickest to the south and west of our study area but extend into the southwest corner of Crockett County (fig. 22). Sandstones occur progressively lower in zone 4 southwestward (fig. 14). Most of the thick "Wolfcamp" sandstones reported in Terrell County (Horton, 1977) are stratigraphically equivalent to and lower than our Ozona zone 4. Although zone 4 sandstone thickness maps display northeast-thinning lobate geometries (figs. 22 and 26), the log facies map reveals narrow, east-trending belts of upward-fining sandstones (fig. 30).

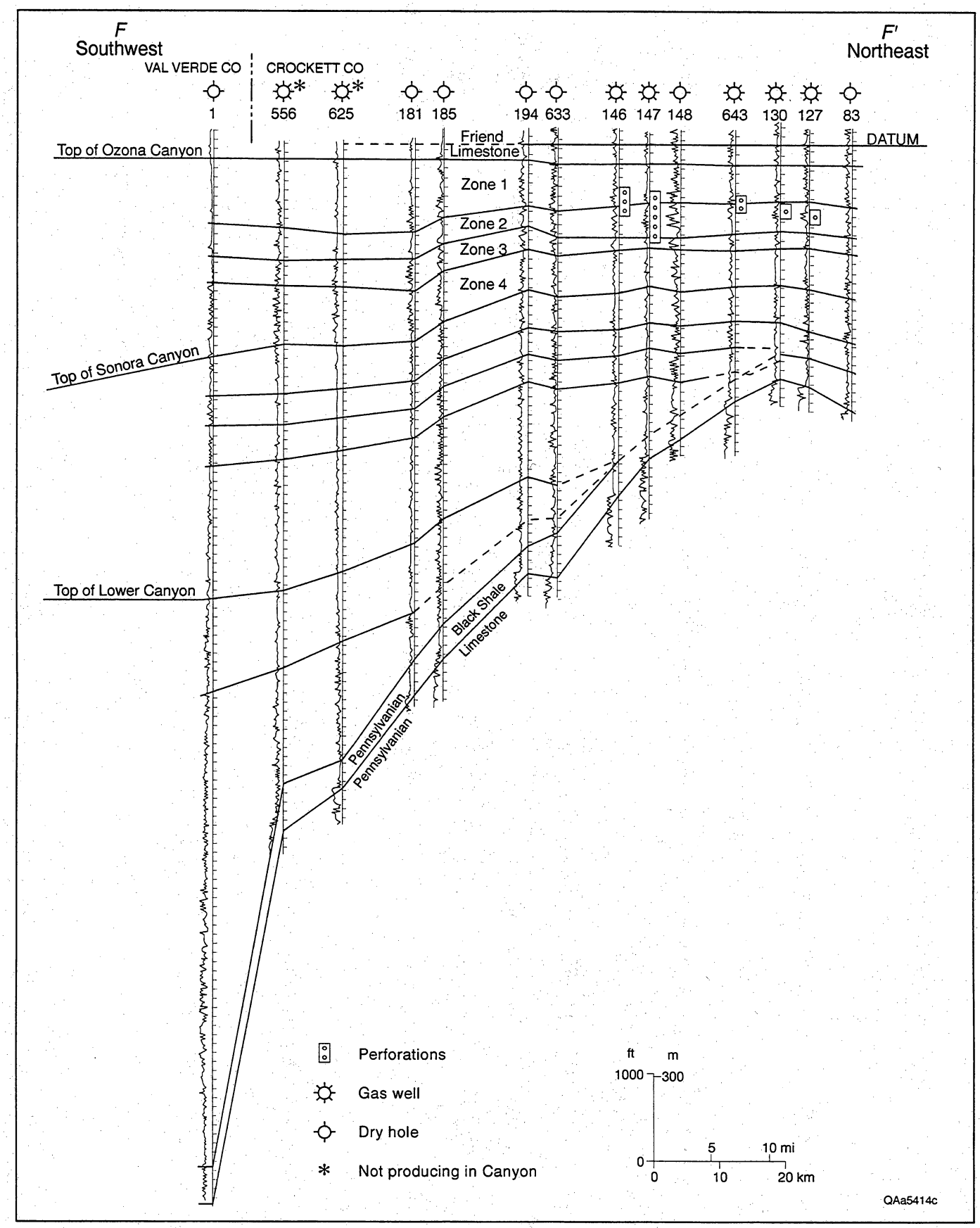

Figure 14. Stratigraphic cross section F–F′ oriented along the axis of the Ozona trend. See figure 3 for location of section line. Gamma-ray logs display sandstone/shale interbedding styles.

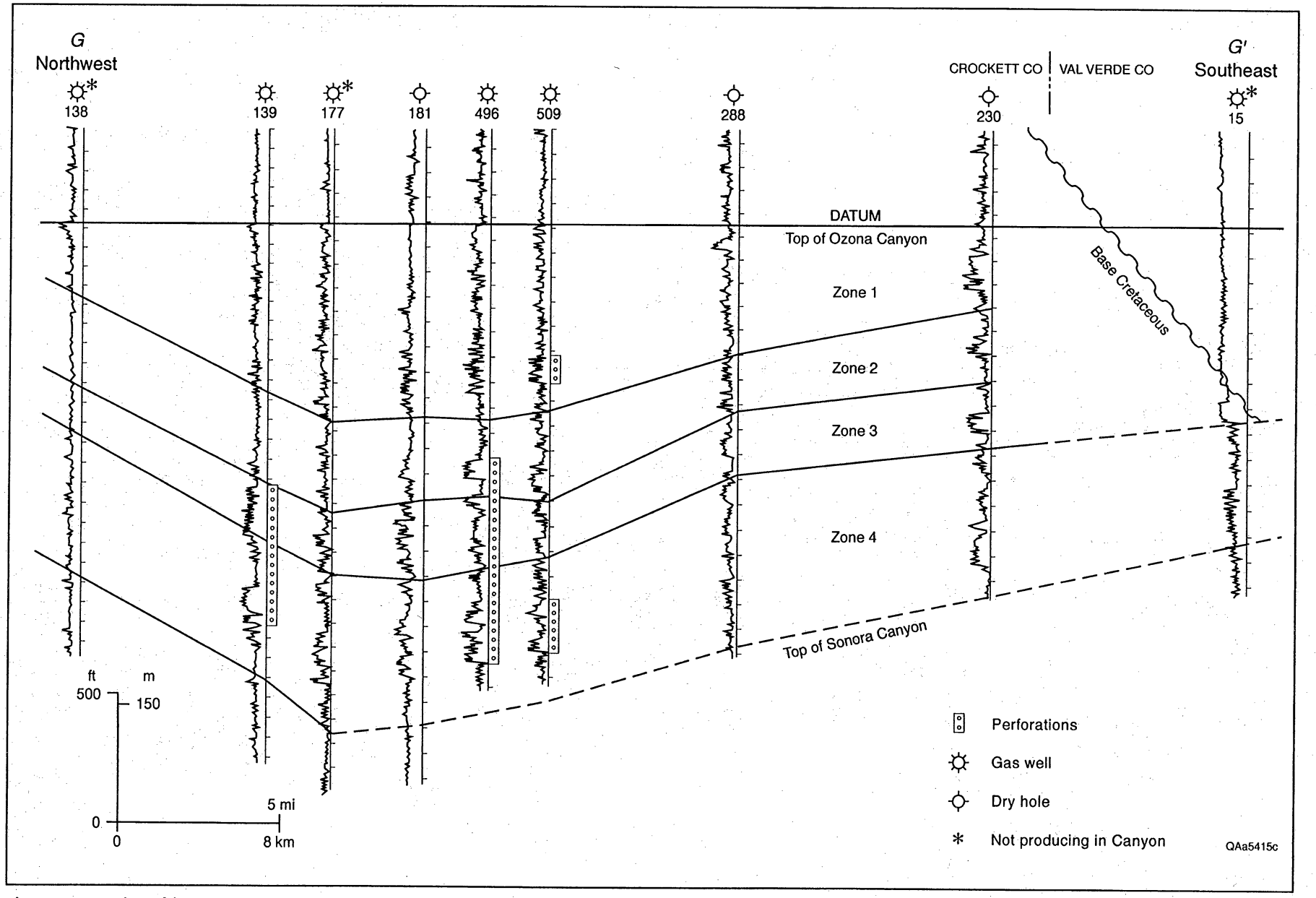

Figure 15. Stratigraphic cross section G–G′ oriented perpendicular to the main Ozona trend. See figure 3 for location of section line. Gamma-ray logs display sandstone/shale interbedding styles.

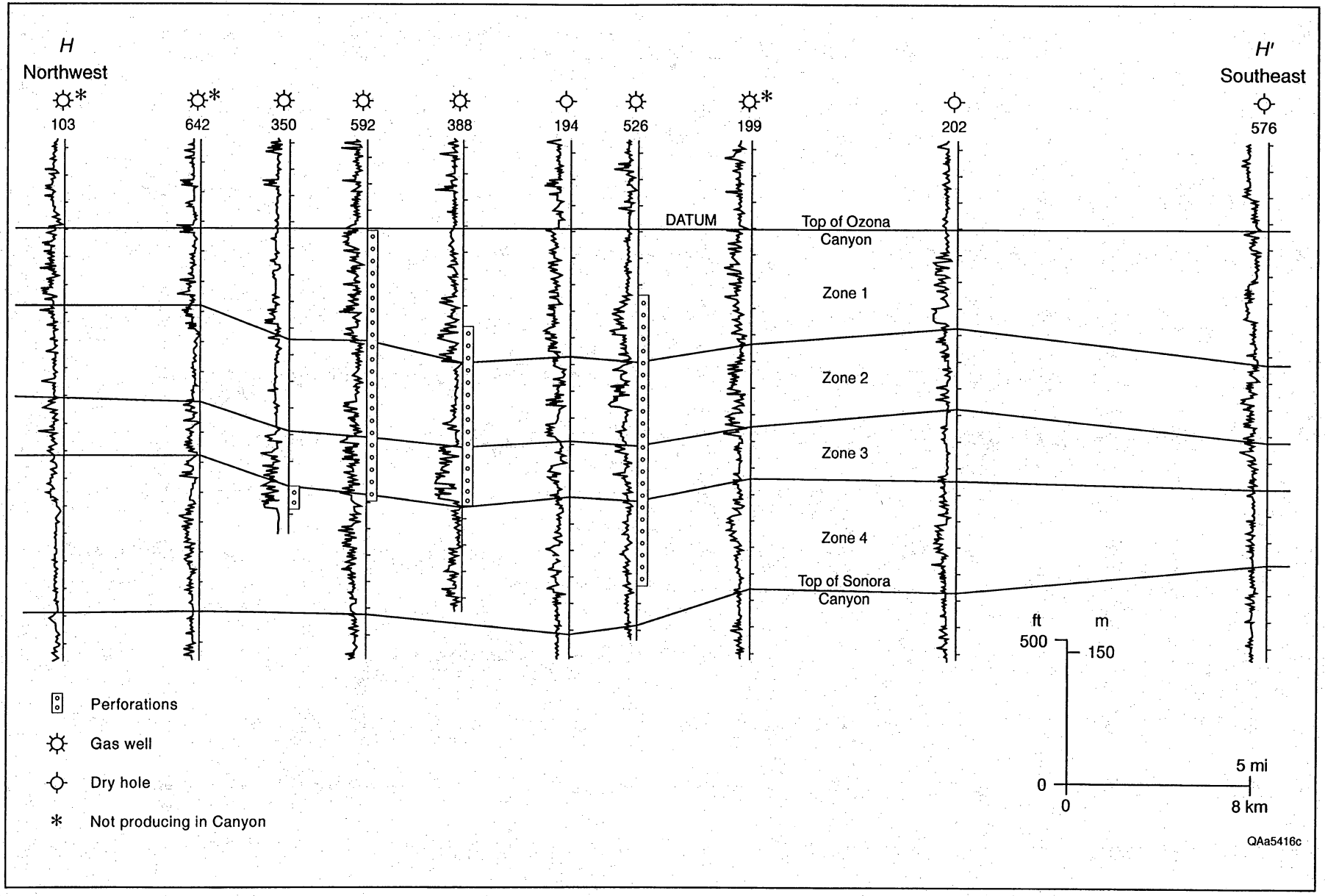

Figure 16. Stratigraphic cross section H–H′ oriented perpendicular to the main Ozona trend. See figure 3 for location of section line. Gamma-ray logs display sandstone/shale interbedding styles.

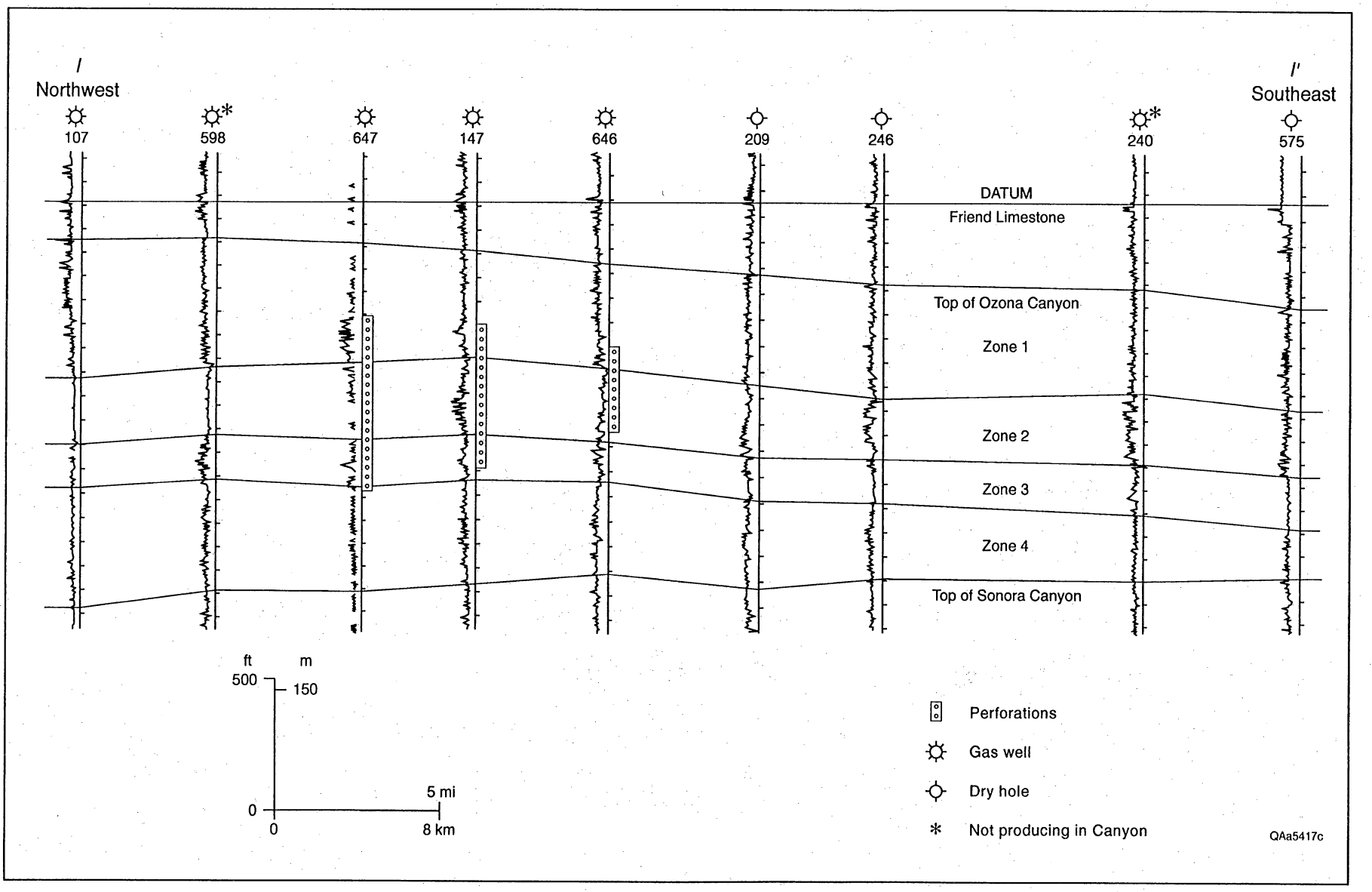

Figure 17. Stratigraphic cross section I–I′ oriented perpendicular to the main Ozona trend. See figure 3 for location of section line. Gamma-ray logs display sandstone/shale interbedding styles.

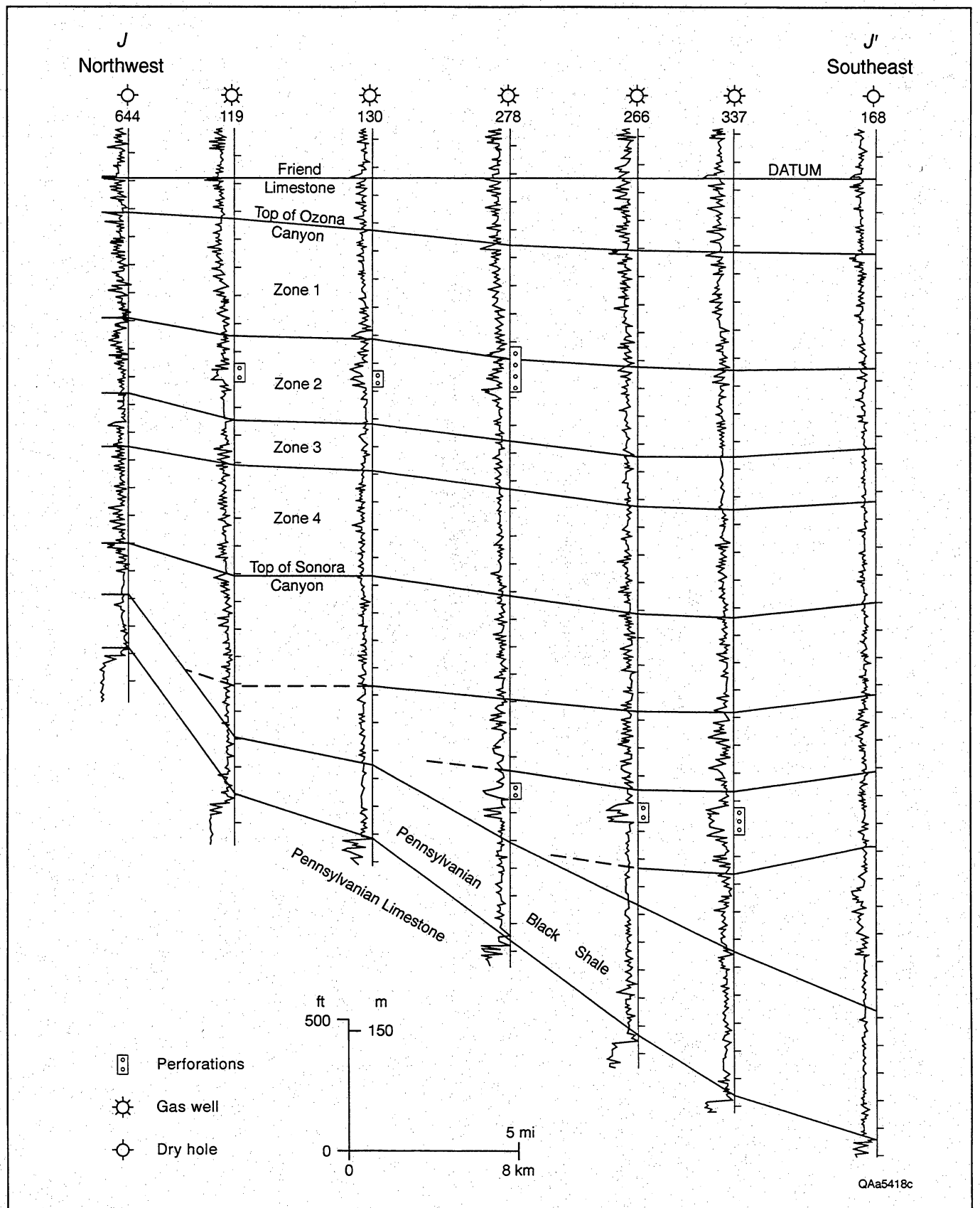

Figure 18. Stratigraphic cross section J–J′ oriented perpendicular to the main Ozona trend. See figure 3 for location of section line. Gamma-ray logs display sandstone/shale interbedding styles.

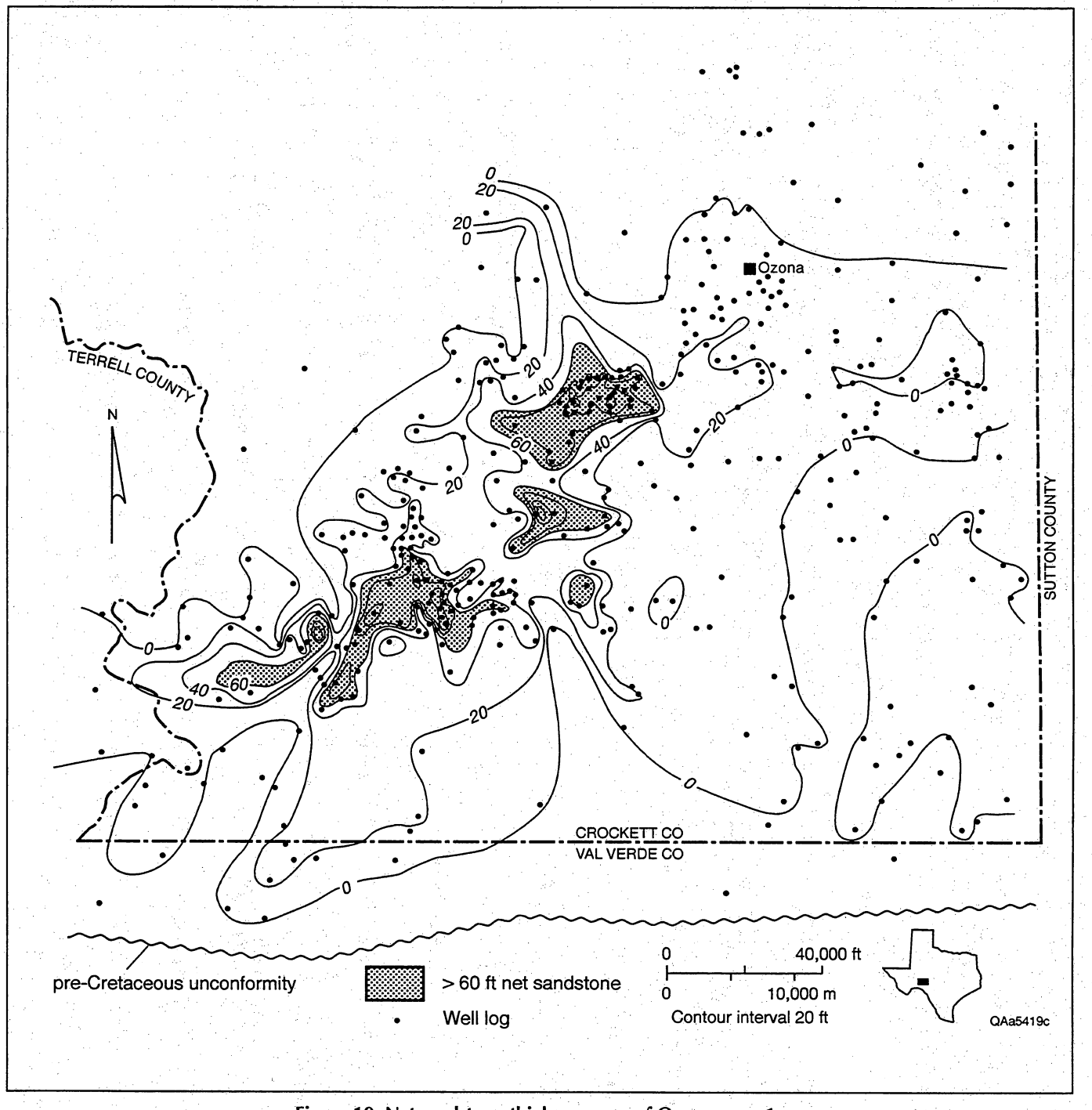

Figure 19. Net sandstone thickness map of Ozona zone 1.

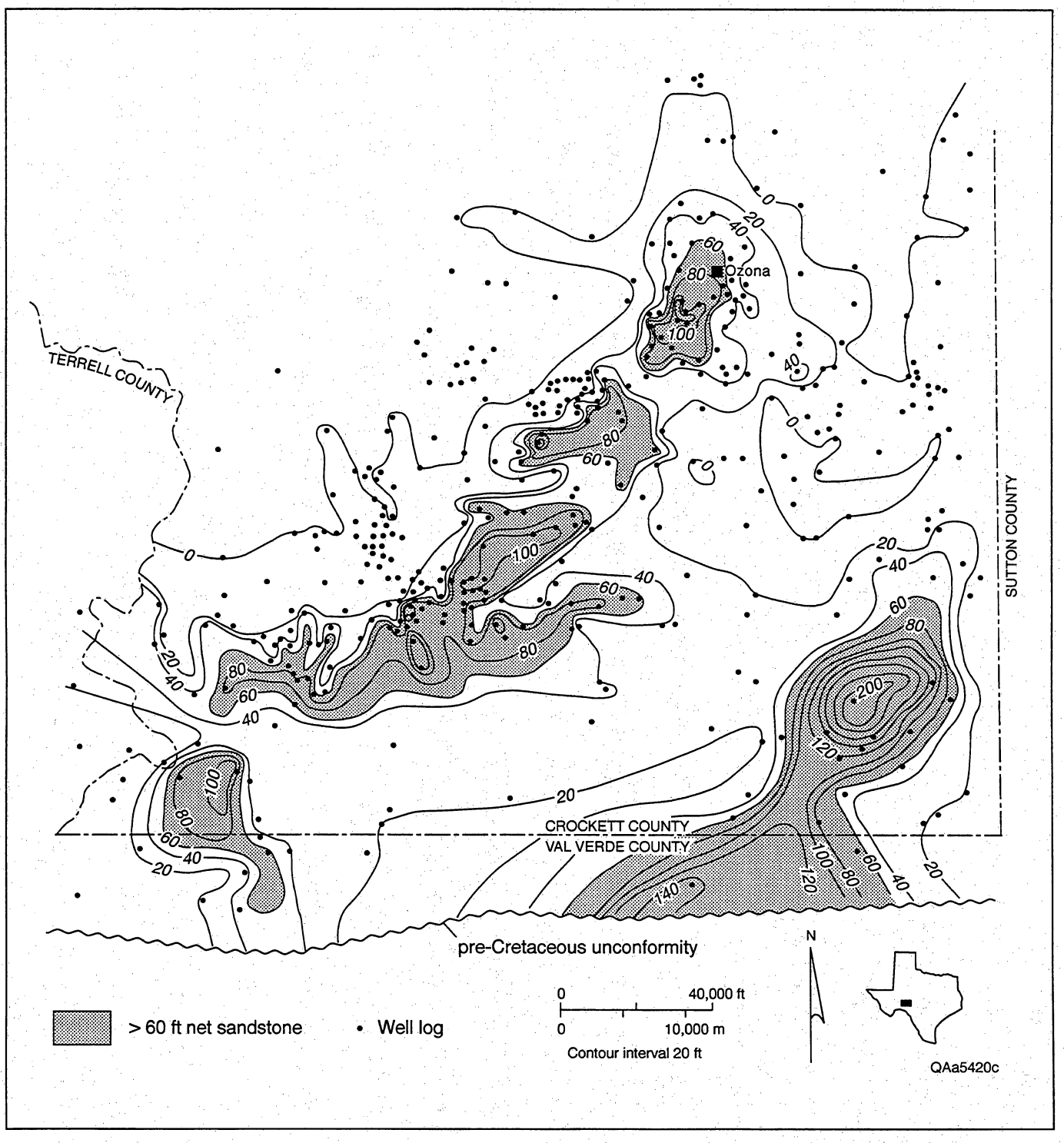

Figure 20. Net sandstone thickness map of Ozona zone 2.

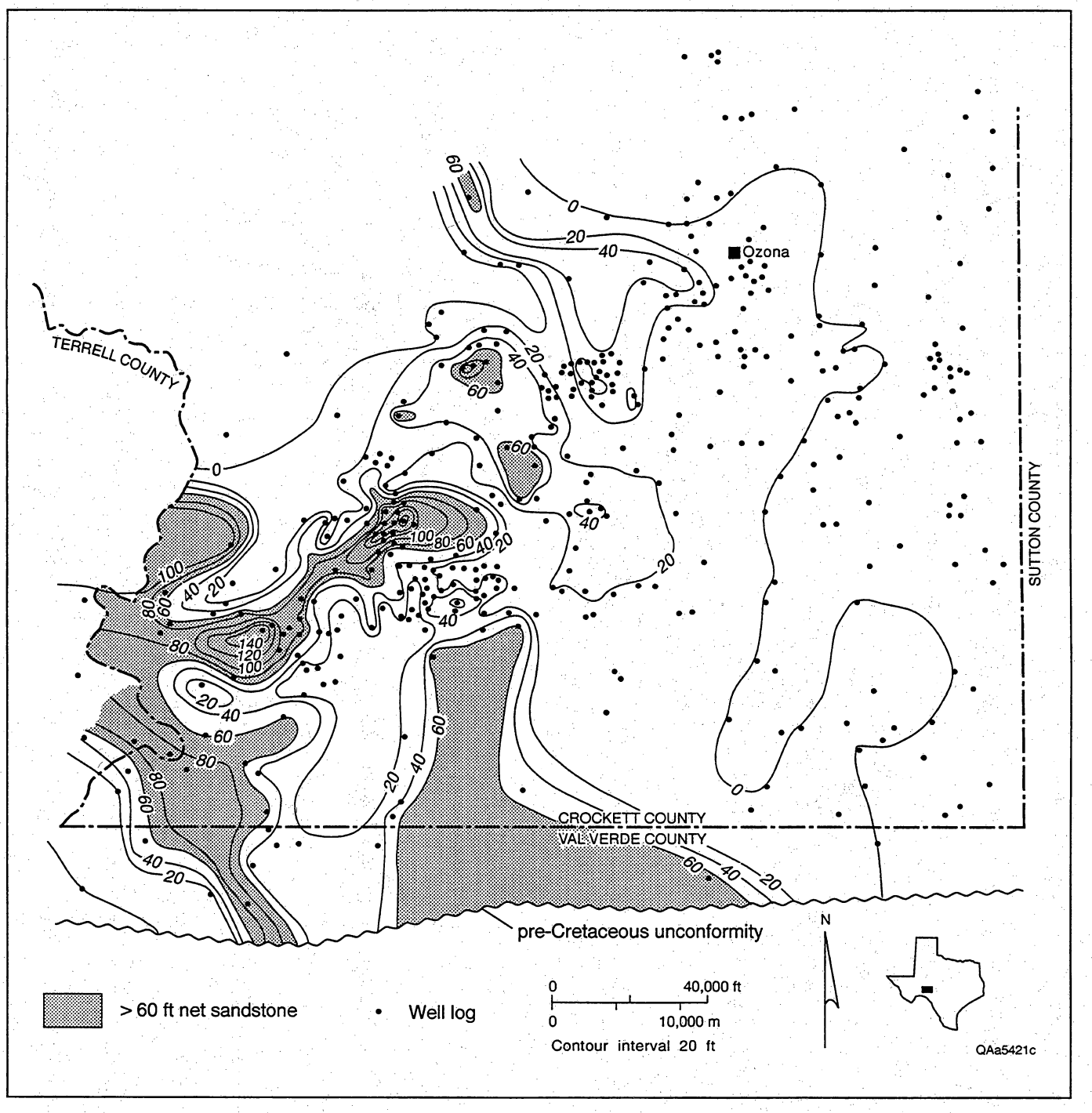

Figure 21. Net sandstone thickness map of Ozona zone 3.

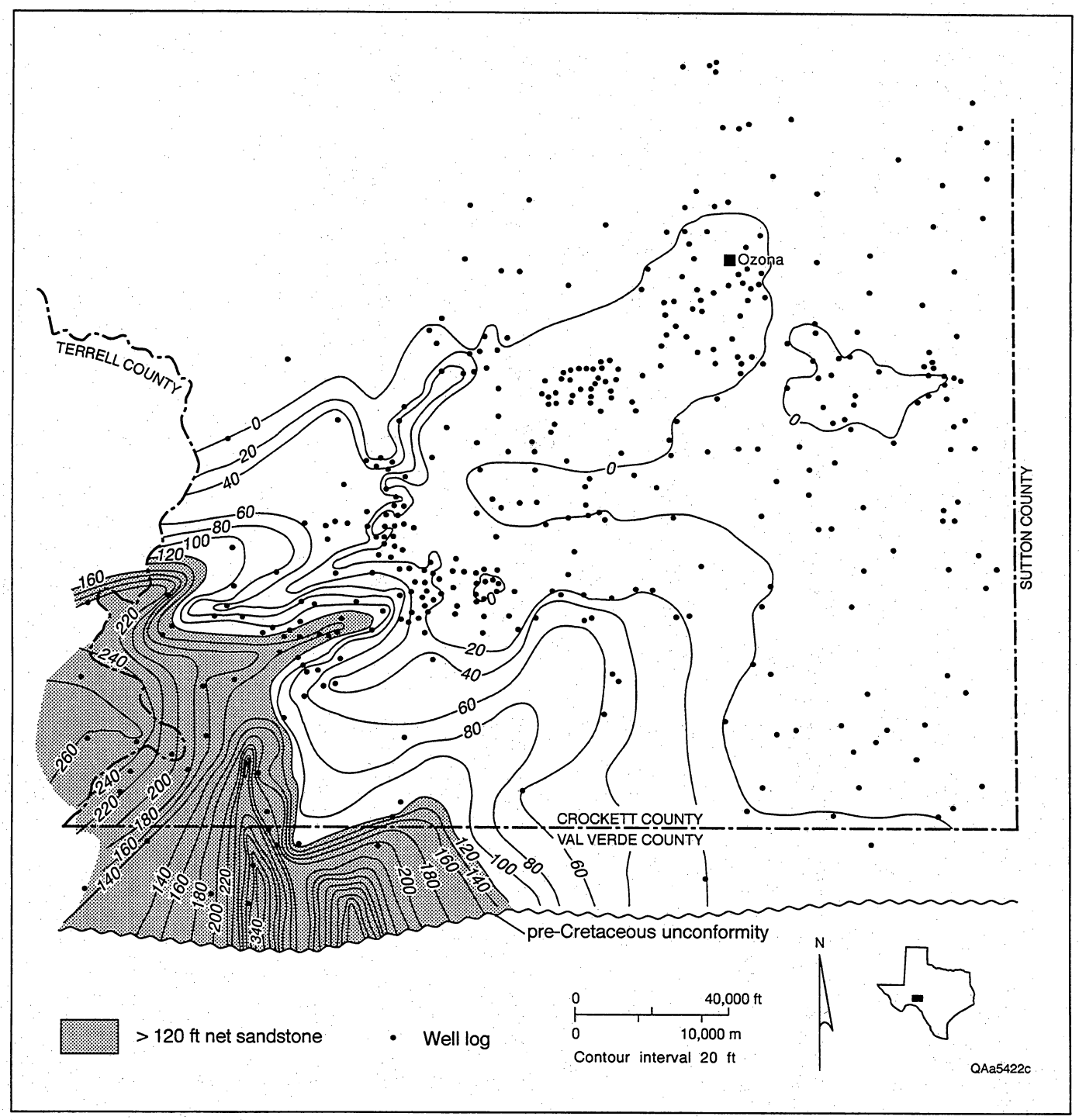

Figure 22. Net sandstone thickness map of Ozona zone 4.

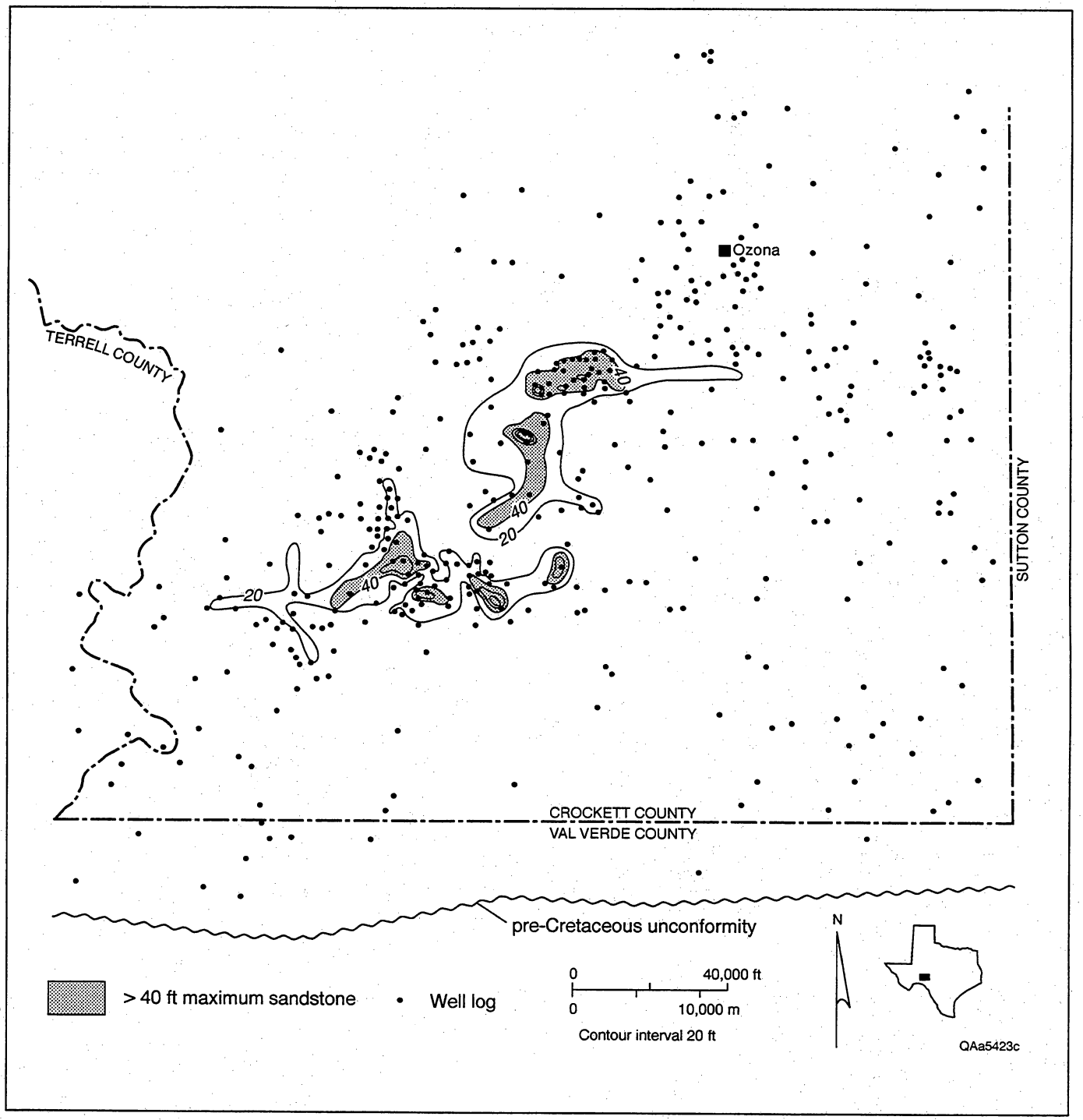

Figure 23. Maximum sandstone map of Ozona zone 1. The thickest individual sandstone at each well is mapped regardless of stratigraphic position within the zone. Individual sandstones are here defined as those containing no shale interbed >5 ft thick.

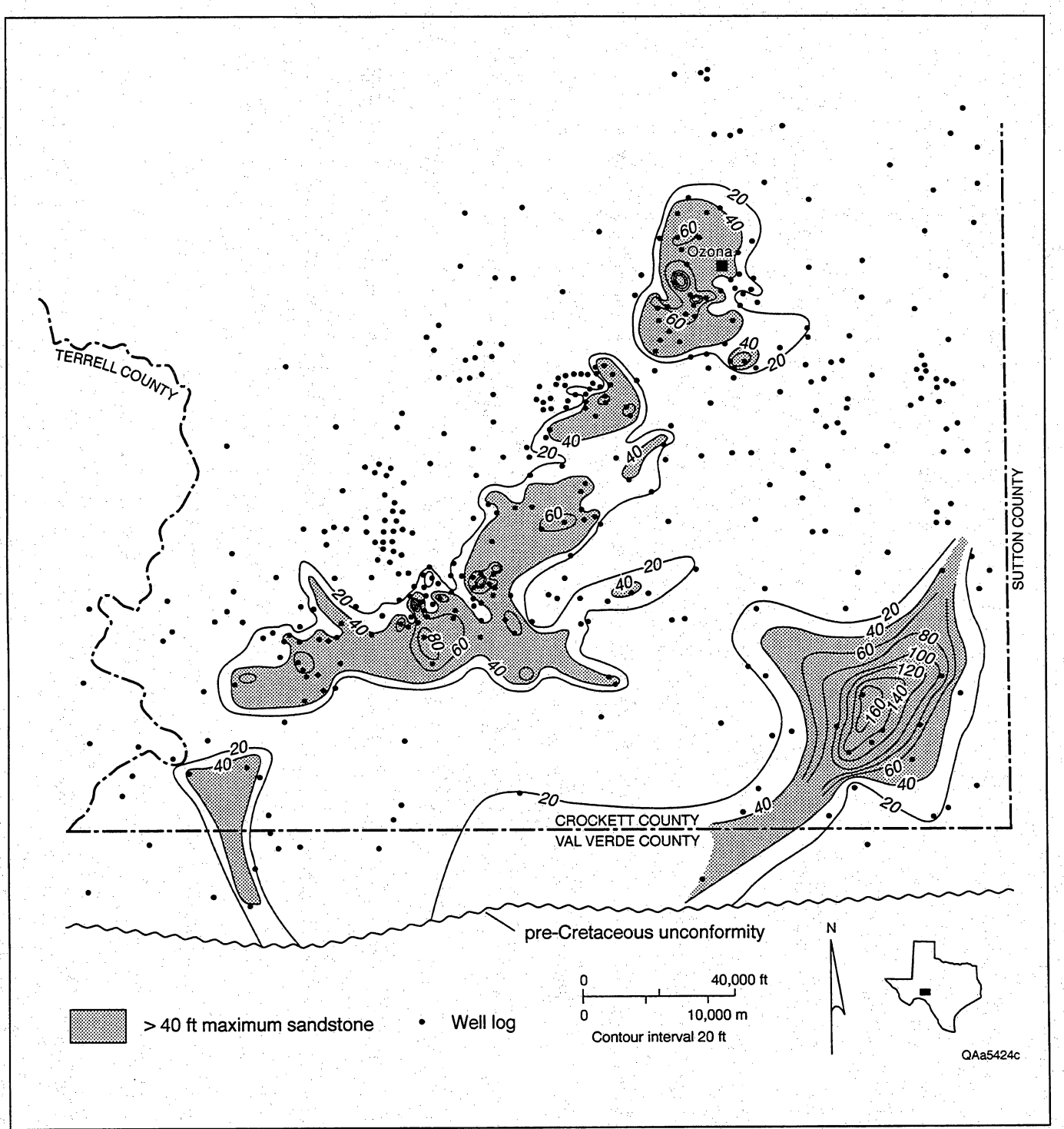

Figure 24. Maximum sandstone map of Ozona zone 2. The thickest individual sandstone at each well is mapped regardless of stratigraphic position within the zone. Individual sandstones are here defined as those containing no shale interbed >5 ft thick.

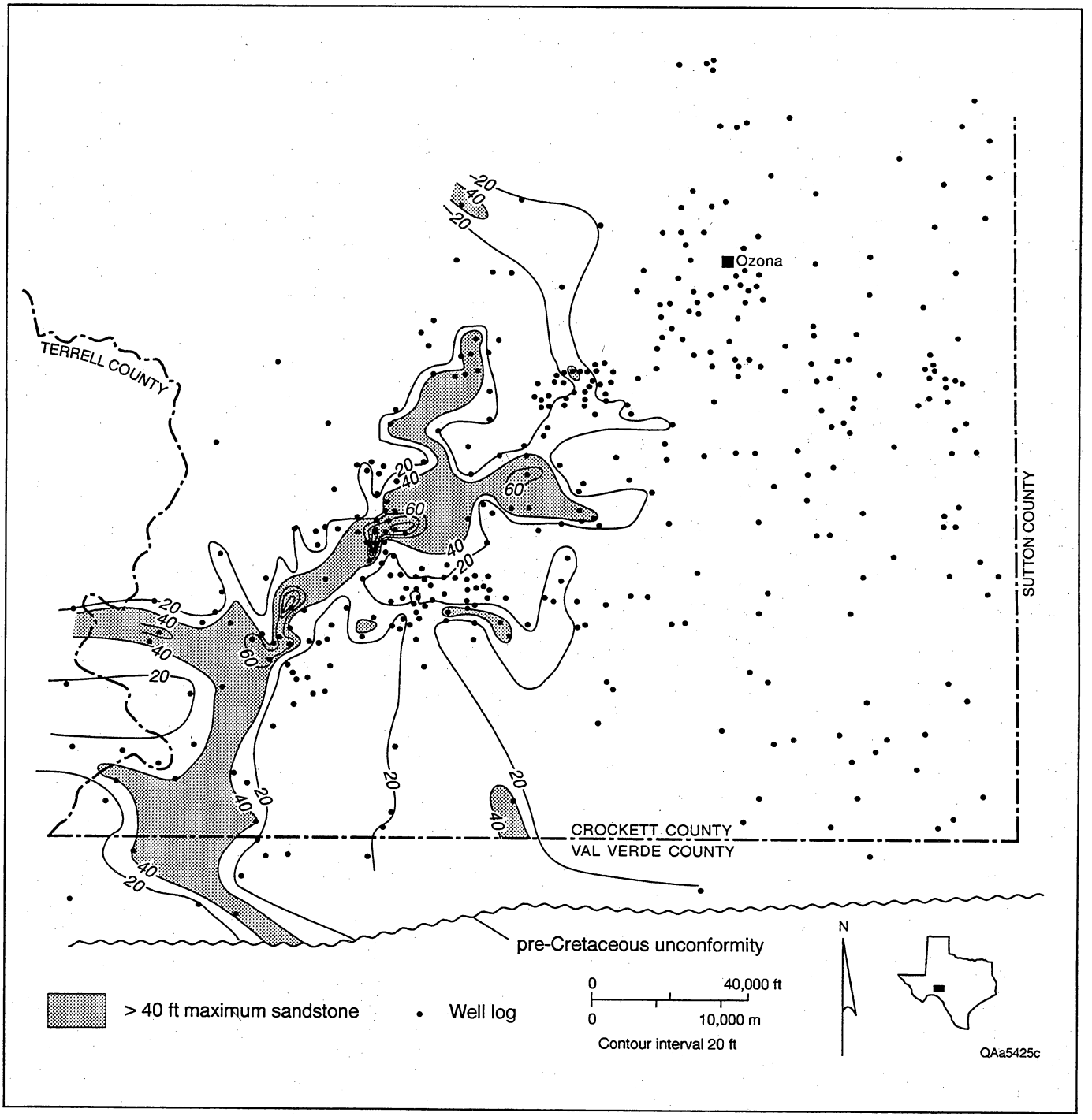

Figure 25. Maximum sandstone map of Ozona zone 3. The thickest individual sandstone at each well is mapped regardless of stratigraphic position within the zone. Individual sandstones are here defined as those containing no shale interbed >5 ft thick.

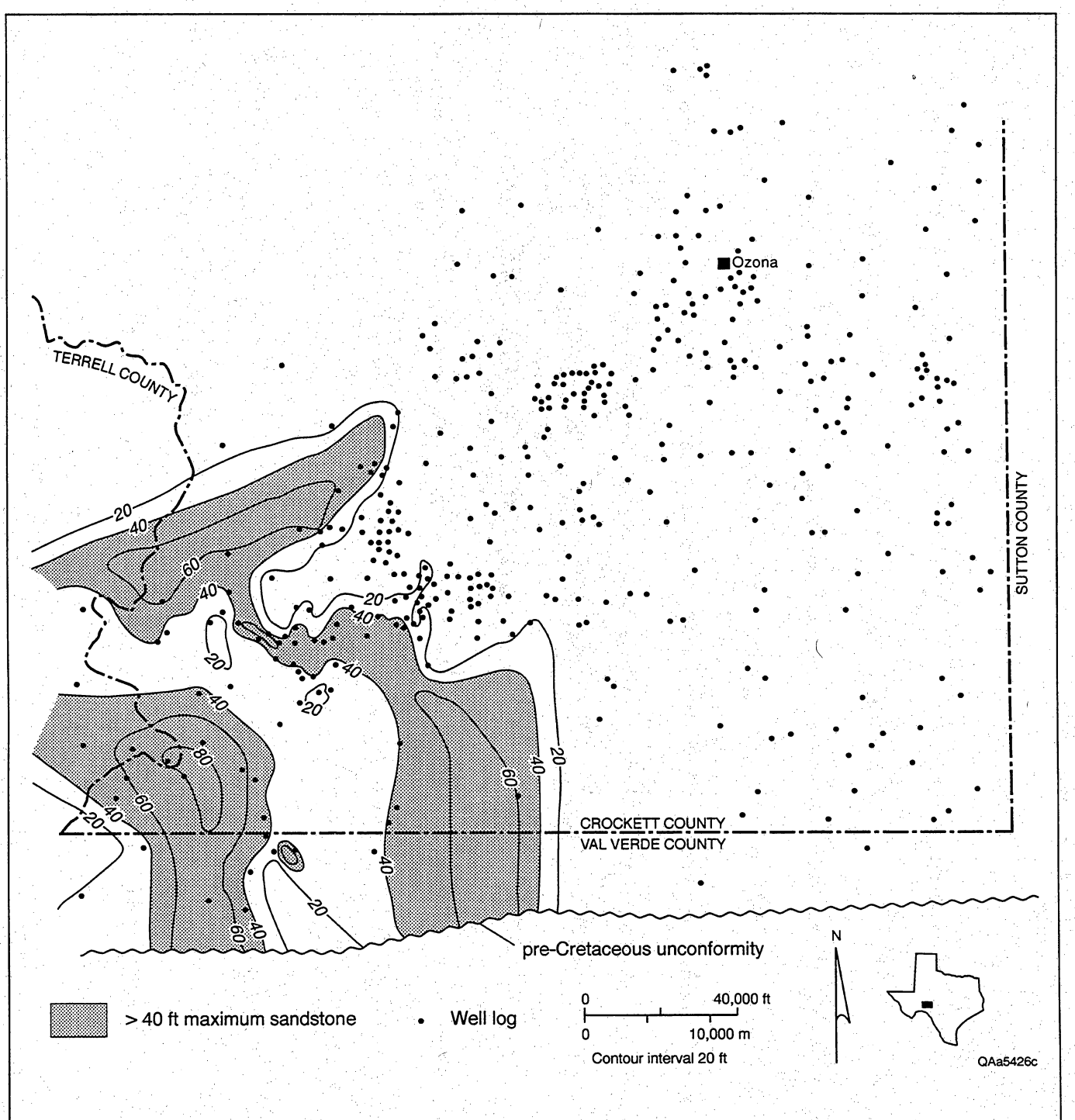

Figure 26. Maximum sandstone map of Ozona zone 4. The thickest individual sandstone at each well is mapped regardless of stratigraphic position within the zone. Individual sandstones are here defined as those containing no shale interbed >5 ft thick.

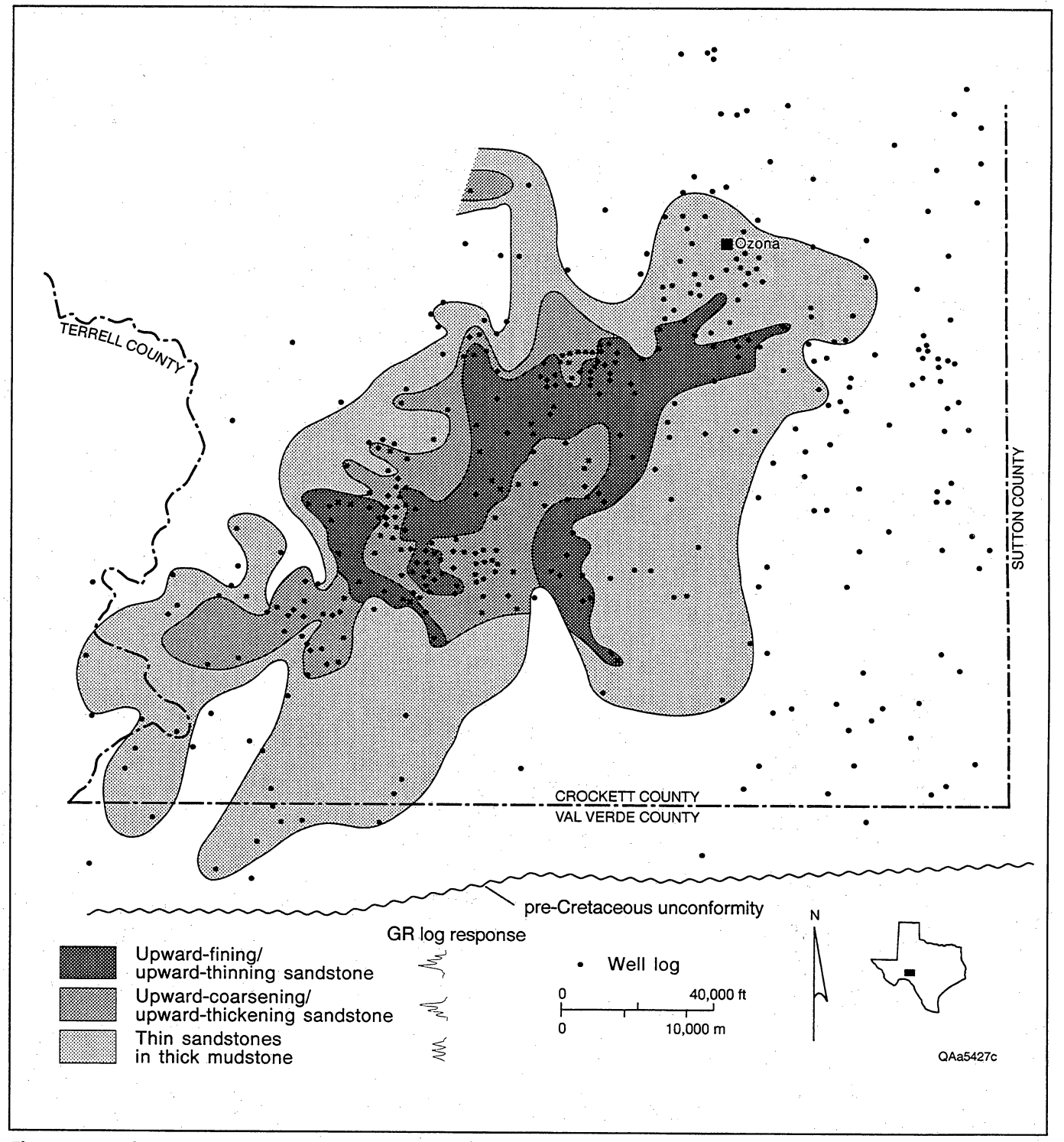

Figure 27. Log facies map of Ozona zone 1. Log facies illustrate vertical trends in sandstone/shale interbedding styles interpreted from gamma-ray log patterns.

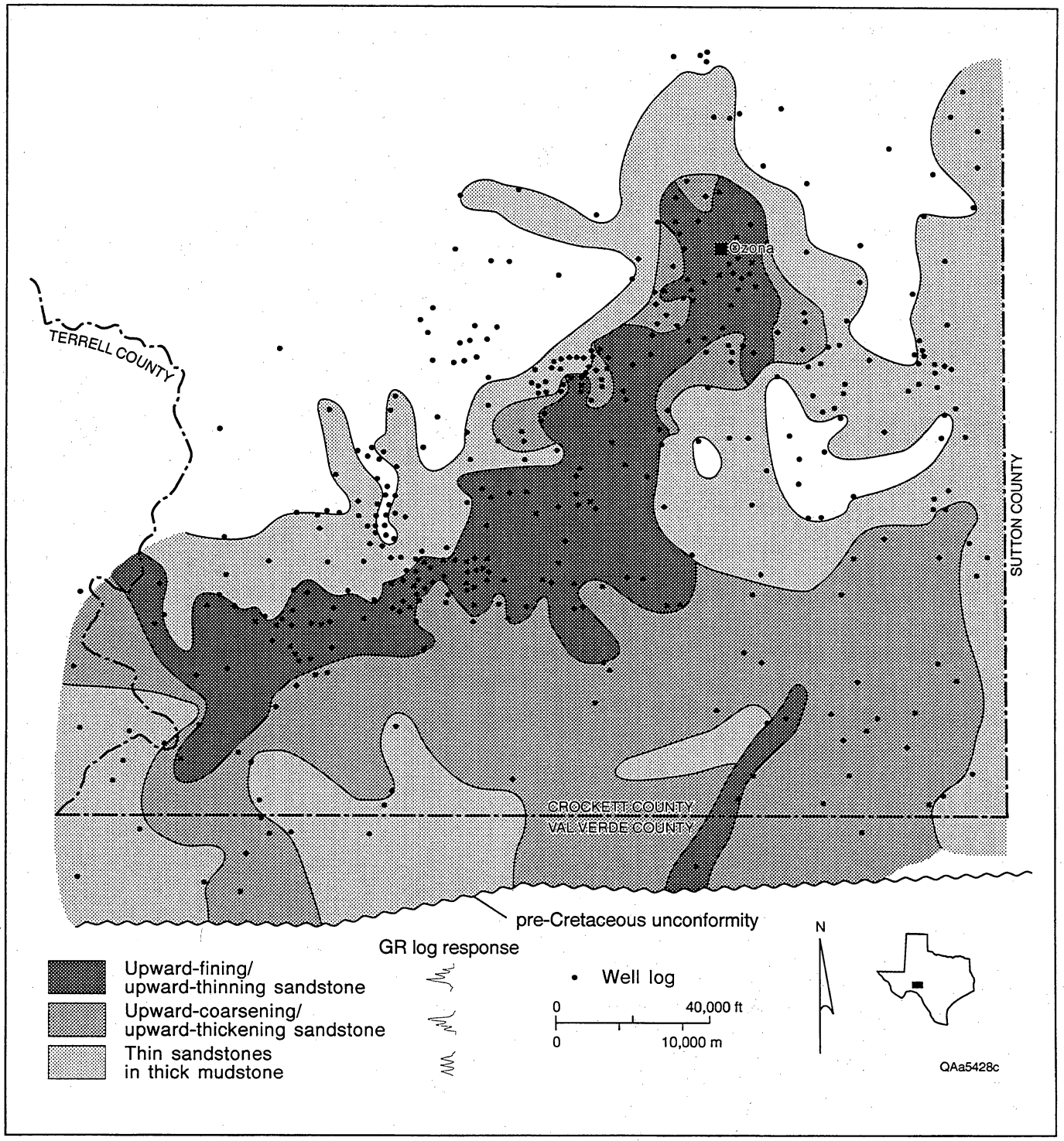

Figure 28. Log facies map of Ozona zone 2. Log facies illustrate vertical trends in sandstone/shale interbedding styles interpreted from gamma-ray log patterns.

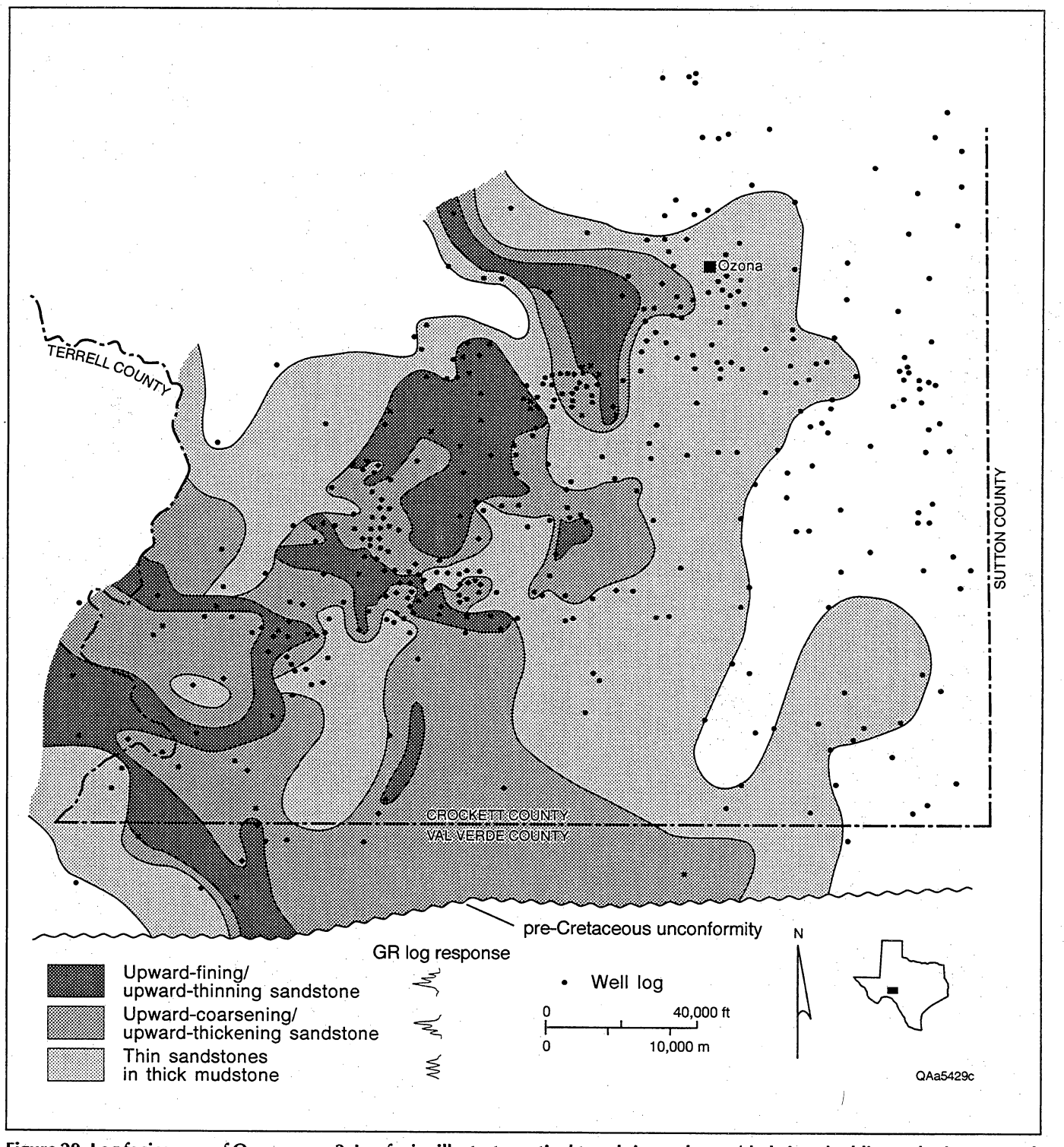

Figure 29. Log facies map of Ozona zone 3. Log facies illustrate vertical trends in sandstone/shale interbedding styles interpreted from gamma-ray log patterns.

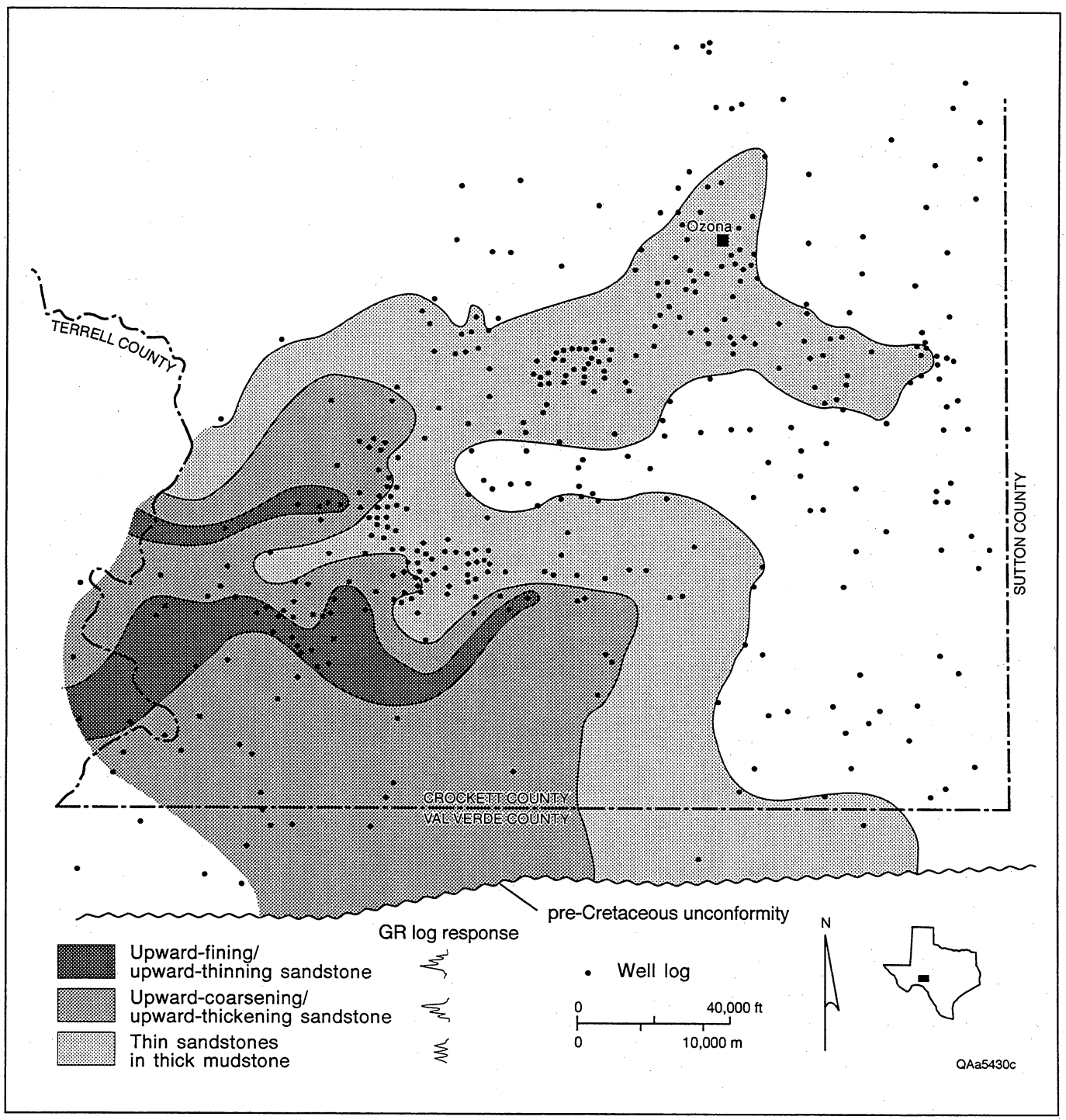

Figure 30. Log facies map of Ozona zone 4. Log facies illustrate vertical trends in sandstone/shale interbedding styles interpreted from gamma-ray log patterns.

Ozona zones 3 and 4 are most commonly productive in wells in the southwest part of the trend, coinciding with the distribution of thick sandstones in these zones. Initial potentials in wells perforated in zones 3 and 4 reach 5,000 to 19,000 Mcf/d in a few wells but generally range between 500 and 3,500 Mcf/d. Although thick sandstones are abundant in the southwest, post-depositional processes, such as cementation, may be responsible for somewhat lower reservoir quality there (National Petroleum Council, 1980). The lack of petrographic data, however, precluded further investigations into the specific mechanisms affecting reservoir quality in the southwest part of the Ozona trend.

Depositional Facies

Ozona cores from two wells located at the northeast edge of the Ozona trend (fig. 3) were the only Ozona formation samples available for direct observation during this study. These cores are mainly from Ozona zone 2, which is well developed in this area (fig. 20). Most of the cored intervals, however, are shale-dominated, distal fan lobe depositional facies. Therefore, published core descriptions from several wells in the heart of the main Ozona trend (Lehtonen, 1987) were used to provide a more complete picture of Ozona core lithofacies.

Submarine fans consist predominantly of turbidites (Shanmugam and Moiola, 1988), and turbidites are the most common sedimentary features identified in Ozona Canyon cores. In a submarine fan depositional context, turbidites are recognized by a typical sequence of sedimentary structures known as the "Bouma sequence" (Bouma, 1962). The Bouma sequence, which may be characterized simply as massive to laminated sandstone overlain by laminated mudstone, records deposition by a waning turbidity flow. All the divisions of the Bouma sequence are found in Ozona cores, but variations from this ideal sequence are useful for identifying depositional facies and interpreting environments. Turbidites having thick lower Bouma divisions (sandstone part) and thin or missing upper divisions (mudstone part) result from higher flow energies in fan channels and on proximal parts of fan lobes, whereas turbidites having thin sandstone and thick mudstone result from lower flow energies in interchannel areas and on distal fan lobes (fig. 13).

Major lithofacies observed in Ozona cores include thick-bedded or massive sandstone (thick turbidites), thinly interbedded sandstone and shale (thin turbidites), contorted muddy sandstone, conglomeratic mudstone, and laminated shale. The thick-bedded sandstone facies consists of sandstone beds, 1 to 5 ft thick, interbedded with mudstone beds less than 0.5 ft thick. The sandstones are predominantly fine-grained and commonly contain carbonate cement. Sharp bases with sole marks, graded bedding, horizontal lamination, and fluid escape structures are the most common sedimentary features in these sandstones. Unlike in Sonora sandstones, in Ozona sandstones organic debris is relatively rare, and siderite staining is absent. Ozona thick-bedded turbidites were probably deposited in channels and proximal lobes on the middle part of the submarine fan (fig. 13). Channel-fill sandstones make the best reservoirs but are laterally discontinuous at typical Canyon well spacing (1,000 to 5,000 ft).

The most common Ozona lithofacies is thinly interbedded sandstone and shale (fig. 31). Sandstone beds are fine grained, less than 1 ft thick, and interbedded with shales of equal or greater thickness. Horizontal, wavy, convoluted, and ripple lamination styles are all common in these thin sandstone beds, which have sharp bases but grade upward into finely laminated shale. In the Ozona Canyon, thinly interbedded sandstones and shales represent classical turbidites, which form mainly in interchannel areas on all parts of the fan but are generally thinner and more shale-dominated on the outer fan (fig. 13). Thin-bedded turbidites are commonly more laterally continuous than are thick-bedded channel-fill turbidites, but the abundant shale laminations adversely affect reservoir quality. Highly serrated gamma-ray and sonic log patterns accurately reflect the fine-scale shale interlamination that is inherent in thin-bedded turbidite facies (fig. 31).

The contorted muddy sandstone and conglomeratic mudstone lithofacies record slumps and debris flows in a gravitationally unstable slope environment. Contorted muddy sandstone displays pronounced soft-sediment deformation, especially complexly folded lamination. Conglomeratic mudstone comprises scattered clasts of sandstone, shale, and limestone in a sandy mudstone matrix. These lithofacies are relatively minor, localized deposits on the steeper parts of the submarine fan surface.

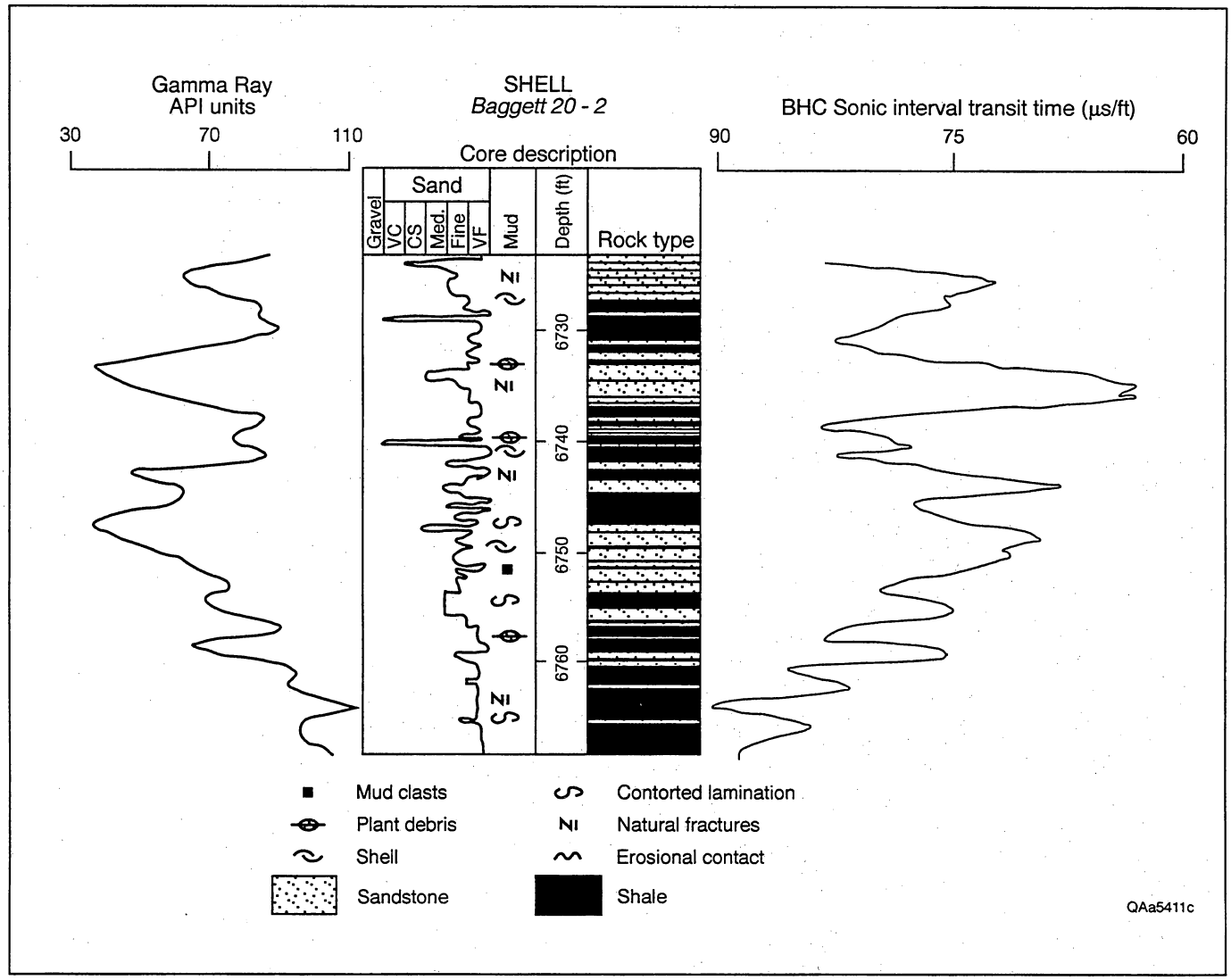

Figure 31. Core description and log responses from Ozona Canyon core. Several upward coarsening, submarine fan lobe sequences are present. Thinly interlaminated, sandstone/shale turbidites are accurately recorded by the gamma-ray and sonic logs.

Ozona Canyon Sandstone Composition

T. F. Hentz

Methods

Sixteen Ozona Canyon sandstone samples from two cores (11 samples from the Texaco Kincaid No. D-7, 5 samples from the Shell Baggett No. 2-20) were examined for texture, composition, and diagenetic history using standard thin-section petrography and scanning electron microscopy (SEM). Thin sections were stained for potassium feldspar and carbonates. Point counts (200 points) of thin sections from representative samples from the two cores were used to determine mineral composition and porosity. SEM inspection of samples enabled more precise identification of grain and clay mineralogy and visualization of mineral and pore morphology. Samples were selected from visually clean (minimal detrital clay matrix) and extensively cemented sandstone intervals and are thus representative of Ozona Canyon reservoir sandstones.

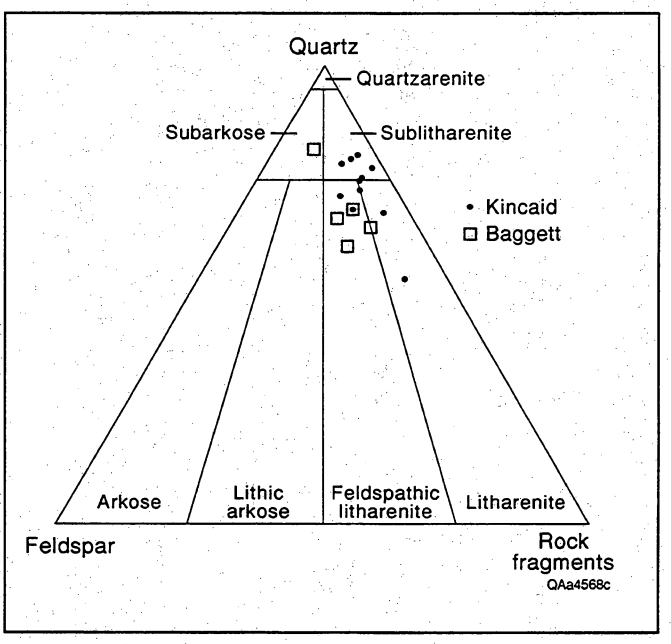

Figure 32. QFR (quartz:feldspar:rock fragments) ternary diagram illustrating detrital components of Ozona Canyon sandstone samples from the Texaco Kincaid No. D-7 and Shell Baggett No. 2-20 cores.

Texture and Composition

The Ozona Canyon sandstone samples used in this study range from very fine to coarse grained, with most samples being in the fine sandstone range (0.125 to 0.25 mm). Sorting ranges from very poor to moderate; most clean sandstones are poorly sorted. Sand grains are angular to subrounded.

All Ozona Canyon sandstones examined are mineralogically immature, and all samples except one are classified as sublitharenites and litharenites by the sandstone classification of Folk (1974) (fig. 32). All samples are quartz-grain dominated. The average composition of essential framework grains (normalized to 100 percent) from all 16 core samples is 72 percent quartz, 8 percent feldspar, and 20 percent rock fragments ($Q_{72}F_8R_{20}$). Mean sandstone composition values for the two cores are $Q_{73}F_6R_{21}$ (Texaco Kincaid) and $Q_{72}F_8R_{20}$ (Shell Baggett). Plagioclase is the most abundant feldspar in the samples, composing from 1.5 to 7.5 percent of whole-rock volume (table 3). Orthoclase occurs as point counts only in the Baggett core where its content ranges from 0 to 2.5 percent of whole-rock volume. Orthoclase is found in only trace amounts in some Kincaid core samples. Rock fragments occur in two categories: metamorphic (MRF) and sedimentary (SRF) types. Low-rank MRFs are the most abundant lithic type and include phyllite, slate, and meta-siltstone. SRFs comprise shale, chert, micritic limestone, and siltstone. Lithic types are consistent with Ozona Canyon source areas in the Ouachita Fold Belt to the south and east (Berg, 1986; Lehtonen, 1987). Mean percentage of whole-rock volume for primary framework grains (both cores) is quartz (43.7), plagioclase (4.3), orthoclase (0.3), MRFs (8.2), and SRFs (3.9).

Diagenesis

Authigenic cements and replacive minerals collectively constitute between 16.0 and 45.5 percent of the whole-rock volume in the sandstone samples, with a mean value of 31.7 percent. Authigenic ankerite, quartz, chlorite, ferroan calcite, pyrite, and ilmenite occur in Ozona Canyon sandstone samples. The primary cements (ankerite, quartz, chlorite, and ferroan calcite) have mean whole-rock volumes of 18.4, 6.4, 3.7, and 3.2 percent, respectively.

The primary diagenetic events in the burial history of Ozona Canyon sandstones were (1) growth of chlorite rims on framework grains, (2) compaction (roughly

Table 3. Petrographic analyses of Ozona Canyon sandstones. Values given in percent of whole rock volume.

	Range (percent)	Constituent mean (percent)
Texaco Kincaid No. D-7		
Framework grains		
Quartz	28.0 to 54.5	45.8
Plagioclase	1.5 to 6.5	3.7
MRF[1]	3.5 to 16.0	8.9
SRF[2]	0 to 13.5	3.8
Other[3]	0 to 15.0	2.4
Cements		
Ankerite	5.5 to 38.0	19.3
Quartz	0 to 12.5	5.0
Chlorite	0 to 11.5	4.7
Matrix	0 to 13.0	4.4
Primary porosity	0 to 6.5	1.7
Secondary porosity	0 to 1.0	0.3
Shell Baggett No. 2-20		
Framework grains		
Quartz	26.0 to 50.5	39.0
Plagioclase	4.0 to 7.5	5.6
Orthoclase	0 to 2.5	0.9
MRF	1.0 to 12.5	6.8
SRF	1.0 to 9.5	4.0
Other[3]	0 to 2.5	1.3
Cements		
Ankerite	9.0 to 32.5	16.3
Ferroan calcite	0 to 34.0	10.4
Quartz	1.0 to 18.0	9.4
Chlorite	0 to 6.5	1.8
Matrix	0 to 9.5	4.5
Primary porosity	0	0
Secondary porosity	0	0

[1]Metamorphic rock fragments
[2]Sedimentary rock fragments
[3]Mostly pyrite, ilmenite, various heavy minerals, and fossil fragments

contemporaneous with stage 1) causing deformation of ductile rock fragments, (3) precipitation of quartz overgrowths, (4) precipitation of ankerite and ferroan calcite, which filled pores not occluded by quartz overgrowths, and contemporaneous dissolution of feldspar and MRFs, (5) pressure solution and additional silica cementation at quartz-to-quartz grain contacts, and (6) late-stage fracturing.

The whole-rock volume of chlorite cement varies from 0 to 11.5 percent (table 3). Chlorite, the first cement to form in Ozona Canyon sandstones, is mostly a grain-rimming cement but also fills a small percentage of intergranular pore space. Chlorite crystal morphology typically takes the form of platelets (fig. 33).

Quartz cementation postdated formation of chlorite rims. Quartz cement formed by (1) development of relatively early quartz overgrowths and (2) additional silica mobilization and subsequent precipitation due to pressure solution between quartz grains during burial compaction. The whole-rock volume of quartz cement ranges from 0 to 18.0 percent. Where quartz overgrowths are abundant, they completely fill some primary, intergranular pores. Generally, in Ozona Canyon sandstones where chlorite cement is common, quartz

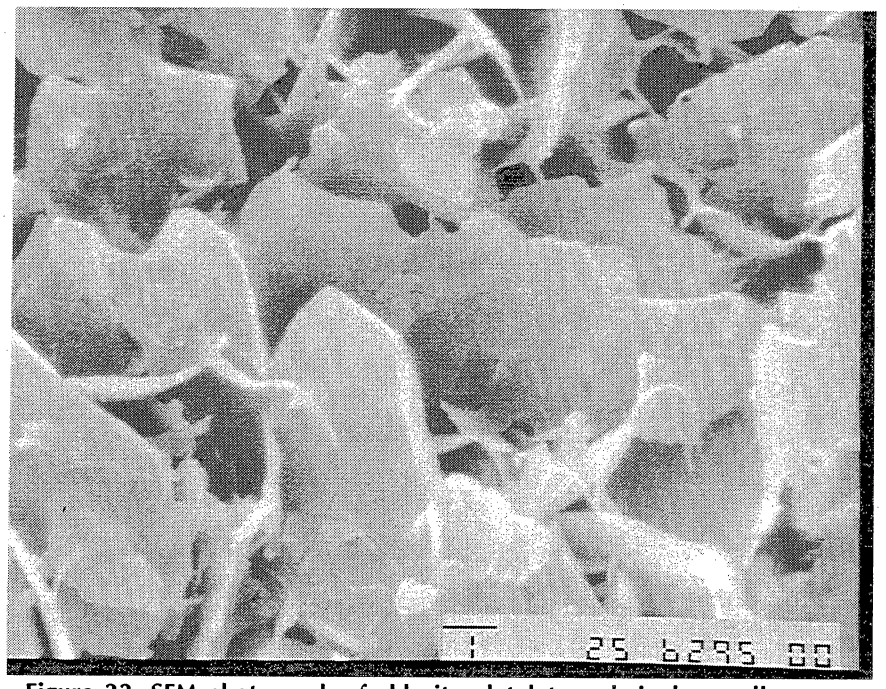

Figure 33. SEM photograph of chlorite platelets and single, small quartz overgrowth (left center, foreground) within a grain-rimming cement. Sample from a depth of 6,295.7 ft in the Texaco Kincaid No. D-7 well. Scale bar is 1 micron. Photograph by S. Clift.

overgrowths are relatively rare. Chlorite rims around quartz grains probably acted as barriers to quartz-overgrowth nucleation. Where chlorite is abundant, most quartz overgrowths are small, apparently having nucleated where breaks occur in the chlorite rims (fig. 33).

Ankerite is the most abundant cement in all Ozona Canyon sandstone samples (fig. 34). Ferroan calcite, another carbonate cement, occurs only in some Baggett core samples. Ankerite whole-rock volume ranges from 5.5 to 38.0 percent, whereas ferroan calcite volume varies from 0 to 34.0 percent (table 3). Ankerite and calcite cements formed late in the diagenetic sequence; textural relations indicate that these cements precipitated after chlorite and quartz cement. Ankerite and ferroan calcite commonly replace framework grains. Partially (fig. 35) and wholly replaced feldspar grains are common in sandstone samples from both cores. Completely replaced feldspars appear as relict, rectilinear patches of the carbonate cement. Both carbonate cements also partially replace MRFs and SRFs, primarily shale, phyllite, and slate grains (fig. 36). Complete replacement of pelitic MRFs is probable but difficult to ascertain because MRFs typically have irregular grain boundaries. The overall abundance of ankerite, which is present in all Ozona Canyon samples and has an average whole-rock volume of 18.4 percent, suggests that these cements may also fill intergranular pores that had remained open throughout earlier phases of diagenesis.

Porosity

Porosity observed in thin section varies from 0 to 6.5 percent; no porosity was observed in samples from the Shell Baggett core (table 3). Average total porosity of samples from both cores is 1.4 percent. Cements and ductile, compaction-deformed MRFs occlude most visible porosity in Ozona Canyon samples (fig. 36). Primary porosity exists as small (several microns) intergranular voids, commonly between quartz grains, and within areas of ankerite and ferroan calcite cement (fig. 34). Secondary porosity is developed as voids within partially dissolved framework grains (mainly feldspar, MRFs, and shale SRFs). Average net-overburden porosity, measured by a porosimeter, is 7.6 percent in clean Ozona Canyon sandstones. Thin section porosity generally is lower than porosimeter porosity because of the presence of micropores between clay flakes and within partly dissolved framework grains. For example, voids between chlorite platelets (fig. 33) may compose some microporosity in Ozona Canyon sandstone samples. Micropores are measured by a porosimeter, but they cannot be accurately quantified in thin section. Microfractures within 4 of the 11 Texaco Kincaid core samples (fig. 37) also enhance porosity and possibly permeability if the microfractures are interconnected. Average Klinkenberg-corrected gas permeability measured at net overburden pressure for the Ozona Canyon sandstone samples is 0.024 md.

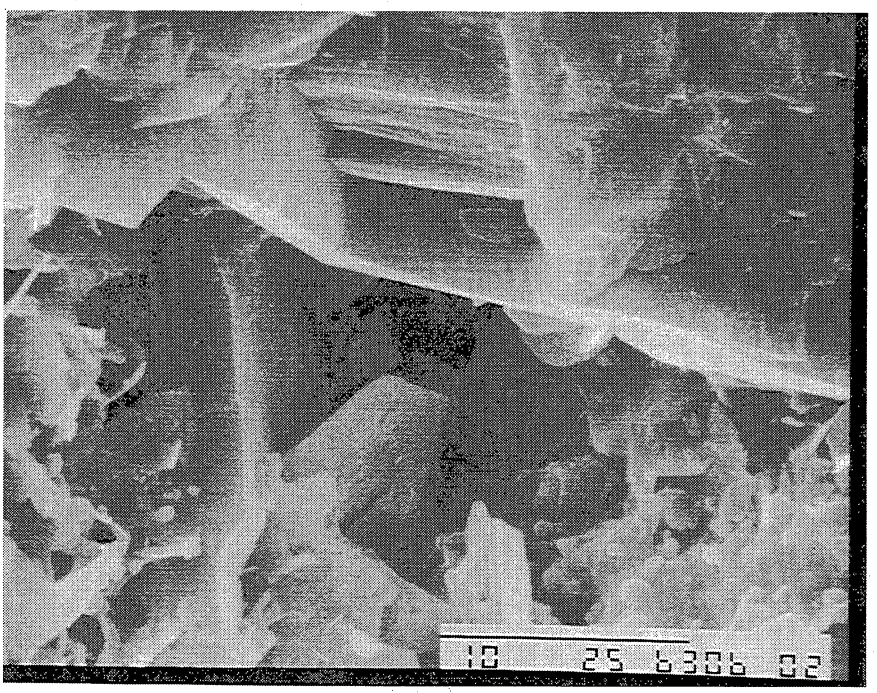

Figure 34. SEM photograph of ankerite (blocky mineral) and chlorite (platelets at far left) cements lining a micropore. Sample from a depth of 6,306.8 ft in the Texaco Kincaid No. D-7 well. Scale bar is 10 microns. Photograph by S. Clift.

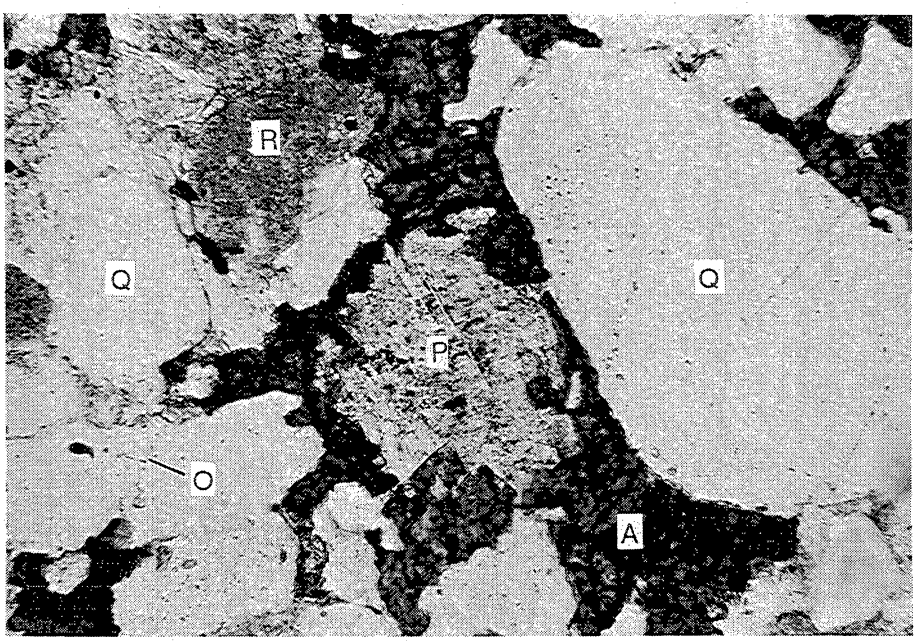

Figure 35. Plagioclase (P) grains are commonly partially replaced by ankerite (A) cement. Quartz (Q) and MRFs (R) are typically the most common framework grains in Ozona Canyon sandstones. Quartz overgrowths (O) are a common cement. Sample from depth of 6,357.7 ft in the Texaco Kincaid No. D-7 well. Long dimension of photo is 1.0 mm. Plane-polarized light with green filter.

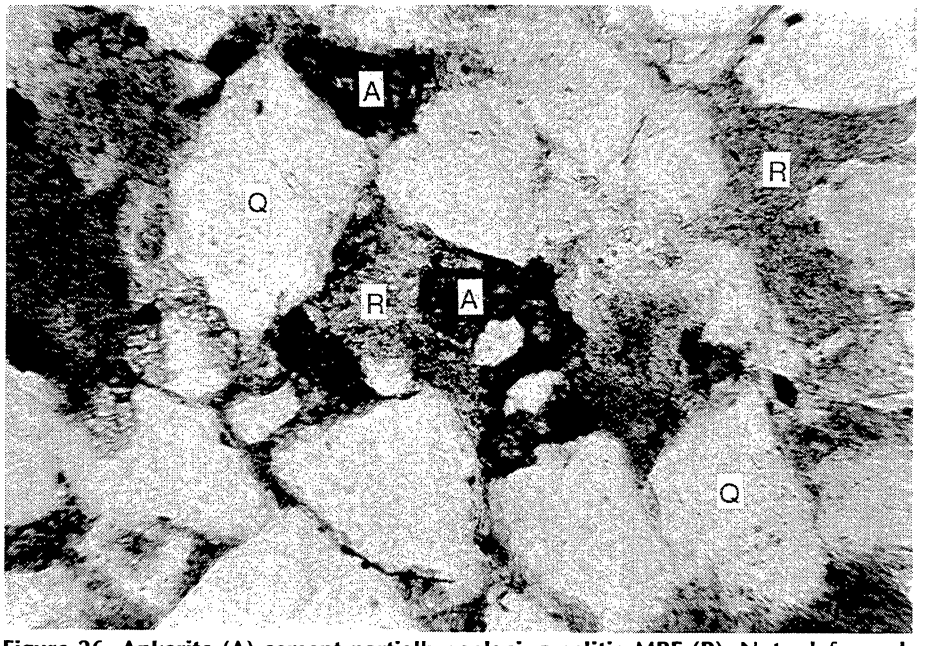

Figure 36. Ankerite (A) cement partially replacing pelitic MRF (R). Note deformed MRF in upper right corner of photo. Ductile deformation of MRFs around rigid framework grains, such as quartz (Q), is a significant contributor to porosity occlusion in Ozona Canyon sandstones. Sample from depth of 6,306.8 ft in the Texaco Kincaid No. D-7 well. Long dimension of photo is 1.0 mm. Plane polarized light.

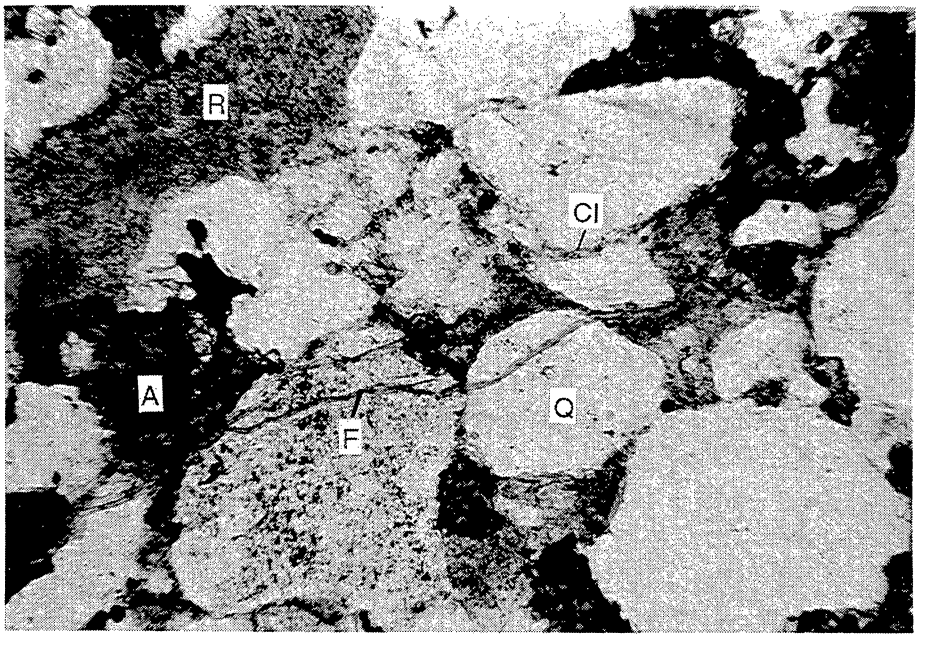

Figure 37. Discontinuous, bifurcating microfractures (F) cutting across and between framework grains contributes to porosity in some Ozona Canyon samples. Chlorite grain-rimming cement (Cl) was the first cement to form during diagenesis of the Ozona Canyon sandstones. Ankerite cement (A), quartz grain (Q), and deformed MRF (R) are also identified. Sample depth from 6,357.7 ft in the Texaco Kincaid No. D-7 well. Long dimension of photo is 1.0 mm.Plane polarized light.

Natural Fractures in Ozona Canyon Sandstone

S. E. Laubach

Natural fractures are widespread in Ozona Canyon sandstone cores from the Baggett "2" No. 20 and the Kincaid "D" No. 7 wells. Most are subvertical, opening-mode fractures that are densely filled with secondary minerals—primarily the iron carbonate mineral ankerite (figs. 38 and 39) although local, isolated areas having quartz fracture fill also exist. Fractures in core are typically short (average height less than 10 cm), narrow (width less than 0.4 mm), and vertically discontinuous (figs. 40 through 43). The principal control on fracture size (height) is the scale (vertical spacing) of thin shale beds and laminae because fractures typically terminate at or before reaching these boundaries. In other words, fractures in core are typically no taller than the thickness of the sandstone that contains them. The core data available does not permit any conclusions regarding lateral (plan view) fracture network connectivity or fracture persistence. Outcrop studies of fractures in sandstone show that these fracture attributes can vary widely and abruptly (e.g., Laubach, 1992).

As described in the previous section, microfractures are also present in Ozona Canyon samples. Where present, these features may influence core-scale tests of permeability.

Ozona Canyon fractures in the cores we examined lack the vertical extent and prominent fracture porosity that would mark these features as probable important fluid conduits. On the other hand, the abundance of small fractures observed in our limited sample, combined with the strong bias against intersecting vertical fractures with vertical core, suggests that fractures are widespread features in Ozona sandstones.

Our observations do not rule out the possibility that there are larger (taller) fractures in the Ozona Canyon sandstone. The available evidence does not permit us to conclude whether fractures elsewhere in the Ozona trend might be larger, more open, or more interconnected. Moreover, it is not the size (height) of fractures at the wellbore that is important for flow through fracture networks. Extent of interconnected fractures, degree of occlussion of fracture porosity by fracture-filling minerals, and persistence of individual fractures are each more important factors than the vertical extent of the fractures in most reservoir rocks. Observations in other areas where similar patterns of small fractures have been observed in core—most notably the [Atoka] Davis sandstone of the Fort Worth Basin (Collins and others, 1992)—shows that such arrays of small, isolated and closed fractures can be accompanied by less-common zones of large, interconnected and open fractures capable of causing significant, abrupt leak off.

The role of fractures in Canyon Sandstone reservoirs is discussed more fully in a later section of this report.

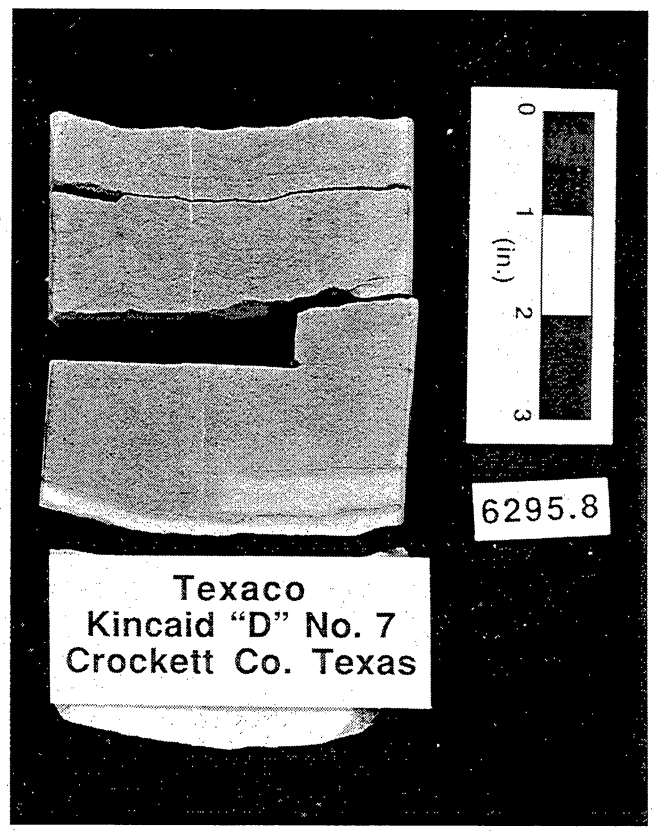

Figure 38. Photograph of opening-mode fractures in Ozona Canyon Sandstone. Kincaid "D" No. 7, depth 6195.8 ft. Fracture is near vertical.

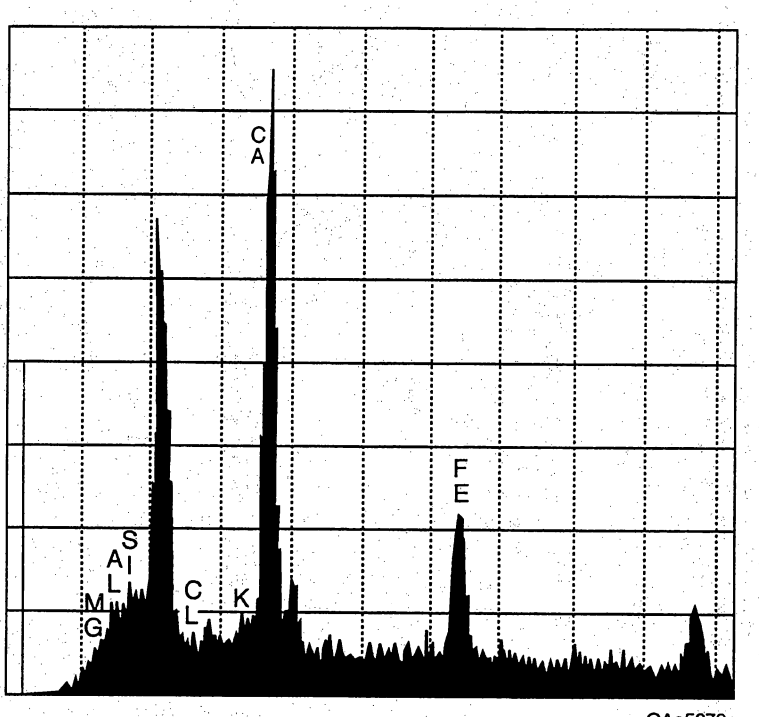

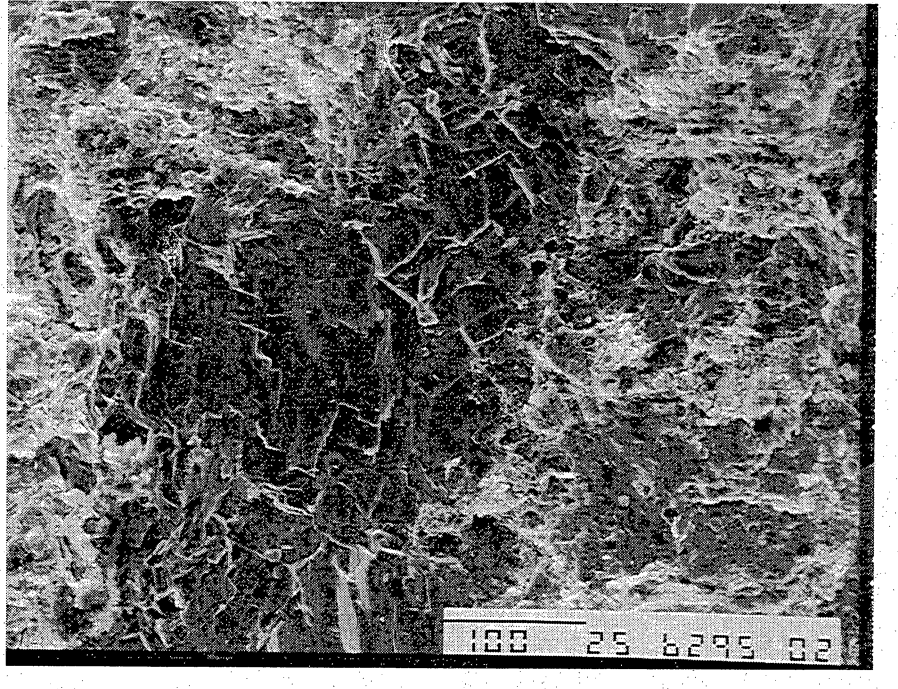

Figure 39. SEM photomicrograph of fracture-filling ankerite, Kincaid "D" No. 7 (depth 6,295.1 ft). Inset shows compositional information (EDX) for vein-fill ankerite from this sample.

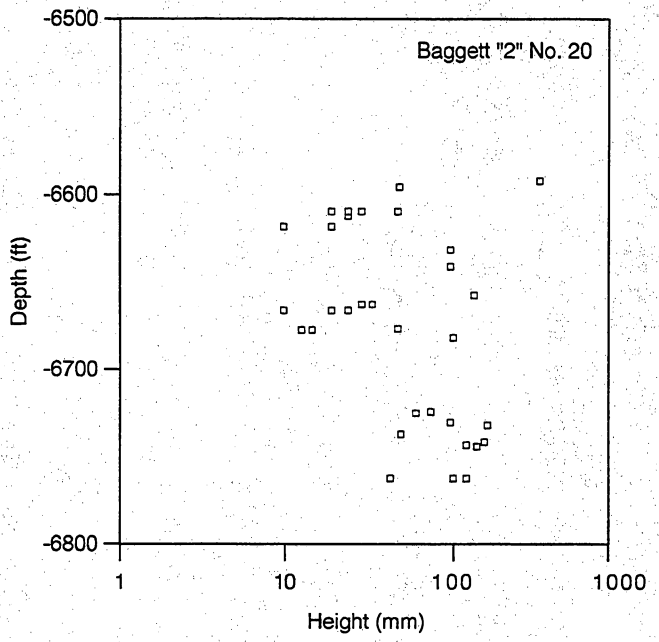

Figure 40. Fracture height versus depth, Baggett "2" No. 20.

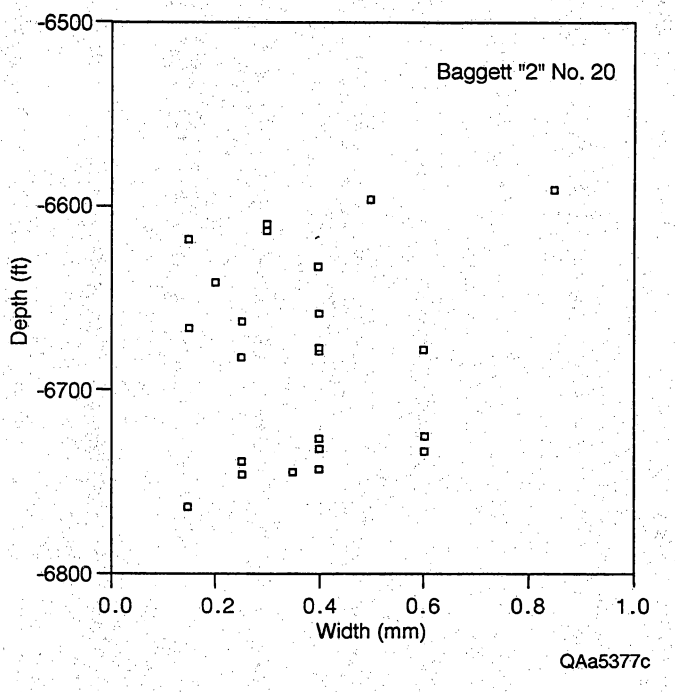

Figure 41. Fracture width versus depth, Baggett "2" No. 20.

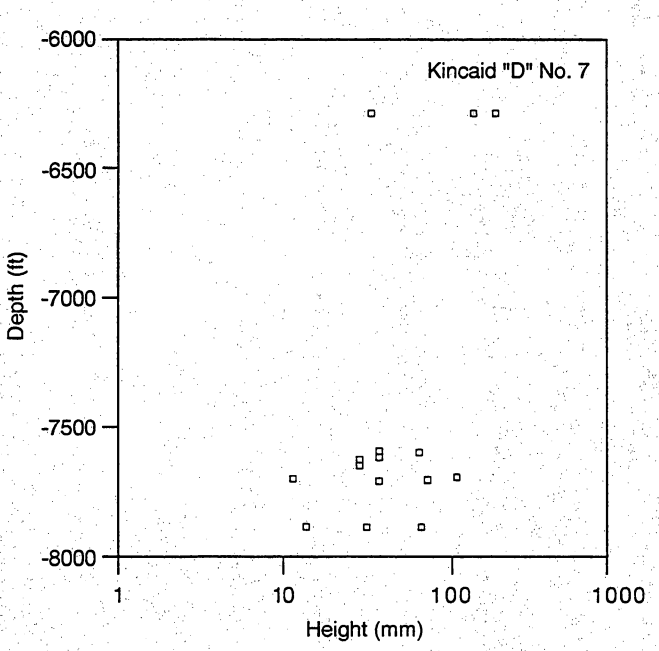

Figure 42. Fracture height versus depth, Kincaid "D" No. 7.

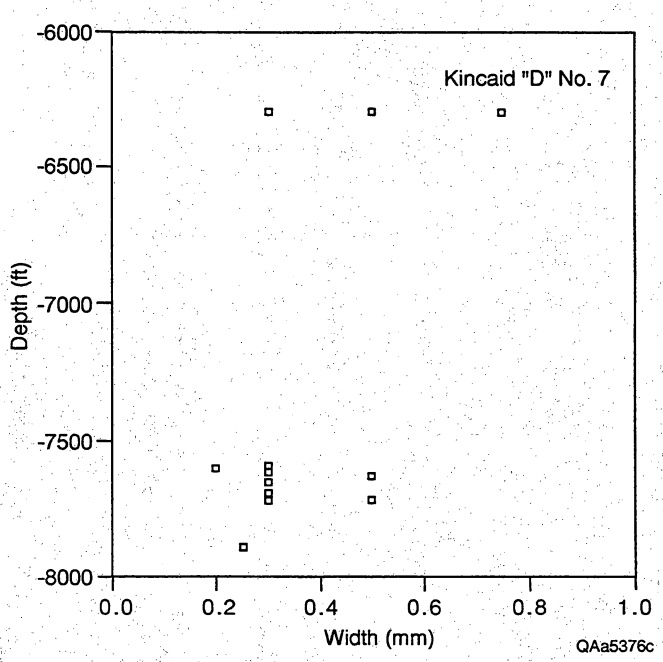

Figure 43. Fracture width versus depth, Kincaid "D" No. 7.

Sonora Canyon Stratigraphy

H. S. Hamlin, S. J. Clift

Sonora Canyon sandstones, which were deposited in shelf-edge, slope, and adjacent basin-floor settings, lie in the northern part of the Val Verde Basin and along the southern margins of the Ozona Arch and the Eastern Shelf (fig. 1). Desmoinesian-Missourian (primarily Strawn) carbonate-bank facies rim the Central Basin Platform, Ozona Arch, and Eastern Shelf (Rall and Rall, 1958; Holmquest, 1965), delineating shelf-margin positions that persisted during deposition of the overlying Sonora Canyon (Wolfcampian) (fig. 5). These shelf edges included both distinct shelf-slope topographic breaks and more irregular and topographically gradational ramps, both of which are identifiable on the present structural configuration of the underlying Desmoinesian-Missourian carbonate surface (fig. 44). The original depositional topography of this pre-Canyon-Sandstone surface, however, has been modified by subsidence of the Ouachita foredeep (fig. 44) and post-Canyon-Sandstone northwest tilting (fig. 45).

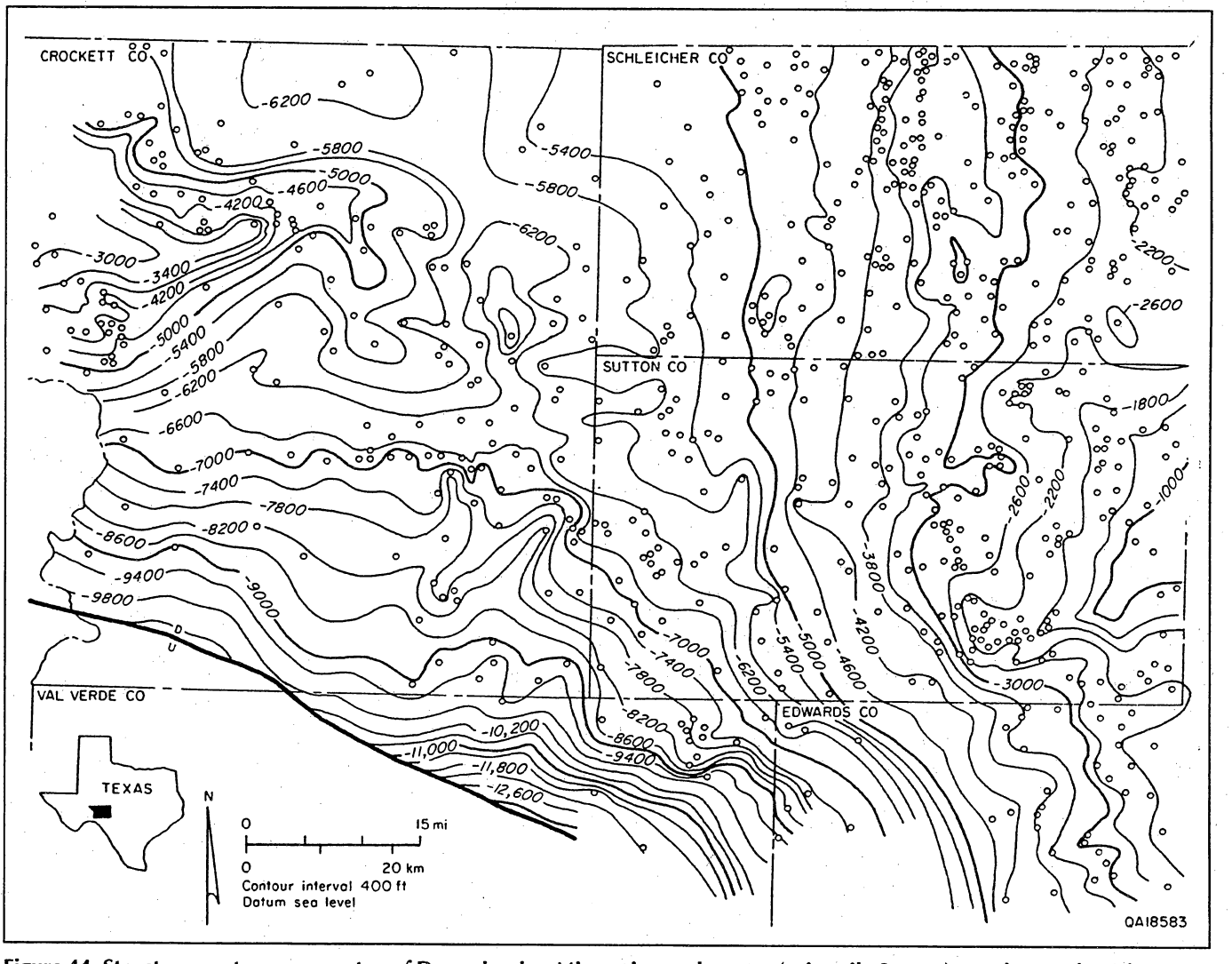

Figure 44. Structure-contour map on top of Desmoinesian-Missourian carbonates (primarily Strawn), northern Val Verde Basin.

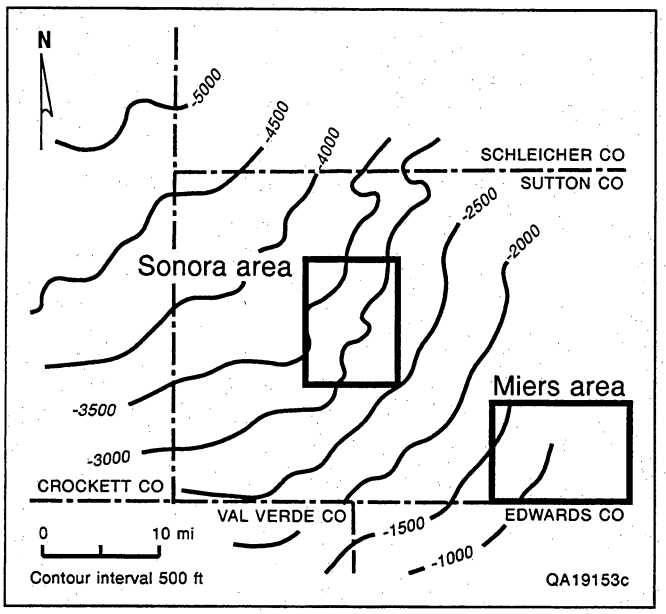

Figure 45. Structure-contour map on top of the Sonora Canyon relative to a sea-level datum. Depths from land surface to Canyon sandstones range from about 3,000 to 7,000 ft in Sutton County. The areas of field-scale studies are outlined.

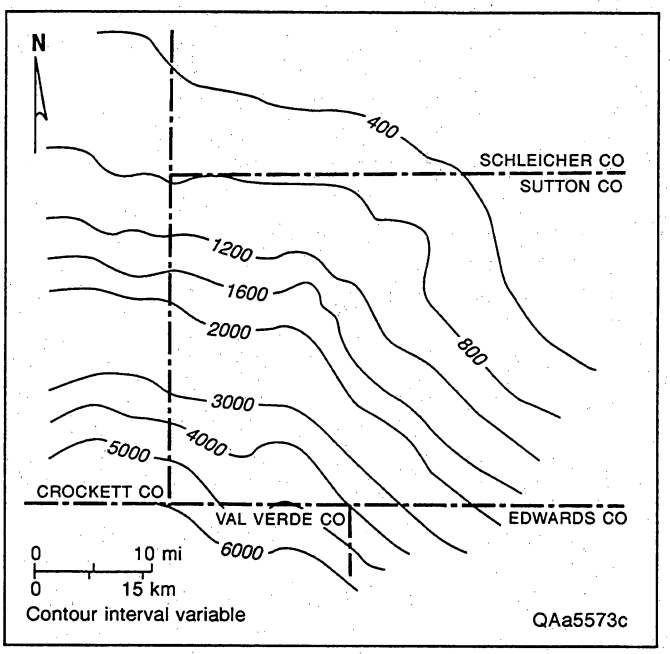

Figure 46. Isopach map of the interval between the top of the Sonora Canyon and the Strawn limestone.

Stratigraphic Framework

Several hundred feet of dark clay shale and thin limestones overlie Desmoinesian-Missourian carbonates and are overlain (locally erosionally) by Sonora Canyon sandstones. The Sonora Canyon is a wedge-shaped interval (fig. 46) composed primarily of coalesced submarine fans forming a slope apron. Sonora Canyon sandstones, which are mainly slope-channel and fan-lobe depositional facies (fig. 13), grade basinward into deep-water mudstones and landward into shallow-shelf mudstones, isolated sandstones, and thin limestones. Deposition of the Sonora Canyon slope wedge prograded the slope and shelf margin, constructing a platform for overlying Wolfcampian carbonate and fine-grained-clastic shelf deposits (fig. 5). The depositional topography of the northern part of the Val Verde Basin is similar to that of the Eastern Shelf and adjacent Midland Basin of North-Central Texas (Galloway and Brown, 1972; Van Siclen and Bloomer, 1988; Brown and others, 1990).

Source areas for Sonora Canyon sandstones lay mainly to the north and east. Both the Central Basin Platform and the Ouachita Fold Belt (fig. 1) were subaerially exposed during the Late Pennsylvanian and Early Permian (Cys and Gibson, 1988). Fluvial-deltaic systems transported sediment from these uplifts across the Eastern and "northern" (Ozona Arch) shelves for deposition in the Sonora Canyon slope system. Depositional patterns suggest that coarse clastic sediment from the southern part of the Ouachita Fold Belt was trapped in the adjacent, rapidly subsiding foredeep (fig. 4) and did not reach the northern part of the Val Verde Basin. The segment of the Ouachita Fold Belt that lies adjacent to the Eastern Shelf and the Llano Uplift (fig. 1), however, was an important source area for the Sonora Canyon.

Although the Sonora Canyon interval is enclosed in regionally extensive mudstones and limestones, it contains few internal horizons that are sufficiently continuous to be used for correlation-based subdivision. Several mudstone-dominated zones were nevertheless used to divide the Sonora Canyon into upper, middle, and lower map units (fig. 47). These subregionally continuous mudstone zones apparently record episodes of reduced delivery of coarse clastics to the outer shelf and slope. Instead, fine-grained clastics (clay and fine silt) slowly settled and accumulated across large areas. Shale layers resulting from this hemipelagic style of deposition have widespread continuity and can be identified using well log correlations. Subdivision of the Sonora Canyon reveals stratigraphic and depositional patterns that are not otherwise obvious. Sandstone thickness maps of each unit are shown in figures 48 through 50, and stratigraphic correlations are displayed on a series of cross sections (figs. 51 through 55).

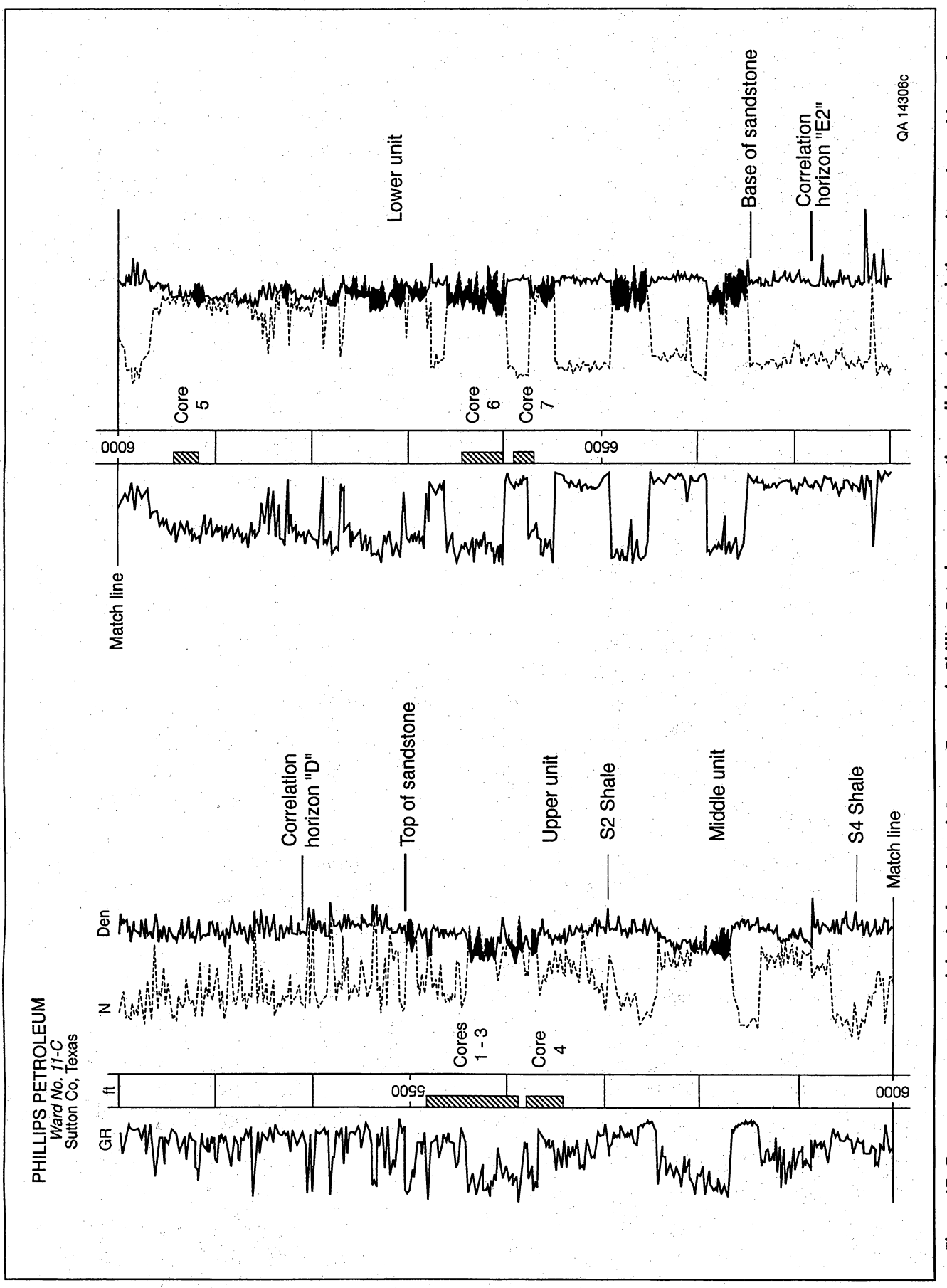

Figure 47. Gamma-ray, neutron, and density logs through Sonora Canyon in Phillips Petroleum cooperative well showing correlation units and cored intervals.

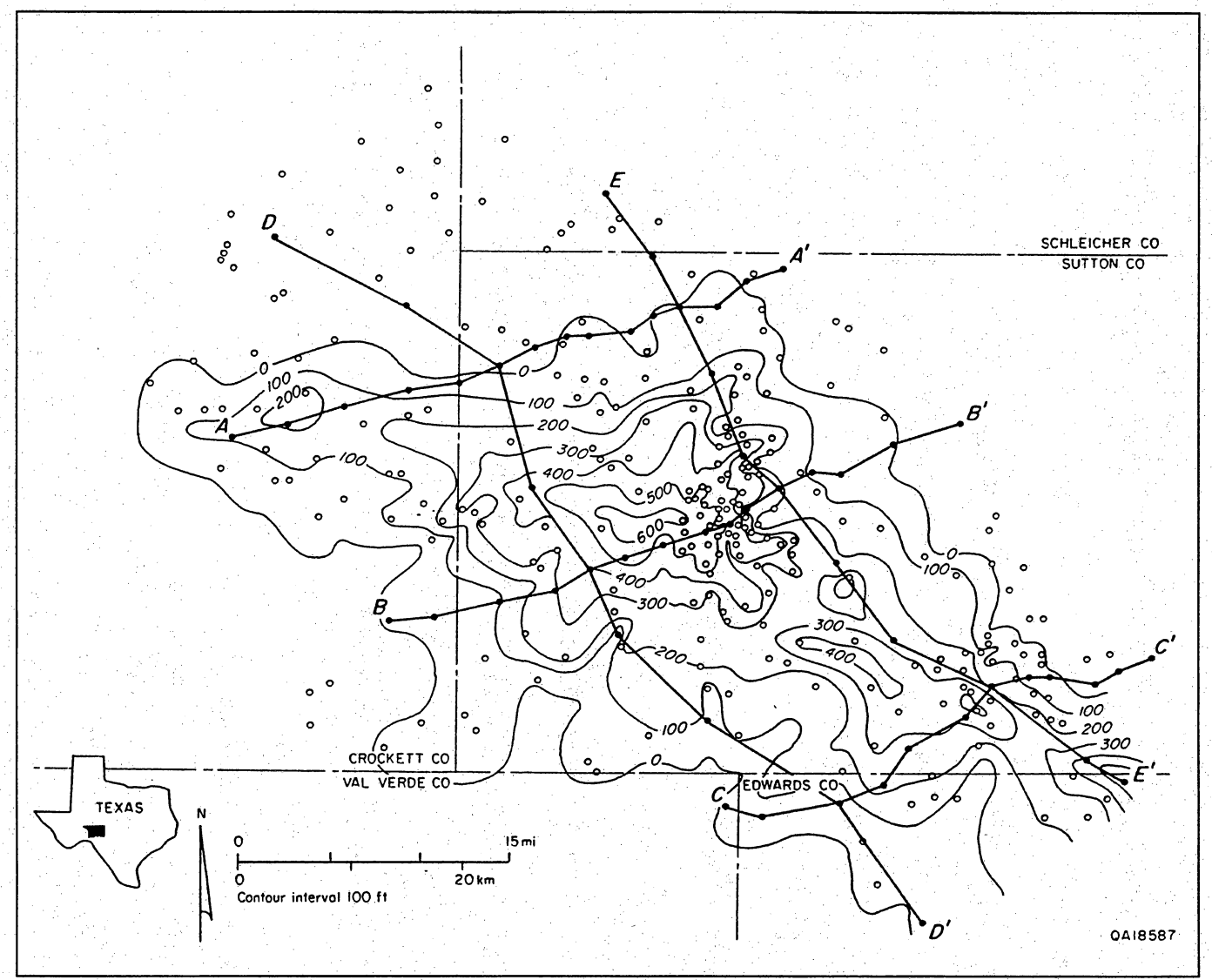

Figure 48. Net-sandstone thickness map of lower Sonora Canyon map unit (fig. 47).

The Sonora Canyon slope wedge thickens to the south-southwest (fig. 46). The thin updip part of the wedge is near the shelf margin and is composed of mudstone and local lenticular sandstone (fig. 51). The thickest net sandstone (figs. 48 through 50) primarily lies in the middle of the wedge, where the Sonora Canyon is composed largely of thick laterally discontinuous sandstones having abundant thin mudstone interbeds (fig. 52). The thickest part of the wedge consists of thick mudstones and thin sandstones in a depositionally distal setting (base of slope or adjacent basin floor) (fig. 53).

Within the larger Sonora Canyon slope wedge, the map units form a series of smaller wedge-shaped bodies, which extend progressively farther updip, onlapping underlying Desmoinesian-Missourian slope and shelf margin facies (figs. 51 through 53). Onlap of Virgilian-Wolfcampian strata in the northeastern Val Verde Basin was first noted by Young (1960). Correlation horizons in the Sonora Canyon and in the lower (Epps) Canyon are relatively flat-lying and converge updip with the more steeply dipping surface of the underlying Desmoinesian-Missourian carbonates and shales (see especially figures 52 and 53). The lower (Epps) Canyon

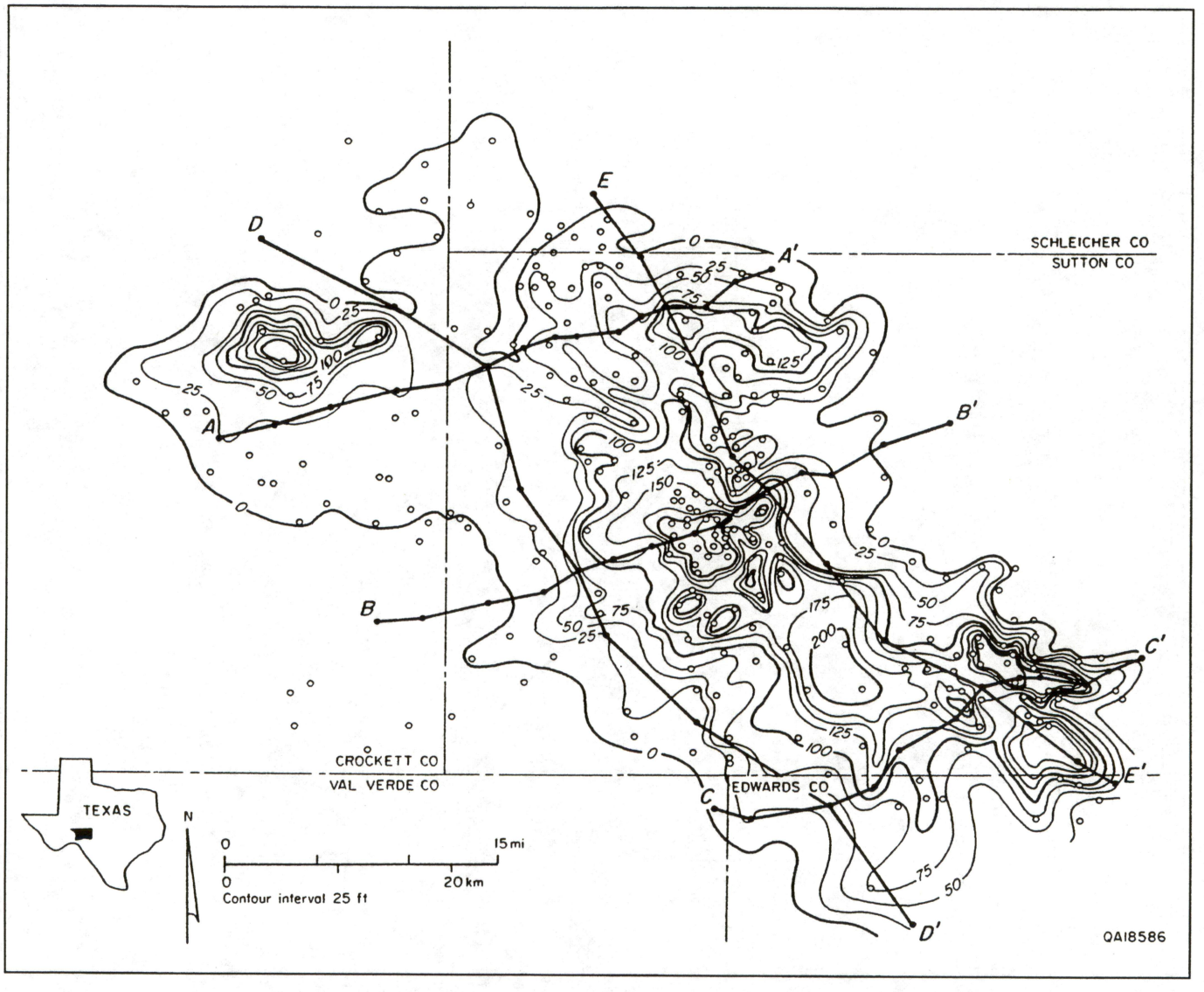

Figure 49. Net-sandstone thickness map of middle Sonora Canyon map unit (fig. 47).

and much of the Sonora Canyon lie below and basinward of preexisting shelf margins. This style of basin fill is similar to that expressed by well-documented sea-level-lowstand depositional systems tracts along the edge of the Eastern Shelf in North-Central Texas (Galloway and Brown, 1972; Bloomer, 1977, 1991; Brown, 1989; Brown and others, 1990). Sonora Canyon lowstand systems tracts are composed of sand-rich basin-floor fans overlain by mixed sand/mud slope wedges. Paleogeographic context, slope-onlap stratigraphic patterns, and a predominance of upward-fining vertical trends in the Sonora Canyon suggest a lowstand setting (Van Wagoner and others, 1990; Posamentier and others, 1991). Thin, laterally continuous shale condensed sections separate the lowstand tracts and provide useful correlation horizons. These thin shales were deposited basinward of the shelf margin in transgressive and highstand systems tracts. A hierarchy of depositional sequences (in the sense of Galloway [1989]) exists in the Sonora Canyon, reflecting variable-duration relative sea-level cycles and interplay between tectonics and eustacy. The largest scale (lowest order) sequence comprises the entire Sonora interval, which is bounded by regionally extensive deep-water shales that record basinwide flooding events. Each Sonora map unit forms a depositional sequence that extends across the northeast part of the Val Verde Basin, and within each map unit, locally developed sequences are a few tens to hundreds of feet thick and extend laterally only a few miles. Smaller scale Sonora sequences formed in response to variations in sediment dispersal patterns, which are discussed below.

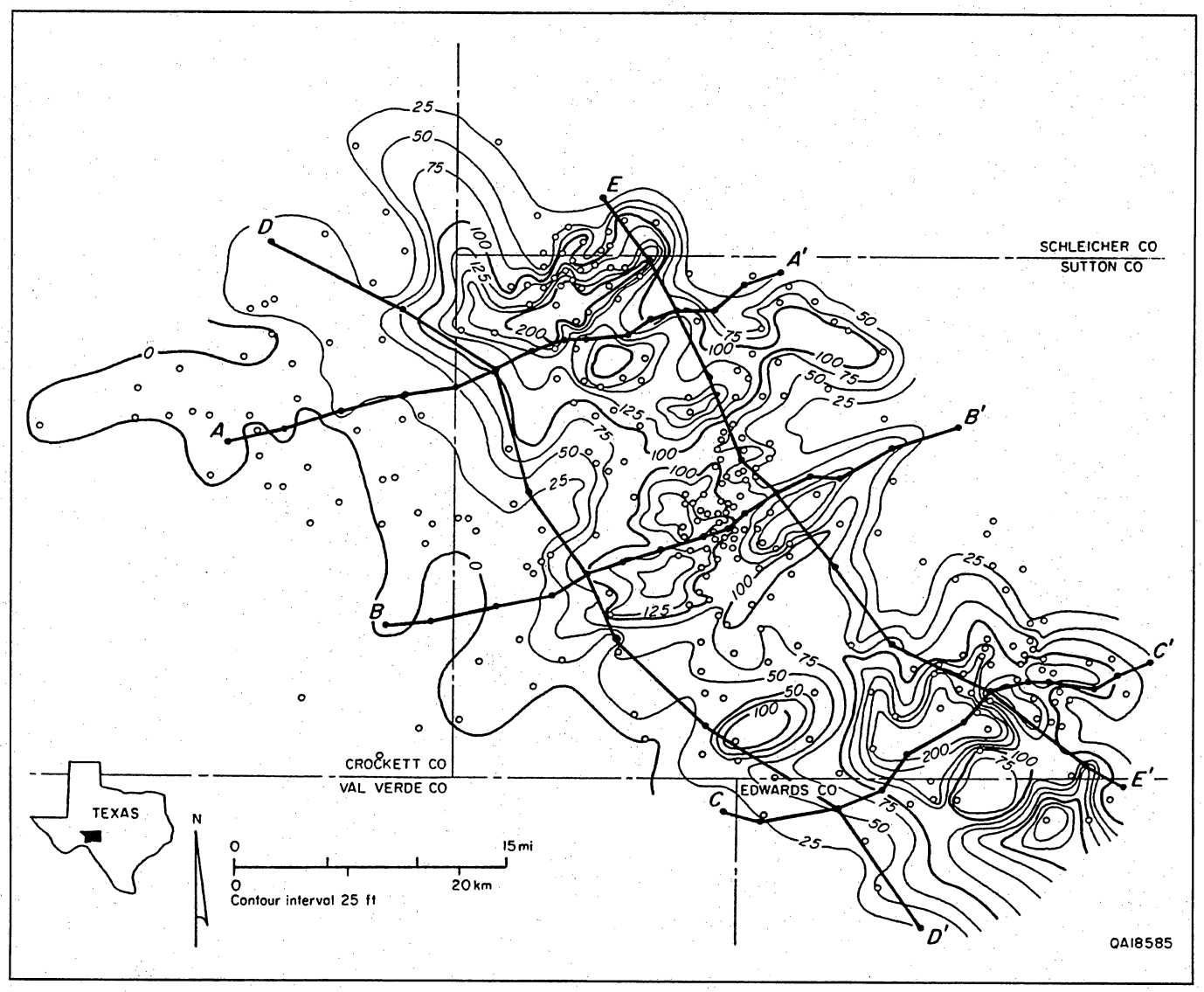

Figure 50. Net-sandstone thickness map of upper Sonora Canyon map unit (fig. 47).

Regional Sandstone Distribution

Regional net-sandstone-thickness patterns reveal the framework of the Sonora Canyon submarine-fan depositional system. Sonora Canyon sandstones form a discrete northwest-trending body that is 20 to 30 mi wide and at least 60 mi long (figs. 48 through 50). This thick body of sandstone extends farther southeastward in Edwards County, where it merges with the lower (Epps) Canyon (fig. 55). Within the Sonora Canyon, net-sandstone thicknesses are greatest (reaching 1,000 ft) in a series of partly coalesced depocenters lying near the long axis of the sandstone trend, which parallels interval isopach contours (fig. 46) and inferred shelf-margin trends. From this axis, net sandstone decreases toward the northeast (depositionally updip) and the southwest (downdip) (figs. 48 through 50). This large-scale geometry probably resulted from lateral coalescence of individual submarine fans, each having its own feeder channel (or canyon) near the shelf edge.

The positions of maximum sandstone accumulation (sandstone depocenters) shifted through time (fig. 56), owing to changing sediment source directions and infill patterns. Sandstone depocenters that shifted along depositional strike (parallel to northwest-trending shelf edge) through time reflect changing sediment input locations along the shelf edge, which, in turn, can be attributed to lateral migration or switching of fluvial-

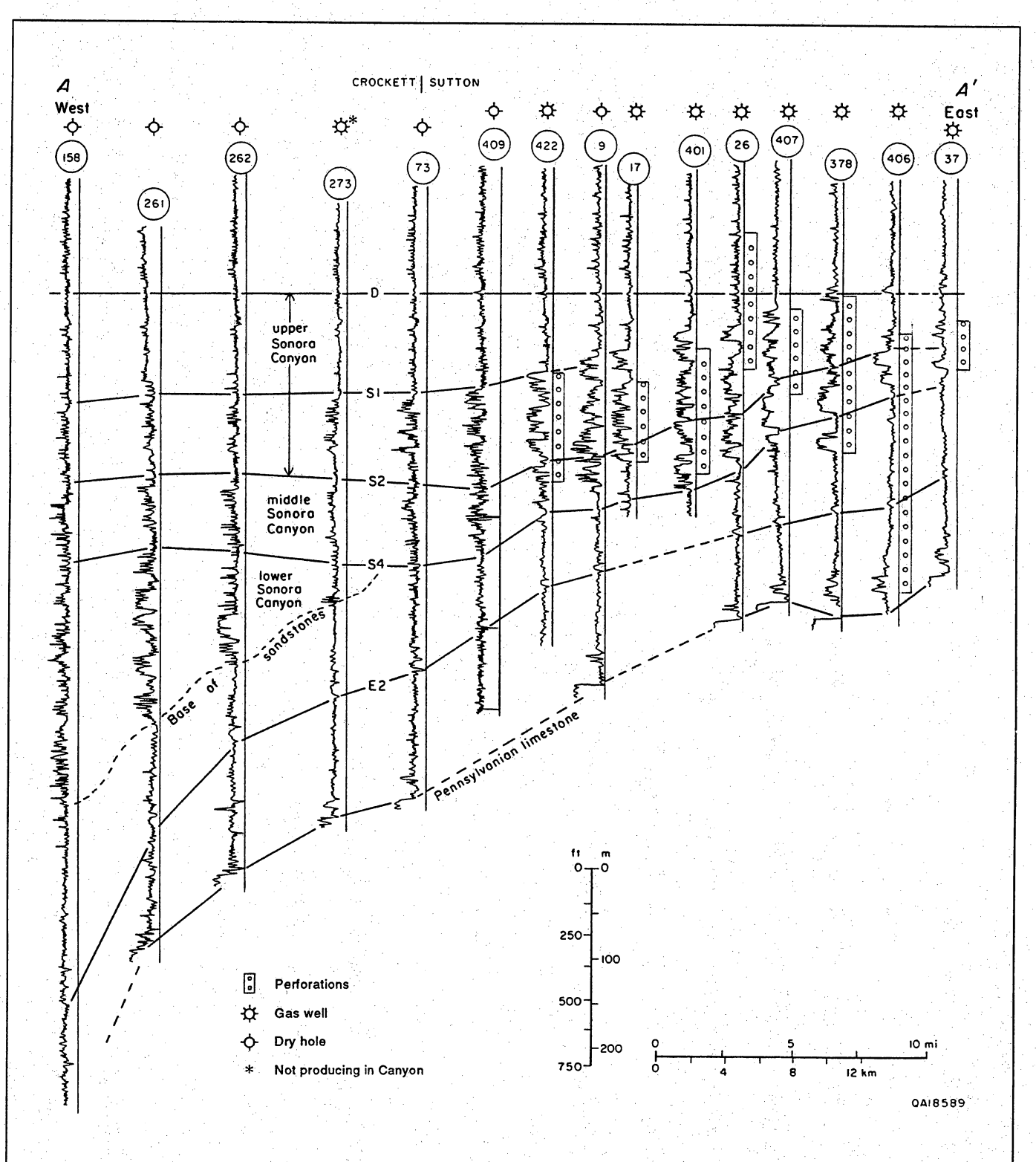

Figure 51. Stratigraphic cross section A–A' oriented approximately parallel to depositional dip. See figure 48 for location of section line. Gamma-ray logs display sandstone/shale interbedding styles. Wells 406 and 37, for example, penetrate isolated sandstones enclosed in thick mudstones characteristic of updip shelf-margin areas.

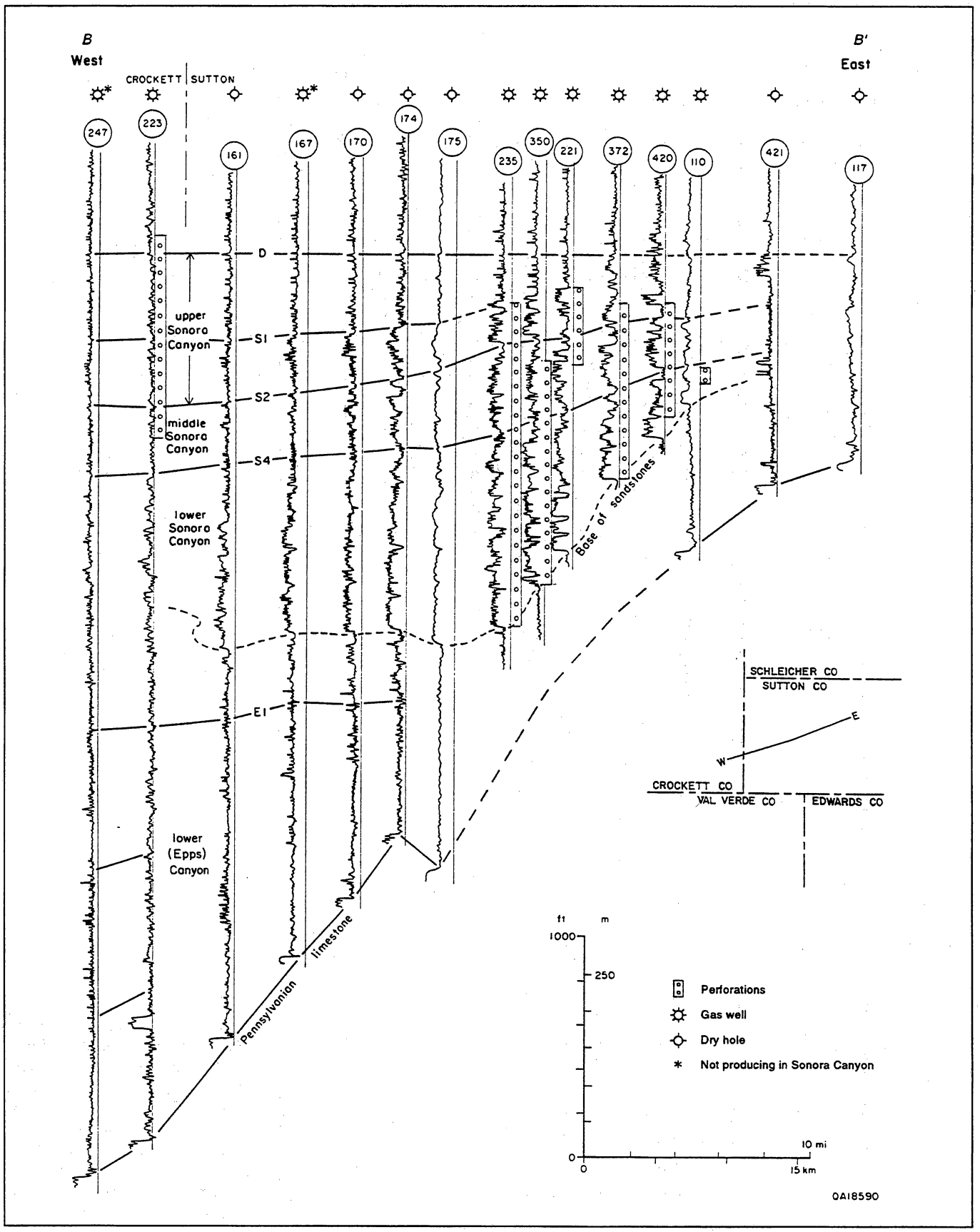

Figure 52. Stratigraphic cross section B–B′ oriented approximately parallel to depositional dip. See figure 48 for location of section line. Gamma-ray logs display sandstone/shale interbedding styles. Wells 235 and 350, for example, penetrate thick sandstones with abundant thin mudstone interbeds characteristic of medial slope areas.

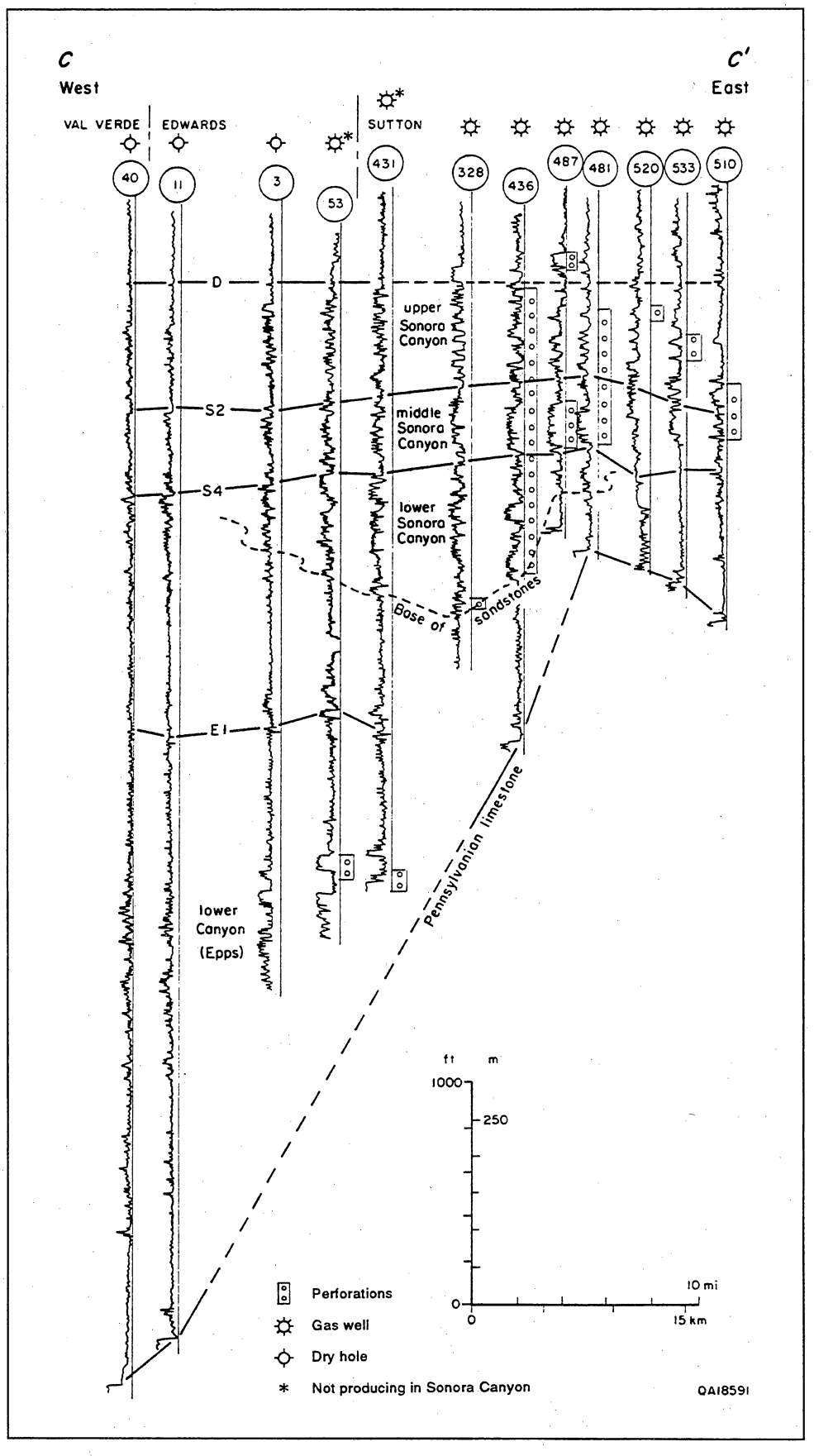

Figure 53. Stratigraphic cross section C–C′ oriented approximately parallel to depositional dip. See figure 48 for location of section line. Gamma-ray logs display sandstone/shale interbedding styles. Wells 40 and 11, for example, penetrate extremely thick mudstones with abundant thin sandstone interbeds characteristic of distal basin-floor areas.

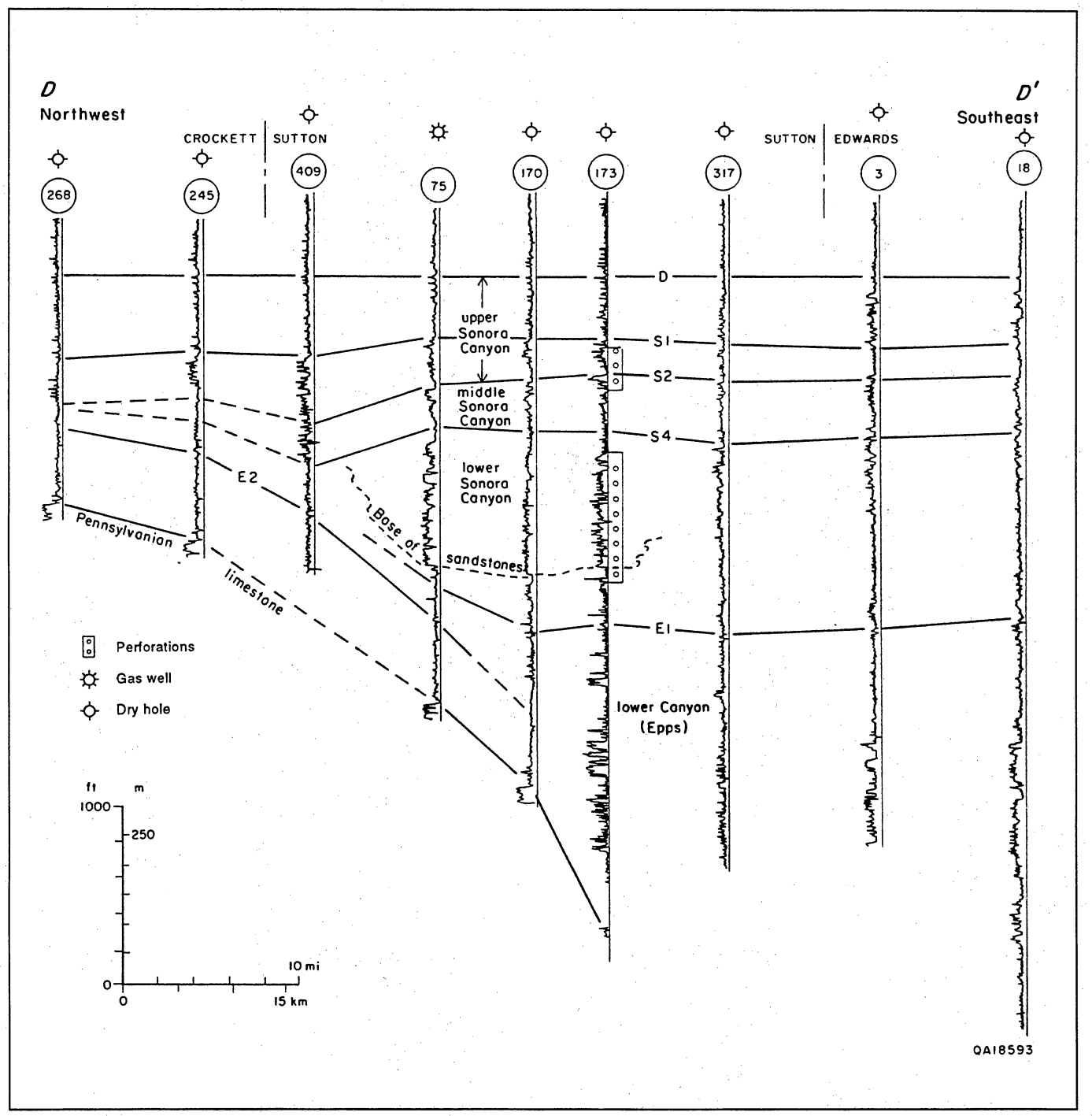

Figure 54. Stratigraphic cross section D–D′ oriented approximately parallel to depositional strike, although it obliquely intersects the shelf margin in the northwest. See figure 48 for location of section line. Gamma-ray logs display sandstone/shale interbedding styles.

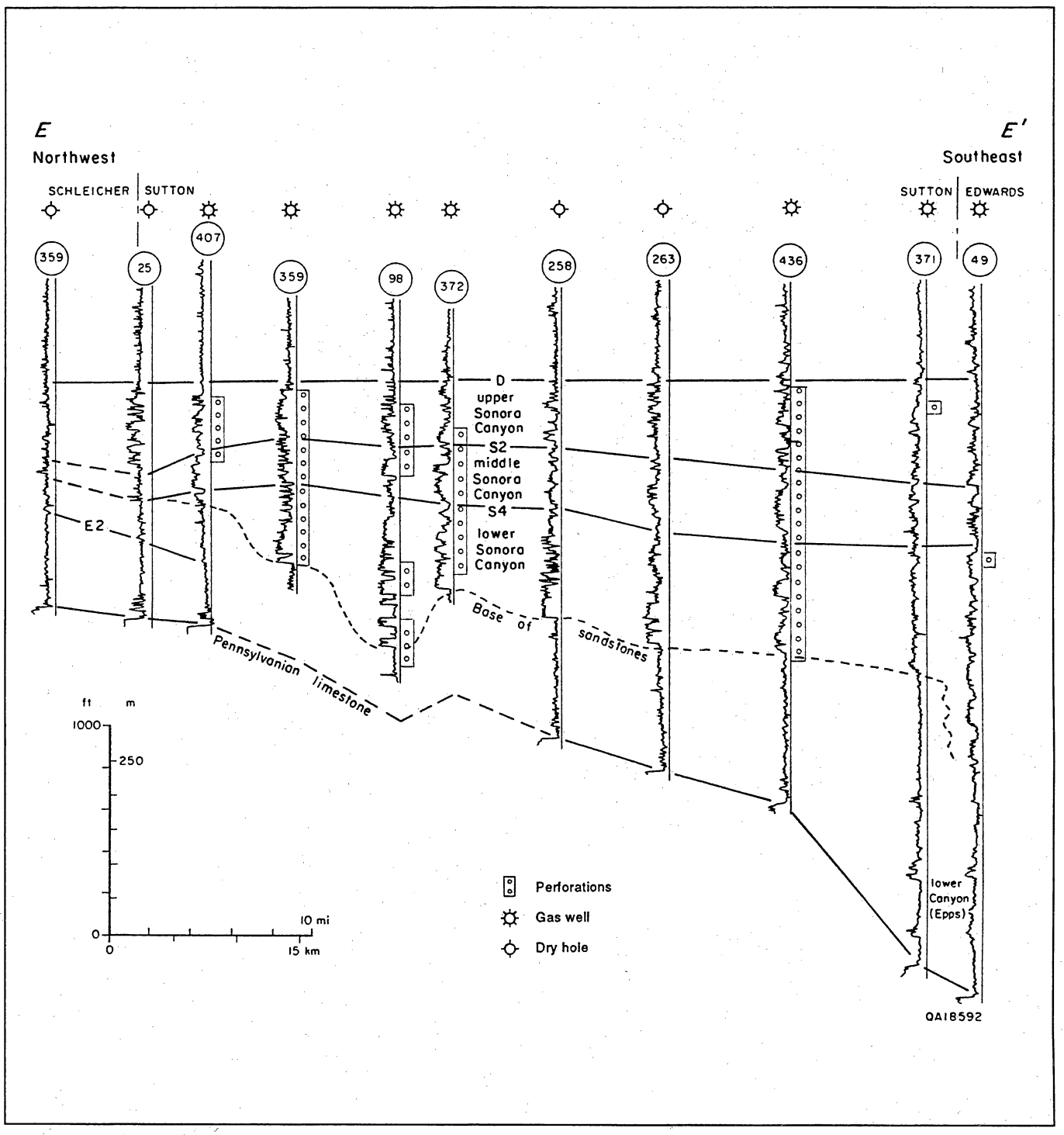

Figure 55. Stratigraphic cross section E–E′ oriented approximately parallel to depositional strike, although it obliquely intersects the shelf margin in the northwest. A slope canyon system centered on well 98 is delineated by erosional "base of sandstones." Lower Sonora Canyon sandstones merge with Lower (Epps) Canyon sandstones in Edwards County. See figure 48 for location of section line. Gamma-ray logs are shown.

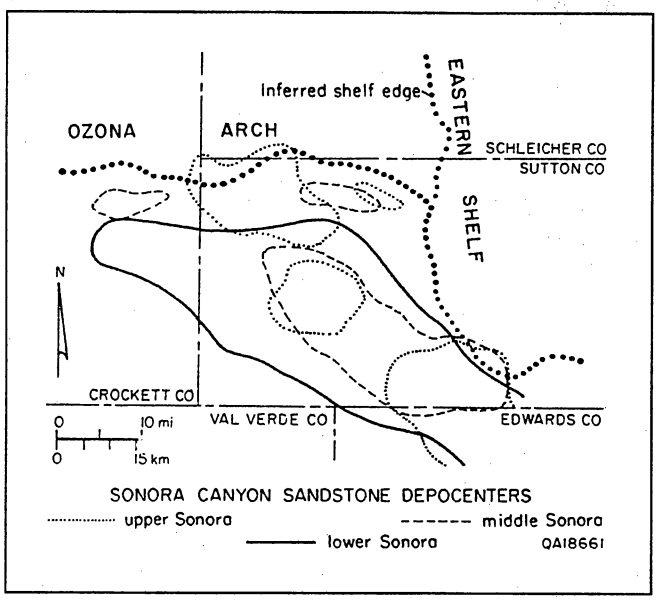

Figure 56. Sonora Canyon sandstone depocenters and inferred shelf-edge positions. Depocenters are areas containing greater than 100 ft of net sandstone.

deltaic feeder systems on the shelf. Shifting feeder systems created a slope apron of coalesced fans, whereas a stable, stationary feeder system would create a single large integrated fan. However, persistent superposition of sandstone depocenters also exists in the Sonora Canyon, especially in west-central and south-central Sutton County (fig. 56), reflecting the dominant influence of feeder systems updip from these locations. The actual locations of Sonora Canyon fluvial-deltaic feeder systems have not been documented but probably lie in incised valleys on the shelf in eastern Sutton, Schleicher, and northern Crockett Counties. Incised valley-fill sandstones in the otherwise mudstone-dominated shelf areas form potential new exploration targets.

Shifting sandstone depocenters confirm the slope-onlap style of Sonora Canyon infill. Sandstone depocenters in the middle and upper map units occur higher on the slope than do those in the underlying lower map unit (fig. 56). This upslope shift is greatest along the northern shelf (Ozona Arch), where middle and upper Sonora Canyon depocenters are 5 to 10 mi nearer the south-facing shelf margin than are lower Sonora Canyon depocenters (fig. 56). Slope onlap is also well displayed in south-central Sutton County (Miers field area). Sandstone depocenters lying near preexisting shelf margins may represent shelf-edge delta systems (similar to those mapped by Neuberger, 1987) and may, therefore, form the distal ends of Sonora Canyon sediment feeder systems.

Field-Scale Mapping

Although coalescence commonly obscures lateral boundaries, the geometries and internal facies frameworks of individual Sonora Canyon submarine fans are recognizable in local areas having dense well control. Inner, middle, and outer components of Sonora Canyon fans are distinguished by the following characteristics: (1) the inner fan consists of isolated channel (submarine canyon) sandstones enclosed in thick slope mudstones, (2) the middle fan comprises a complex crosscutting network of channel-fill and proximal fan lobe (sheet) sandstones and interchannel mudstones, and (3) the outer fan is composed of distal fan-lobe sheet sandstones and hemipelagic mudstone (Shanmugan and Moiola, 1988) (fig. 13). Inner-fan channel-fill sandstones have been penetrated by wells locally on the upper slope but are generally too narrow to be mapped using the commonly available 0.5- to 1.5-mi well spacing. The Sonora Canyon depocenters contain hundreds of feet of thick but laterally discontinuous sandstones that probably represent channelized proximal fan lobes within coalesced middle fans (fig. 13). Most Sonora Canyon sandstone lies in middle-fan facies. Thin, laterally continuous sandstones of the distal fan lobes (fig. 13) form the basinward fringe of the fan system.

Miers Area

In the Miers field area in south-central Sutton County (fig. 45), dense well control was used to map individual fans and to further document stratigraphic relationships between Sonora Canyon sandstone distribution and the preexisting carbonate shelf margin. In the Miers field the middle map unit forms what is probably a single submarine fan (fig. 57). Although coalescence with adjacent fans prevents complete boundary delineation (only the inner and middle fan components are distinguishable), the fan is roughly cone-shaped and is about 5 mi in diameter. It converges updip into several narrow feeder channels (fig. 57). The broad mid-fan region is composed of a single thick sandstone (up to 250 ft) having abundant thin mudstone interbeds; this middle Sonora Canyon sandstone thins and pinches out relatively abruptly updip (fig. 58). The inner-fan channel-fill sandstones are 20 to 60 ft thick and less than 0.5 mi wide and lack the abundant mudstone interbeds that characterize the middle fan.

In the Miers field area, a Strawn carbonate buildup overlies a preexisting (early Paleozoic) uplift (Brian, 1955; Rall and Rall, 1958), forming an unusually pronounced (for this region) shelf-slope topographic break; this shelf-margin carbonate buildup also dips shelfward (figs. 53 and 58). The lower and middle Sonora Canyon map units pinch out toward the crest of the Strawn buildup in an

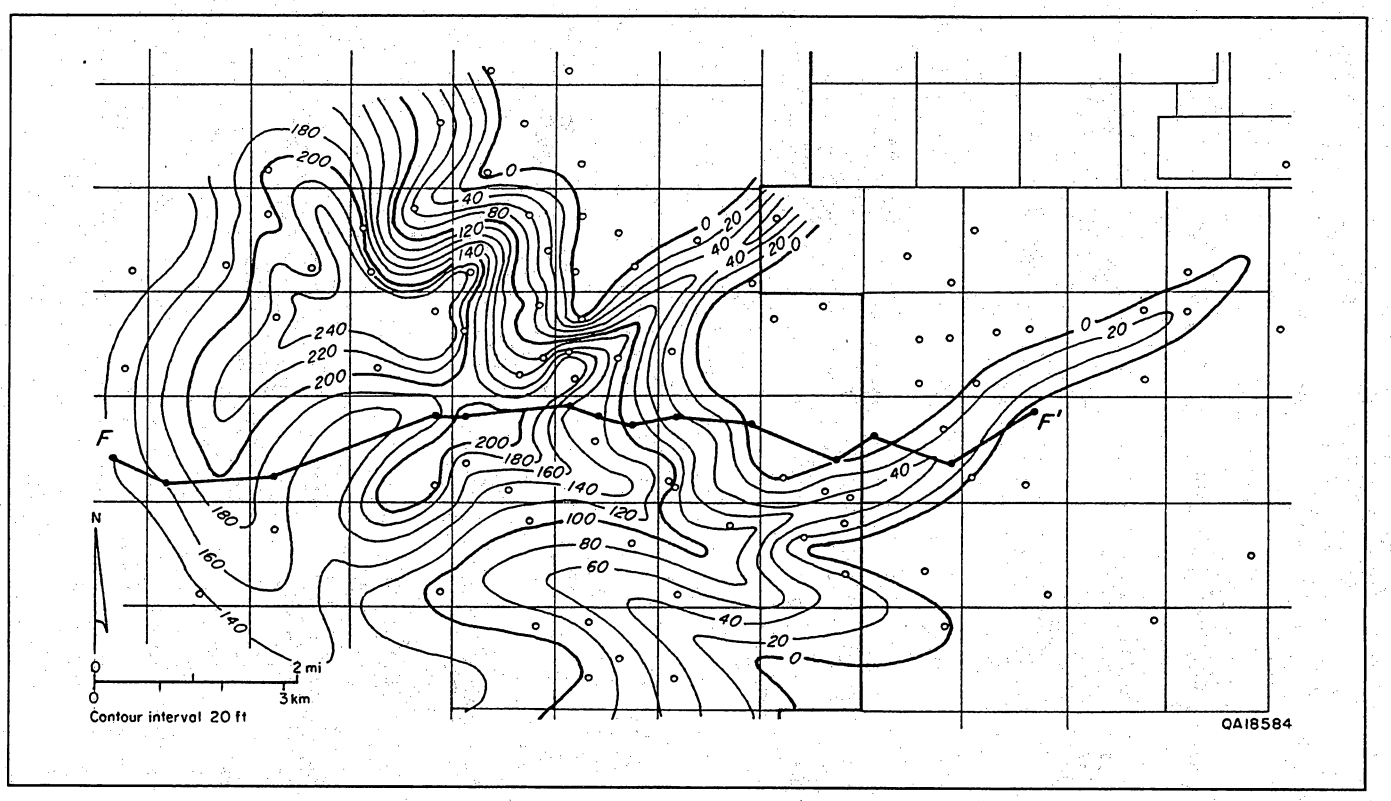

Figure 57. Net-sandstone thickness map of middle Sonora Canyon map unit in Miers field area south-central Sutton County (fig. 45). This sandstone is known locally as the Canyon "Stray" zone.

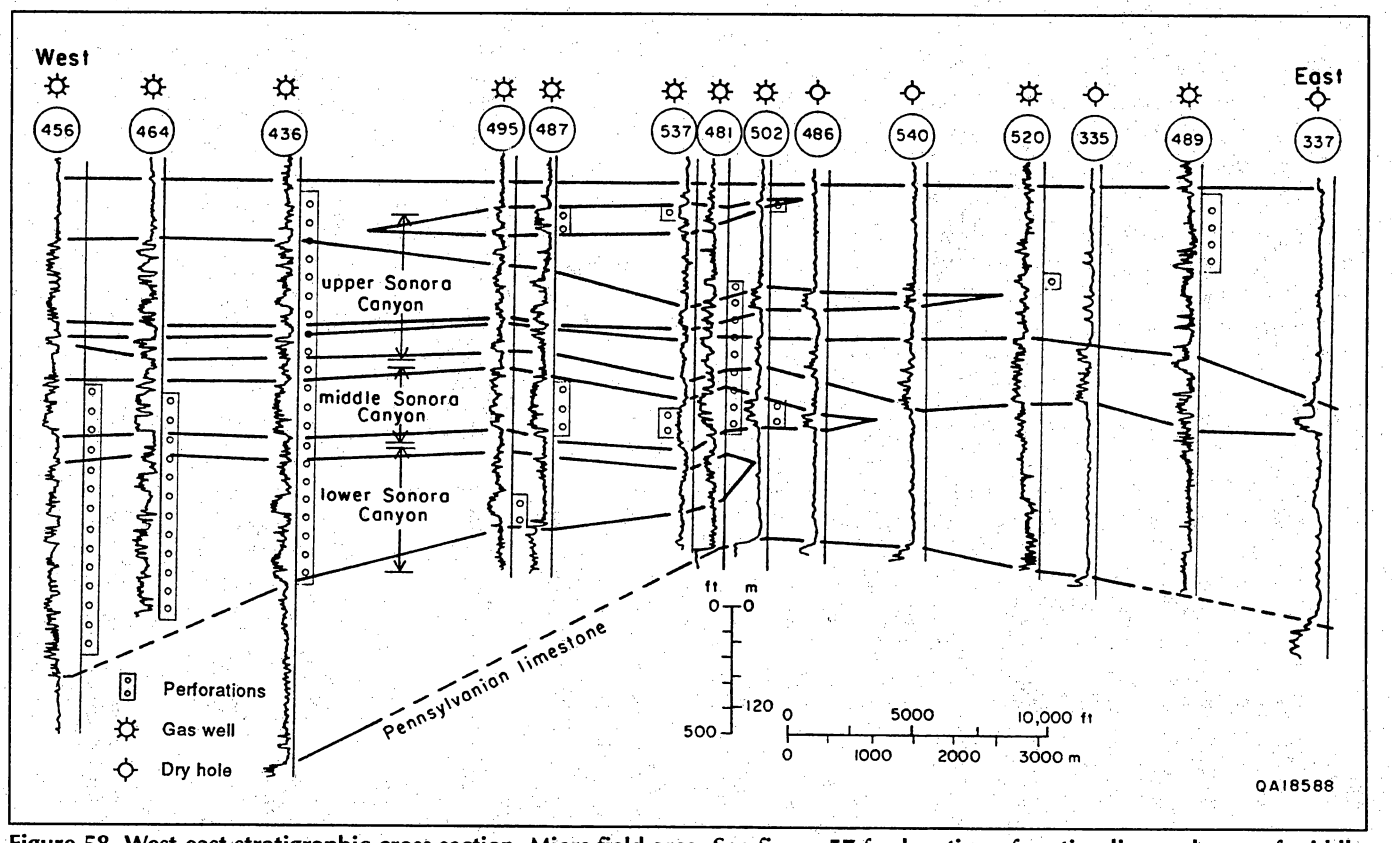

Figure 58. West-east stratigraphic cross section, Miers field area. See figure 57 for location of section line and map of middle Sonora Canyon unit. Anticlinal surface of "Pennsylvanian limestone" (Desmoinesian-Missourian) delineates shelf-margin carbonate buildup with the slope to the west and the shelf to the east.

onlapping relationship, whereas sandstones in the upper map unit extend across the crest and onto the outer shelf (fig. 58). Sonora Canyon sandstones on the shelfward side of the Strawn buildup are probably fluvial-deltaic in origin.

Sonora Area

The Sonora area in west-central Sutton County (fig. 45) lies in a major Sonora Canyon sandstone depocenter, where wells commonly encounter as much as 1,000 ft of sandstone (fig. 47). Because the depositional setting is farther basinward from the shelf margin than is that of the Miers area, middle fan channelized proximal lobes (fig. 13) predominate in the Sonora area. Sonora Canyon sandstones in the Sonora area are thick (50 to 300 ft) but display a high degree of lateral variability and contain abundant shale laminations. Complex cross-cutting relationships and lateral amalgamation make it difficult to map individual channel or fan-lobe sandstones, but composite intervals can be identified and mapped using closely spaced well logs and core.

In the Sonora area the lowermost Sonora Canyon sandstones were deposited in erosional submarine canyons on the slope, but the upper sandstones are mostly fan-lobe deposits. An isopach map of the lower map unit displays northeast-trending canyon fills (fig. 59), and the irregular base of the Sonora Canyon delineates canyon erosion into underlying slope shales (fig. 60). Sandstones near the base of the Sonora Canyon commonly have blocky and upward-fining gamma-ray log patterns (fig. 60), which suggest that these sandstones are channel-fill deposits (fig. 13). The upper map units lack well-defined canyon fills (fig. 61) and are dominated by the serrated gamma-ray log patterns (fig. 60) that characterize fan-lobe sandstones (fig. 13). Mudstone interbeds are more continuous in the middle and upper map units than they are in the lower map unit (fig. 60), highly channelized facies being inherently more discontinuous than sheet-like lobe facies.

Stratigraphic influences on gas productivity in the Sonora area can be documented using maps of initial potential data and sandstone geometries. Although highly variable, initial potentials in Sonora Canyon wells display systematic map patterns having a northeastward elongation (fig. 62), an orientation which occurs on lower Sonora isopach, net sandstone, and maximum sandstone maps (figs. 59, 63, and 64). Several northeast-trending belts of wells having high initial potentials coincide with the lower Sonora slope-canyon fills (compare figs. 59 and 62). Net sandstone trends are thin and lenticular in the east part of the Sonora area but thicken and become more lobate toward the west (fig. 63), suggesting a westward transition from channel-dominated to lobe-dominated. Initial well potentials, however, are generally higher in the eastern channel-dominated area (fig. 62), even though net sandstone thicknesses are lower there. The maximum sandstone map, which emphasizes the thickest individual sandstone bodies, highlights the lenticular channel trends in the east part of the Sonora area (fig. 64). Although initial potentials are generally higher in wells within belts composed of thick-bedded channel-fill sandstone, the correlation is imperfect for several reasons: (1) post-depositional diagenetic processes pervasively modify original reservoir quality (see next chapter), (2) natural fractures may have a large influence on well productivity (also discussed in a later chapter), and (3) initial potential data are subject to artificial factors associated with their measurement and reporting. Nevertheless, isopach and sandstone maps in small areas, such as this Sonora example, help delineate the geometries and distribution of the most prospective reservoir facies.

Depositional Facies

Submarine fans consist predominantly of turbidites (Shanmugam and Moiola, 1988), and turbidites are the most common sedimentary features identified in Sonora Canyon cores. Turbidites are recognized by a typical sequence of sedimentary structures known as the "Bouma sequence" (Bouma, 1962). The Bouma sequence, which may be simply characterized as massive to laminated sandstone overlain by laminated mudstone, records deposition by a waning turbidity flow. All the divisions of the Bouma sequence are common in Sonora Canyon cores, but variations from this ideal sequence are useful for identifying depositional facies and interpreting environments. Turbidites having thick lower Bouma divisions (sandstone part) and thin or missing upper divisions (mudstone part) result from higher flow energies in fan channels and on proximal parts of fan lobes, whereas turbidites having thin sandstone and thick mudstone result from lower flow energies in interchannel areas and on distal fan lobes.

Sonora Canyon channel-fill facies are composed mainly of massive, locally conglomeratic sandstone. Thin mudstone beds and laminations occur locally, but bedding is irregular, and complete Bouma sequences are rare. Distinctive features in cored intervals of fan channel-fill facies include normally graded beds, disseminated organic debris, mud clasts, shell fragments, contorted bedding, and fluid escape structures. Combined core and log analysis suggests that Sonora Canyon channel-fill facies are 10 to 60 ft thick. Contorted mudstone/sandstone and conglomeratic sandy mudstone, which are interpreted to be slump and debris-flow deposits, are commonly associated with channel-fill facies.

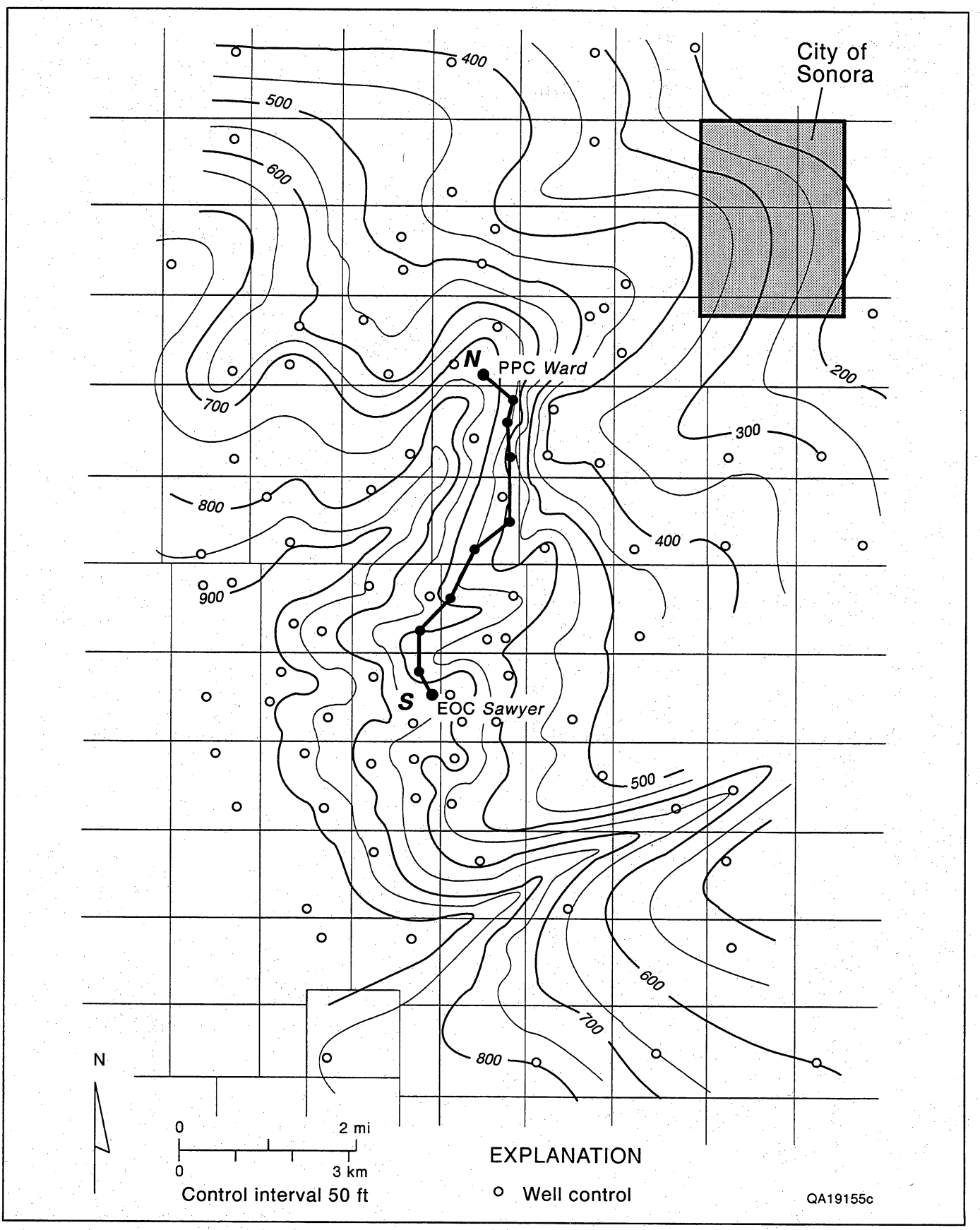

Figure 59. Isopach map of the lower Sonora Canyon map unit in the Sonora area (fig. 45). Narrow northeast-trending zones of maximum thickness represent infilling of submarine canyons that were eroded into underlying slope shales.

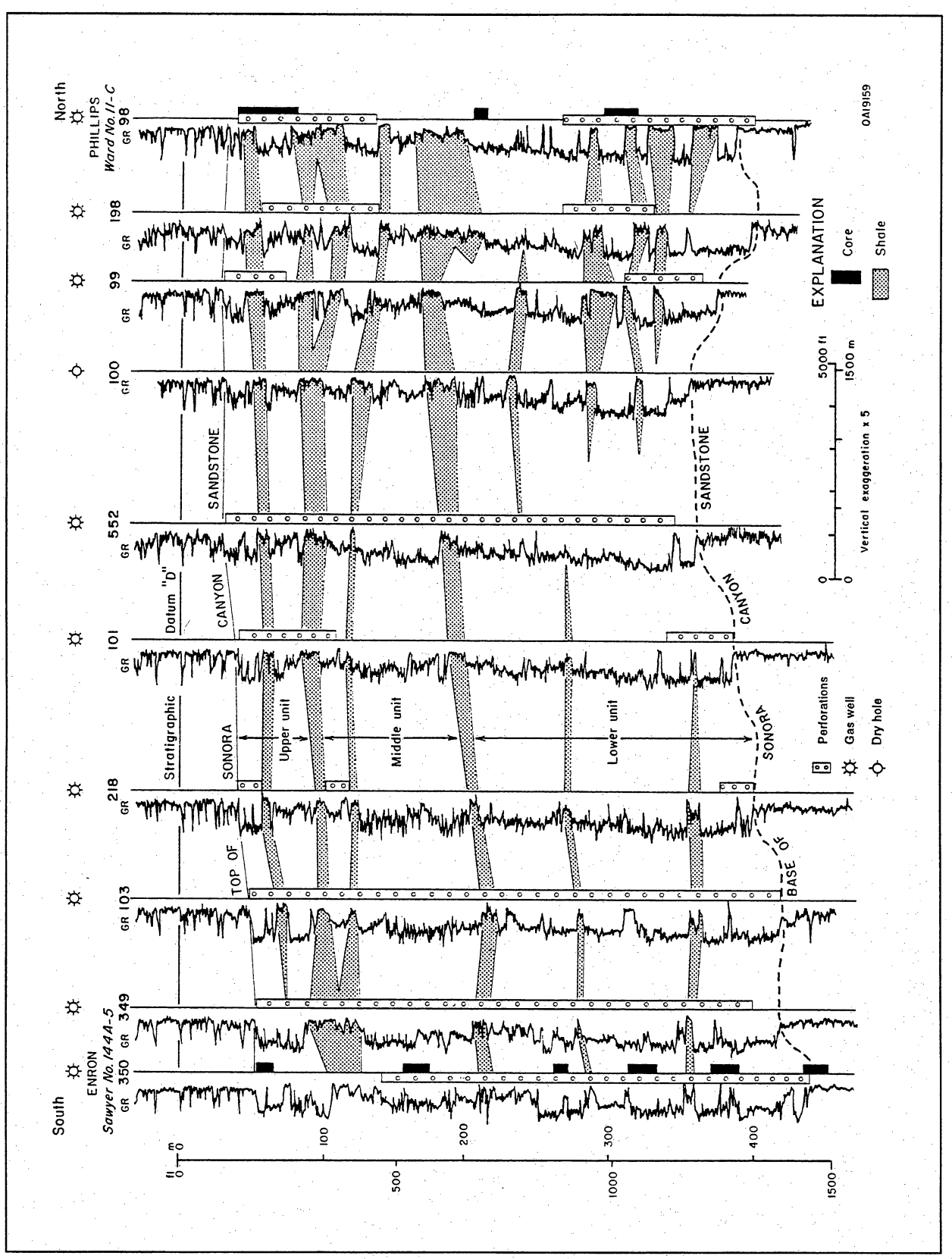

Figure 60. South-north stratigraphic cross section connecting the Enron and Phillips cooperative wells. See figure 59 for location of section line. Thicker, more laterally continuous mudstones are shaded. The irregular base of sandstone delineates submarine canyon erosion. The abundance of shale interbeds and laminations is reflected in highly serrated gamma-ray patterns. Lateral variability in sandstone development is also evident.

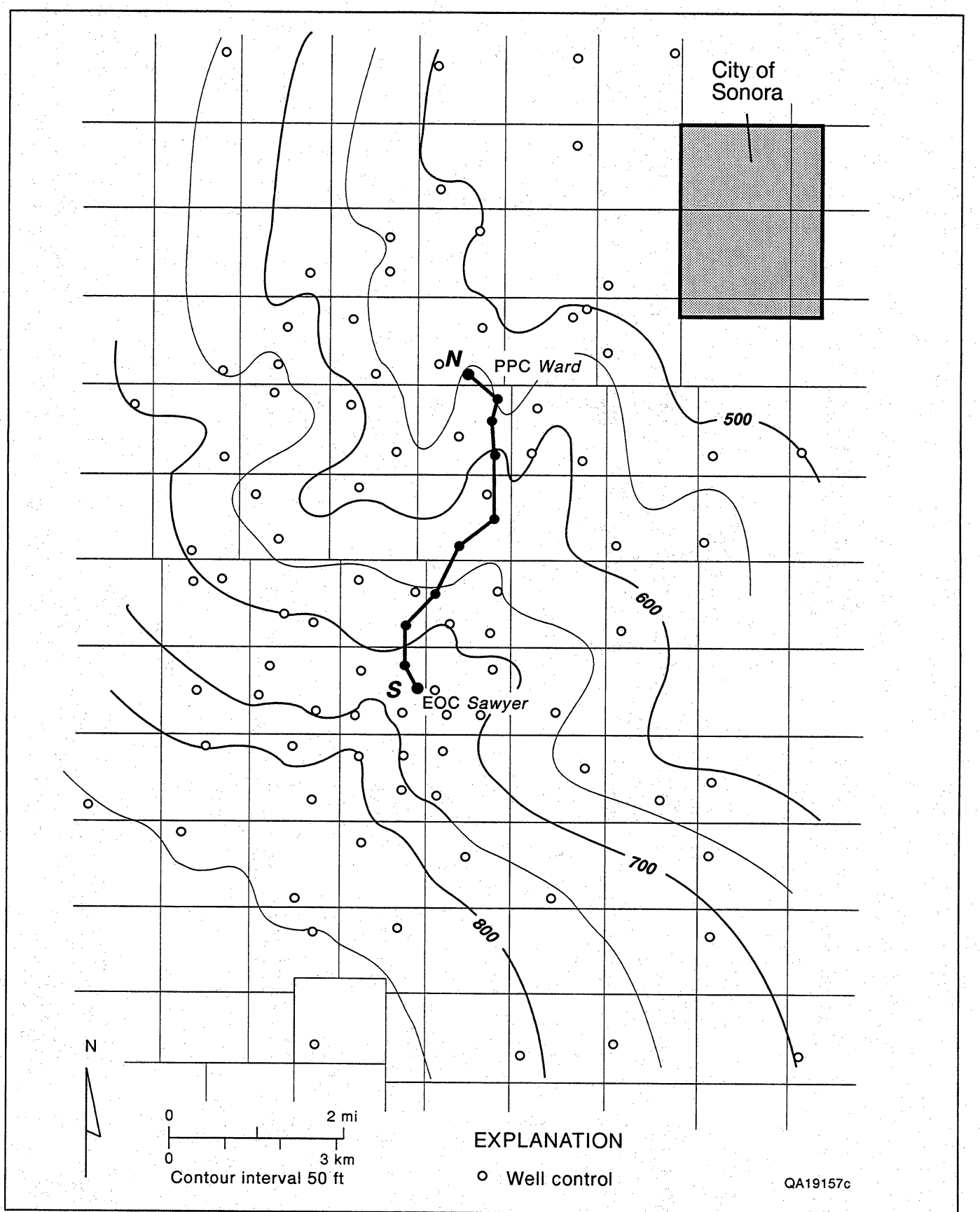

Figure 61. Isopach map of the middle and upper Sonora Canyon map units combined (fig. 60) in the Sonora area (fig. 45). Lack of well-defined canyon fills suggests that this interval is composed mainly of fan-lobe facies.

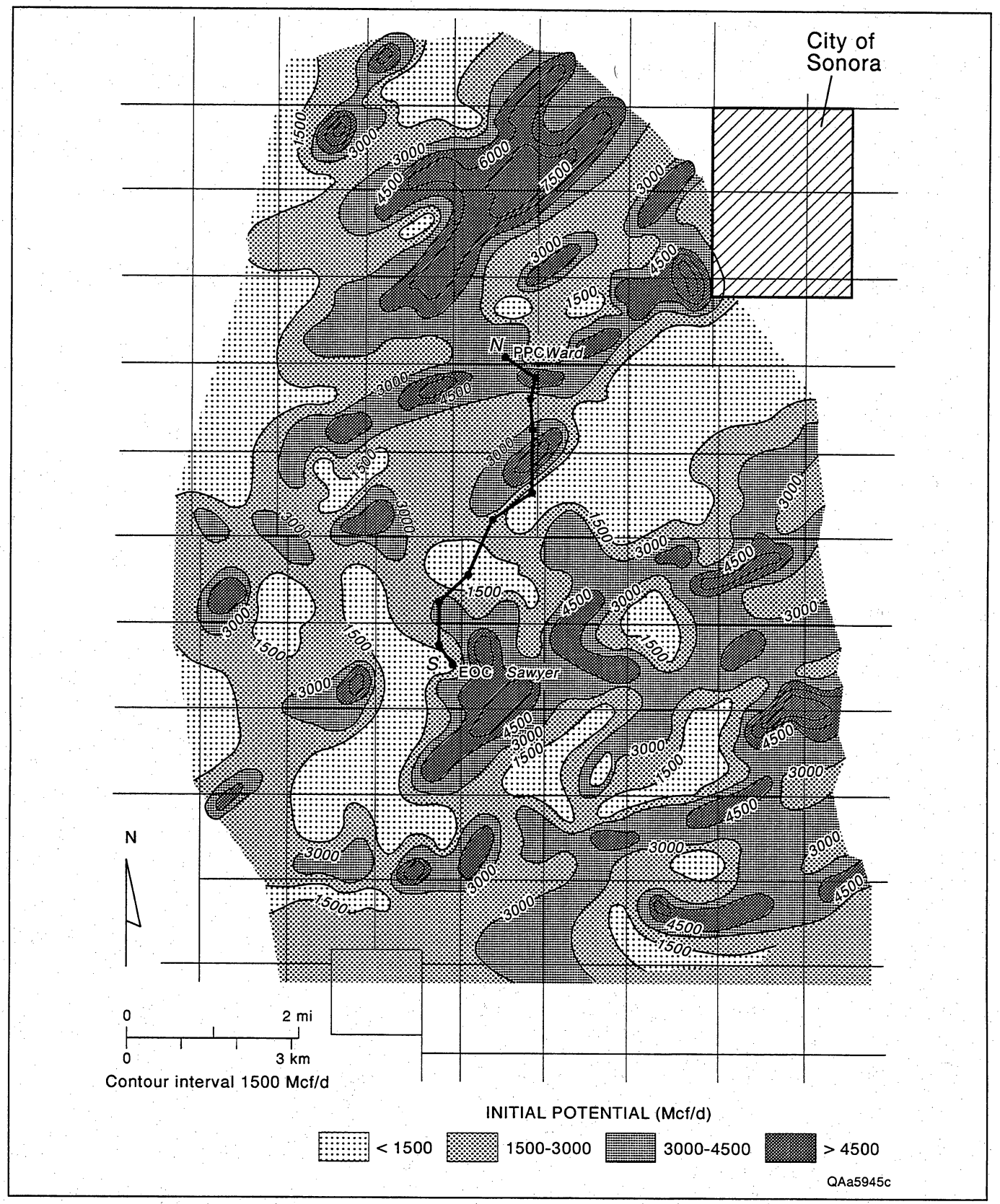

Figure 62. Map of initial well potentials (IP's) from wells completed in the Sonora interval in the Sonora area (fig. 45). These IP's are from calculated open-flow tests conducted after fracture stimulation. Contours are based on approximately four values per section (wells not shown).

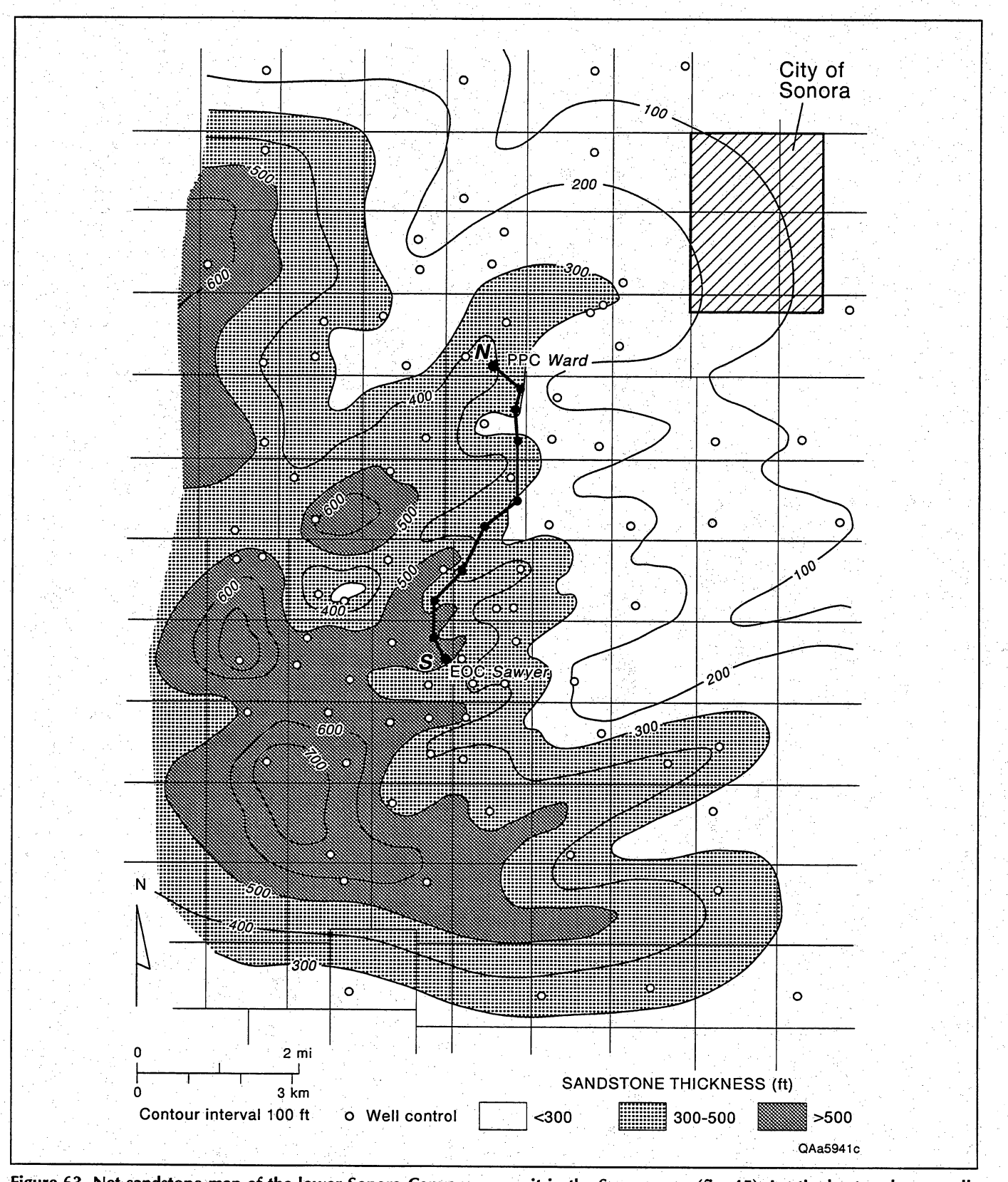

Figure 63. Net-sandstone map of the lower Sonora Canyon map unit in the Sonora area (fig. 45). Lenticular trends are well displayed in the east, whereas more lobate patterns characterize the west, suggesting dominance of fan channels and lobes, respectively.

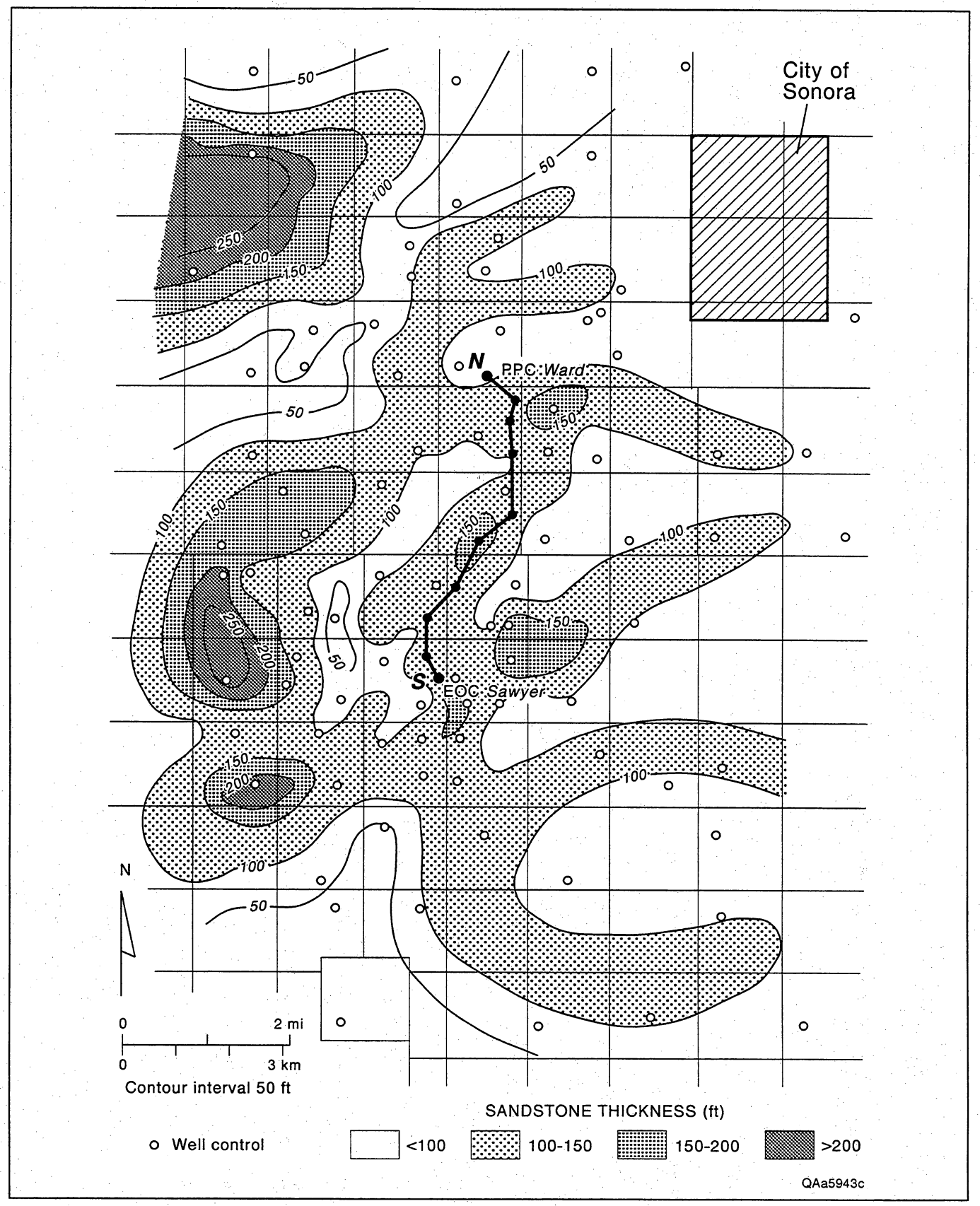

Figure 64. Maximum-sandstone map of the lower Sonora Canyon map unit in the Sonora area (fig. 45). Isolating and mapping the single thickest sandstone in this unit in each well highlights the lenticular, fan-channel trends.

Thick sequences of regularly bedded turbidites characterize Sonora Canyon fan-lobe facies. Proximal fan-lobe turbidites are composed of sandstone beds, 1 to 5 ft thick, and mudstone beds less than 0.5 ft thick. Distal lobe-fringe turbidites have sandstone/siltstone beds less than 1 ft thick interbedded with thicker mudstones. All gradations between these two end-member bedding styles exist intimately interbedded in cores from the Sonora area (fig. 65). The sandstone depocenters in the middle of the Sonora Canyon slope wedge are composed largely of hundreds of feet of fan-lobe turbidites, having highly serrated log responses, and local channel-fill facies, displaying more blocky gamma-ray patterns (fig. 60).

Reservoir Stratigraphy

Sonora Canyon gas reservoirs are found primarily in the submarine-fan, channel-fill and lobe sandstones (fig. 13). Although shelf-edge deltaic sandstones are also productive locally (Miers field), most Virgilian-Wolfcampian shelf facies, which lie north and east of the Sonora Canyon gas-producing trend (fig. 7), are composed of nonproductive mudstone and limestone. The basinal facies that lie southwest of the Sonora Canyon trend are also nonproductive mudstones. The large "Canyon Sands" gas fields that extend across western Sutton County coincide with the regional distribution of Sonora Canyon submarine-fan sandstones. The most prolific of these gas fields, Sonora and Sawyer fields, lie in the thick sandstones that form the Sonora Canyon depocenters (fig. 56). Wells in these fields commonly penetrate 1,000 ft of gross sandstone that is composed of hundreds of turbidites interbedded with channel-fill sandstones and deep-water mudstones (fig. 60). Comparisons of initial well potentials and sandstone maps indicate that the relatively thick-bedded channel-fill sandstones form the most prospective reservoir facies.

Most Sonora Canyon reservoirs, although thick, are compartmentalized vertically by the fine-grained components of the turbidites (fig. 65). Channel-fill sandstones are more homogeneous in the vertical dimension but are highly lenticular (typically less than 1 mi wide). Even the more sheetlike fan-lobe sandstones, because they formed in numerous small submarine fans, do not extend more than a few miles (fig. 57). Both lateral and vertical stratigraphic variability in Sonora Canyon sandstones is well displayed in the Sonora area cross section, where well spacing is only a few thousand feet (fig. 60).

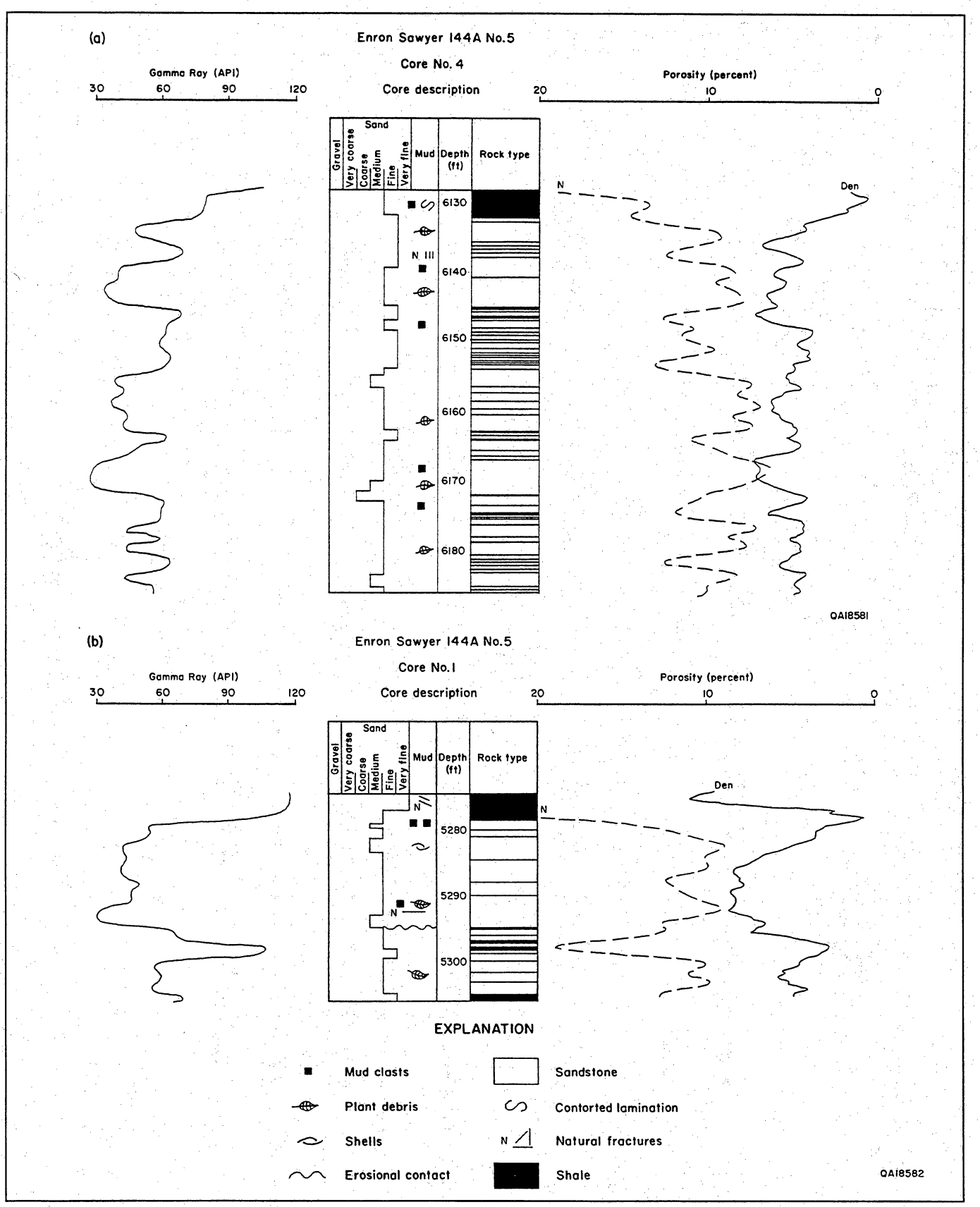

Figure 65. Core description and log responses from the Enron Sawyer cooperative well. (a) Interbedded sandstones and mudstones are thick- and thin-bedded turbidites. (b) Sandstone between 5,278 and 5,294 ft is probably a small channel fill. The underlying thin sandstones are turbidites.

Sonora Canyon Diagenesis

S. P. Dutton

Sonora Canyon sandstones contain abundant natural gas resources, but the gas is difficult to extract at economic rates because extensive diagenesis has reduced average permeability in these sandstones to less than 0.1 md. One of the most common diagenetic changes was precipitation of grain-rimming siderite cement, and, contrary to what might be expected, reservoir quality is best in sandstones that contain the most abundant siderite. The purposes of this section are to (1) describe the detrital and authigenic mineralogy of Sonora Canyon sandstones, (2) ascertain the geochemical and hydrologic conditions under which the siderite precipitated, and (3) quantify the effect of siderite cementation on reservoir quality. An understanding of the diagenetic variability of Canyon sandstones can help to predict zones of higher permeability and identify appropriate production methods.

Previous studies of the deposition and diagenesis of the Canyon sandstones conducted by Rall and Rall (1958), Holmquist (1965), Hills (1968), Mitchell (1975), National Petroleum Council (1980), Berg (1986), Huang (1989), Hamlin and others (1992a and b), and Marin and others (1993) formed the background for this investigation. The study by Mack (1984) of the diagenesis of Pennsylvanian submarine fan sandstones on the Eastern Shelf of the Midland Basin provided detailed geochemical information on authigenic cements from a similar depositional setting. In addition, recent research on siderite geochemistry, particularly the work of Curtis (1978), Berner (1981), Maynard (1982), Gautier and Claypool (1984), Rosenbaum and Sheppard (1986), Carothers and others (1988), Mozley (1989), Hesse (1986), Mozley and Carothers (1992), Mozley and Wersin (1992), and Coleman and Raiswell (1993), provided the geochemical foundation necessary to interpret the Canyon siderite.

Methods

Fifty-one thin sections were examined from cores from two wells, the Phillips Ward "C" No. 11 and the Enron Sawyer 144-A No. 5, in Sonora Canyon gas fields in Sutton County, Texas. The thin sections were taken from a total of 480 ft (146 m) of core that gave good coverage of the entire 1300-ft- (400-m-) thick Sonora Canyon interval (Hamlin and others, 1992a). Core depths range from 5,274 to 6,576 ft (1,608 to 2,005 m) below ground surface. Matrix-free sandstones were sampled preferentially because cementation was more extensive in them than in sandstones with detrital clay matrix.

Composition of Canyon sandstones was determined by standard thin-section petrography and scanning electron microscopy (SEM) with an energy dispersive X-ray spectrometer. Thin sections were stained for K-feldspar and carbonates. Point counts (200 points) of thin sections from representative samples from the two cores were used to determine mineral composition and porosity. Counting error varies with the percentage of the constituent. A constituent that is 50 percent of the sample (whole-rock volume) has the maximum error of ±3.6 percent, whereas a constituent that is 10 percent of the sample has an error of ±2.1 percent, and one that is 2 percent of the sample has an error of ±0.9 percent (Folk, 1974). Grain size and sorting were determined by grain-size point counts (50 points).

Stable isotope measurements of siderite cement were accomplished by the reaction of carbonate samples with phosphoric acid to release CO_2 gas. The gas preparation procedure used in the stable isotope measurements applied the reaction rates and $\delta^{18}O$ variations for carbonates and phosphoric acid described by Walters and others (1972) for rocks with mixed carbonate mineral assemblages. The CO_2 recovered in one hour at 25°C, considered to represent the calcite fraction in each sample, was discarded. The gas evolved after two hours at 150°C represented the siderite in each sample. We used the equilibrium fractionation factor (a = 1.00771) for siderite-phosphoric acid of Rosenbaum and Sheppard (1986). The siderite CO_2 was then analyzed for carbon and oxygen stable isotopes with a VG SIRA 12 triple collection mass spectrometer. Results of oxygen isotopic analyses are reproducible to ±0.2 ‰ and results of carbon analyses to ±0.1 ‰. Oxygen isotope ratios determined at 150°C were corrected to 25°C by linear interpolation (Rosenbaum and Sheppard, 1986), and all values are reported in per mil (‰) deviations relative to the CO_2 liberated from the PDB standard at 25°C by reaction with >100 percent phosphoric acid. Delta values were corrected for ^{13}C and ^{17}O variations according to Craig (1957).

Canyon Sandstone Composition

Sonora Canyon sandstones are typically composed of very fine to medium grained sandstone, although coarser, locally conglomeratic sandstone is present in the channel-fill facies. In general, upper Sonora Canyon sandstones are finer grained than are lower Sonora Canyon sandstones. Sorting ranges from good to poor, but most clean sandstones (defined as containing ≤2 percent clay matrix) are moderately well sorted.

Framework Grains

Sonora Canyon sandstones are mineralogically immature and are classified as sublitharenites and litharenites in the sandstone classification of Folk (1974). Average composition of the essential framework grains (normalized to 100 percent) is 77 percent quartz, 4 percent feldspar, and 19 percent rock fragments ($Q_{77}F_4R_{19}$). Plagioclase is the most abundant feldspar, composing from 0 to 8 percent of the whole-rock volume; orthoclase is rare. Sedimentary rock fragments, including chert, sandstone, siltstone, shale, and mud rip-up clasts, are the most abundant lithic grains. Fine-grained, low-rank metamorphic rock fragments, such as slates or phyllites, also are common. The composition of the rock fragments is consistent with the sediment source being from the Ouachita Structural Belt, which shed detritus from older sedimentary rocks and their metamorphosed facies into the adjacent basin. Detrital organic matter, such as wood fragments, occurs in many of the sandstones and mudstones in volumes ranging from 0 to 10 percent.

Cements and Replacive Minerals

Authigenic cements and replacive minerals constitute between 7 and 52 percent of the whole-rock volume in the sandstone samples. Authigenic quartz, siderite, ankerite, calcite, chlorite, illite, kaolinite, and pyrite all occur in Canyon sandstones. Major diagenetic events in the burial history of Sonora Canyon sandstones were (1) siderite cementation, (2) mechanical compaction, (3) quartz cementation, (4) feldspar dissolution and illite and kaolinite precipitation, (5) iron-bearing calcite and ankerite precipitation.

Siderite

The volume of siderite cement in Sonora Canyon sandstones varies from 0 to 38 percent (median volume = 2 percent). Siderite was one of the first cements to precipitate, and it commonly forms rims around detrital grains in Sonora Canyon sandstones (figs. 66 and 67). The siderite rims are formed of clusters of 1- to 2-μm-long siderite rhombs (fig. 68). Many siderite rims contain flakes of authigenic chlorite (fig. 69), suggesting that chlorite and siderite both formed relatively early in the diagenetic history.

When an opaque white card is inserted beneath the thin section and it is examined in strong oblique reflected light, the siderite rims and masses appear pale smoky brown, quite different from the orange-brown colors of oxidized siderite. This is the clue that the siderite crystals contain disseminated organic matter. To determine the source of this coloration, we etched the siderite for a half hour in 10 percent HCl at 50°C. SEM examination then revealed the presence of subspherical nannobacterial bodies (0.05 to 0.15 μm; Folk, 1993). We presume that the brown color is due to the presence of carbon-rich remnants of cell walls that are invisible at the SEM scale. Nannobacteria are locally abundant, ranging up to 100 bodies per μm^2 on the siderite crystal surfaces; other portions of the crystals contain virtually no bodies. As we discuss in the section on siderite diagenesis, bacteria presumably helped trigger siderite precipitation by consuming organic matter and reducing Fe^{3+} in the unconsolidated sediment and producing Fe^{2+} and HCO_3^-.

Most Sonora Canyon sandstones contain some siderite, but certain layers and patches are extensively cemented by siderite. Abundant siderite cement commonly occurs in bedding-parallel layers that average 3 to 4 in (8 to 10 cm) thick and are rarely >10 in (25 cm). Abundant siderite also occurs in indistinct, irregular patches that are typically 1 to 3 in (3 to 8 cm) in diameter. Distribution of siderite can be estimated qualitatively by measuring the number of feet of sandstone that are stained red-brown by oxidation of siderite cement. An average of 30 percent of all Sonora Canyon sandstones in the two cores are siderite stained; in some intervals, as much as 47 percent of the sandstones are siderite stained. The percentage of siderite-stained sandstone increases upward slightly. Siderite concretions and layers also occur in the interbedded shales.

A comparison of siderite-rich and siderite-poor sandstones reveals similarities and differences between them (table 4). Siderite-rich Canyon sandstones, arbitrarily defined as sandstones having ≥10 percent siderite cement, have similar grain size and sorting as siderite-poor sandstones (sandstones having <10 percent siderite). The average depth of occurrence of siderite-rich sandstones is shallower than that of siderite-poor sandstones. All of the siderite-rich samples occur in basal, Bouma A (massive or graded sandstone) turbidite divisions, whereas siderite-poor samples are equally divided between Bouma A and Bouma B (parallel laminated sandstone) divisions. Point counts reveal that the siderite-rich samples contain less organic matter but more pyrite than

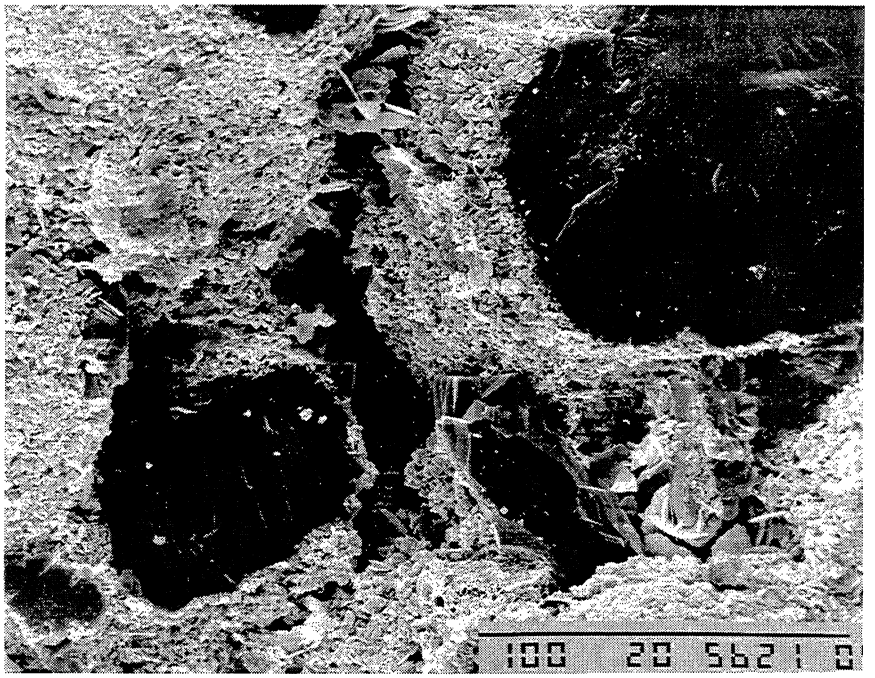

Figure 66. SEM photograph of siderite and chlorite cement rimming detrital quartz grains. Sample from a depth of 5,621 ft in the Phillips Ward "C" No. 11 well. Scale bar is 100 μm. Photo by J. Mendenhall.

Figure 67. SEM photograph showing close-up view of the contact between a detrital quartz grain (top of photo) and rhombs of grain-rimming siderite cement. Sample from a depth of 6,370 ft in the Phillips Ward "C" No. 11 well. Scale bar is 10 μm. Photo by J. Mendenhall.

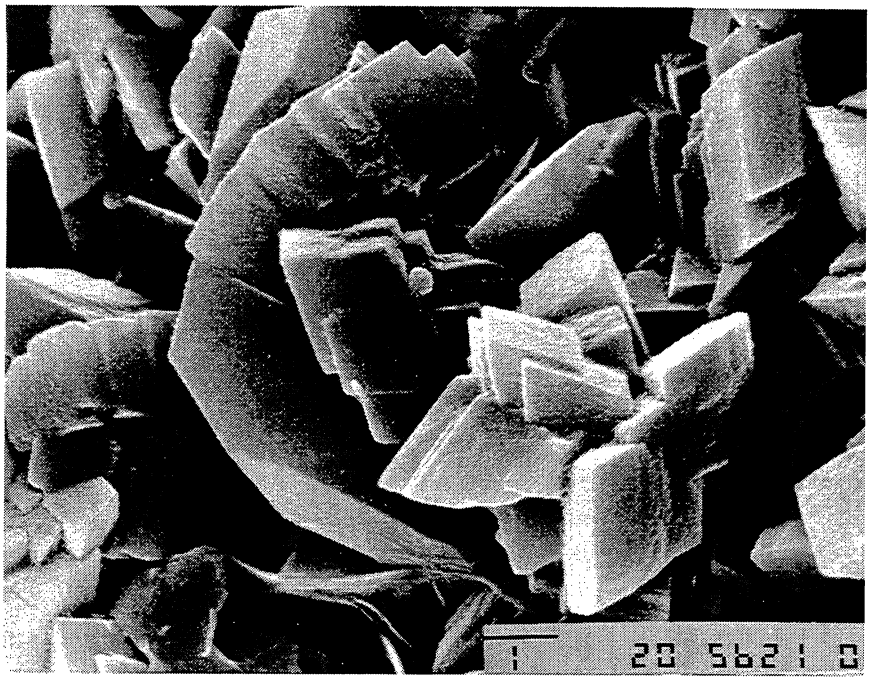

Figure 68. SEM photograph of a cluster of siderite rhombs. Sample from a depth of 5,621 ft in the Phillips Ward "C" No. 11 well. Scale bar is 1 μm. Photo by J. Mendenhall.

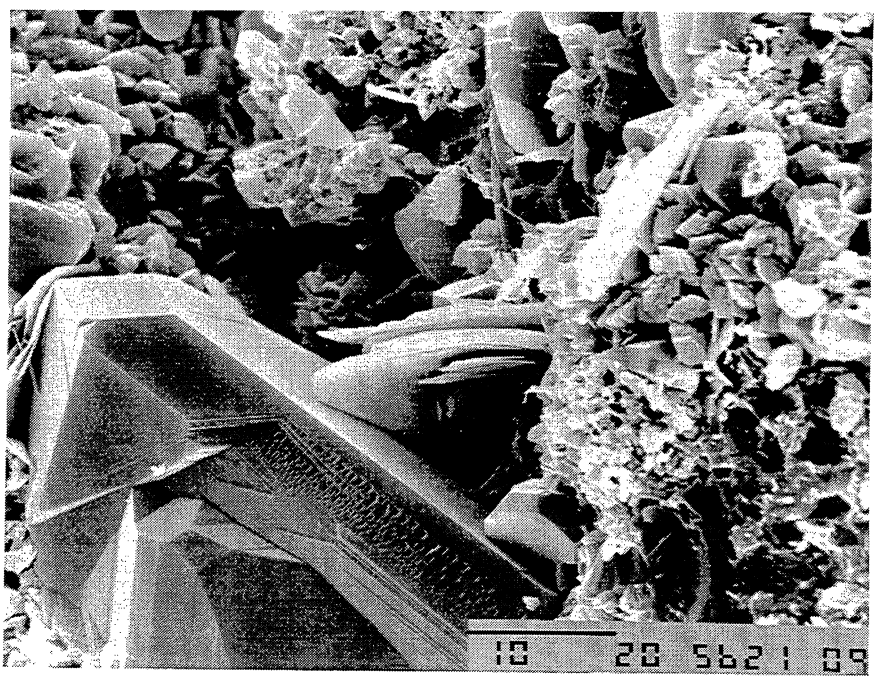

Figure 69. SEM photograph of a quartz overgrowth (lower left), flakes of authigenic chlorite cement (center), and small rhombs of siderite (center right), probably projecting into a primary pore. Sample from a depth of 5,621 ft in the Phillips Ward "C" No. 11 well. Scale bar is 10 μm. Photo by J. Mendenhall.

Table 4. Comparison of siderite-poor and siderite-rich Sonora Canyon sandstones.

	Siderite-Rich (≥10 %)	Siderite-Poor (<10 %)
Average depth (ft)	5,640	6,050
Bouma division	A only	A or B
Framework-grain composition	$Q_{78}F_4R_{18}$	$Q_{75}F_4R_{21}$
Mean grain size (mm)	0.131	0.143*
Sorting (phi standard deviation)	0.66	0.62
Detrital clay matrix (%)	0.1	1.0
Organic matter (%)	0.1	0.7
Quartz cement (%)	6	11
Siderite (%)	24	2
Pyrite (%)	0.8	0.1
Total cement (%)	32	15
Primary porosity (%)	1.5	0.4
Minus-cement porosity (%)	33	15
Porosimeter porosity (%)	7.9	6.3
Geometric mean permeability (md)†	0.042	0.006
Number of samples	14	30

*Includes three samples of chert-pebble conglomerate and conglomeratic sandstone that were probably deposited in a channel or a slope canyon near the head of a submarine fan. If those three samples are omitted, mean grain size is 0.132 mm.

†Permeability measured at restored reservoir pressure.

do the siderite-poor zones (table 4). In general, organic matter visible in core is absent or rare in most Bouma A facies but is common to abundant in Bouma divisions B to E, with the D (parallel laminated siltstone) and E (mudstone) divisions apparently the most organic-rich.

Oxygen and carbon isotopic compositions of siderite cements were determined for five samples. Siderite $\delta^{18}O$ values (corrected to 25°C) have a narrow range from -0.7 ‰ to +1.2 ‰ (PDB) (table 5). The average $\delta^{18}O$ composition is +0.3 ‰ (PDB), which is equivalent to 31.1 ‰ (SMOW). Carbon-isotope $\delta^{13}C$ values range from +0.6 ‰ to +4.0 ‰ and average +2.4 ‰ (PDB). The average $\delta^{18}O$ and $\delta^{13}C$ values of Canyon siderite are heavier than most values of marine siderite reported in the literature (summarized in Mozley, 1992) but still within the range of reported values. Interpretation of the carbon and oxygen isotopic composition of siderite cement will be discussed in the section on siderite diagenesis.

Other Cements

Pyrite is not abundant in Canyon sandstones. It occurs in volumes of up to 5.5 percent (average = 0.3 percent), but in most samples no pyrite was counted in 200 points. It is more abundant in the siderite-rich zones (arithmetic mean = 0.8 percent) than in the siderite-poor zones (0.2 percent) (table 4). Pyrite apparently precipitated before siderite, because where it is most abundant, it forms the first rims around detrital grains and is overlain by siderite. Some detrital grains are partly surrounded by pyrite and partly by siderite, but the pyrite appears to have precipitated first. Pyrite also replaces organic particles and fossils.

Quartz cement precipitated after siderite. The volume of quartz cement in these samples varies from 0 percent (in mudstones) to 20 percent. Quartz overgrowths are well developed in clean sandstones, with an average volume of 9 percent. Where quartz overgrowths are abundant, they completely fill some primary, intergranular

Table 5. Isotopic composition of siderite cements (PBD).*

Well	Depth	$\delta^{18}O$	$\delta^{13}C$
Phillips Ward	5516.7	–0.34	0.56
Phillips Ward	6056.1	0.65	3.66
Enron Sawyer	5289.5	0.70	0.82
Enron Sawyer	5642.2	1.16	3.95
Enron Sawyer	6181.3	–0.66	2.76

*All values given in per mil (‰) relative to CO_2 liberated from PDB-1 at 25°C by attack with >100% phosphoric acid.

pores (fig. 70). An inverse relationship exists between quartz and siderite cement; quartz cement is most abundant in samples containing little siderite cement (table 4). Where siderite is abundant, most quartz overgrowths are small, and they apparently nucleated where breaks occurred in the siderite rims (fig. 71).

Authigenic chlorite, illite, and kaolinite occur in clean, matrix-free sandstones. Most illite has a fibrous morphology, but chlorite mainly occurs as platelets. Chlorite apparently precipitated early in the burial history, whereas illite and kaolinite probably precipitated relatively late.

Iron-bearing calcite and ankerite cements also precipitated late in the diagenetic sequence; textural relationships show that they precipitated after quartz cement. They both replace framework grains (mainly feldspars) and fill intergranular pores that had remained open throughout earlier phases of diagenesis. Ankerite volume ranges from 0 to 7 percent and calcite volume from 0 to 5 percent.

Porosity

Porosity observed in thin section varies from 0 to 5 percent; in clean sandstones the average volume of primary porosity is 0.8 percent and average secondary porosity is 0.6 percent. Most secondary pores formed by dissolution of framework grains, mainly feldspar, chert, and clay clasts. Average porosity measured by porosimeter is 6.9 percent in clean sandstones. Thin section porosity generally is lower than porosimeter porosity because of the presence of micropores between clay flakes and within partly dissolved grains; the micropores cannot be accurately quantified in thin section. Although the total volume of micropores may be greater than that of macropores, microporosity contributes little to permeability. The difference between porosimeter-measured porosity and thin section porosity provides an estimate of the volume of microporosity, which in clean Sonora Canyon sandstones averages 5.5 percent.

Interpretation of Siderite Diagenesis

Geochemical Conditions of Siderite Precipitation

Because siderite will only precipitate under certain narrow chemical conditions, it should be possible to closely constrain the conditions under which the Canyon siderite formed. The conditions necessary for siderite precipitation include low oxidation potential (low Eh), high partial pressure of CO_2 (high P_{CO_2}), very low sulfide concentration (low $[S^{-2}]$), and high ratio of ferrous iron to calcium ion (high $[Fe^{+2}]/[Ca^{+2}]$) (Berner, 1971). Sulfide concentration must be low or pyrite will form, and the $[Fe^{+2}]/[Ca^{+2}]$ ratio must be high or calcite will form. The conditions necessary to precipitate siderite are met in two anoxic-nonsulfidic geochemical environments—the weakly reducing post-oxic environment and the highly reducing methanic environment (fig. 72) (Berner, 1981; Maynard, 1982).

Although siderite has long been recognized as a common authigenic mineral in fresh-water environments because of the low sulfate concentration in meteoric water, many examples also have been reported in the literature recently of early siderite cement that formed in marine environments (see summary of references in Mozley, 1989). Berner (1981), Maynard (1982), and Mozley and Wersin (1992) suggest that anoxic, nonsulfidic geochemical conditions may be more common in marine sediments than previously recognized. For post-oxic conditions to develop (fig. 72), deep-sea sediments must contain sufficient metabolizable organic matter that all dissolved oxygen is consumed in the sediment during organic decomposition by aerobic bacteria (Berner, 1981). However, there must be insufficient organic matter to bring about sulfidic conditions, so that further bacterially mediated organic matter decomposition takes place by successive reduction of nitrate, manganese, and iron, but not by sulfate

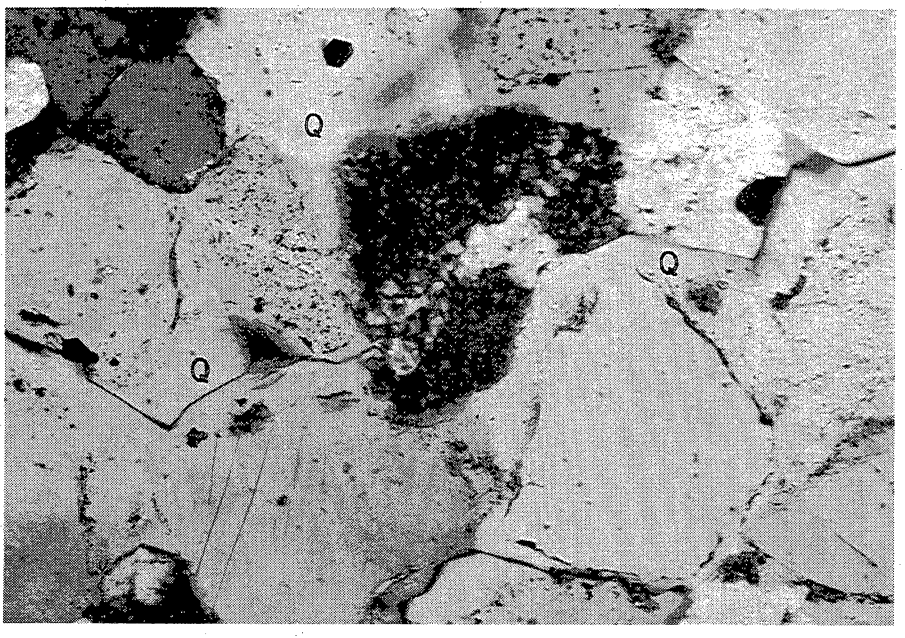

Figure 70. Sandstones that lack early siderite cement experienced considerable quartz cementation. Quartz cement (Q) occludes much of the intergranular porosity. Sample from 6,383 ft in the Phillips Ward "C" No. 11 well. Long dimension of photo is 0.65 mm. Cross-polarized light.

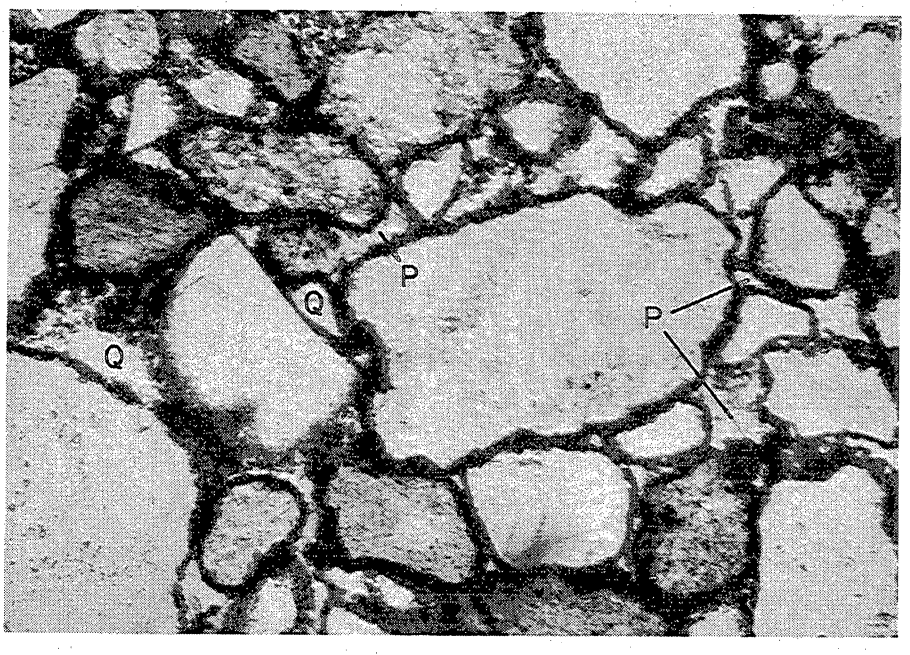

Figure 71. Thick, continuous siderite rims (dark) around quartz grains inhibited precipitation of quartz cement, thus preserving some intergranular porosity (P). Small quartz overgrowths (Q) nucleated where breaks occurred in the siderite rims. Sample from 5,621 ft in the Phillips Ward "C" No. 11 well. Long dimension of photo is 0.65 mm. Plane-polarized light.

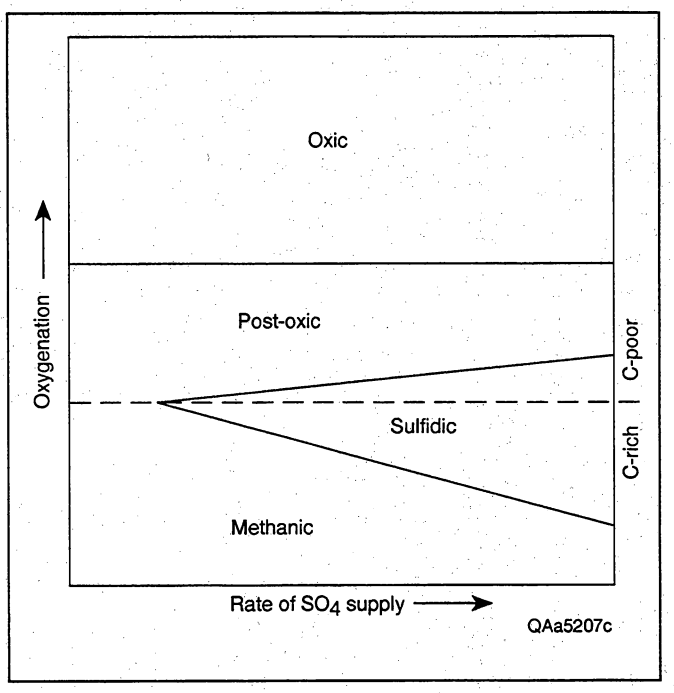

Figure 72. Classification of diagenetic environments (from Maynard, 1982; modified from Berner, 1981). Siderite can form in post-oxic and methanic environments; canyon siderite is interpreted to have formed in a methanic environment.

reduction (Berner, 1981). This anoxic-nonsulfidic geochemical environment is referred to as the suboxic environment by Froelich and others (1979) and post-oxic by Berner (1981) (fig. 66). Bacterial reduction of Fe^{3+} in this environment increases the Fe^{2+} in the pore fluids, and in the absence of sulfide, siderite precipitates.

The methanic environment forms under more strongly reducing conditions (fig. 72). For methanic conditions to develop, there must be sufficient organic matter for sulfate-reducing bacteria to first reduce all sulfate in the pore waters to sulfide. If any reduced iron is present in the pore fluids of the sulfate-reduction zone, pyrite precipitates. Once all sulfate has been reduced, continued organic decomposition occurs by microbial methanogenesis (Curtis, 1986), resulting in production of methane and CO_2 (fig. 73). Assuming there is still a supply of reduced iron, siderite precipitates.

Siderite that formed in a post-oxic environment can be distinguished from that which formed in a methanic environment by the isotopic composition of the carbon (Maynard, 1982). Carbon in CO_2 produced by oxidation of organic matter and corresponding bacterial reduction of nitrate, manganese, iron, and sulfate is isotopically light (-25 ‰ PDB), whereas CO_2 produced during methanogenesis is isotopically heavy (+15 ‰ PDB) (Curtis, 1978, 1986) (fig. 73). Thus, the $\delta^{13}C$ of the Canyon siderite should identify the geochemical zone in which it formed.

Interpretation of Canyon Siderite

The relatively heavy values of carbon (average of +2.4 ‰ PDB) indicate that most if not all of the Canyon siderite formed in a methanic environment. This interpretation is supported by the presence of pyrite in the siderite-rich samples (table 4), which indicates that the sediments passed through the zone of sulfate reduction. Furthermore, the pyrite appears to have precipitated before siderite. Textural evidence indicates that siderite cement in Sonora Canyon sandstones formed relatively early in the burial history of these deep-water marine sediments. Except where pyrite is present, siderite is the first cement around detrital grains, and the high minus-cement porosity of siderite-rich sandstones (33 percent) indicates that they were cemented prior to much compaction. This interpretation of early siderite cementation is consistent with siderite precipitating at the shallower end of the depth range at which bacterial methanogenesis occurs, from approximately 30 to 300 ft (10 to 1000 m) below the sediment-water interface (Curtis, 1978) (fig. 73). The following discussion outlines our interpretation of how siderite precipitation occurred in Canyon sandstones.

Bioturbation is common in Canyon deposits, indicating that the bottom water in the basin could support organisms and thus was oxygenated. The oxidation zone in the sediment probably was quite thin, approximately 10^{-2} m (fig. 73), and below that depth a zone of anaerobic sulfate reduction developed. Pyrite precipitation occurred in this zone. The source of the Fe^{2+} in the pyrite was probably from microbial iron reduction of semi-amorphous, colloidal particles of iron oxide and oxyhydroxide on larger detrital grains and clay flakes (Berner, 1981; Hesse, 1986; Coleman and Raiswell, 1993).

The relatively low volume of pyrite in the sandstones (average of 0.8 percent in siderite-rich sandstones) compared with siderite suggests that the supply of sulfide must have been limited. Because a limitless supply of sulfate existed in the ocean water, there must have been very limited or no diffusion of sulfate from the water column into the pore fluids of the sulfate-reduction zone, perhaps because rapid sedimentation of turbidite packages quickly isolated the sediment from sea water (Curtis and Douglas, 1993). Thus, the volume of pyrite that precipitated may have been limited to the supply of sulfate buried with the sea water in the pores. When all that sulfate was reduced to sulfide, no more pyrite precipitated. In general, rapid sedimentation rates move sediment quickly through a narrow sulfate-reduction

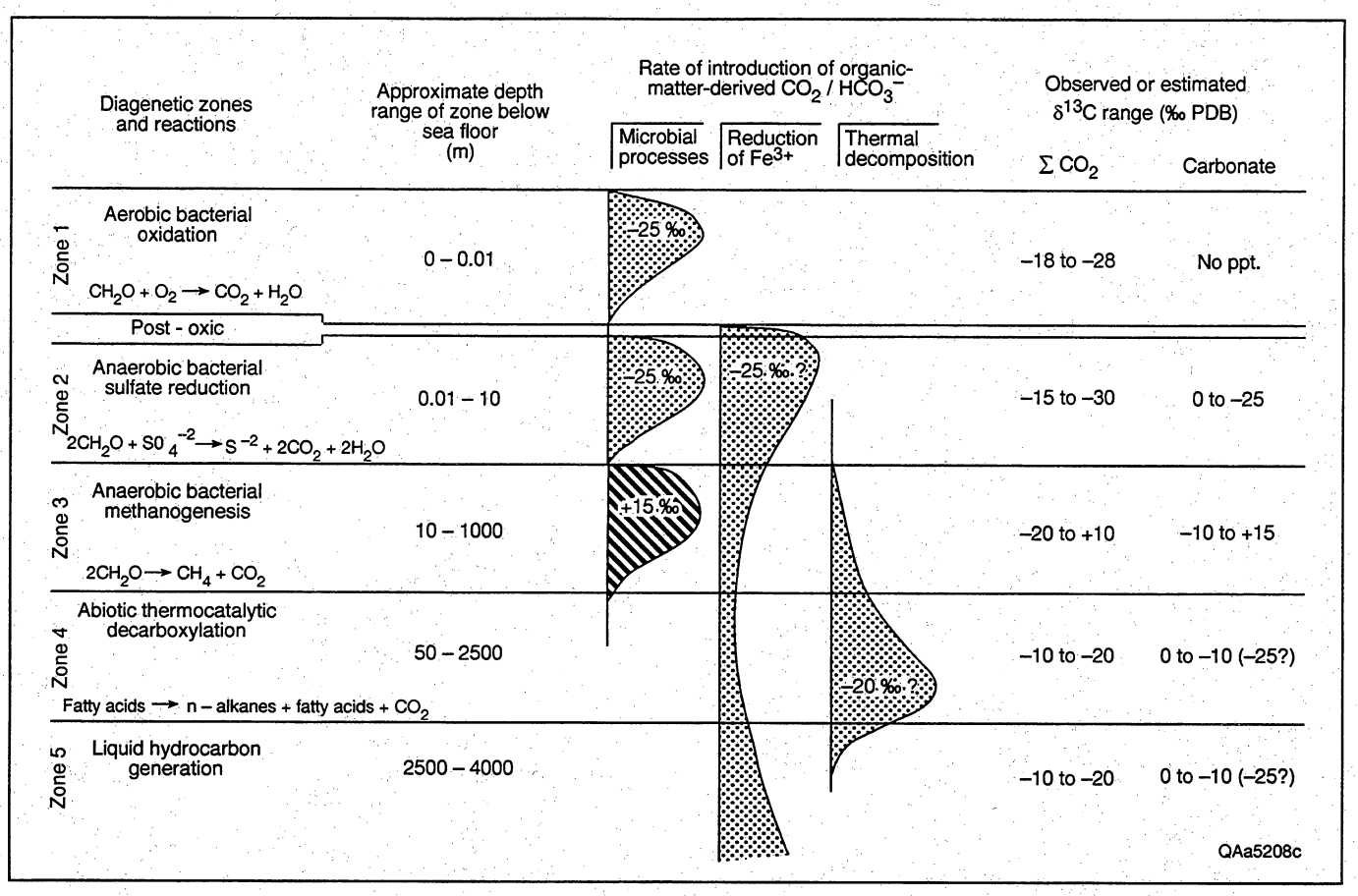

Figure 73. Zones of burial diagenesis of organic matter and resulting range of $\delta^{13}C$ values in dissolved carbon species (ΣCO_2) and of carbonates precipitated in the different zones (after Mack, 1984; modified from Curtis, 1978; Pisciotto, 1981; Garrison; 1981). In this diagram, the post-oxic environment is represented by the narrow band between zones 1 and 2, in which microbial reduction of Fe^{+3} occurs but sulfate reduction has not begun.

zone, seldom more than 3 to 7 ft (1 to 2 m) deep, and into the methanogenesis zone (Curtis, 1986). Thus, rapid sedimentation can limit the amount of pyrite that precipitates in a sediment. An alternative explanation of the low pyrite volume was suggested by Mozley and Carothers (1993), who also observed a paucity of pyrite associated with siderite. Following Berner (1985), they suggested that significant sulfate reduction can occur without the formation of pyrite if H_2S gas escapes from the system.

Once sulfate reduction in the Canyon sandstones ended, the concentration of Fe^{2+} in the pore fluids began to rise because bacterial iron reduction continued (fig. 73) but pyrite precipitation had ended. With sulfate depleted, organic decomposition continued by microbial methanogenesis in reactions of the general form $2CH_2O = CH_4 + CO_2$ (Irwin and others, 1977) (fig. 73). Simultaneous iron reduction increased the pore water alkalinity (Coleman and Raiswell, 1993), so that in the presence of bicarbonate derived from methanogenesis, siderite precipitated.

The siderite has heavy carbon isotope values (average = 2.4 ‰ PDB) because of the fractionation of light carbon into methane and the heavy carbon into CO_2 (Curtis, 1978). The carbon isotopic values of Canyon siderite, however, are not as heavy as the predicted value of +15 ‰ (Curtis, 1978), suggesting that some light carbon from CO_2 produced in the sulfate-reduction zone may also have precipitated in the siderite. There is no evidence for calcite precipitation in the sulfate-reduction zone and thus some of the light CO_2 generated there may have diffused into the underlying methanic zone (Gautier and Claypool, 1984). Claypool and Kaplan (1974) observed that in the early stage of methane production, the $\delta^{13}C$ of dissolved bicarbonate in deep sea sediments most commonly shifts from about -23 ‰ to a moderately heavy +5 ‰. Garrison (1981) and Pisciotto (1981) stated that carbonates that precipitate in the methanogenic zone have $\delta^{13}C$ values ranging from -10 ‰ to +15 ‰ (fig. 8). Finally, Gautier and Claypool (1984, p. 121) noted that carbonates with $\delta^{13}C$ values as high as +15 ‰ are rare and that lower values such as those observed in

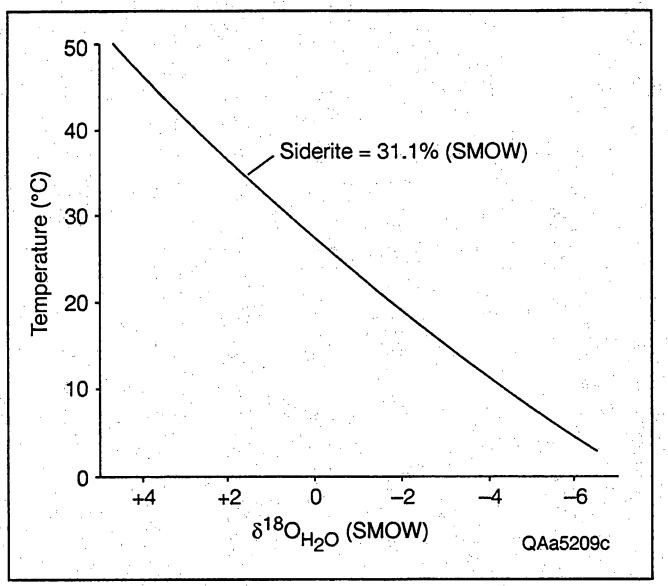

Figure 74. Loci of possible water temperatures and $\delta^{18}O$ compositions that could have precipitated Canyon siderite with the average $\delta^{18}O$ composition of 31.1 ‰ (SMOW). Equation relating temperature, $\delta^{18}O$–water, and $\delta^{18}O$–mineral is: $10^3 \ln a = 3.13 \times 10^6 \times T^{-2} - 3.50$ (Carothers et al., 1988).

Canyon siderite may reflect "some commonly achieved dynamic balance between isotopic fractionation resulting from methane generation and the continued addition of isotopically light carbon through fermentation reactions."

Alternatively, the moderately positive $\delta^{13}C$ isotopic values may reflect a mixture of two generations of siderite that could not be separated when the samples were prepared for isotopic analyses. If some siderite formed in a post-oxic environment, it would be expected to have light carbon values (Maynard, 1982). If that siderite were analyzed along with siderite that formed later in the methanic zone, the resulting $\delta^{13}C$ values would represent a mixture of light carbon from the post-oxic siderite and heavy carbon from methanic siderite. Mozley and Carothers (1992) identified two siderite generations that formed in post-oxic and methanic environments by differences in $\delta^{13}C$ composition and by zonation of siderite crystals that are Fe-rich in the center and Mg-rich along the crystal margins. Zonation in the Canyon siderites has not been observed, but the measured $\delta^{13}C$ isotopic values nevertheless may reflect mixtures of two generations of siderite. However, at least some, if not all, of the siderite must have precipitated in the methanic zone because of the heavy $\delta^{13}C$ values.

Oxygen isotopic composition of the siderite also provides information about the conditions under which it precipitated. The fractionation equation between siderite and water of Carothers and others (1988), $10^3 \ln a = 3.13 \times 10^6 T^{-2} - 3.50$, relates isotopic composition of siderite to the temperature and isotopic composition of the water from which the siderite precipitates. The possible combinations of temperature and water compositions that could have precipitated siderite with the observed average composition of 31.1 ‰ (SMOW) are plotted in figure 68. Assuming that the $\delta^{18}O$ composition of the water from which the siderite precipitated was that of normal sea water, or 0 ‰ (SMOW), the temperature at which the siderite formed was about 81°F (27°C) (fig. 74). Using the present day geothermal gradient of 1.6°F/100 ft (29°C/km) and assuming a temperature of 64°F (18°C) at the sediment-water interface in water depths of about 650 ft (200 m), the siderite would have precipitated at a depth of about 1,000 ft (300 m) below the sea floor. This interpreted depth of siderite precipitation is within the typical depths of the methanic zone, from 30 to 3,300 ft (10 to 1000 m) below the sea floor (Curtis, 1978) (fig. 73). It is also similar to the depth of siderite formation, from about 400 to 3,900 ft (120 to 1,200 m), in Cretaceous and Tertiary sediments on the continental rise off the east coast of the United States (Botz and von Rad, 1987). Thus, Canyon siderites have $\delta^{18}O$ values compatible with precipitation at relatively shallow burial depths from interstitial pore fluids derived from normal sea water. Precipitation of the siderite at 1,000 ft (300 m) is also consistent with the amount of compaction in the siderite-rich zones, based on their minus-cement porosity values of about 33 percent. Experimental work by Pittman and Larese (1991) predicts that well-sorted sandstones with a composition similar to that of the Canyon sandstones would reach a porosity of 33 percent after compaction to about 3,900 ft (1,200 m). A decrease in sorting lowers porosity, thus the moderately sorted Canyon sandstones could have had porosity reduced to 33 percent at shallower depths, possibly by 1,000 ft (300 m).

In contrast to the Canyon siderite, measured $\delta^{18}O$ values for many marine siderites reported in the literature are not compatible with the interpreted low temperature of formation or expected sea-water compositions (Gautier and Claypool, 1984; Mack, 1984; Carpenter and others, 1988; Mozley and Carothers, 1992). Mozley and Carothers (1992) even suggested that anomalously low values of $\delta^{18}O$ are "the norm" for marine siderites. One difference between many of those studies and this one is the water depth at which the sediments containing the siderite were deposited. Most of the formations with the anomalously light $\delta^{18}O$ values, the Gammon Shale (Gautier and Claypool, 1984), Fox Hills Formation (Carpenter and others, 1988), and Kuparuk Formation (Mozley and Carothers, 1992), were deposited in marine shelf environments that could potentially be exposed to meteoric-water incursion during lowstands of sea level.

In contrast, the Canyon sandstone was deposited in considerably deeper water on the slope and basin floor and thus would be highly unlikely to have any exposure to meteoric water. Thus, the commonly observed but anomalously low values of $\delta^{18}O$ in marine siderites may be explained by meteoric water incursion, as each of these authors has suggested. The Canyon sediments were deposited at such great water depths that meteoric water did not penetrate them even during sea level lowstands, and the early siderite cement precipitated from connate, sea-water-derived pore fluids. However, there may be other factors in addition to meteoric-water penetration causing the anomalously light $\delta^{18}O$ values observed in many marine siderites. Siderite in Pennsylvanian submarine fans deposited on the Eastern Shelf of the Midland Basin have anomalously light $\delta^{18}O$ values of -0.1 to -3.2 ‰ (PDB) (Mack, 1984), and early flushing by meteoric water would seem as unlikely in that setting as for the Sonora Canyon submarine fan deposits. One possible hypothesis to explain the commonly observed light $\delta^{18}O$ values in marine siderite could be preferred selection of light oxygen isotopes by bacteria and subsequent incorporation of those isotopes into siderite.

Siderite Distribution in Canyon Sandstones

The factors that controlled the particular location of siderite layers and patches in Canyon sandstones are unclear. The horizontal layers of siderite may correspond to horizons in the sediment where iron-reducing bacteria were particularly abundant, and patches of siderite may arise from bacteria flourishing at a point in the sediment, which triggered precipitation of siderite spherically around that point. Work on siderite concretions in salt-marsh sediments has shown that microbial populations are not homogeneously distributed, and siderite concretions form in association with localized microbial populations (Coleman, 1993). It is not known, however, why the bacteria flourished in those particular layers or spots in the Canyon sandstone. Because the grain size and sorting of the siderite-rich zones are the same as the siderite-poor zones, there does not appear to be a textural control on the distribution of the siderite layers. The amount of organic matter apparently does not control the location of the siderite layers either. One might expect sulfate reduction and methanogenesis to be most extensive in organic-rich intervals, which would then develop the most abundant siderite, but instead siderite-rich zones contain less organic matter than do siderite-poor zones (table 4). One possibility is that the siderite-rich zones used to contain more organic matter, but it was consumed by bacteria during the methanogenesis reactions that led to siderite precipitation. However, the general paucity of organic matter in Bouma A divisions in Canyon core suggests that, for some reason, the siderite developed preferentially in organic-poor zones. The explanation for this may not lie in the amount of organic matter, but in another factor that is correlated negatively to organic matter. For example, variations in the amount of oxidized iron available to bacteria for reduction would influence the location of siderite layers (Coleman, 1993), and oxidized iron should be most abundant in organic-poor sediments.

An additional control on the location and spacing of siderite layers may have been the distance over which diffusion was effective in the sediments. For example, if iron-reducing bacteria flourished in a layer with abundant oxidized iron and triggered the precipitation of siderite, the pore fluids in that immediate layer would become depleted in bicarbonate. Bicarbonate generated by microbial methanogenesis in the surrounding sediment would then diffuse through the pore fluids to that layer, where it would encounter the high iron concentration from continued microbial iron reduction and precipitate as siderite. Siderite layers are rarely more than 6 in (15 cm) thick, and they are generally spaced at least 4 inches (10 cm) apart. Both the thickness and the spacing between layers may reflect the distance over which bicarbonate could diffuse to supply ions for siderite precipitation.

Reservoir Quality

The location of siderite-rich zones in the Canyon sandstone has economic importance because the National Petroleum Council (1980) reported that the highest porosity in Canyon sandstones occurs in association with abundant siderite. Data from the two wells in this study support this observation. Siderite-rich sandstones have an average of 1.5 percent primary porosity measured in thin section, whereas siderite-poor sandstones have an average of 0.4 percent primary porosity (table 4). Average porosimeter porosity of siderite-rich sandstones is 7.9 percent, compared with 6.4 percent in siderite-poor sandstones (table 4).

Siderite-cemented Canyon sandstones also have higher permeability than do sandstones without siderite, as previously noted by the National Petroleum Council (1980), Berg (1986), and Huang (1989), although they presented no supporting data. Siderite-rich sandstones in this study have geometric mean permeability of 0.042 md, compared with siderite-poor sandstones with mean permeability of 0.006 md (table 4). Similarly, the range of permeability is higher in siderite-rich than in siderite-poor sandstones (0.009 to 0.592 md versus 0.002 to 0.168 md, respectively; permeability measurements were made at calculated in-situ overburden pressure). Therefore, core-analysis data from this study confirm that

the best matrix reservoir quality in Canyon sandstones apparently occurs in siderite-cemented zones.

On the basis of petrographic evidence, it appears that siderite-cemented sandstones have the highest remaining porosity because they lost less intergranular porosity by compaction and quartz cementation than did sandstones without siderite. Siderite formed before significant burial occurred and provided siderite-cemented sandstones with a rigid framework, so that loss of porosity by mechanical compaction during burial was arrested. Sandstones with little siderite cement lacked this rigid framework and thus were more intensely compacted during burial. Average minus-cement porosity, a measure of the amount of porosity remaining after compaction (Rosenfeld, 1949), is 33 percent in siderite-rich sandstones, compared with 16 percent in siderite-poor sandstones (table 4). Assuming the Canyon sandstones had porosity of about 40 percent at the time of deposition, siderite-rich sandstones lost only 7 percent porosity by compaction, but siderite-poor sandstones lost considerably more porosity, an average of 24 percent, by compaction. Furthermore, as previously noted by Berg (1986) and Huang (1989), thick coats of siderite around detrital quartz grains inhibited some later nucleation of quartz cement (fig. 71), thus preserving primary intergranular porosity. Siderite-rich sandstones contain an average of 6 percent quartz cement, but siderite-poor sandstones contain an average of 11 percent quartz cement (fig. 70). Therefore, even though the siderite itself fills primary porosity, the overall effect of the siderite is to preserve porosity.

Conclusions: Sonora Diagenesis

Siderite cementation was a major diagenetic modification of Sonora Canyon sandstones, which were deposited in submarine fans on the slope and basin floor along the northeastern margin of the Val Verde Basin. Siderite precipitated fairly soon after deposition, at depths of about 1,000 ft (300 m) and temperatures of about 81°F (27°C) from connate, sea-water-derived pore fluids having oxygen isotopic composition of 0 ‰ (SMOW). The siderite formed in a methanic geochemical environment in which bacterial processes controlled the chemistry of the pore fluids by organic matter decomposition. Siderite layers and patches developed preferentially in organic-poor, Bouma A divisions of turbidites. The main control on the location of siderite layers probably was availability of oxidized iron. Once iron-reducing bacteria became established in a layer or spot and precipitation of siderite began, diffusion of bicarbonate from the surrounding sediment caused siderite precipitation to continue in that zone.

Siderite-rich layers retain the highest porosity and permeability in the overall low-permeability Canyon sandstones. Early siderite cementation preserved some intergranular porosity by inhibiting mechanical compaction and precipitation of quartz cement. Currently, siderite-cemented areas cannot routinely be recognized on well logs. Development of the techniques or tools to do so would aid Canyon development.

Natural Fractures in Sonora Canyon Sandstones

S. E. Laubach, B. A. Marin

Natural fractures are widespread in Sonora Canyon sandstones in Sutton County, Texas. Data obtained from three cored wells through a cooperative research program conducted by the Gas Research Institute and industry show that at least two distinct vertical opening-mode (joint/vein) classes coexist that have contrasting distributions, characteristic sizes, and/or mineral fills. The most abundant fracture class in core consists of generally small (less than 1 ft vertical extent) clay- or clay- and carbonate mineral-filled opening mode fractures existing only in siderite-cemented zones in sandstones. Another fracture class—characterized by greater fracture size and spacing and carbonate- and/or quartz mineralization—may be as widespread but is underrepresented in core due to sampling bias. Owing to their clay content, some fractures in siderite layers locally may be barriers to fluid flow and their presence could cause reservoir heterogeneity and anisotropy if permeable siderite layers are the flow units that dominate overall Sonora Canyon reservoir flow behavior. Carbonate- and quartz-lined fractures are larger (greater vertical extent) than those in siderite layers and are partly open. Closure of these fractures owing to changes in effective reservoir stress would be inhibited by fracture-bridging minerals.

These observations show that fractures in Sonora Canyon sandstones should be considered in completion and stimulation design. Quartz- and carbonate-lined fractures are potential targets for directional drilling. High treatment pressures observed in some Canyon Sandstone stimulations may be due to natural fractures promoting near-wellbore propagation of multiple fracture strands leading to fracture tortuosity. Inconsistencies between hydraulic fracture strike and maximum horizontal stress may be due to natural fractures guiding hydraulic fracture growth. Considerations of fracture-fill paragenesis suggests that some flow pathways in Canyon natural fracture networks may be susceptible to improvement (increased interconnection) by acid treatment, although this approach remains to be tested.

Why Natural Fractures are Important

In rock having low matrix permeability, natural fractures can significantly affect reservoir properties and the success of gas exploration and development. Open fractures can enhance and filled fractures can impede fluid flow, and fractures in many cases produce anisotropic and heterogeneous rock permeability. When hydraulic fracture treatments are performed to stimulate gas reservoirs, natural fractures can cause high treatment pressures by promoting development of multiple fracture branches near the wellbore (near-wellbore tortuosity) that impedes movement of fracture fluids and proppant. Because they are commonly planes of low tensile strength, natural fractures can also cause treatment fractures to grow in a direction that differs from that predicted from analysis of principal stress directions. This can be a key consideration where permeability anisotropy or interwell communication is important for engineering assessment or where closely spaced wells (100–1,000 ft interwell distance) are being fracture stimulated. For these reasons the presence and attributes of natural fractures may be important factors to take into account in exploration, development, and well completion and stimulation design.

Prior to this study, natural fractures in Canyon sandstones had not been described in the literature. Our preliminary observations on fractures in Sonora Canyon sandstones were reported at the SPE Rocky Mountain Regional/Low Permeability Reservoir Symposium (Marin and others, 1993). We document the occurrence and attributes of natural fractures Sonora Canyon core from 3 wells (fig. 75). Maps showing the occurrence of all fractures in core is our basic data set. Typical maps are illustrated in figures 76 through 80.

In Situ Stress

Where natural fractures are key reservoir elements, knowledge of in situ stress conditions is needed because subsurface fracture and fracture network properties are potentially susceptible to alteration as a result of ambient or changing effective stress. In situ stress measurements in the Phillips Ward "C" No. 11 and Enron Sawyer "A" 144 No. 5 wells indicate stress gradients of 0.61 to 0.65 psi/ft in sandstone and 0.73 to 0.83 psi/ft in shale (Miller and others, 1991). A typical Canyon stress profile from is shown in Dutton and others (1993).

The orientation of maximum horizontal compressive stress (SHmax) was studied by measuring the direction

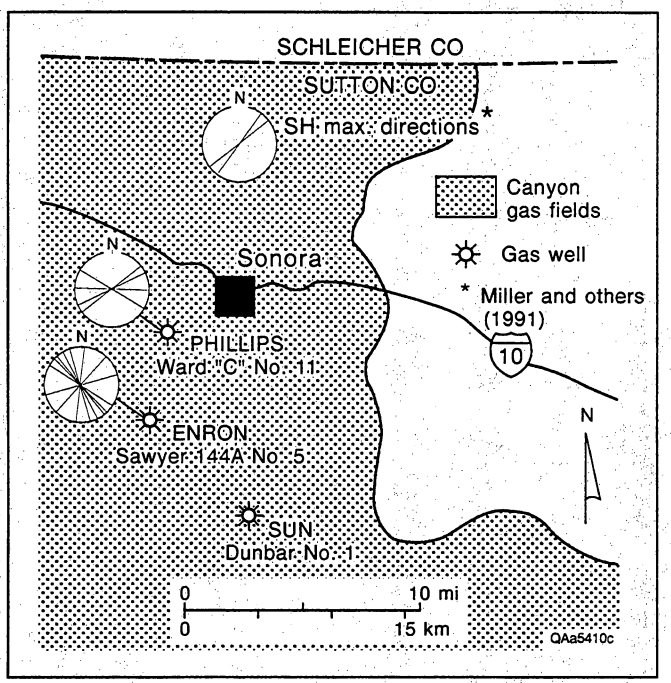

Figure 75. Location of Phillips Ward "C" No. 11, Enron Oil & Gas Sawyer "A" 144 No. 5, and Sun Oil Co. Dunbar No. 1 wells in Val Verde Basin; 842.5 ft of core from these wells contained 191 natural fractures and evidence for a link between diagenesis and fracturing that was used to predict fracture occurrence and attributes.

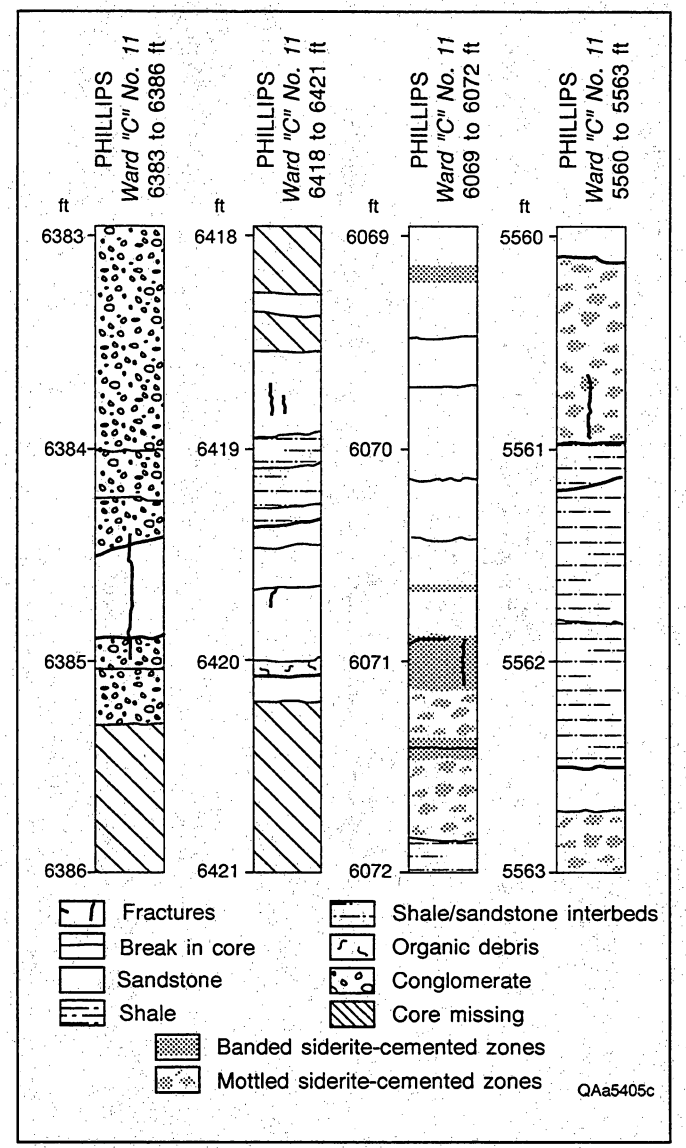

Figure 76. Fractures in Sonora Canyon Sandstone core, Phillips Ward "C" No. 11. Maps show fracture traces, rock types, and location of siderite-cemented zones. A quartz-lined fracture occurs at -6384.5 ft.

of anelastic core strain relaxation (ASR) and the strike of fractures induced by both stress tests and drilling (Miller and others, 1991). ASR results were inconclusive, but induced fracture strikes in core and visible on logs indicate SHmax trends north-northeastward (approximately 035 degrees), broadly consistent with SHmax from wellbore breakout directions (SHmax = 046 degrees) in the Sawyer "A" 144 No. 5 well and results of regional studies (Zoback and Zoback, 1989). Monitoring of microseismic signals from hydraulic fracture treatments in the Ward "C" No. 11 well suggests that a stimulation fracture grew east-northeastward (085 degrees), an orientation significantly different from measured SHmax directions.

Fracture Description

Figure 75 shows the location of three study wells: (1) the Phillips Ward "C" No. 11 well, in which 204 ft of core was obtained in 1990; (2) the Enron Oil & Gas Sawyer "A" 144 No. 5 well, in which 281.5 ft of core was obtained in 1990; and (3) the Sun Oil Company Dunbar No. 1, in which 357 ft of core was obtained in 1959. The amount of sandstone in these three cores is 92 ft, 128 ft, and 215 ft, respectively.

Natural and drilling-induced fractures are present in all three Sonora Canyon cores. Natural fractures were distinguished from drilling-induced fractures by the presence of vein-filling minerals in natural fractures and by surface marks and distinctive shapes (such as downward-steepening profiles of petal-centerline fractures) that are typical of drilling-induced fractures. Standard criteria used to identify drilling-induced fractures are described by Kulander and others (1990). Natural fractures are also predominantly intragranular, whereas various types of fractures induced in the coring process are typically transgranular. Not all natural fractures contain infilling minerals that are readily apparent, and

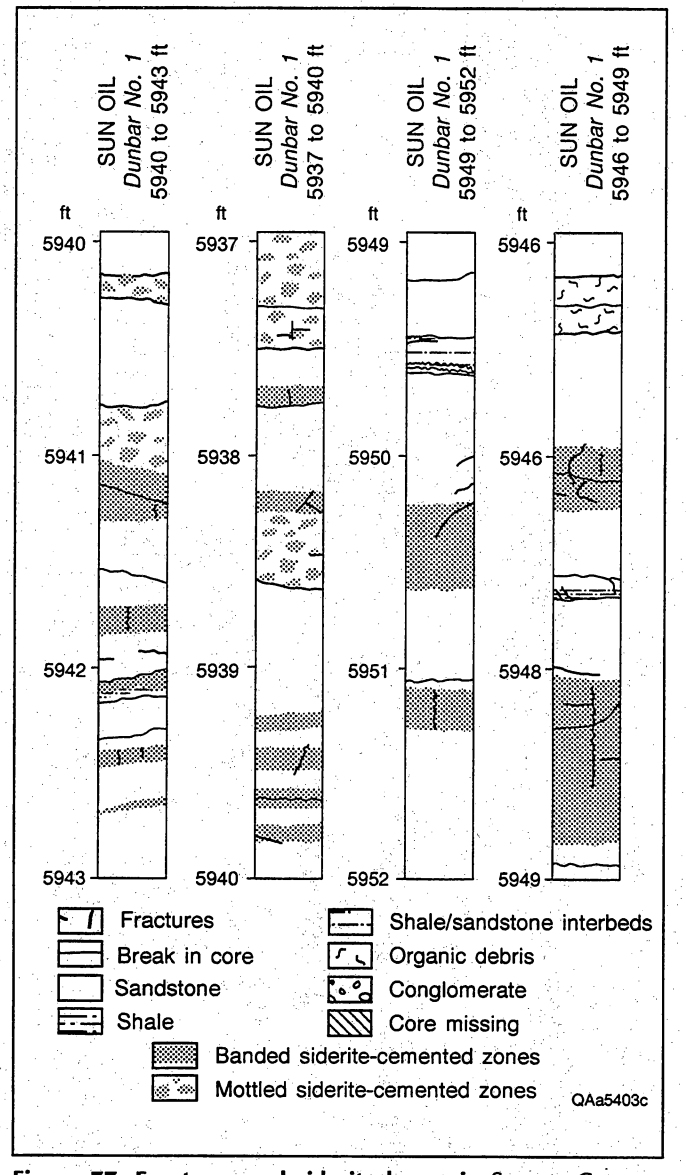

Figure 77. Fractures and siderite layers in Sonora Canyon Sandstone core, Sun Dunbar No. 1. Maps show fracture traces, rock types, and location of siderite-cemented zones. Note fractures localized in siderite layers.

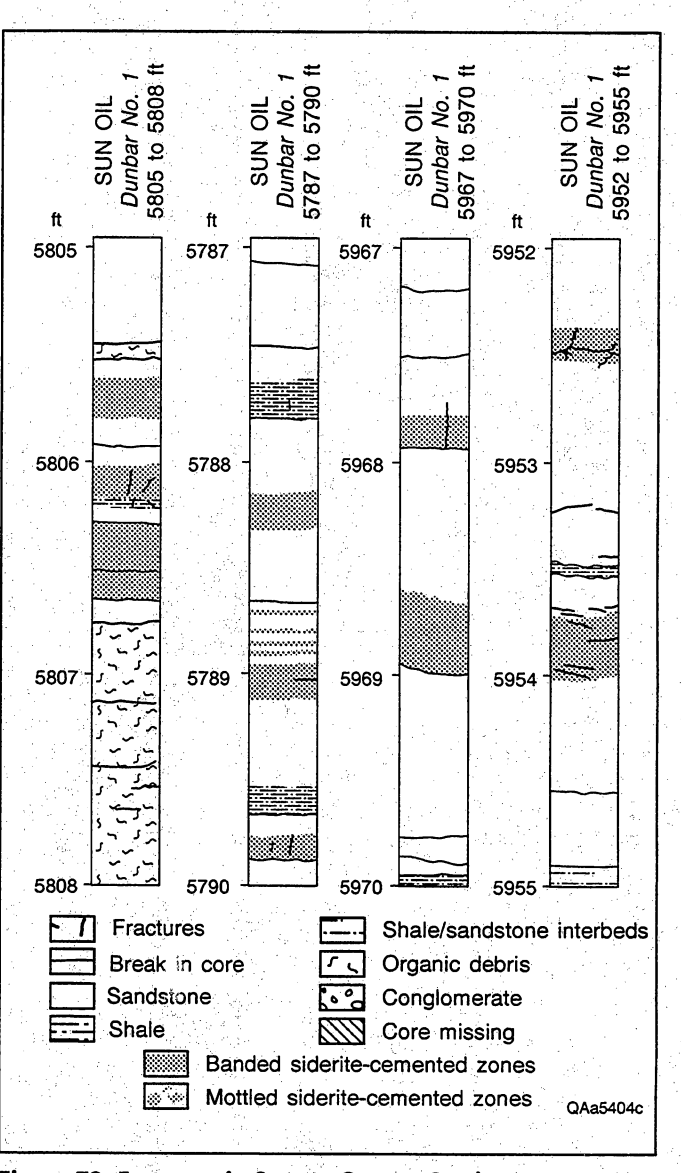

Figure 78. Fractures in Sonora Canyon Sandstone core, Sun Dunbar No. 1. Maps show fracture traces, rock types, and location of siderite-cemented zones. Note that some fractures in siderite layers do not extend across entire layer.

some induced fractures lack distinctive surface marks and shapes, so the classification of a few fractures is uncertain. More than 200 drilling-induced fractures were logged in the three cores, of which 22 are petal-centerline fractures.

General Attributes

Abundance of natural fractures is high; 191 fractures are present in 842.5 ft of core, with most of the natural fractures confined to sandstones (435 ft of core). A few fractures are evident on Formation Microscanner (FMS) logs, but fracture abundance from these logs may be biased because fractures less than a few inches long can easily be missed on images and some fractures in core that likely extended into the borehole wall are not visible on logs. In this case the FMS log was not as reliable a guide to natural fracture abundance as was core.

As described below, core observations and petrographic data show that many fractures have preserved primary fracture porosity, as described below. Moreover, a Repeat Formation Tester (RFT) log in the Ward "C" No. 11 well recorded an instant pressure buildup (R. E. Peterson, personal communication, 1992)

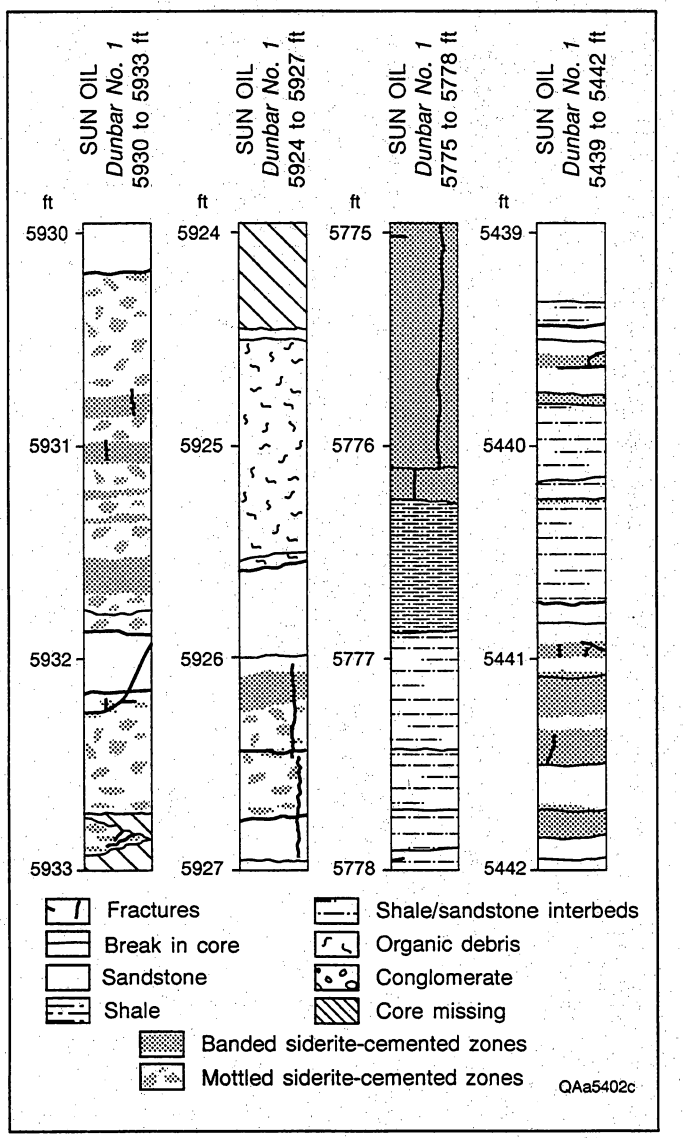

Figure 79. Long fracture in thick siderite layer, Sonora Canyon Sandstone core, Sun Dunbar No. 1. Maps show fracture traces, rock types, and location of siderite-cemented zones.

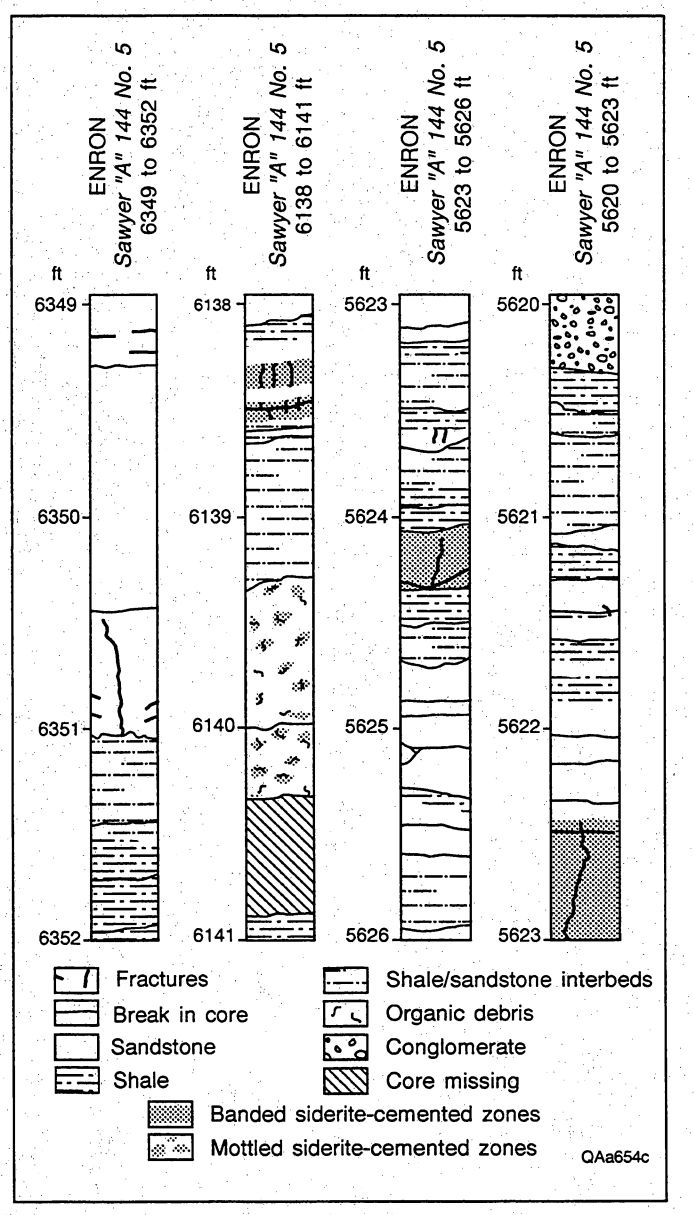

Figure 80. Fractures in Sonora Canyon Sandstone core, Enron Sawyer "A" 144 No. 5. Maps show fracture traces, rock types, and location of siderite-cemented zones.

when a test was conducted over a natural fracture at 6,384.7 ft, indicating that the fracture is permeable. Other indicators that some fractures are open or can transmit fluid, such as lost circulation and instantaneous mud loss while drilling, have not been reported by operators. Monitoring mud loss while drilling could be a useful method for delineating areas having conductive fractures.

Natural fractures in the Canyon Sandstone are primarily vertical to subvertical opening-mode fractures (figs. 76 through 81). A few fractures have gentle dips (less than 10 degrees) and some moderately to gently dipping fractures having striated surfaces are localized in mudstone beds and probably are laterally discontinuous faults caused by burial and consolidation. The latter fracture type is particularly common in Sun Dunbar No. 1 core in shale and debris-flow intervals with mudstone matrix at depths of 5,810 to 5,811 ft and 6,018 to 6,020 ft, but these fractures are the least likely to influence gas production since they are completely closed. We therefore focus our description on the vertical and subvertical opening-mode fractures.

Widths of fractures are generally less than 0.35 mm (fig. 82). Average fracture width is 0.17 mm, and maximum and minimum fracture widths are 0.4 mm and 0.06 mm, respectively. Open fracture porosity is marked by fractures that are lined by faceted crystals. There is

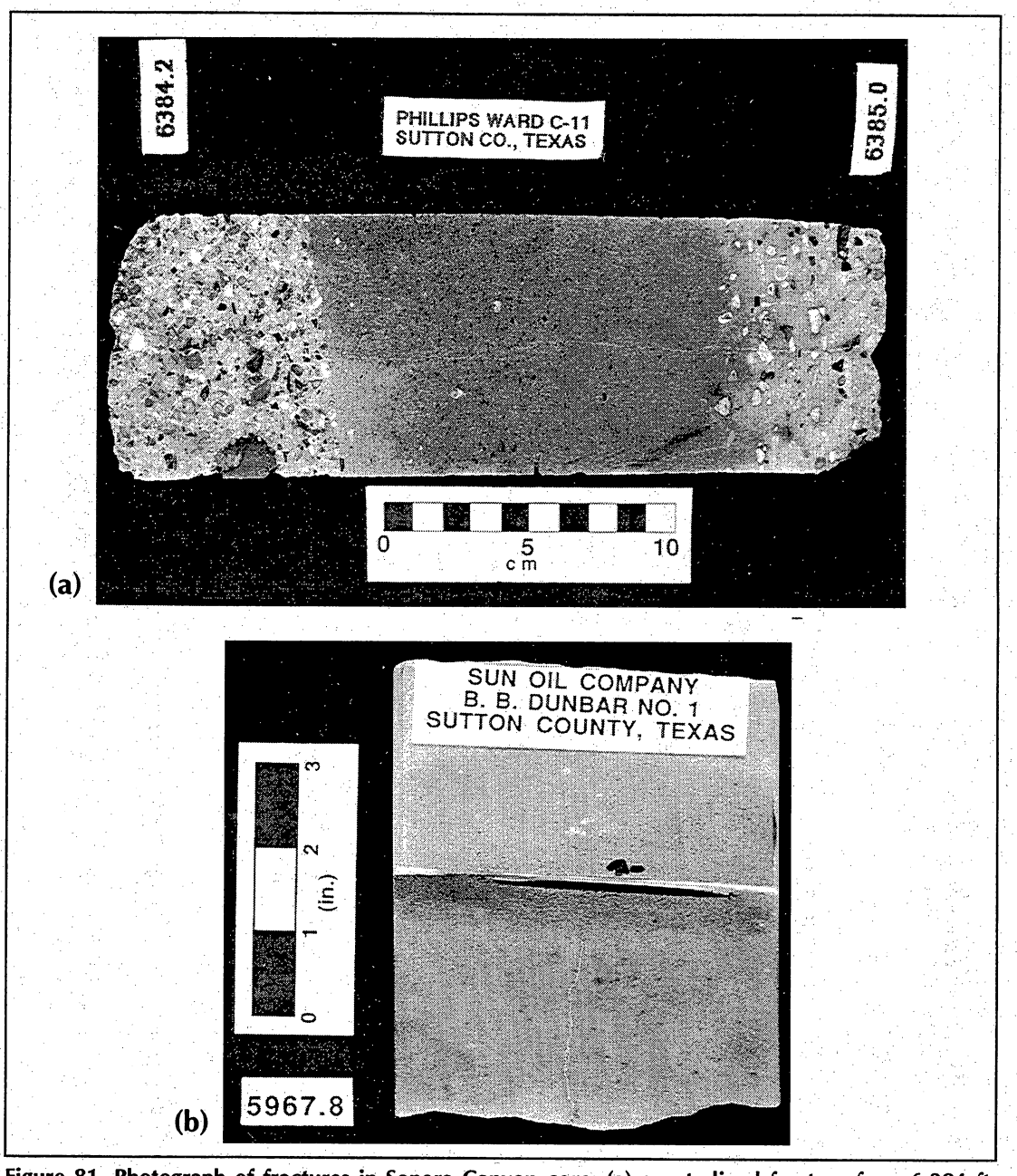

Figure 81. Photograph of fractures in Sonora Canyon core: (a) quartz-lined fracture from 6,384 ft, Phillips Ward "C" No. 11, (b) fracture in siderite layer, 5,967.8 ft, Sun Dunbar No. 1.

little difference between widths of open and filled fractures, and the range of fracture apertures is similar for the three wells. No trends are apparent in fracture width with depth or with stratigraphic position. Although many fractures are completely or nearly completely filled, the amount of fracture fill varies sharply along some fracture traces, and open fractures grade laterally into filled fractures over distances of as little as 1 mm. The pattern of mineral fill in these fractures shows that the assumption commonly made in modeling fluid flow in fractures—namely that fracture porosity can be approximated as a persistent parallel-sided slot—is far from being satisfied in this case.

The main fracture-filling minerals are quartz, a carbonate mineral (calcite; possibly some ankerite) and the clay mineral dickite. Carbonate minerals and dickite are the most abundant fracture filling minerals, but they rarely occur together in the same fracture. Quartz forms a volumetrically minor component; where present it typically is an inconspicuous veneer on fracture walls.

In Canyon sandstones, most natural fractures are short (less than 3 inches tall) and vertically discontinuous, but

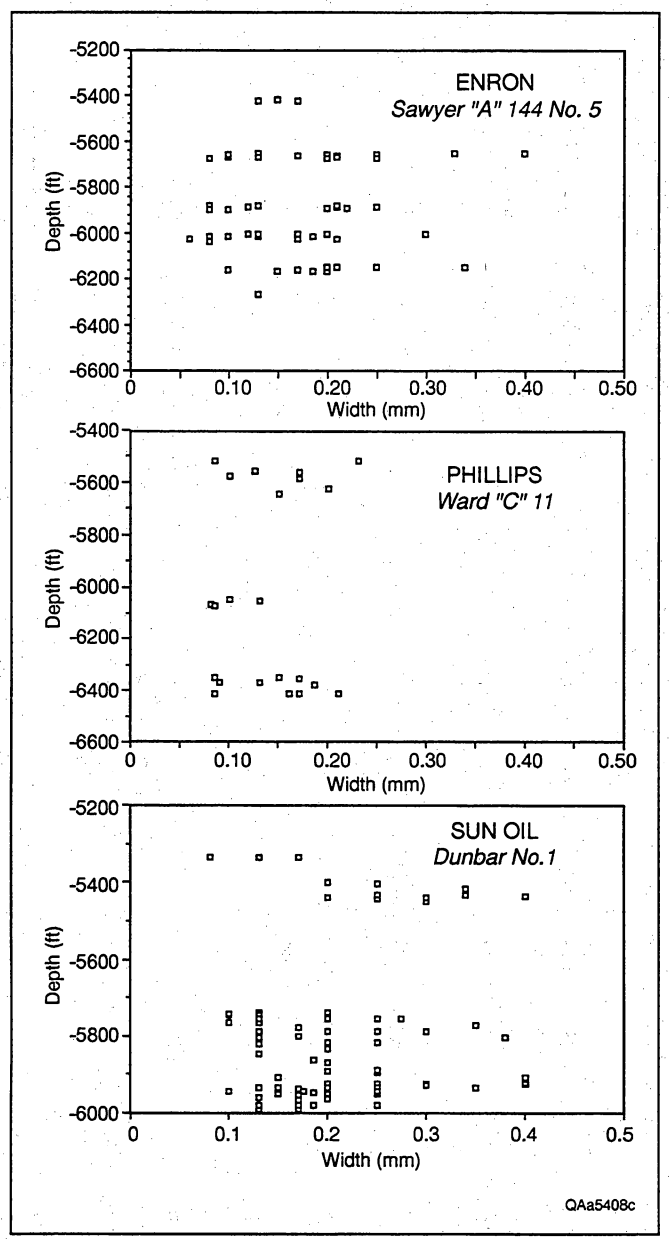

Figure 82. Fracture width versus depth for three Canyon Sandstone wells.

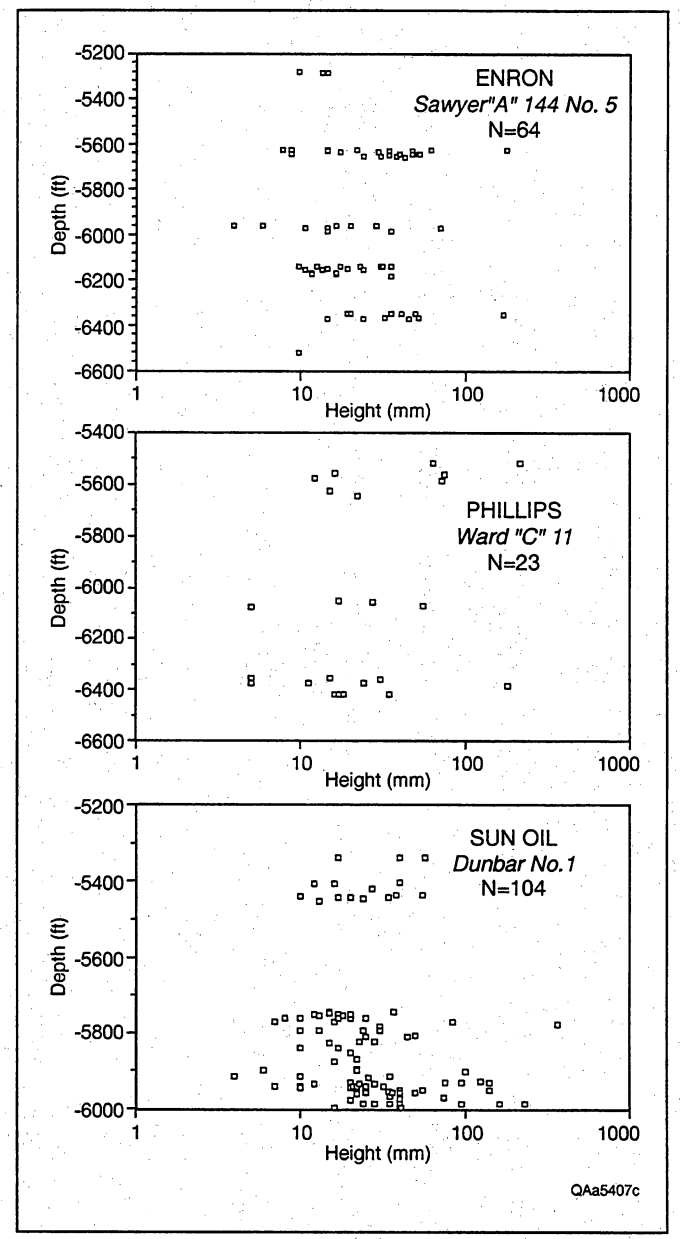

Figure 83. Fracture height versus depth for three Canyon Sandstone wells.

a few fractures have heights of greater than 1 ft (figs. 83 and 84). The range of fracture heights is similar for all cores, and no trends are evident in fracture height with depth. Fractures generally end by intersecting shale interbeds or at gradually tapering blind terminations within sandstone. Some fractures are confined to zones of diagenetic alteration, as will be described herein, and these fractures terminate at or near the abrupt margins of cemented zones. Fractures in sandstone also commonly end at mudstone interbeds. In core, fractures rarely intersect fractures above or below them. These observations, combined with termination of fractures at bed boundaries, suggest that fractures do not form interconnected networks from the top to the base of sandstone beds. Based on core observations, interconnected networks, if they exist at all, are likely to exist only within individual sandstones or parts of sandstones.

Table 6 and figure 85 summarize natural fracture orientations (strike). In the Ward "C" No. 11 and Sawyer "A" 144 No. 5 wells, some core was oriented by using downhole methods and comparing features in core to

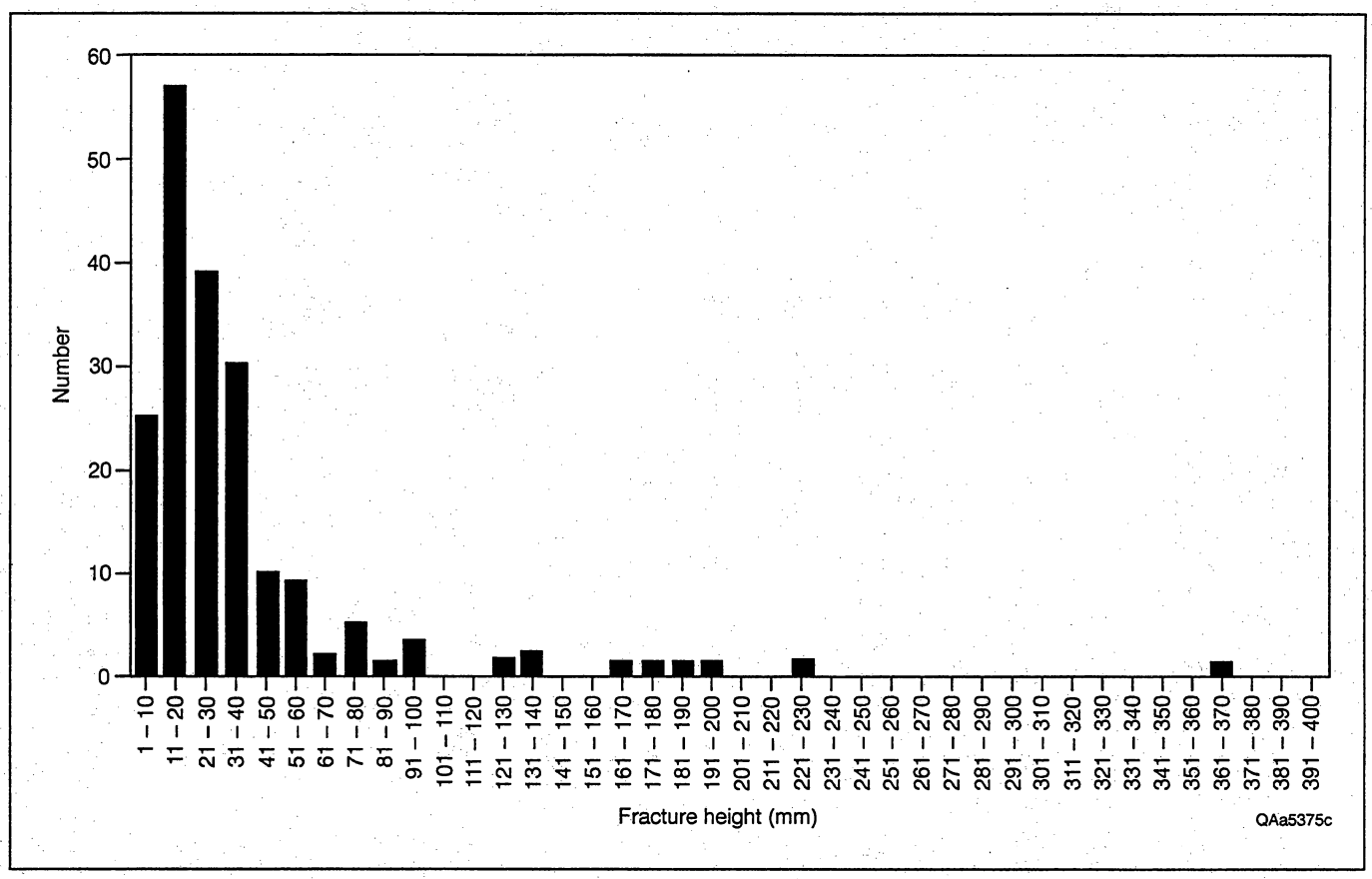

Figure 84. Histogram of fracture heights for fractures in siderite-cemented zones.

oriented borehole images from FMS logs. Fractures in the Ward "C" No. 11 well strike northeastward and northwestward. In the Sawyer "A" 144 No. 5 well, five fractures strike northwestward, two strike northeastward, and one strikes east-northeastward. In this well four fractures visible only on FMS images and interpreted to be natural fractures strike northwestward (mean strike 319 degrees).

A range of natural fracture orientations in Canyon sandstones is confirmed by inspecting fractures in intact sections of core. In the Ward "C" No. 11 well, two fractures in the same core interval differ in strike by 12 degrees (strikes of 244 degrees and 232 degrees). In Sawyer "A" 144 No. 5 core, three fractures in the same core interval have strikes of 006 degrees, 165 degrees, and 074 degrees, indicating that fractures are present that are oriented at nearly right angles. Four oriented fractures in core from this well are in a continuous core interval and have differences in strikes ranging from 12 degrees to 71 degrees. In a single shale layer two fractures in this well have strikes that differ by 30 degrees. The wide dispersion in fracture strikes shown in table 6 therefore cannot result entirely from core orientation errors.

Because lateral intersections of vertical fractures are rarely seen in core, evidence is sparse for estimating the relative age of fractures on the basis of abutting and crossing relations. One fracture in the Sawyer "A" 144 No. 5 core (strike 044 degrees) crosscuts an older clay-filled fracture (strike 136 degrees), showing that fractures of more than one age are present. The observed dispersion in fracture strike and evidence for more than one generation of fractures precludes identifying a dominant fracture orientation from this data set. Because they strike parallel to SHmax, fractures having east-northeast or northeast strikes are most prone to be open in the subsurface on the basis of subsurface loading conditions.

Fracture spacing is challenging to quantify with vertical core in the Canyon Sandstone because fracture dip is subparallel to the core axis and in most cases spacing of fractures is greater than the wellbore diameter. The only direct evidence for systematic spacing in Canyon Sandstones where more than one fracture is present; this is observed only in thin beds, where fractures are short (less than 4 inches [10.2 cm] about equal to the diameter of the core). For example, in the Sawyer "A" 144 No. 5 core, fracture spacing in siderite-cemented layers is

Table 6. Fracture orientations from core data.

PHILLIPS Ward "C" No. 11 Fracture No.	Depth (ft)	Azimuth	Comments
N-16	5646.75	300	1
N-20	5560.80	091	1
N-22	5516.65	244	1, 3
N-23	5515.68	232	1, 3

ENRON Sawyer "A" No. 144-5 Fracture No.	Depth (ft)	Azimuth	Comments
N-33	5969.93	006	1
N-34	5968.78	165	1
N-35	5968.72	074	1
N-36	5960.30	141	1, 4
N-38	5958.08	123	2
N-39	5958.08	153	2
N-40	5957.35	044	1
NI-1	5957.35	044	5

Comments

1. Fracture in siderite-cemented layers
2. Fracture in shale
3. Fracture in same cored interval
4. Orientation uncertain
5. Possibly a drilling-induced fracture

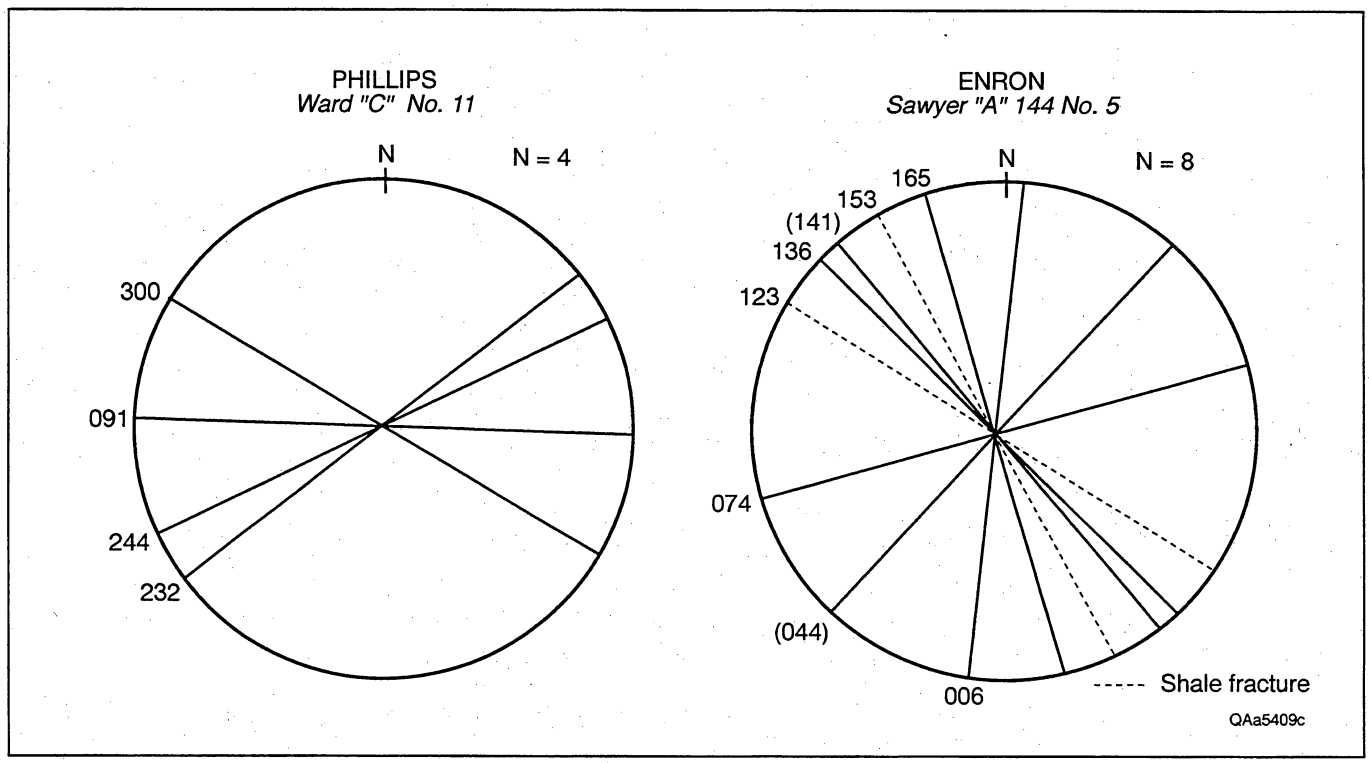

Figure 85. Natural fracture strikes in Phillips Ward "C" No. 11 and Enron Sawyer "A" 144 No. 5 core.

Table 7. Summary of fracture class attributes.

	Fractures in quartz- and calcite-cemented layers Class I	Fractures in siderite-cemented layers Class II
Height	Many >10 inches tall	10 inches tall (average)
Aspect ratio	Tall and narrow	Short and wide
Visible porosity	Common	Rare
Mineral fill	Quartz; followed by ankerite in some cases. A few fractures lack early quartz.	Clay minerals (dickite); some later calcite
Roughness	Fairly smooth walls	Rough, irregular walls
Occurrence	Cross zones of various cement types	Confined to siderite cemented zones

16 mm in a layer 30.5 mm thick and 23 mm in a layer 36.5 mm thick. Fracture spacing in mudstone beds is highly variable; in one example spacing is 21 mm in a bed 27.9 mm thick.

The spacing of larger fractures can only be inferred, and the possibility that fractures are arranged in swarms or other patterns rather than in evenly spaced sets cannot be ruled out. Even spacing for some closely spaced small fractures is consistent with fractures being arranged in sets having regular patterns of spacing and orientation. Evidence that siderite-cemented layers typically contain fractures and have a fracture stratigraphy and decreasing abundance of fractures with increasing mechanically significant bed thickness suggests that a relationship between systematic fracture spacing and bed thickness exists for siderite-cemented layers.

Fracture Classes

Opening-mode fractures in Sonora Canyon core can be separated into at least two categories. We informally designate these categories as fracture classes rather than fracture sets, because we were able to determine fracture orientations or relative ages for only a few fractures. Fractures in the two classes have contrasting distributions, characteristic sizes, and/or mineral fills (table 7). It is likely that they also are of different ages and have contrasting patterns of orientation.

Fractures Predominantly in Quartz-Cemented Zones

The first fracture class in Canyon Sandstone cores are carbonate- and quartz-filled fractures that lack dickite and that typically are predominantly in quartz-cemented zones, but these fractures are not confined to layers that have a particular cement type. Most commonly, these fractures are observed in areas having moderate to extensive quartz and carbonate cement. Fractures in this class could be separated into two classes based on mineral composition of vein fill as we initially did (Marin and others, 1993), but because of the small number of fractures involved and the variability in vein-filling mineral paragenesis this distinction may not be useful. This fracture class exists in all three wells. Unlike fractures within siderite-cemented layers (described below), these fractures cross sandstone containing various cement types. Tall fractures within this class locally cross shale interbeds. These fractures are generally taller and tend to have somewhat greater height-to-width ratios than fractures in siderite layers. Both carbonate- and quartz-filled fractures are typically smooth-sided with smoothly curved to planar walls, in contrast to rough-walled fractures characteristic of many siderite-cemented layers. Nevertheless, intragranular fracture pathways characterize these fractures and distinguish them from fractures created by drilling and coring processes and fractures created in laboratory tests of these sandstones (Baek and Laubach, this volume).

Quartz- or carbonate-filled fractures are far less common (n=48) than those in siderite-cemented layers (n=116). In the 3 wells there are 40 quartz-filled fractures and 8 carbonate-filled fractures. Quartz-filled fractures range in height from 5 to 230 mm, and calcite-filled fractures range from 11 to 368 mm. This range of measured fracture heights probably underestimates fracture size for these classes of fracture because many do not end within core. From the observation that these fractures end at shale interbeds or at other major changes in rock type (figs. 76 through 80), rather than at boundaries between rock having contrasting cement types, we infer that fracture heights for this class of fracture are most likely comparable to sandstone bed thicknesses. Carbonate- or quartz-filled fractures rarely contain both minerals, and where both are present, quartz is the first phase to have precipitated.

Quartz fracture-fill mineralization is typically manifested as a thin (less than 0.5 mm) veneer of faceted or subhedral growth on broken or intact (more common) grains on fracture walls. Intact quartz bridging and occluding fracture porosity can be present at any point along fractures, but in our samples is most readily observed near fracture terminations. Locally, fracture-filling quartz displays parallel planes of minute fluid-filled cavities that we interpret to be traces of healed or sealed fractures ("crack-seal" microstructure). Such features may result from the process of fracture propagation (opening) during quartz precipitation. Similar features are common in quartz-cemented Cretaceous Travis Peak Formation tight sandstones in East Texas (Laubach, 1988).

Isolated fluid-inclusion planes, representing micron- to millimeter-scale healed or sealed fractures are also evident in Sonora Canyon sandstones (fig. 86). As is the case for similar features in Travis Peak sandstones (Laubach, 1989b) these healed microfractures are more common near large (macroscopic) features. Post-depositional microfracture strikes are in many cases subparallel to macrofracture orientation. While they are unlikely to have any influence on the physical properties of the sandstone that contains them, these features are potentially useful as guides to macroscopic fracture orientation if they occur in oriented core.

Calcite in carbonate-lined and filled fractures typically is massive and, locally, twinned and fractured. Texture of vein-filling calcite suggests that several phases of carbonate fill may have been precipitated in these fractures (fig. 87). The overall pattern of vein carbonate precipitation may not have been uniform throughout the Sonora Canyon, but from the wells in our study the following sequence of events is evident. The earliest phase of calcite in fractures is found overgrowing fracture-fill quartz, and this generation of calcite was precipitated in fractures that did not break (cross cut) quartz cement—we infer that if filled in pre-existing open quartz-lined fractures. Locally, isolated calcite crystal-lined pores existed along these fractures after the first generation of calcite vein fill was deposited. Horizontal stylolites, small fractures, and twin lamellae are evident in a few samples of this older generation of vein carbonate. Much of the fracture porosity in the older fracture-lining calcite was filled by a texturally younger phase of carbonate (locally, ankerite). In some cases this younger carbonate generation is associated with short horizontal carbonate-filled fractures emanating from the vertical fractures. These horizontal fracture segments may be indicative to fracturing at shallow depths (possibly less than 1 km) where fractures could open against the load of overlying rock.

A few fractures have only one generation of infilling carbonate that we interpret to be equivalent to the younger generation of vein fill because these fractures

Figure 86. Fluid-inclusion planes (healed microfractures), Sun Dunbar No. 1, depth 5,335 ft. Bar = 0.01 mm.

crosscut quartz cement (fig. 88). These textural relations suggest that two episodes of fracture growth occurred while carbonate minerals were precipitating in these sandstones.

Primary fracture porosity is preserved along both quartz- and carbonate-filled fractures. Visual inspection of fracture traces on core edges suggests that quartz-lined fractures have the greatest preserved porosity (locally as much as 75 percent). In the Ward "C" No. 11 well, an RFT log recorded an instant pressure buildup when a test was conducted at a depth from which a partly open quartz-lined fracture had been recovered in core (fig. 76), indicating that fracture porosity exists at depth for this fracture class. Petrographic examination shows that parts of quartz-lined fractures are open for distances of several inches, but transitions to filled fracture or areas of disconnected fracture porosity (on the scale of fractions of an inch) are abrupt. Carbonate-filled fractures in the cores we logged are largely filled and calcite is locally highly twinned, but primary fracture porosity is present locally. This fracture porosity typically does not appear

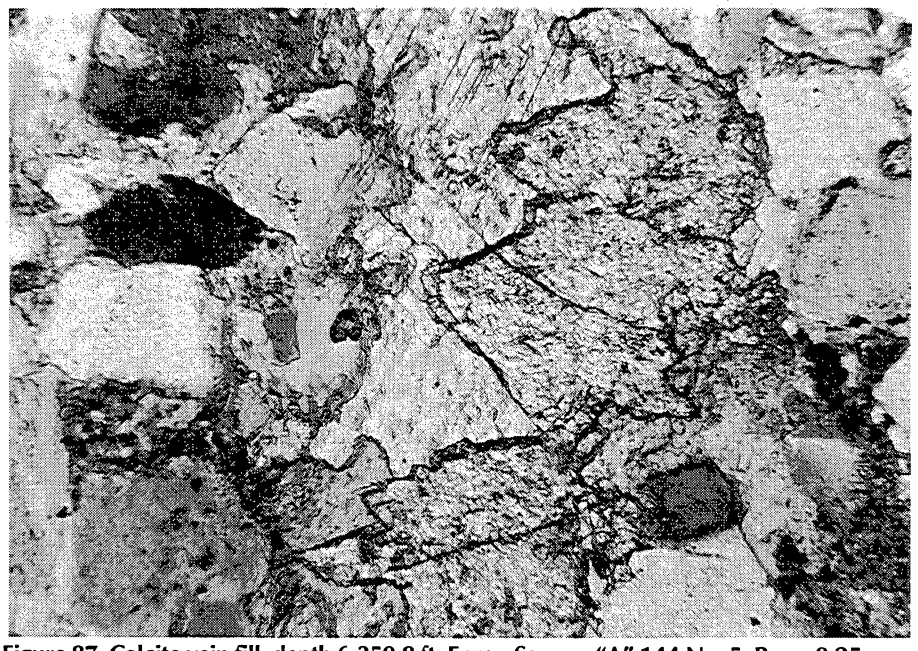

Figure 87. Calcite vein fill, depth 6,350.8 ft, Enron Sawyer "A" 144 No. 5. Bar = 0.25 mm.

Figure 88. Calcite-filled vein crosscutting grains and quartz cement, Enron Sawyer "A" 144 No. 5, depth 6,350 ft. Also note later handling-induced fracture (unfilled, dark). Bar = 1 mm.

to be connected within the plane of the fracture. We infer that compared to quartz-lined fractures, fractures having extensive carbonate fill are less likely to preserve fracture porosity.

Fractures in Siderite Cement Layers

The most abundant fracture class comprises fractures that exist only in siderite-cemented layers and in isolated patches of siderite cement in sandstones (fig. 79). Fractures in this class cross siderite-cemented zones and typically end abruptly at the edges of siderite-cement layers. The tallest fractures are as tall as the thickest layers of siderite cement. Only rarely do fractures extend beyond boundaries of siderite-cemented layers. Fractures are typically narrow, commonly less than 0.25 mm wide (average 0.17 mm), but short (less than 100 mm tall). Fractures in siderite-cemented layers have a range of height-to-width ratios of 25:1 to more than 2500:1, but most are between 100:1 and 300:1. Locally fractures have height-to-width ratios of as much as 25:1 where short fractures are exceptionally wide. Fractures of a given height in siderite-cemented layers are commonly wider than fractures of comparable height in other classes.

Fractures in siderite-cemented layers are the most abundant, constituting 116 (61 percent) of the natural fractures documented in Canyon core. Fractures are in 16.5 percent of the siderite-cemented zones in the Dunbar No. 1 core, in 5.3 percent of these zones in Ward "C" No. 11 core, and in 9.7 percent of those zones in Sawyer "A" 144 No. 5 core. Fracture abundance varies with layer thickness, that is, thin layers have greater numbers of fractures. Many thick siderite-cemented layers lack

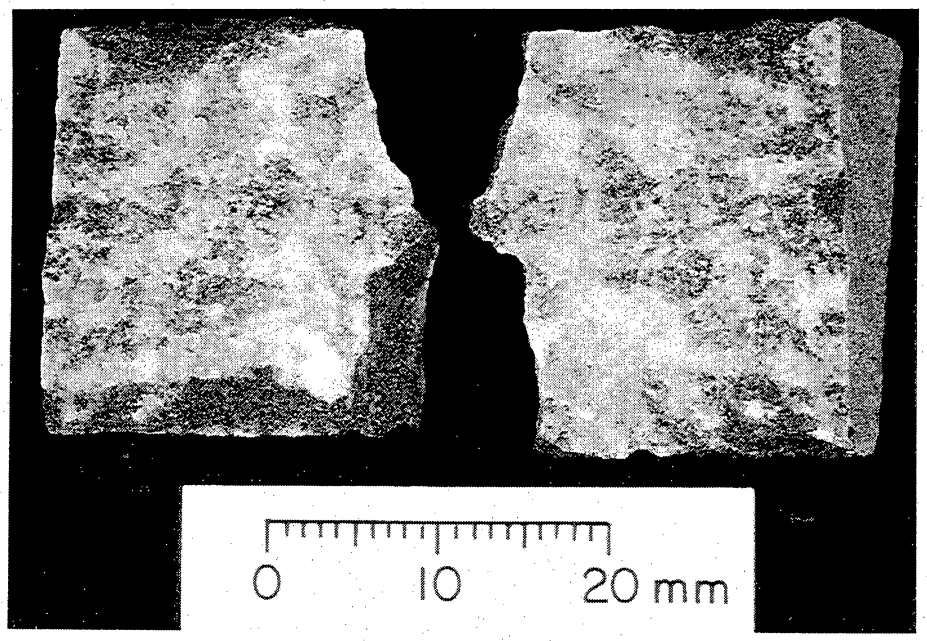

Figure 89. Photograph of natural fracture surface showing dickite mineralization, Enron Sawyer "A" 144 No. 5 core, depth 5,644.8 ft.

fractures in core. The range of siderite-cemented layer thickness measured from core is 6 mm to more than 1,000 mm. For layers ≤130 mm, the percentage containing at least one fracture is 18.5 percent of siderite-cemented zones in the Dunbar No. 1 core, 11 percent in Ward "C" No. 11 core, and 9.5 percent in Sawyer "A" 144 No. 5 core.

Siderite-cemented layers were categorized as either light, medium, or dark, corresponding roughly to increasing degree of cementation. Light layers typically have less than 10 percent siderite cement; medium and dark layers range from 10 to 30 percent siderite. There is little variation in fracture shape or mineral fill in layers of differing degree of cementation, but fractures are somewhat more common in the darker layers. In the Dunbar No. 1 core, 77 percent of the fractures are in medium to dark siderite layers, and 78 percent are in layers having a banded appearance and abrupt boundaries. The overall attributes and abundance of fractures in siderite-cemented layers are similar in all three wells, but the Dunbar No. 1 core contains a slightly higher density of fractures than do the other two wells, corresponding to a higher proportion of thin, discrete layers of medium- to dark-colored siderite-cemented layers in this well than in the other two wells, where diffuse, mottled, and light-colored siderite-cemented zones are prevalent.

Mineralization in fractures in siderite-cemented layers is predominantly dickite (fig. 89), a clay mineral that is a polymorph of kaolinite. Petrogenetic evidence shows that dickite-filled fractures formed later than siderite cement but prior to quartz cement. Dickite mineralization typically forms a dense fracture fill with little or no visible fracture macroporosity, but scanning electron microscope images show that fracture microporosity exists within these fractures. In some fractures minor calcite accompanies and textural evidence suggests that it is younger than dickite. Some fractures in siderite layers in the Ward "C" No. 11 well are calcite filled.

Timing of Fracturing

Dickite-filled fractures in siderite layers were the first fractures to form. Later quartz-lined fractures formed in part in rock lacking siderite cement, but quartz does not appear to have been precipitated in fractures having dickite fill, possibly because these fractures were closed (filled) at the time. Petrographic studies show that several generations of fracture-filling calcite exist in Canyon Sandstones and that fracture-filling calcite locally postdates dickite in fractures in siderite layers. Carbonate vein fill also postdates precipitation of quartz in some fractures. Early calcite vein fill experienced burial loading and compaction after their formation, manifested by twinned calcite and subhorizontal stylolites. Some later-stage carbonate precipitated in short fracture segments that may have formed at shallow burial depths. One crossing relationship, where fractures intersect, shows the relative age of fracture classes. In the Sawyer "A" 144 No. 5 core, a quartz-filled fracture (strike 044 degrees)

cuts across a siderite-layer fracture at nearly right angles, showing that quartz-filled fractures formed later.

Bearing in mind the limited evidence for true ages of fracture formation and the very limited oriented fracture data, we speculate that dickite-filled fractures formed shortly after sediment deposition at relatively shallow burial depths (but possibly, based on the presence of dickite, in an area of elevated heat flow). The orientation (strike) of these fractures is likely highly variable. Quartz-lined fractures developed at greater depths, and if the limited information from oriented fracture is representative, in a tectonic regime of northwest-trending extension and northeast-oriented SHmax. The orientation of these fractures is not diagnostic of the age of fracture growth, since several tectonic events in the Paleozoic to Recent history of the region could have been responsible. Based on crosscutting relations among fracture-filling minerals, calcite-filled fractures may be the youngest fracture set observed in core, but internal deformation in vein filling minerals and crosscutting subhorizontal stylolites are evidence that these fractures formed prior to an episode of burial. Uplift rather than burial has affected the Canyon since at least the late Tertiary; we infer that these fractures formed in the Cretaceous or earlier. More complete evidence of the timing and circumstances of fracture formation in Canyon Sandstones would help improve estimates of fracture orientation and interconnection.

Fracture Stratigraphy

Siderite-cemented layers and their associated fracture class in Canyon sandstones are a particularly clear example of a fracture (or mechanical) stratigraphic unit: fractures are localized within layers, they stop at cement-layer boundaries, fracture height increases with increasing layer thickness, and fractures are less abundant in thick siderite-cemented layers than in thin layers, as is expected if there is wider fracture spacing in thick beds. We speculate that early siderite cement caused these layers to be brittle at an early stage of burial loading, resulting in a concentration of burial-related fractures in these layers. Because compaction and authigenic cements subsequently modified the mechanical properties of non-siderite-cemented parts of the sandstone, the mechanical contrast caused by siderite cement became less pronounced with time, and later fractures are not concentrated in siderite layers. Data from the Ward "C" No. 11 well suggest that Canyon Sandstone layers having high quartz (10 percent to 20 percent) and/or siderite (20 percent to 30 percent) cement volumes have higher static Young's modulus (3.5 to 4 MMpsi) and slightly higher dynamic Young's modulus (7 to 8 MMpsi) (Miller, 1991) than rock having lower volumes of these authigenic phases. Fracture toughness measurements give similar

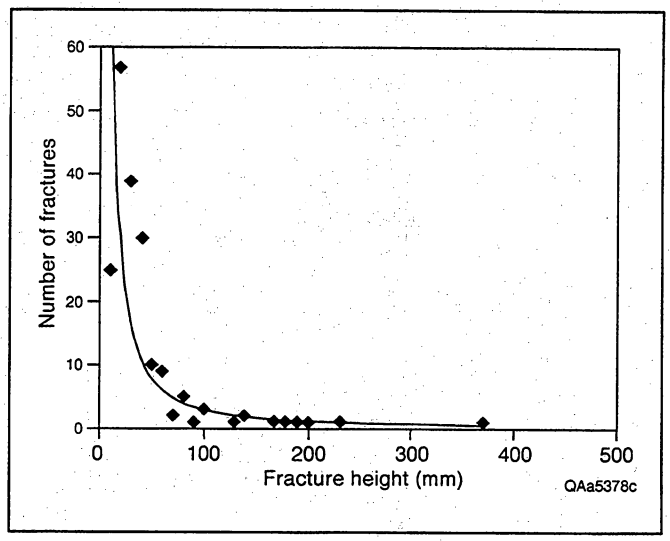

Figure 90. Number of fractures versus fracture height (interpreted to be equal to fracture spacing) and probability of fracture intercept for that fracture spacing and four-inch-diameter core (solid curve).

results for both siderite- and non-siderite cemented beds (Baek and Laubach, this volume).

The probability of encountering a fracture where the wellbore is perpendicular to bedding and fractures are vertical is equal to the core diameter (4 inches) divided by the median fracture spacing. When fracture spacing is less than or equal to the core diameter, a fracture intersection is certain. If typical spacing in siderite-cemented layers is about the same as layer thickness (6 to 8 inches thick and rarely more than 10 inches), then we should expect to find intersecting fractures in many thin siderite-cemented layers, as is observed.

Where a single joint set is present in mechanically significant beds or in layers of different thickness, the distance between joints in thick beds commonly is greater than in thin beds. The ratio of bed thickness to joint spacing can vary with a number of factors, including rock properties and length of time that fracture-producing processes have been active, but in thin beds, spacing in many cases is close to, or slightly less than, bed thickness. This may be also true for fractures in siderite-cemented layers (fig. 90). Although estimates of spacing using probabilistic methods (Aguilera, 1988) could be made, to a first approximation siderite-cemented-layer thickness provides a reasonably accurate estimate of spacing for this fracture class.

Fracture Networks

Core provides information on attributes of individual fractures, but the influence that fractures exert on the

permeability of a fractured rock is, to a large extent, controlled by the connectivity of fractures in a network. Unfortunately, the attributes of lateral (plan view) fracture connectivity are not apparent at the wellbore. Outcrop studies of other sandstones show that connectivity of sandstone fracture networks can be low but highly variable (Laubach, 1992). Fractures of all sizes may belong to interconnected networks having a wide range of sizes, and thus observed flow along fractures intersecting a borehole need not correlate with fracture aperture, length, or height in the wellbore. Short naturally fractured intervals can have high production levels (Missman and Jameson, 1991). Core data from Canyon sandstones are consistent with the thickness of fractured intervals being equal to or less than bed thickness. In the case of fractures confined to siderite-cemented zones, fractured layers are typically less than 1 ft thick.

Core evidence does not indicate what fracture network patterns may exist in Sonora Canyon sandstones, but fractures in siderite-cemented zones are the most likely to be interconnected because they have diverse strikes (based on fractures that occur together in the same core interval) and high fracture density. However, even if high connectivity exists between these fractures, fluid flow may be hampered or blocked by infilling minerals, such as the abundant clay minerals in Dunbar No. 1 siderite-layer fractures. Despite the higher porosity and permeability that has been described in some siderite-cemented Canyon sandstones (Dutton, this volume), filled fractures in these layers could possibly impede or compartmentalize fluid flow. Connectivity of fracture porosity in quartz- and carbonate-lined fractures is at least locally interrupted by mineralization within fractures (filled fractures).

Predicting Fracture Occurrence

Diagenetic attributes are useful for predicting the occurrence of siderite-layer fractures. Because siderite cementation occurred in the shallow subsurface and was influenced by sediment composition, depositional patterns may be useful for predicting where abundant siderite is likely to be found. Areas or intervals with dense siderite cement are likely to be highly fractured, with fracture spacing about equal to the thickness of individual siderite layers. Highly productive channel belts—with their propensity for siderite cementation—may also be highly fractured areas. Predicting the presence of other classes of natural fracture in Canyon sandstones is problematic because fewer of these fractures were seen in core, and it is challenging to recognize factors that control their appearance.

That conductive networks of fractures exist in subsurface rocks that lack folds and faults has been shown in several recent studies. For example, study of the Paleozoic Davis sandstone in North-Central Texas shows that in rock with a structural history similar to the Canyon sandstone, numerous fractures that can conduct significant volumes of fluid occur in areas that lack folds and faults (Collins and others, 1992). Our Canyon Sandstone well control and maps suggest that fractures are not confined to the vicinity of faults or fold hinges in these reservoirs, but our observations of vertical fractures are limited to a few vertical cores; it is possible that fractures are more numerous in other structural settings and that fault geometry or bed curvature analysis (Laubach and others, 1992b; Schultz-Ela and Yeh, 1992) may be useful for fracture prediction. Data from deviated wells may be the best way to test these methods.

Implications for Evaluation and Stimulation

Natural Fracture-Enhanced Permeability

Maximum annual production and cumulative production per Sonora Canyon Sandstone well vary by substantial amounts over distances of less than a mile in areas of uniformly low matrix permeability. Locally, Canyon Sandstone wells have moderate production rates that are anomalous if production is entirely from low-permeability matrix rock (Hamlin and Clift, this volume; R. E. Peterson, personal communication, 1992). These variations could stem in part from differences in thickness of pay intervals in these complexly interbedded sandstones and shales and from contrasts in the success of well completion and stimulation. The presence of open natural fractures in Canyon Sandstone core indicates that they might also contribute to fluid production and the observed variability in production, and that they are a potential target for development. Anomalies on temperature logs that have been reported by operators are possibly another manifestation of natural fractures.

In thick and otherwise vertically homogeneous Canyon sandstones directional drilling is a potentially appropriate method to tap vertical fractures. However, such sandstones are not widespread in the Canyon. Numerous thin interbeds, which interrupt vertical continuity of fracture systems, are the rule. Such sedimentary fractures cannot necessarily be distinguished on commonly used geophysical well logs, although they would be evident on Formation Microscanner Logs. In

any case, the depositional environment of Canyon Sandstones suggests that these features are widespread, whether detected or not. These thin beds appear to control the height (vertical extent) of most Canyon Sandstone fractures. In view of the short natural fracture heights and prevalence of underpressure in the Canyon, horizontal drilling—with current technology—may not be an effective development strategy.

On the other hand, where sandstone beds are thicker or where they lack interbeds of great lateral extent, as in some channel belt areas, fractures may be 10 ft or more in height and therefore potentially viable targets. In a pervasively gas-saturated sandstone, these features could possibly be effectively targeted. Additional information on fracture orientations and connectivity would be helpful for evaluating this possibility. In the absence of such information, stress-direction information and limited information on fractures in core suggests that fractures striking north or northeast are most likely to be open conduits for gas.

Of the fracture classes observed in Sonora Canyon core, quartz- and carbonate-lined fractures have the greatest vertical extent and the best evidence for preserved fracture porosity. They also pass through sandstone having the greatest degree of fracture-occluding quartz and carbonate cements, rock that might otherwise have poor reservoir quality. If natural fractures in these rocks form laterally extensive, hydraulically interconnected networks—and there is currently no direct observational evidence for this—then wellbores in contact with such networks would likely drain much larger areas than wellbores in contact with sandstone lacking fractures. Although preferred fracture orientations have not been established by our study owing to the small number of oriented fractures (fig. 85), fractures striking eastward or northeastward are aligned with regional SHmax and may be prone to be open. One quartz-lined fracture in core strikes northeastward (044 degrees), suggesting that it is possible that there is a population of fractures having this orientation.

Efficient Sonora Canyon reservoir management should take the likely presence of natural fractures into account. According to Dyke (1992a, 1992b), natural fracture permeability is easily damaged by small amounts of solids contained within drilling mud; it is therefore possible that blockage by mud solids may obscure or damage permeable Sonora Canyon fractures. Natural fractures in these reservoirs may be more common than previously determined from interpretation of well test results, and care is warranted in treating these reservoirs to avoid damage to fractures. Owing to their clay (dickite) content, many of the fractures in siderite layers may be impediments or barriers to fluid flow, and their presence could promote reservoir heterogeneity and anisotropy without necessarily augmenting production. Moreover, although not filled with swelling clay minerals, clay-filled fractures may be sensitive to fluids introduced during completion and stimulation (possibly including fines migration). The significance of these effects for overall reservoir quality and performance depends on the extent that siderite-cemented layers govern reservoir flow properties. With their relatively higher porosity and permeability (Dutton, this volume) these siderite layers and the fractures within them could be key elements of reservoir plumbing where damage should be particularly avoided.

If interconnected natural fractures are a component of reservoir porosity and permeability, the fracture network may be sensitive to changes in effective stress caused by long-term pressure drawdown, which might cause fractures to close and overall reservoir permeability to decrease. On the other hand, quartz and calcite mineralization in some large Canyon fractures suggests that fracture porosity and fracture permeability (open channels within mineralized fractures) may be relatively insensitive to increases in effective stress, because bridging minerals can hold fractures open. The highly variable degree of occlusion of fracture porosity by infilling minerals suggests that flow channeling can occur within some fractures.

New Stimulation Method to Exploit Natural Fractures

The attributes of minerals precipitated in Canyon Sandstone fractures suggest that acid treatment would improve the effectiveness of natural fractures as flow pathways to the wellbore. The justification for this suggestion is as follows. The tallest and widest and most porous class of fractures in Sonora and Ozona Canyon sandstones contain quartz and a carbonate mineral—calcite, Fe-calcite, or ankerite. Quartz precipitated first and generally either lines or partially bridges fractures. Rarely are fractures completely filled by quartz. Carbonate minerals precipitated later than quartz; these carbonate minerals are primarily responsible for occluding fracture porosity. Dissolution of carbonate would improve fracture porosity and permeability and enlarge connected flow networks.

Even where primary fracture porosity is visible in cored fractures, it is possible that the continuity of fractures and/or fracture networks is interrupted by fracture-filling carbonate minerals. Outcrop studies of fracture networks in sandstones have shown that interconnections among large, persistent fractures may be through arrays of small, narrow, easily occluded minor fractures (Laubach, 1992). Carbonate minerals fill these choke points of the fracture network and effectively block or impede flow in natural fracture systems, even where

the network has significant overall fracture porosity or porosity at the wellbore.

Removal of carbonate fracture-fill minerals could substantially improve the natural fracture flow network plumbing, and this could possibly be accomplished by acid treatment. Mild acid treatments were carried out by applying a dilute 2 percent HCL solution to polished Canyon Sandstone samples containing fractures. We found that fracture-filling carbonate minerals were preferentially dissolved compared to pore-filling carbonate minerals. This is likely due to twinning and microfracturing present in fracture-filling carbonate minerals that increase mineral surface area and thus make them more susceptible to attack by acid. These tests merely show that fracture-fill minerals can be preferentially dissolved; design of in situ tests and treatments is beyond the scope of this study. An issue that needs to be considered in any future work is the potential for formation damage from reactions between acids and iron-carbonates such as ankerite.

Would acid-treated, widened natural fractures in Canyon Sandstones remain open? Observations of fractures in other sandstones suggest that they could. Quartz-lined and quartz-bridged fractures having extensive fracture porosity exist at depths greater than -10,000 ft in normally pressured quartz-cemented sandstone. One formation where this is the case is the Travis Peak Formation of East Texas (Laubach, 1989a). Fracture-bridging quartz would tend to prop open Canyon Sandstone fractures after carbonate minerals were partly removed.

If effective in the Canyon, the proposed acid treatment approach for interconnecting natural fractures in networks may also be useful in other tight gas sandstones having similar fracture-fill paragenesis. Precipitation of synkinematic quartz in fractures accompanies quartz cement precipitation in several tight gas sandstones that have extensive quartz cement. Fracturing and the resultant quartz-lined fracture porosity may be a natural outcome of the quartz cementation process (Laubach, 1988). Later carbonate mineral precipitation is commonly responsible for filling these fractures. Techniques that can remove carbonate minerals from fractures in such sandstones have the potential to open up permeability pathways in rocks that are otherwise among the least prospective for gas production owing to extensive quartz cement.

Acid treatments are carried out in many formations including Canyon Sandstones, but it is doubtful that current acid treatment practices are best for the proposed application. Acid treatments prior to hydraulic fracture treatment for general wellbore cleanup have become common in the Canyon in the past several years. We speculate that optimum treatments for this new application would involve small fluid volumes injected at low pressure (less than the fracture gradient) in order to minimize damage to the natural fracture system, and that treatments would be targeted in intervals of the borehole that core, geophysical well log (including temperature log), or other information indicated contained partly open fractures that could accept fluid. Such treatments might not necessarily be carried out in conjunction with hydraulic fracture treatments and concentrations should be designed to enhance penetration into existing fractures. Further analysis of the issues involved in design of successful treatments was beyond the scope of our study.

Natural Fractures and Hydraulic Fracture Stimulation

There is some evidence that natural fractures can affect the outcomes of Canyon Sandstone hydraulic fracture stimulations. The orientation of fractures created in hydraulic fracture treatments can be modified by natural fractures; created fractures are generally assumed to align perpendicular to the least principal compressive stress, but in naturally fractured rock this may not be the case if preexisting fractures are opened by the fracturing fluid. This is a viable explanation for the discrepancy between hydraulic fracture strike detected by remote measurement of treatment-induced microseismicity and SHmax (Fix and others, 1989), and it is a phenomena that has been proposed to operate in other tight gas sandstones (Laubach and others, 1992a). For the Sonora Canyon, microseismic results in the Ward "C" No. 11 well indicate that treatment fractures strike eastward (085 degrees), whereas stress indicators predicted northeastward (035 degrees) fracture growth (Miller and others, 1991). If natural fractures are influencing hydraulic fracture growth direction, efficient well placement plans should take this phenomenon into account.

Another consequence of natural fractures in Canyon Sandstones may be unexpectedly high treatment pressures. In a study of hydraulic fracture treatments in the Sawyer "A" 144 No. 5 well, Miller (1991) concluded that modeled net fracture pressures were lower than measured pressures by 1,100 to 1,300 psi, and that the likely explanation was stiffening of the formation (increased "effective" modulus) resulting from the growth and interference of multiple fractures during treatment near the wellbore (near-wellbore tortuosity). In some low-permeability Travis Peak sandstones in East Texas (Laubach, 1989a) and Frontier Formation sandstones, Wyoming (S. A. Holditch, personal communication, 1992), development of multiple fractures was ascribed to hydraulic fracture branching caused by preexisting natural fractures, and this phenomena may also occur in Canyon Sandstones. Observations described in a later

section of this report (Baek and Laubach, this volume) show that natural fractures in core have grown significantly under the influence of the relatively mild loads imposed by the coring process.

Thus, engineers designing fracture treatments in Canyon Sandstone likely need to consider and design for near-wellbore and far-field growth of multiple fracture strands during hydraulic fracture treatment. In the near-wellbore region, this process can lead to high net treatment pressures that may require adjustments in planned treatment viscosity and pumping rates (Wright and others, 1993). Distant from the wellbore, multiple fracture strands affect proppant movement and placement.

A range of natural fracture strikes has been observed in Canyon core. Higher than expected treatment pressures can also result from opening of natural fractures that are not aligned with SHmax because these fractures would not be opening against the least principal horizontal stress. This discrepancy would affect the interpretation of stress profiles used in hydraulic fracture treatment design. Core or well log information may need to be taken into consideration in hydraulic fracture treatment design and interpretation where fractures are plentiful in perforated intervals.

A Key Reservoir Element: Summary

Natural fractures are abundant in Sonora Canyon gas reservoir sandstones. Two different types or classes of subvertical extension fracture are locally present. In core, clay- or clay- and calcite-filled fractures that are in thin siderite-cemented zones are the most common fracture class. Owing to infilling clay minerals (dickite), these fractures may be barriers to lateral fluid flow within siderite layers and could promote reservoir anisotropy and local reservoir compartmentalization if flow in siderite layers is the key to overall reservoir flow communication. A second class of fractures that is not confined to siderite layers—carbonate- and quartz-lined fractures—are larger (greater vertical extent) than fractures in siderite-cemented layers, and they locally preserve fracture porosity along their traces; these fractures could be conduits of fluid flow. These observations show that fractured zones in Sonora Canyon sandstones are possible reservoir elements that assist production. Sampling bias does not permit an accurate estimate of the abundance of this class of fractures, but vertical fractures are typically underrepresented in vertical core, and it is probable that these fractures are more common than is suggested by core observations. To a first approximation, fracture spacing is likely to be similar to the thickness of quartz-cemented intervals—in the range of several feet to tens of feet. Fractures with this spacing will be rare in core, but they will likely be intersected by hydraulic fractures created during well stimulation.

In Sonora Canyon reservoirs, manifestations of natural fractures influencing hydraulic fracture growth may include elevated net pressures during hydraulic fracture treatments and discrepancies between measured SHmax directions and growth directions of hydraulic fractures. These results have implications for well placement and the design and modeling of hydraulic fracture treatments in these rocks.

Fracture Mechanics Property Evaluation, Canyon Sandstone

Hwanjo Baek, S. E. Laubach

Fracture toughness values for 36 Canyon Sandstone specimens average 1.77±0.46 MN/m$^{1.5}$ for siderite-cemented sandstones and 1.72±0.60 MN/m$^{1.5}$ for non-siderite-cemented sandstones. The significant variability in fracture toughness—a range of values from 0.90 MN/m$^{1.5}$ to 2.94 MN/m$^{1.5}$—primarily reflects the influence of compositional attributes other than the presence of siderite cement. Poorly sorted sandstones tend to have higher fracture toughness values. The volume and distribution of clay particles and cements may be a key attribute, with clay-rich specimens having lower fracture toughness. The measured fracture toughness values of Canyon sandstones are comparable to those obtained in previous studies of Travis Peak Formation (Cretaceous, East Texas) sandstones. Quantitative studies of the surface roughness profiles of both natural and induced fractures in Canyon sandstones suggest that petrographic methods can distinguish these fracture types where fracture-filling minerals are absent. Petrographic study of Canyon Sandstone fractures suggests that in low-porosity sandstone having fracture toughness values in a range typical of tight gas sandstones, natural fractures are readily reactivated and grow under the influence of perturbations due to drilling activity.

Fracture Toughness

Fracture toughness is a measure of the ease of fracture propagation in a material. It is generally measured by monitoring load, displacement, and crack growth during laboratory tests on specimens having a specific shape that contain an initial notch of known length. Fracture toughness is calculated from the critical load and critical crack length corresponding to onset of crack propagation. Mode I fracture toughness K_{Ic}—or critical stress intensity factor in opening mode crack propagation—has been widely used in application of linear elastic fracture mechanics (LEFM) principles to rock. As such, K_{Ic} is potentially an important material property in industrial applications related to natural gas production such as assessment of rock drillability, borehole stability, behavior of natural fractures under changing effective stress conditions during drilling and production, and design of hydraulic fracture treatment. Few reliable fracture toughness values have been published for sandstones similar to those in low-permeability gas reservoirs, and no studies have explored fracture toughness variations caused by differences in cement type within low-permeability gas sandstone sequences. No measurements of fracture toughness for Canyon sandstones have been published.

The purpose of this study is to document fracture toughness values for Canyon Sandstone and to investigate the role of sandstone diagenesis in controlling fracture properties. This study also documents the microstructural contrast between fractures created under controlled conditions during fracture toughness tests and fractures formed in the subsurface by natural processes. In addition to characterizing a key Canyon Sandstone rock property, results of this study have implications for methods of predicting fracture toughness based on rock composition, texture, and porosity and for understanding the conditions of natural fracture growth and natural fracture reactivation during drilling and completion. This study also documents the use of a non-standard sample preparation method for fracture toughness testing that is particularly well suited to core analysis.

Laboratory Methods

Specimens were taken from 3.5-inch (89 mm) diameter Canyon sandstone core, from both siderite and non-siderite-cemented sandstones. Mineralogical composition and microstructure of specimens are described in a following section.

Mode I fracture toughness values were measured using either notched Brazilian disc or semi-circular bend specimens (fig. 91; Baek, 1994), depending on the character of intact rock materials available at a given core depth. These testing methods are relatively simple, in sample preparation. ISRM-suggested test methods (ISRM, 1988) could not be employed in this study due to limited amounts of intact rock materials. Furthermore, the fracture direction induced by those test methods would be parallel to bedding, an unrepresentative direction considering that induced and natural fractures are mostly orthogonal to bedding and possible bed-parallel planes of weakness.

The Brazilian test was originally developed as an alternative method for measuring Poisson's ratio and

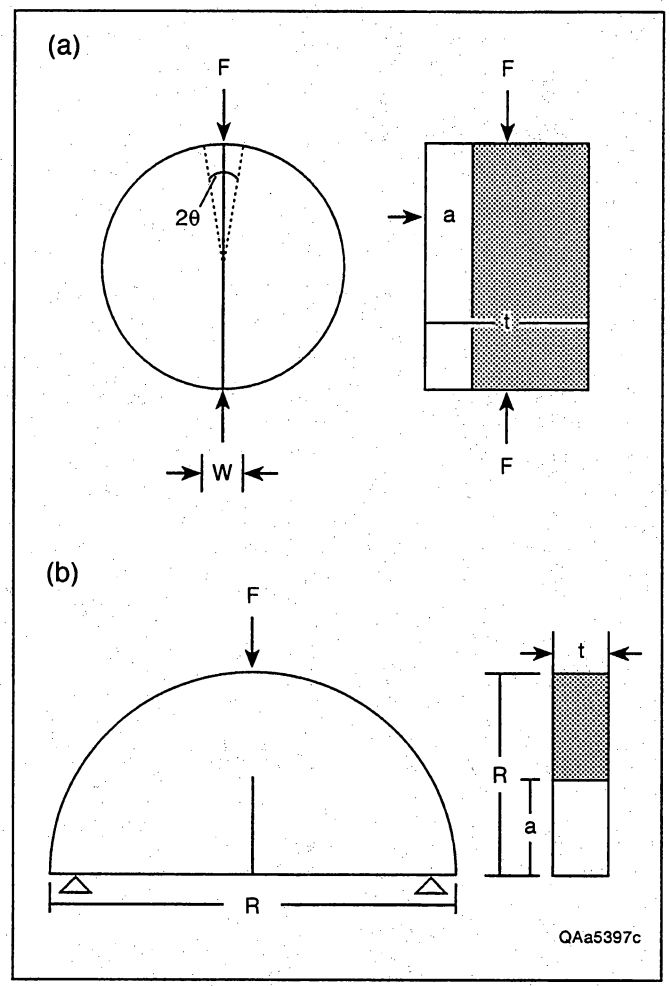

Figure 91. Specimen geometries used for determining fracture toughness of the Canyon Sandstones. (a) Notched Brazilian disc specimen; (b) semi-circular bend specimen.

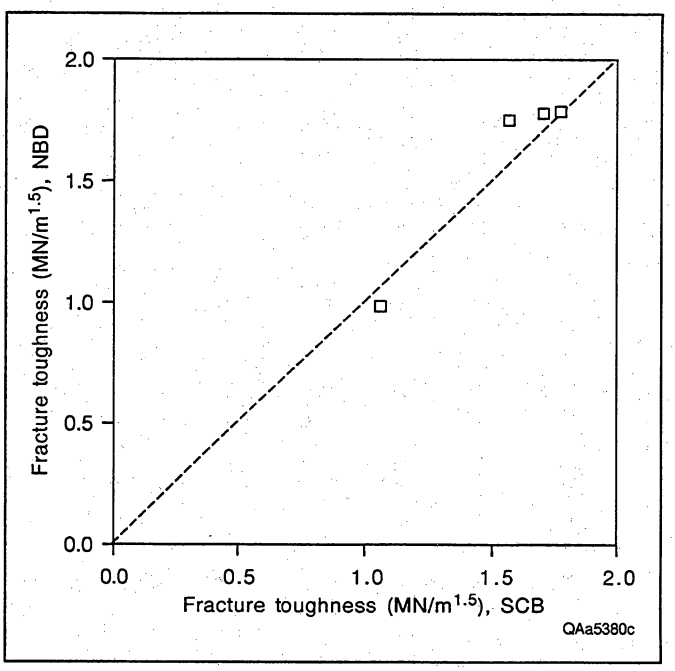

Figure 92. Comparison of the measured fracture values by two different test methods; NBD, notched Brazilian disc; SCB, semi-circular bend specimen.

elastic modulus of brittle materials (Wright, 1955; Olszak and others, 1957), and has been adopted for determining tensile strength of rocks (Bieniawski and Hawkes, 1978). The straight-edge-notched Brazilian disc in diametral compression was first used by Szendi-Horvath (1980) for fracture toughness measurement of brittle materials. For this test, two diametrically opposite faces of a disc specimen are ground flat on a surface grinder to make loading faces parallel and smooth. An initial notch is cut through one face of the specimen along the diametral axis as a stress raiser. Specimens are diametrally loaded in such a way that the notch remains parallel to the loading line while the load is applied by the rig through flat platens. The semi-circular bend test was introduced by Chong and Kuruppu (1984). In this test, a core half with a single straight notch along the centerline is loaded under three-point bending. This method is suitable for applications that require duplicate specimens having similar composition since a circular disc can be cut into halves to make two duplicate specimens.

Although closed-loop, servo-controlled loading frames can provide more precise information during testing, a conventional screw-driven type loading frame was used that could accommodate higher loads than possible for the servo-controlled rig in our laboratory. Higher loads are required for the notched Brazilian disc specimens. Crack-mouth opening displacement (CMOD), which is the distance change between points on opposite sides of the initial notch, was monitored with an MTS model 632-03c clip-on gage. Load point displacement (LPD) was also monitored by a Trans Tek, Inc., Model 0240 displacement transducer.

Measured fracture toughness values of heterogeneous rock materials can be affected substantially by the test geometry adopted. Since two different specimen geometries were employed in this study, a calibration procedure for the measured fracture toughness values was necessary to make them comparable to each other. This was done by testing identical specimens from the same core depth with the two specimen geometries. Fracture toughness values were compared and, as shown in figure 92, the notched Brazilian disc and semi-circular bend specimen yielded similar test results. Hence, considering the variability inherent in heterogeneous rock materials, the effect of different specimen geometries on the measured fracture toughness appears to be negligible.

Calculation of Fracture Toughness

Fracture toughness is calculated from the maximum test load and the specimen geometry based on analysis of stress-strain behavior of a circular (or semi-circular) element under loading. Assuming no significant change in shape of the boundary line of the compressive field due to introduction of flat surfaces on top and bottom of the circular element, the expression for evaluating fracture toughness by the notched Brazilian disc specimen is (Szendi-Horvath, 1980)

$$K_{Ic} = 1.264 \cdot (\sin 2\theta - \theta) \cdot \frac{F_{max} \cdot \sqrt{a}}{w \cdot t} \qquad (1)$$

where notations are given in figure 91.

For semi-circular bend specimens, the fracture toughness is calculated as (Chong and Kuruppu, 1984)

$$K_{Ic} = \frac{F_{max} \cdot \sqrt{\pi \cdot a}}{2R \cdot t} \cdot Y' \qquad (2)$$

where Y′ is a dimensionless stress intensity factor, given by

$$Y' = 5.64 - 22.16\alpha + 166.90\alpha^2 - 576.23\alpha^3 + 928.83\alpha^4 - 505.92\alpha^5 \qquad (3)$$

$$(\alpha = a / R)$$

The tests and expressions described above were used on Canyon Sandstone core samples representing the range of Canyon Sandstone composition.

Fracture Toughness Values

Fracture toughness values of 36 siderite- and non-siderite-cemented sandstone specimens are summarized in tables 8 and 9. Difference in the average fracture toughness values for the two rock types is negligible. Siderite-cemented sandstones average 1.77±0.46 MN/m$^{1.5}$, and non-siderite-cemented sandstones average 1.72±0.60 MN/m$^{1.5}$. High standard deviations and coefficients of variation (26 percent for siderite-cemented sandstones and 35 percent for non-siderite-cemented sandstones) indicate significant variability in fracture toughness within each rock type. Fracture toughness of siderite-cemented sandstone ranged from 0.98 MN/m$^{1.5}$ to 2.83 MN/m$^{1.5}$. For sandstone lacking or having very small amounts of siderite, values ranged from 0.90 MN/m$^{1.5}$ to 2.94 MN/m$^{1.5}$. These values are comparable to fracture toughness values of Travis Peak Formation sandstone measured by Ferm and others (1990) using the modified ring test. For that sandstone and those tests, fracture toughness values range from 0.74 MN/m$^{1.5}$ to 2.16 MN/m$^{1.5}$. The Travis Peak Formation is a Cretaceous low-permeability gas sandstone of the East Texas Basin (Dutton and others, 1991) having quartz cementation similar to parts of the Canyon.

No significant variation is evident in Canyon sandstone fracture toughness with depth (fig. 93), but there is variability among wells. Non-siderite-cemented sandstone fracture toughness values are lower than siderite-cemented sandstone values in samples from the Enron Sawyer "A" No. 5 well and the Kincaid "D" No. 7 well, and are mostly lower in samples from the Dunbar No. 1 core, but values for both sandstone types are closely similar for samples from the Phillips Ward "C" No. 11 well (fig. 94). There is an overall pattern in which samples having low fracture toughness values tend to be from non-siderite-cemented rock, whereas samples with high values of fracture toughness are more common among siderite-cemented rocks, but this pattern is obscured when data from all wells is plotted together.

Canyon sandstone fracture toughness varies linearly with dry density (fig. 95; table 8). For non-siderite-cemented sandstones, the relationship is marginally significant (Pearson correlation coefficient, r=0.72). In contrast, for siderite-cemented sandstones, there is no statistically significant relationship (r=0.26). On average, siderite-cemented sandstone has a higher dry density than that of non-siderite-cemented sandstone, but the difference is negligible, with most values clustered between 2.5 and 2.7 g/cm^3. Dry density of compact silicic sandstones commonly is lower for rocks containing greater pore volume (including microfractures). Previous studies suggest, however, that Canyon siderite-cemented zones have higher porosity than non-siderite-cemented zones, but the difference is slight (National Petroleum Council, 1980; Dutton, this volume). Siderite-rich sandstones have porosity of about 7.9 percent compared to 6.4 percent for siderite-poor sandstones. The high specific gravity of siderite may be responsible for compensating for higher porosity in siderite-cemented sandstone, resulting in an average density close to that of less-porous non-siderite-cemented sandstone.

In porous and uncompacted sandstone, a plausible expectation is that greater porosity will correspond to lower fracture toughness, since a crack may propagate through less resistant pore spaces. In compact, low-porosity rocks such as the Canyon sandstone and many other low-permeability gas sandstones, this relationship is less likely to hold, since pore space is a volumetrically minor microstructural component. This has been documented for the Travis Peak Formation, where there appears to be little relationship between fracture toughness and whole-rock porosity (Ferm and others, 1990). For such rocks the proportion of weak elements in the rock (in addition to porosity), such as volume of

Table 8. Fracture toughness test results of the dry Canyon sanstones.

Sonora Canyon Sandstone (Notched Brazilian disc specimen)

Well (company)	Depth (ft)	Cement	Diameter (mm)	Thickness (mm)	Height (mm)	2α (radian)	Notch (mm)	Load (KN)	Dry Density (gram/cm^3)	Toughness (MN/m$^{1.5}$)
Kincaid, #D-7	7748.4	Siderite	51.1	49.6	49.6	0.50	15.8	30.66	2.71	1.78
(Texaco Inc.)	7734.4	"	51.1	50.0	49.5	0.51	15.7	30.66	2.60	1.75
"	7623.9	"	51.1	49.1	49.5	0.51	15.0	55.00	2.72	2.13
"	7622.3	"	51.1	49.3	49.4	0.52	15.5	17.19	2.49	0.98
"	7620.7	"	51.1	49.6	49.7	0.48	20.4	31.41	2.63	2.09
"	7732.8	Non-siderite	51.1	48.5	49.8	0.46	12.9	33.54	2.63	1.82
"	7648.5	"	51.1	49.6	49.8	0.46	20.7	22.88	2.57	1.54
Ward, "C" No. 11	6354.9	Siderite	51.1	49.8	49.4	0.52	15.6	25.33	2.49	1.45
(Phillips Petroleum)	6353.8	"	51.1	50.8	49.5	0.51	16.7	39.47	2.53	2.29
"	6379.3	Non-siderite	51.1	48.3	49.5	0.51	14.4	28.35	2.50	1.61
"	6378.1	"	51.1	49.6	49.4	0.53	15.8	26.37	2.48	1.51
"	6353.5	"	51.1	49.4	49.5	0.51	15.5	30.46	2.54	1.75
"	5518.0	"	51.1	51.3	49.8	0.46	22.4	21.54	2.45	1.45
Sawyer, "A" 144	6186.0	Siderite	51.1	53.2	49.7	0.47	24.2	41.76	2.63	2.83
No. 5	5963.6	"	51.1	50.1	49.4	0.53	16.1	23.78	2.48	1.37
(Enron)	5644.7	"	51.1	49.0	49.5	0.51	15.0	34.43	2.64	1.97
"	5642.3	"	51.1	51.9	49.5	0.51	17.7	31.00	2.63	1.81
"	5961.7	Non-siderite	51.1	49.4	49.5	0.51	15.6	23.64	2.51	1.37
"	5961.1	"	51.1	50.8	49.3	0.54	16.8	25.04	2.50	1.45
Dunbar, No. 1	5948.6	Siderite	51.1	48.5	49.4	0.53	14.5	27.02	2.50	1.52
(Sun Oil Co.)	5882.8	"	51.1	50.9	49.2	0.55	17.1	24.96	2.56	1.44
"	5836.7	"	51.1	50.3	49.3	0.53	16.4	22.73	2.58	1.31
"	5964.4	Non-siderite	51.1	49.4	49.5	0.51	15.4	17.13	2.46	0.98
"	5814.2	"	51.1	49.4	49.4	0.52	15.3	22.67	2.49	1.39

Ozona Canyon Sandstone (Notched Brazilian disc specimen)

Well (company)	Depth (ft)	Cement	Diameter (mm)	Thickness (mm)	Height (mm)	2α (radian)	Notch (mm)	Load (KN)	Dry Density (gram/cm^3)	Toughness (MN/m$^{1.5}$)
Baggett "2"	5992.9	Non-siderite	37.9	37.8	36.3	0.59	12.0	30.76	2.62	2.67
No. 20	5967.9	"	37.9	34.4	36.7	0.50	14.3	18.08	2.51	1.95
(Sun Oil Co.)	5915.0	"	37.9	33.8	36.8	0.49	9.8	31.95	2.65	2.90
"	6657.5	"	38.0	31.9	37.1	0.43	17.5	17.84	–	2.32
"	6724.0	"	38.1	24.3	37.2	0.42	10.7	14.46	–	1.93
"	5866.0	"	37.8	39.4	36.7	0.48	13.6	31.95	2.68	2.94
Kincaid, #D-7	6366.2	Non-siderite	51.1	48.9	49.8	0.45	20.1	35.01	2.64	2.25
(Texaco Inc.)	6205.2	"	51.1	47.3	49.7	0.47	18.2	13.71	2.52	0.90

Ozona Canyon Sandstone (Semi-circular bend specimen)

Well (company)	Depth (ft)	Cement	Thickness (mm)	Height (mm)	Notch (mm)	a/R	Y'-scb	Load (KN)	Toughness (MN/m$^{1.5}$)
Kincaid, #D-7	6342.4	Non-siderite	24.4	45.2	24.7	0.5	7.5	1.75	1.66
(Texaco Inc.)	6295.3	"	29.7	44.4	23.5	0.5	7.1	1.58	1.16
"	6220.9	"	28.2	45.1	24.1	0.5	7.2	1.96	1.53
"	6209.1	"	18.7	45.9	25.4	0.6	7.7	0.72	0.91

Table 9. Mineralogical composition and fracture toughness values of the Canyon sandstone specimens.

Well	Depth (ft)	Cement	Fracture toughness ($MN/m^{1.5}$)*	Hard contact (%)	Quartz (%)	Feldspar (%)	Rock fragments (%)	Quartz overgrowth (%)	Carbonates (%)	Clays (%)	Siderite (%)	Others (%)	Primary porosity (%)	Secondary porosity (%)
Kincaid "D," No. 7	6344.0	Non-siderite	1.66	10	28	4	19.5	0	33.5	0	0	15	0	0
"	6295.7	"	1.16	39	54	2	11	12.5	9	4.5	0	0.5	6.5	0
"	6221.0	"	1.53	11	40.5	2.5	10.5	0	38	3	0	4.5	0	1
"	6209.0	"	0.91	41	54.5	1.5	14	4.5	16.5	5.5	0	2.5	0.5	1
Baggett "2," No. 20	6657.6	"	2.32	13	33	4.5	13.5	2.5	43	0	0	3.5	0	0
Dunbar, No. 1	5964.4	"	0.98	58	51	5.5	20	13.5	0.5	4	0	0.5	0	5
"	5882.8	Siderite	1.44	5	41	3	10	0	0	0	41.5	0	3.5	1
"	5814.2	Non-siderite	1.29	54	48	6	21	18.5	0	0	0	2.5	0	4
Sawyer "A" 144, No. 5	5644.7	Siderite	1.97	5	43	3	8	0	0	2	38.5	0.5	5	0

*$MN/m^{1.5}$ (meganewton/$m^{1.5}$)

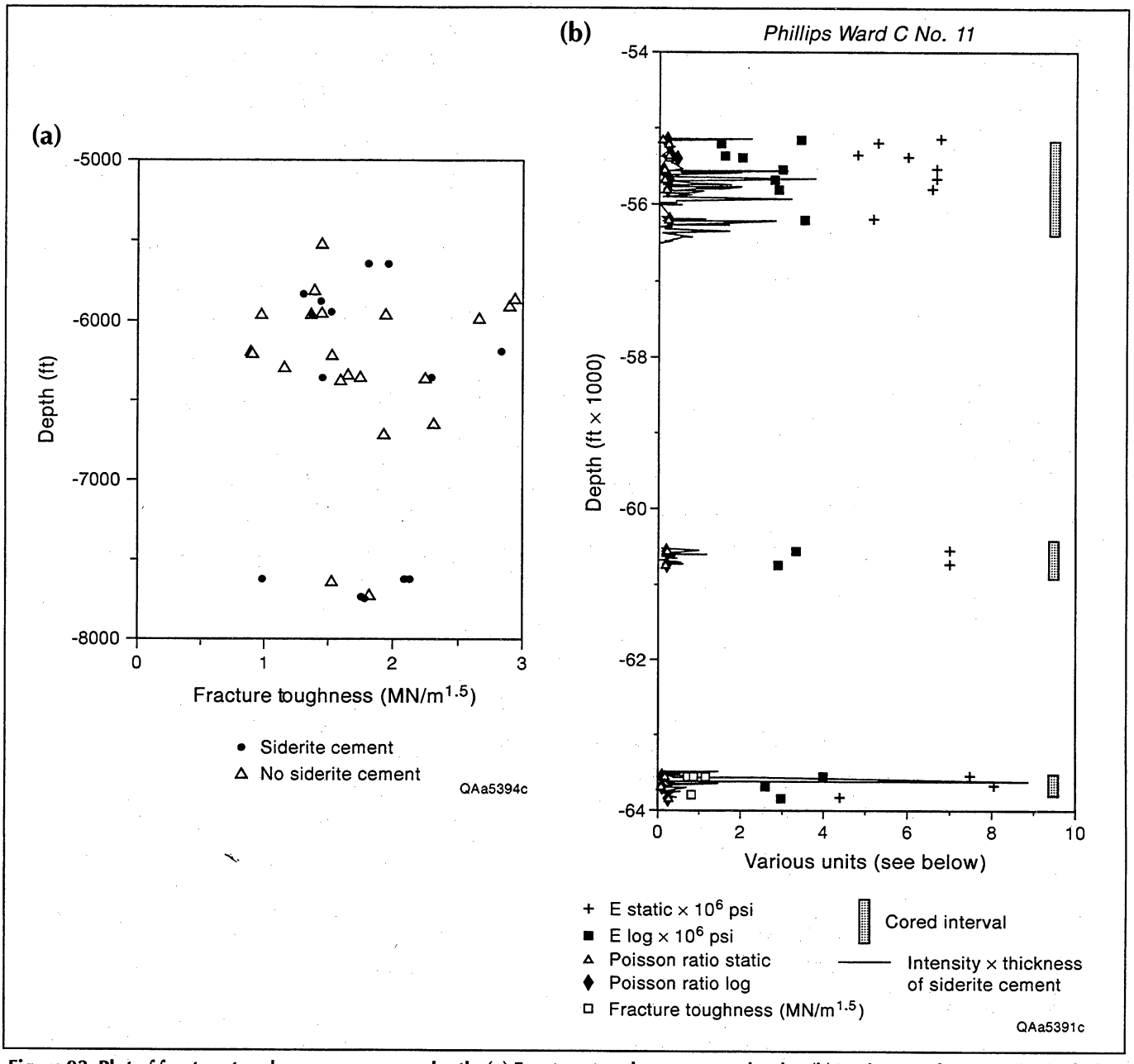

Figure 93. Plot of fracture toughness versus core depth. (a) Fracture toughness versus depths. (b) Various rock properties including fracture toughness versus depth.

lithic grains or clay-mineral cement, or the microstructure of grain boundaries, may control fracture toughness.

We found that, for the narrow range of low porosity values in nine samples (all having porosity less than 7 percent), there is no distinct trend in fracture toughness (table 9). Figure 90 illustrates how fracture toughness values vary with other petrographic parameters. As the number of quartz and feldspar detrital grains in direct contact with each other increases (hard contact percent increases) fracture toughness decreases (fig. 96a, r=-0.73). An increase in percent quartz corresponds to decreasing fracture toughness (fig. 96b, r=-0.77). Although our samples only cover a small range of quartz-overgrowth-cement volume and the trend is not statistically significant (r=-0.54), an increase in this cement type appears to correspond to a decrease in fracture toughness (fig. 96c). Samples that lack or have very small volumes of clay minerals have a range of fracture toughness values, but for samples having measurable clay mineral contents, increasing clay content corresponds to decreasing fracture toughness (fig. 96d, r=-0.93; -0.65 if samples lacking clay are included). The volume and distribution of clay particles and cements may be key to fracture toughness with clay-rich samples having lower values.

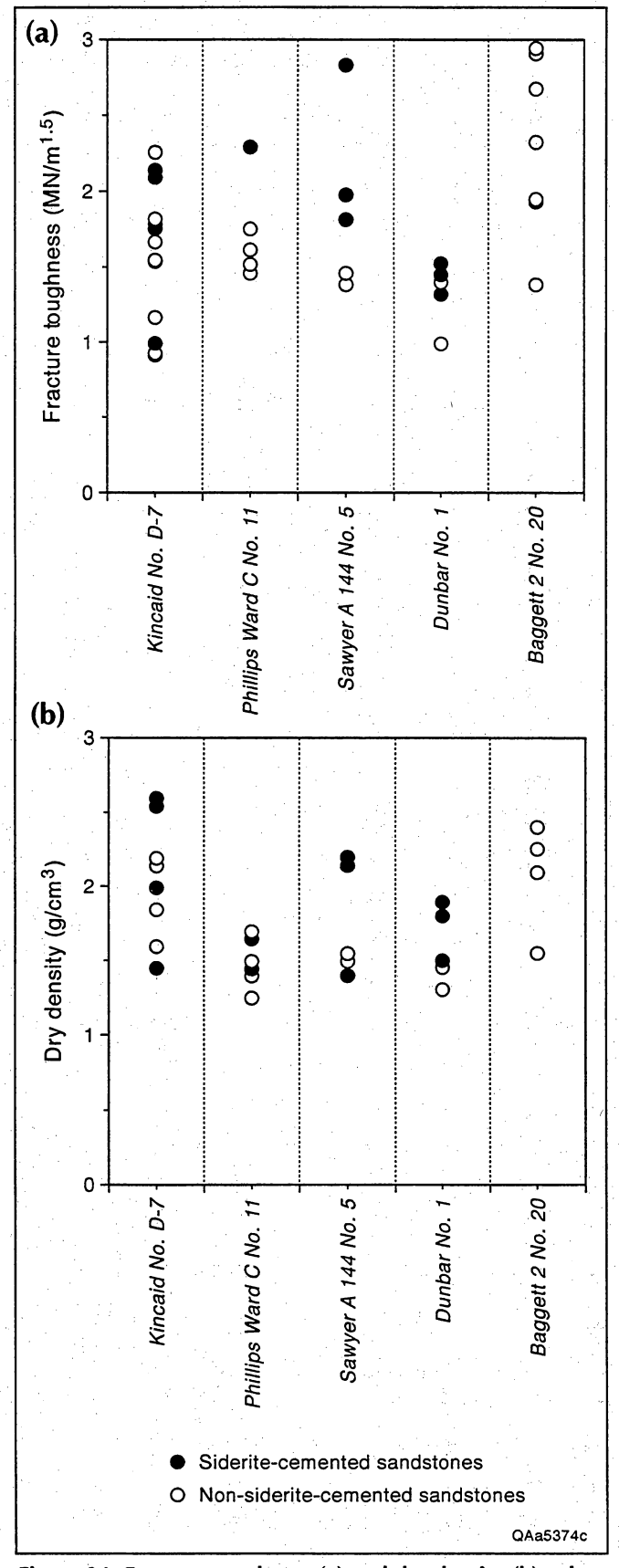

Figure 94. Fracture toughness (a) and dry density (b) values of the Canyon Sandstones. Closed circle for siderite-cemented sandstone, open circles for non-siderite-cemented sandstone.

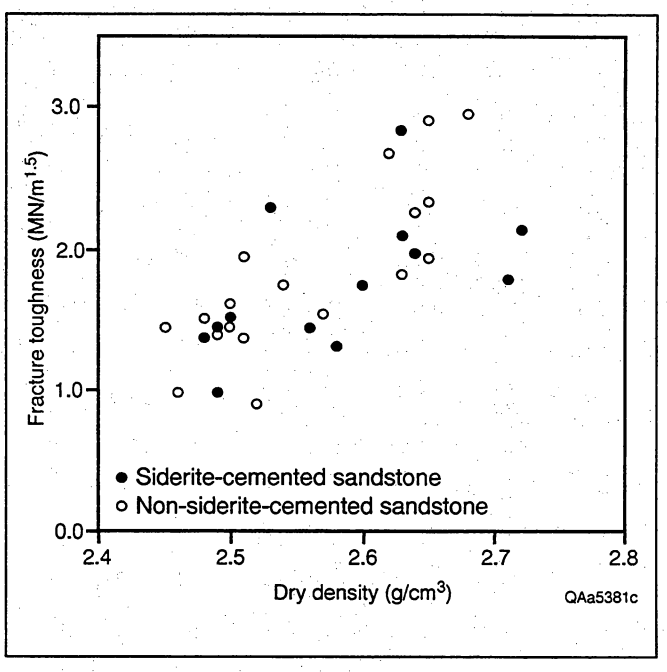

Figure 95. Dry density versus fracture toughness values of the Canyon Sandstones.

Ferm and others (1990) measured the fracture toughness of Travis Peak sandstones using the modified ring test, obtaining values that range from 0.74 MN/m$^{1.5}$ to 2.16 MN/m$^{1.5}$. They concluded that, for these strongly indurated quartzarenites, increasing amounts of ductile matrix (mainly clay minerals) can reduce fracture toughness. As the matrix becomes more abundant, measured fracture toughness will approach values typical of matrix rather than those of framework grains. Sandstones with well-rounded quartz grains and calcite cement have fracture toughness values well below that of the mineral quartz, suggesting that failure in these materials is controlled by the weak cement matrix between quartz grains (Meredith, 1989). Our results for the Canyon sandstone are consistent with those of Ferm and others (1990).

Poorly sorted Canyon sandstones also tend to have higher fracture toughness values. Large grains within clastic rocks may act as crack impeders, increasing measured fracture toughness because more energy is required to break intact grains that make up a greater proportion of coarse-grained rock (transgranular crack propagation), or force longer travel paths as the crack detours around large intact grains. For example, fracture toughness of rock commonly increases with increasing grain size due to a transition from intergranular crack propagation in fine-grained materials to transgranular crack propagation in coarser-grained materials. Microscopic crack propagation within rock is related to the local stress field and, more importantly, to physical properties including porosity distribution and dimensions

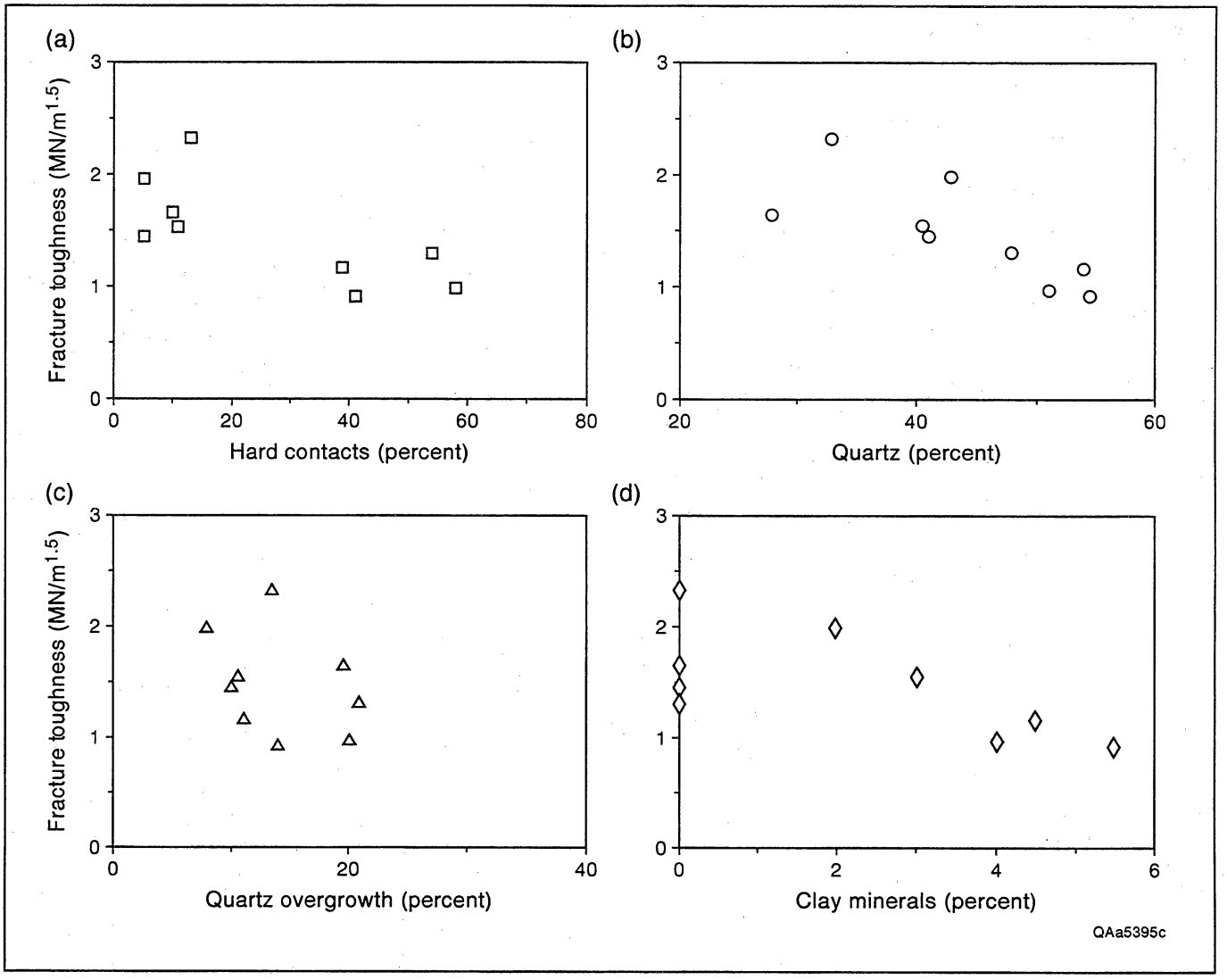

Figure 96. Relationships between fracture toughness and mineralogical composition. (a) Hard contacts (percentage of grains touching counted grain). (b) Percent quartz. (c) Percent quartz overgrowths. (d) Percent clay minerals. Petrographic measurements by T. F. Hentz.

and packing of granular mineral constituents and materials (cements and matrix) binding grains together.

Other Mechanical Properties

Static and dynamic measurements of Young's modulus and Poisson ratio were obtained for the Phillips Ward "C" No. 11 well (Miller and others, 1991). Results are summarized in figure 97. We compared rock composition with test results after eliminating test samples that contained fractures or marked lithologic variability. Results suggest that as quartz cement and/or siderite cement increase in rocks having low amounts of matrix and porosity, both static and dynamic elastic moduli increase. There also is a qualitative increase in elastic modulus within siderite cemented samples as the percent of siderite cement increases from low values (less than 10 percent) in slightly siderite-cemented sandstone to high values in moderately to highly siderite-cemented sandstone (more than 25 percent).

Microstructural Attributes of Fractures

In some instances the morphology of fractures propagating through a material can provide evidence of the properties of the rock at the time the fractures grew

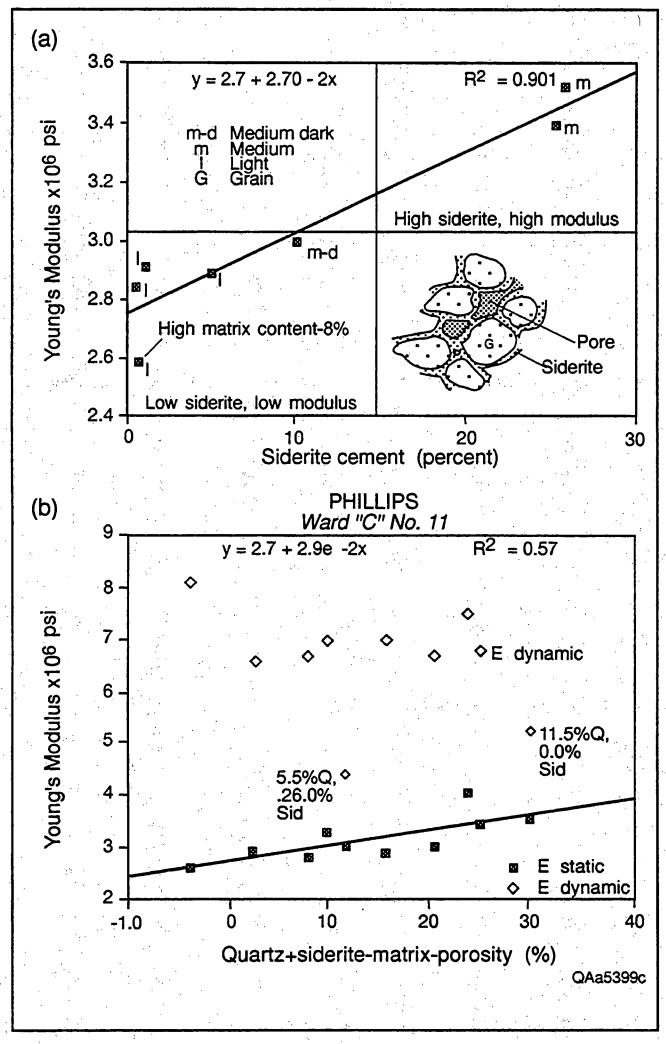

Figure 97. Mechanical properties and composition comparisons. (a) Young's modulus (from log data) versus percent of siderite cement from point counts of thin section. Visual estimates of degree of cementation (light-, medium-, and dark-colored core) are also shown. Inset shows distribution of pores, cement, and grains in siderite-cemented rocks. (b) Young's modulus (from core data) versus a cementation parameter (quartz and siderite cement volume, minus matrix and porosity).

(Bahat, 1991). Petrographic study of natural and experimentally induced Canyon Sandstone fractures shows that even where the fracture-filling minerals distinctive of natural fractures are absent, these two fracture types can be distinguished based on microstructural criteria. Natural fractures are rougher and have broken around sedimentary grains (intergranular), whereas experimentally induced fractures predominantly are planar and mostly transgranular. To illustrate how these results were obtained and quantified, in the following sections we describe our sample preparation procedures and the methods used for petrographic mapping of crack trajectories. Results have implications for the behavior of Canyon Sandstones during drilling, completion, and hydraulic fracture treatment. Results also have implications for proper interpretation of measured fracture toughness values.

Sample Preparation

Samples containing natural and experimentally induced fractures were carefully cut with a diamond saw blade of 0.71 mm (0.028 inch) thickness. In the case of experimental fractures for which crack propagation had been controlled, thin sections were made from the plane perpendicular to the fracture surface. For natural fractures, the major direction of fracture propagation was assumed to be horizontal, and thin sections were cut in the horizontal plane.

During sample preparation, rock samples containing fractures can easily be broken by vibrations associated with cutting by the rock saw. To avoid creating additional fractures during sample preparation, the samples were hardened prior to cutting with a specially prepared concrete restorer. This material is used for sealing cracks and repairing delaminations in concrete structures. A 4R concrete restorer (1000 ml) from 3M, which contains mainly dicyclpentadienyl methacrylate was mixed with cumyl hydroperoxide (40 ml). The solution can be hardened by adding a small amount of cobalt or by heating in an oven.

After 24 hours of soaking with the solution, each sample was placed in a plastic bag and then put in an 82°C (180°F) oven for 24 hours to promote methacrylate hardening and stabilization of fractures. Hardened samples were then cut with a rock saw and impregnated with a blue-dyed epoxy following standard procedures. Under the microscope, blue epoxy facilitated identification of fracture porosity.

Fracture Characterization

Five thin sections of experimental fractures and an equal number of thin sections of natural fractures were described. A special point-counting procedure was employed to characterize the crack trajectory. Thin sections were advanced with a counting stage along a reference line parallel to the fracture trace in 300 μm intervals. At each interval the character of the fracture section under the cross hair of the microscope was described in terms of the upward or downward deviation of the crack path from the reference line and the type of crack propagation increment in the vicinity. Categories were transgranular crack increment and intergranular crack increment. Transgranular crack increments cross individual grains, whereas intergranular crack increments pass through cement or pore space and commonly curve

around boundaries of mineral grains. Other properties noted at each interval were mineralogy, size, shape, and (where appropriate) orientation of grains and cement. The initial notch tip was taken as the start point for measurement along experimental fractures, and a point toward the center of the core was used as a reference for natural fractures.

A transgranular increment from an experimentally created fracture is illustrated in figure 98. Also visible is grain-rimming siderite cement. Despite numerous poorly bonded, siderite-coated grain contacts, the fracture extends with little deviation across grains. An intergranular increment from a natural fracture is shown in figure 99, an example having angular to sub-angular quartz grains and thick siderite cement rims and quartz cement. Despite the lack of porosity or other weak pathways, the fracture extends across the sample with numerous deviations from a straight trace.

Quartz cement can have similar mechanical properties as primary quartz grains, and should not necessarily be regarded as a "weak" element in resisting crack propagation. Although the join between grains and cement in quartz-cemented sandstones can be weak (for example, mild grinding was used to disaggregate grains and cement for geochemical studies of Travis Peak sandstones; Dutton and Land, 1988), crack pathways between quartz grains and quartz cement are rare in both natural and induced fractures in both the Canyon and Travis Peak sandstones. In this study, for petrographic traverse points near quartz overgrowth cements, the state of adjacent crack increments was used to define the nature of the crack increment. Where cracks propagated through quartz cement that formed a clear boundary between primary quartz grains, the increment was described as an intergranular crack increment. In contrast, if adjacent crack increments were through a zone of secondary quartz, more or less perpendicular to the major opening direction, then a transgranular crack increment was assigned. A schematic description of this procedure is depicted in figure 100. Figure 101 illustrates an example of the point counting procedure in which the length of each segment line connecting two adjacent data points sums to the "real" extension length of the crack. Here transgranular crack propagation is dominant.

For the cracks in this study, deviation from the straight reference line is commonly due to intergranular crack propagation. The crack front takes a less resistant path by extending through weaker but off-line grains or cementing materials. However, large grains of quartz resisted fracture and commonly forced the crack to detour.

Percent fracture length is defined as the ratio of length occupied by a certain crack increment type, either intergranular or transgranular, to total crack length. Hence, final values of percent intergranular and percent transgranular crack propagation sum to 100 percent at the right end of each plot. These graphs show the spatial distribution of two types of propagation behavior along a crack.

Figure 102 shows percent cumulative length of both intergranular and transgranular crack increments observed in natural fractures. Dotted lines represent intergranular propagation, whereas solid lines represent transgranular propagation. The higher slope of the dotted line in each plot shows that intergranular propagation dominates in natural fractures. There are sections where slopes of the two lines are similar (N2 and N3), but intergranular crack propagation is far more common.

Specimen N4 shows less intergranular crack propagation compared to that of other natural fractures. Percent lengths of both intergranular and transgranular crack propagation are similar, and the final percent intergranular propagation length is less than 50 percent. This is the only natural fracture specimen from non-siderite-cemented sandstone. Admittedly, this is only one example, but it is consistent with the interpretation that rims of siderite cement promotes intragranular fracture under natural conditions.

Figure 103 shows the microstructural pattern that typifies experimental fractures. Transgranular propagation is dominant with the exception of specimen E14. Among experimental fractures, E21 and E23 were obtained in non-siderite-cemented sandstone. However, no significant effect of siderite cementation on fracture propagation behavior is evident. It may be that effects of other test variables associated with experimental fracturing overwhelmed a possible effect of siderite cement on crack propagation.

Overall, a difference between natural and experimental fractures was observed in crack propagation behavior. Cumulative percentages of intergranular and transgranular crack propagation are listed in table 10. In contrast to the case of natural fractures, siderite cement rims are not markedly associated with intragranular cracking in experimental fractures.

These results raise questions about proper interpretation of fracture toughness values from tests. Comparison of fracture toughness and percent transgranular, or intergranular, crack propagation is inadequate. Figure 103 shows initially flat curves of percent intergranular propagation, particularly in specimens E20 and E21. These flat curves indicate that initial crack extension from the notch tip is mostly transgranular, whereas percent intergranular propagation increases as crack propagation continues. Therefore, fracture toughness values measured from peak load and initial crack extension would not necessarily represent the whole process of crack propagation. The fracture toughness value—ostensibly a material property—in these cases appears to reflect the summation of two distinct cracking processes that change in relative importance

Figure 98. Transgranular crack propagation in a specimen tested for fracture toughness. Cross-polarized light, 77× magnification.

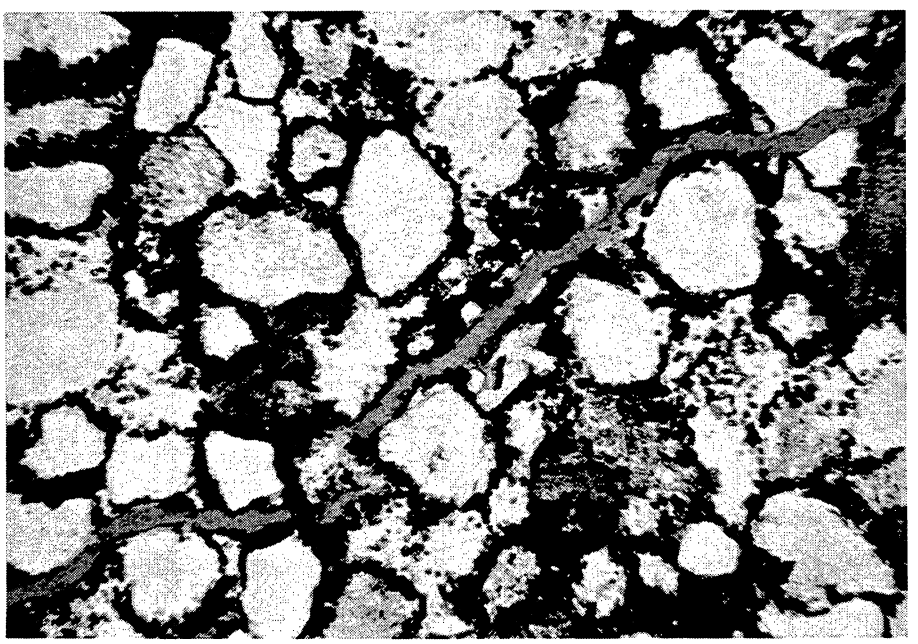

Figure 99. Intergranular crack propagation in a natural fracture sample. Plane-polarized light, 77× magnification.

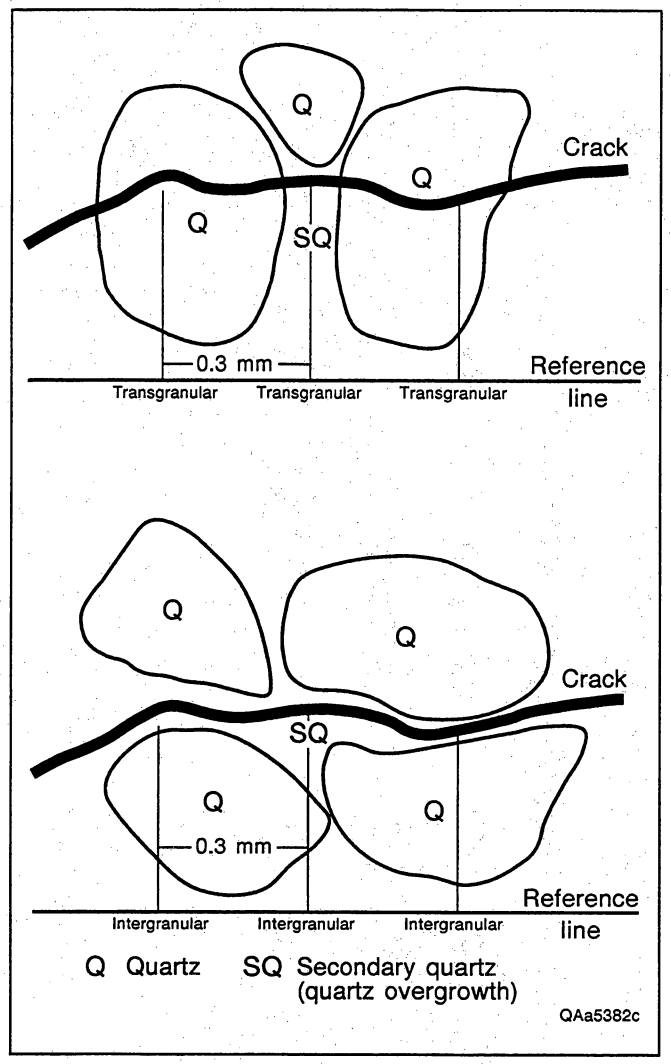

Figure 100. Criteria for counting fracture segment type.

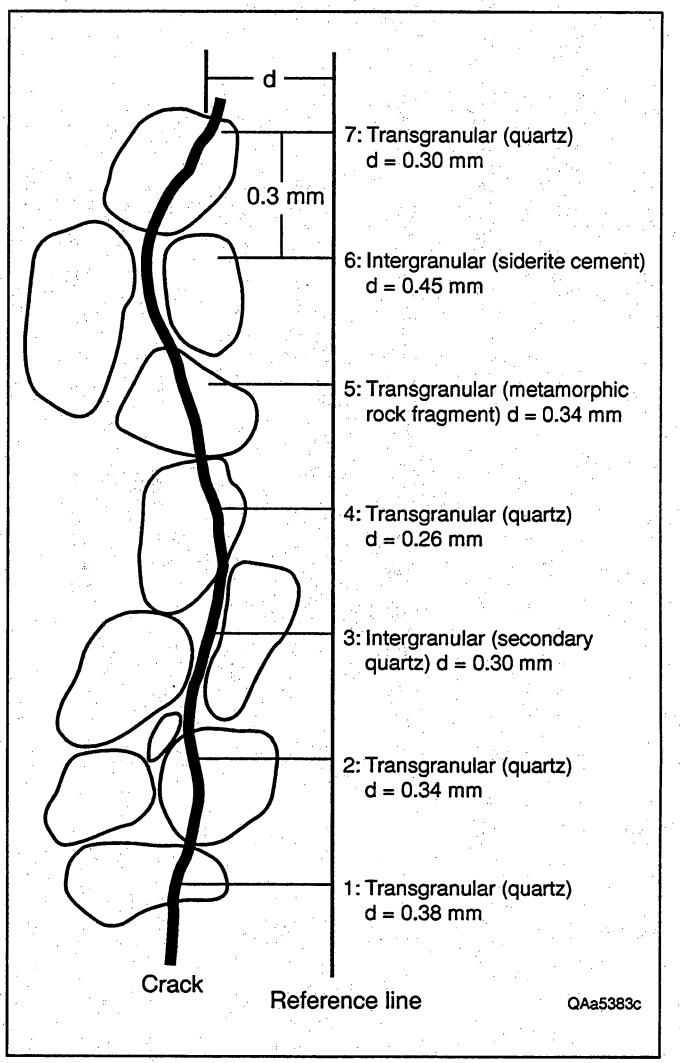

Figure 101. Illustration of point counting procedure for fracture profiles.

during the course of the experiment. A measure of the energy of fracture growth over a finite width of the specimen would be a more useful parameter.

Surface Roughness Profiles

Intergranular crack propagation is dominant in natural fractures, whereas transgranular crack propagation is far more common in experimental fractures. Natural fractures exhibit wavy and rough surface profiles as a result of dominance of intergranular crack propagation. In contrast, experimental fractures show straight and smooth profiles as a result of dominant transgranular crack propagation.

The wall roughness of a rock discontinuity is a potentially important contributor to fracture shear strength, dilatancy, and stiffness, especially in the case of undisplaced and interlocked features. Surface roughness can be described both quantitatively and qualitatively. Qualitative descriptions can be subjective and misleading, so quantitative descriptions should be sought. A semi-quantitative description of fracture (joint)-wall roughness summarized by the ISRM commission on Testing Methods (ISRM, 1981) is shown in figure 104. This classification system, originally proposed by Barton and Choubey (1977), was based on observations made primarily in underground openings and on results of simple tests involving direct shear offsets parallel to the plane of the discontinuity. In this scheme the joint roughness coefficient (JRC) has a value from 0 (smooth) to 20 (rough), representing the full range observed in discontinuity joint wall roughness. The JRC of a surface profile is estimated either by visual matching

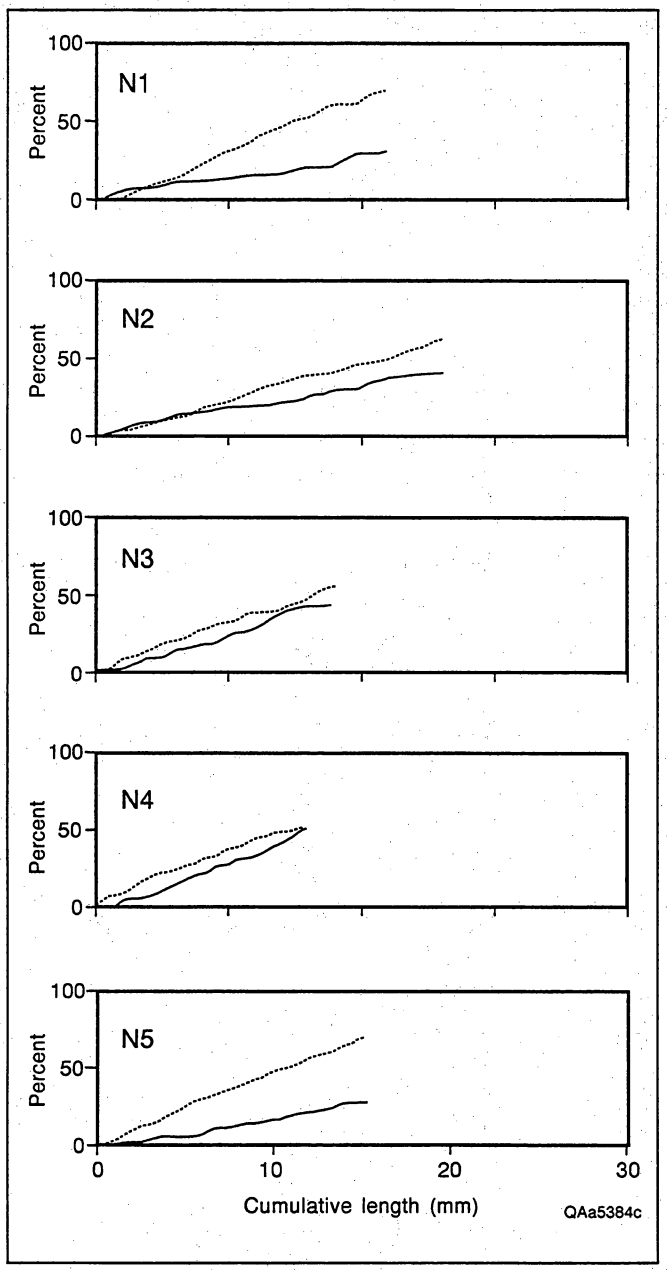

Figure 102. Cumulative inter- (dotted line) and transgranular (solid line) crack propagation of natural fractures.

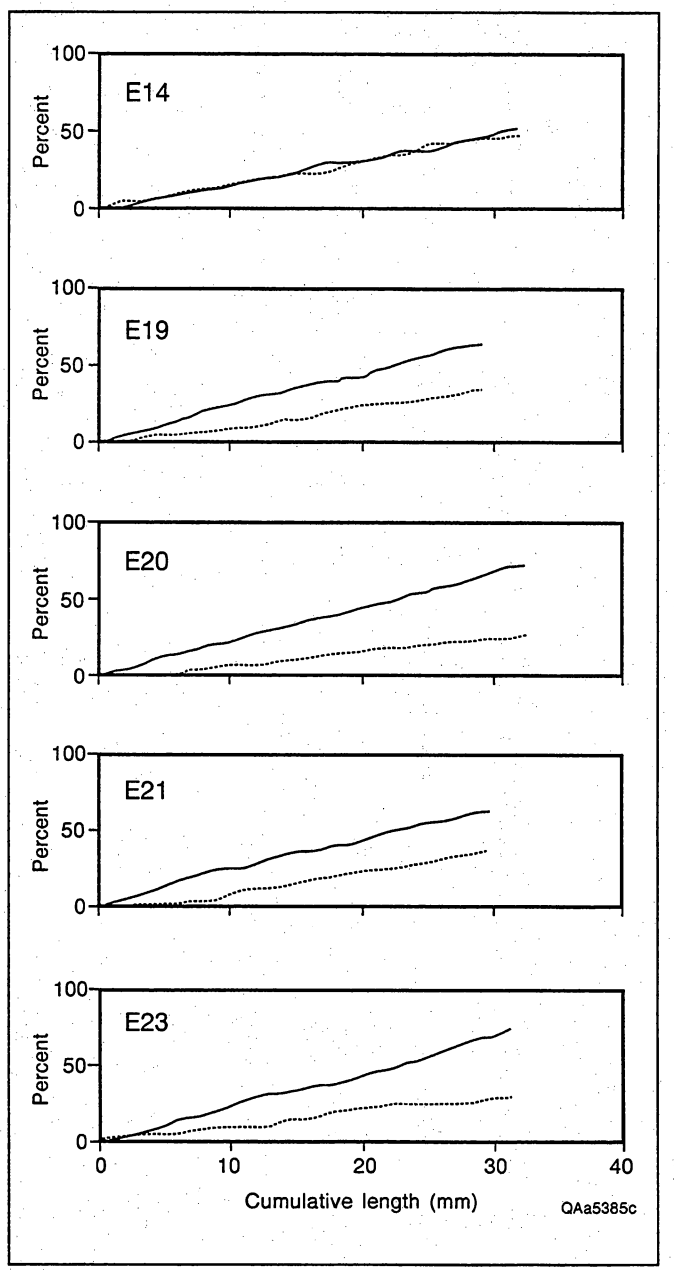

Figure 103. Cumulative inter- (dotted line) and transgranular (solid line) crack propagation of experimentally induced fractures.

with standard profiles such as those in figure 104, or by back-calculation using peak shear strength and basic friction angle in conjunction with joint-wall compressive strength. The latter approach is obviously impractical, considering the purpose of the JRC classification is to predict some of these attributes.

Although the JRC classification has been widely used, it may be subjective in practice. Fractal geometry of rock fracture surfaces has also been used in engineering practice (Brown and Scholz, 1985; Aviles and others, 1987; McWilliams and others, 1990). In this approach, numerical parameters are determined from fractal analyses of digitized surface profiles; drawbacks of this method include the cumbersome data collection requirements.

Another quantitative description of roughness profile, related to performance of side resistance in rock socketed piles, was introduced by Lam and Johnston (1985). Their approach is adopted in this study.

Table 10. Summary of intergranular and transgranular crack propagation in natural and experimental fractures.

Specimen	Cement	Fracture toughness ($MN/m^{1.5}$)	Intergranular propagation (%)	Transgranular propagation (%)
N1	siderite	–	70	30
N2	siderite	–	61	39
N3	siderite	–	55	45
N4	non-siderite	–	49	51
N5	siderite	–	72	28
E14	siderite	1.97	47	53
E19	siderite	1.44	35	65
E20	siderite	1.52	27	73
E21	non-siderite	1.29	38	63
E23	non-siderite	0.98	29	71

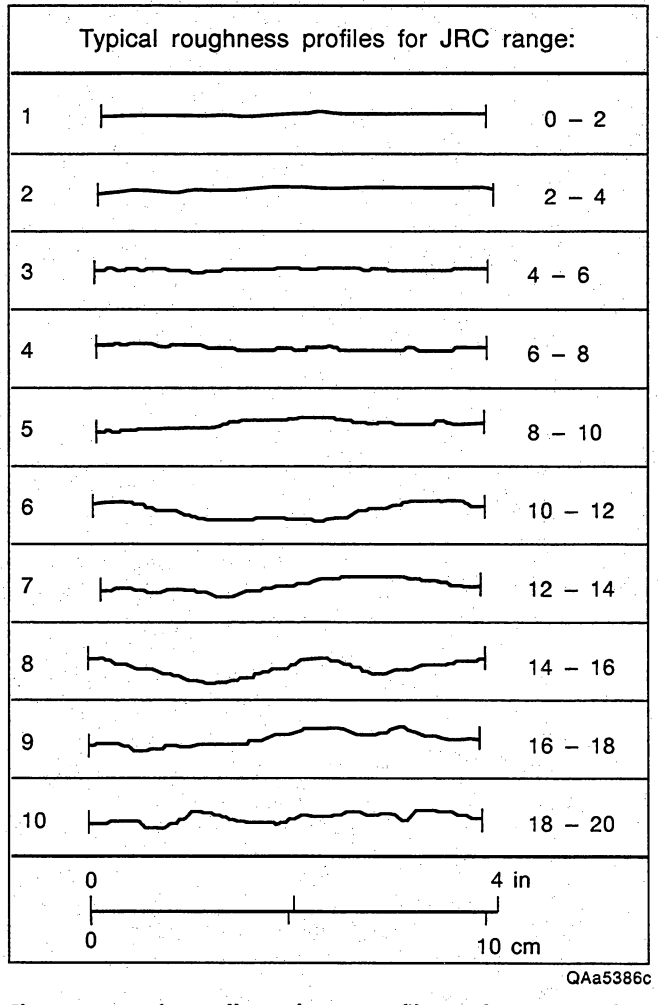

Figure 104. Joint-wall roughness profiles and corresponding range of JRC values (from Barton and Choubey, 1977).

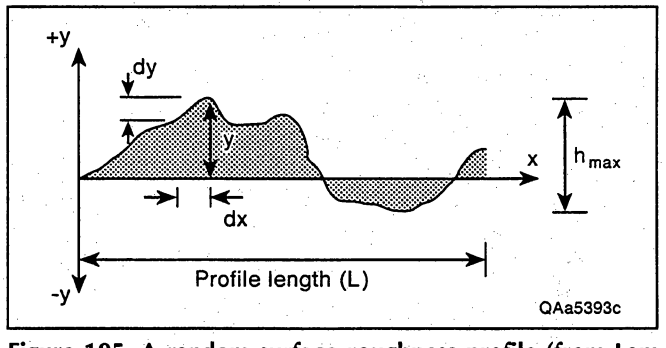

Figure 105. A random surface roughness profile (from Lam and Johnston, 1985).

Roughness of a fractured surface (fig. 105) is described by several statistical terms including maximum asperity height h_{max}, mean asperity height h_{ave}, standard deviation of the heights SD_h, mean asperity angle i_{ave}, and standard deviation of the angles SD_i. Maximum asperity height is the height difference between highest and lowest points on the profile, as shown in the figure. Other terms are calculated by (Lam and Johnston, 1985):

$$h_{ave} = \frac{1}{L}\int_0^L |y|\,dx \qquad (4)$$

$$SD_h = \sqrt{\frac{1}{L}\int_0^L \left(|y| - h_{ave}\right)^2 dx} \qquad (5)$$

Table 11. Statistical parameters of surface roughness of standard profiles of the JRC classification.

Group	JRC	h_{max} (mm)	h_{ave} (mm)	SD_h (mm)	SD_i (deg.)	Ratio, R
1	0–2	0.57	0.21	0.14	7.4	1.01
2	2–4	0.95	0.47	0.21	13.9	1.03
3	4–6	1.30	0.30	0.23	17.3	1.04
4	6–8	1.71	0.49	0.31	20.4	1.06
5	8–10	3.39	0.90	0.84	21.7	1.07
6	10–12	5.77	1.97	1.43	22.2	1.07
7	12–14	5.09	1.20	0.93	21.7	1.07
8	14–16	6.48	2.44	1.88	24.6	1.09
9	16–18	4.92	1.14	0.94	24.9	1.09
10	18–20	4.25	1.05	0.78	26.6	1.10

$$i_{ave} = \tan^{-1}\left[\frac{1}{L}\int_0^L \left(\frac{dy}{dx}\right) dx\right] \quad (6)$$

$$SD_i = \tan^{-1}\sqrt{\frac{1}{L}\int_0^L \left(\frac{dy}{dx} - \tan i_{ave}\right)^2 dx} \quad (7)$$

Parameters h_{ave} and SD_h provide an indication of the position of the mean line of profile and deviation of the heights from this mean line, respectively. The parameter i_{ave} indicates average inclination of each segment line, connecting two data points, to the horizontal of the mean line through asperities. In this study, the first and last data points of the crack profile were connected to draw a horizontal reference line, so that i_{ave} will be zero. Parameters h_{max} and SD_i are the most relevant terms with regard to assessment of shear performance of rough rock joints (Lam and Johnston, 1985). Accordingly, these parameters were used to compare roughness profiles of natural and experimental fractures.

An objective basis for JRC classification can be obtained by applying these numerical parameters to measured data. Standard profiles in figure 104 were digitized using a scanner. Parameters were then calculated and listed in table 11. The ratio, R, between linear length of a profile, measured by straight line distance between first and last data points, and real length measured along actual profile represents relative tortuosity of different fracture profiles. Figure 106 is digitized from figure 104.

As listed in table 11, no general relationship between JRC values and statistical parameters of roughness profiles are evident. Most parameters, with exceptions of SD_i and R, are fluctuating for higher JRC values (Groups 7 to 10). This is because in estimating shear resistance of rock discontinuities the number of asperities is a more important parameter than individual asperity height (for example figs. 98 and 100, where higher JRC values are given to profiles with more asperities). Therefore, it is questionable if these statistical parameters apply to JRC profiles in general. However, microscopic profiles of rock fractures are expected have low JRC values, where all statistical parameters are in step with JRC values.

Microscopic roughness profiles of natural fractures in figure 107. Vertical and horizontal scales are the same in this figure. Fractures depicted in this figure may be roughly described as exhibiting a undulating surface, following the descriptive terms for the roughness profiles suggested by the ISRM Commission on Testing Methods (ISRM, 1981). Typical roughness profiles and suggested nomenclature are shown in figure 108. Roughness profiles of experimental fractures are shown in figure 109. Figures 107 and 109 are drawn to the same scale, so they can be compared directly. Roughness profiles of experimental fractures are smooth and planar compared to those of natural fractures (fig. 107). However, such a general distinction cannot be documented for all cases, in particular when comparing profiles E19 or E20 with N1 or N5.

Statistical parameters of surface profiles of natural and experimental fractures are listed in table 12. It was expected that experimental fractures with dominant transgranular crack propagation would have lower

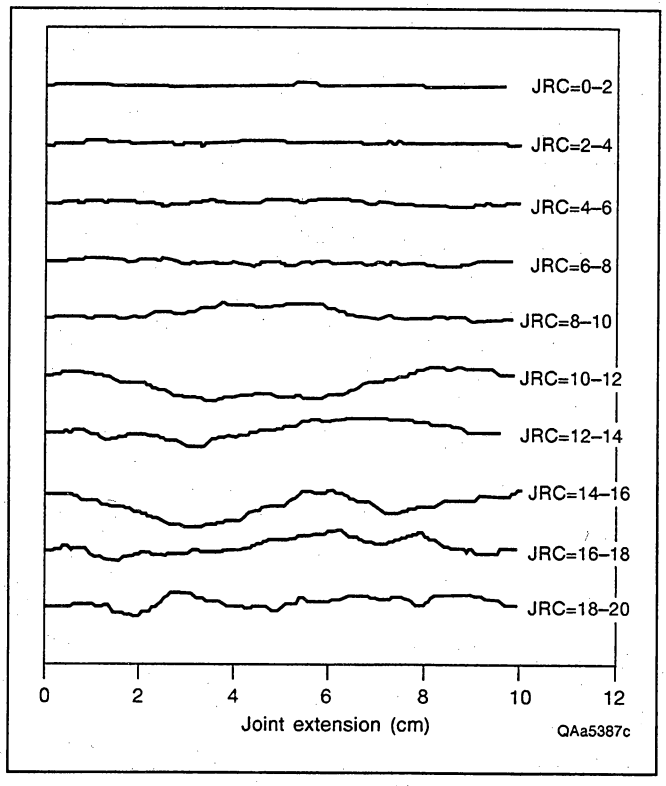

Figure 106. Digitized roughness profiles of the JRC classification.

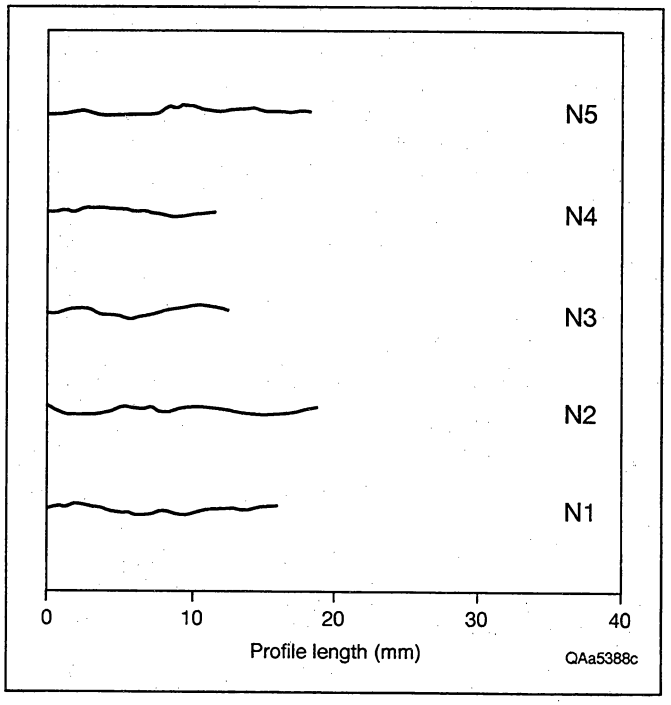

Figure 107. Surface roughness profiles of natural fractures, Canyon Sandstone.

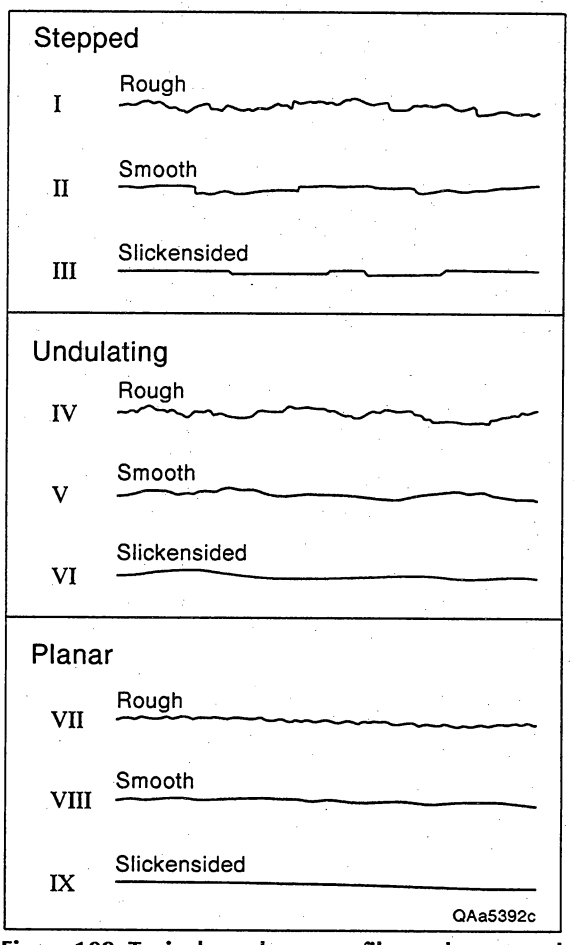

Figure 108. Typical roughness profiles and suggested nomenclature (from ISRM, 1981).

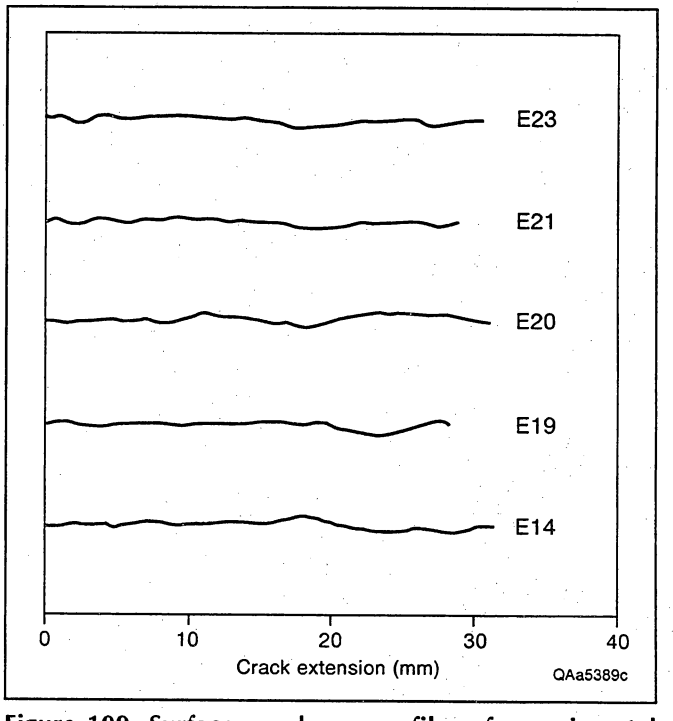

Figure 109. Surface roughness profiles of experimental fractures.

Table 12. Statistical parameters of roughness profiles of natural (N) and experimental (E) fractures.

Specimen	Cement	h_{max} (mm)	h_{ave} (mm)	SD_h (mm)	SD_i (deg.)	R
N1	siderite	0.83	0.28	0.16	12.1	1.02
N2	siderite	0.82	0.24	0.17	17.8	1.04
N3	siderite	1.10	0.24	0.15	17.6	1.05
N4	non-siderite	0.70	0.18	0.12	10.3	1.02
N5	siderite	0.63	0.20	0.16	12.1	1.02
E14	siderite	1.16	0.23	0.16	2.2	1.02
E19	siderite	1.09	0.17	0.19	3.4	1.03
E20	siderite	1.09	0.30	0.23	4.7	1.04
E21	non-siderite	0.83	0.15	0.13	2.7	1.03
E23	non-siderite	0.85	0.17	0.14	2.6	1.02

values of SD_i and R, compared to natural fractures in which wavy and rough intergranular crack propagation was dominant. As shown in table 12, the parameter SD_i shows a clear distinction between natural and experimental fractures. This reflects rougher surface profiles of natural fractures, since a low SD_i value indicates a smooth and planar surface. However, other statistical parameters, as well as R, do not clearly distinguish between the two fracture types.

Among natural fractures sampled from siderite-cemented sandstones, specimens N2 and N3 have thicker siderite cementation compared to that of N1 and N5. Higher values of SD_i and R of these fracture profiles reflects thicker siderite cementation. Experimental fractures exhibit a similar trend. In fact, more undulating surface profiles were observed for fractures in siderite-cemented sandstones. It may be that for each grouping of natural and experimental fractures, siderite-cemented sandstones have higher values of all parameters, that is rougher surface profiles. This conclusion is consistent with the high percent intergranular crack propagation associated with siderite cementation. A comparison of tables 11 and 12 shows that all fractures belong to the range of groups 1 to 3 of the JRC classification. However, experimental fractures have much lower SD_i values than that of group 1 profile, while other parametric values mostly belong to groups 2 or 3.

Although originally developed for estimating frictional resistance of larger scale surface profiles, statistical parameters of Lam and Johnston (1985) provide a reasonable basis for describing surface roughness of fractures under the microscope. Significantly lower SD_i values of experimental fractures may be interpreted as an indication of smooth and planar profiles caused by transgranular propagation.

The effect of siderite cementation on crack propagation is also evident in more intergranular crack propagation and rougher surface profiles. This may be an indication of natural fracturing associated with early siderite cementation, in which fractures were more likely to have propagated along grain boundaries rather than passing through framework grains surrounded by brittle siderite cements.

These observations also suggest that natural and induced fractures in the subsurface will have different sensitivity to changes in effective stress proppant distribution and other properties affecting post-stimulation fluid flow. This is due to the sensitivity of these parameters to fracture surface roughness.

Fracture Growth during Drilling/Completion

Using the criteria developed in the preceding section it is possible to determine if natural fractures have been reactivated during core recovery (fig. 110). Petrographic observations of Canyon Sandstone natural fracture tips suggest that during coring, natural fractures were

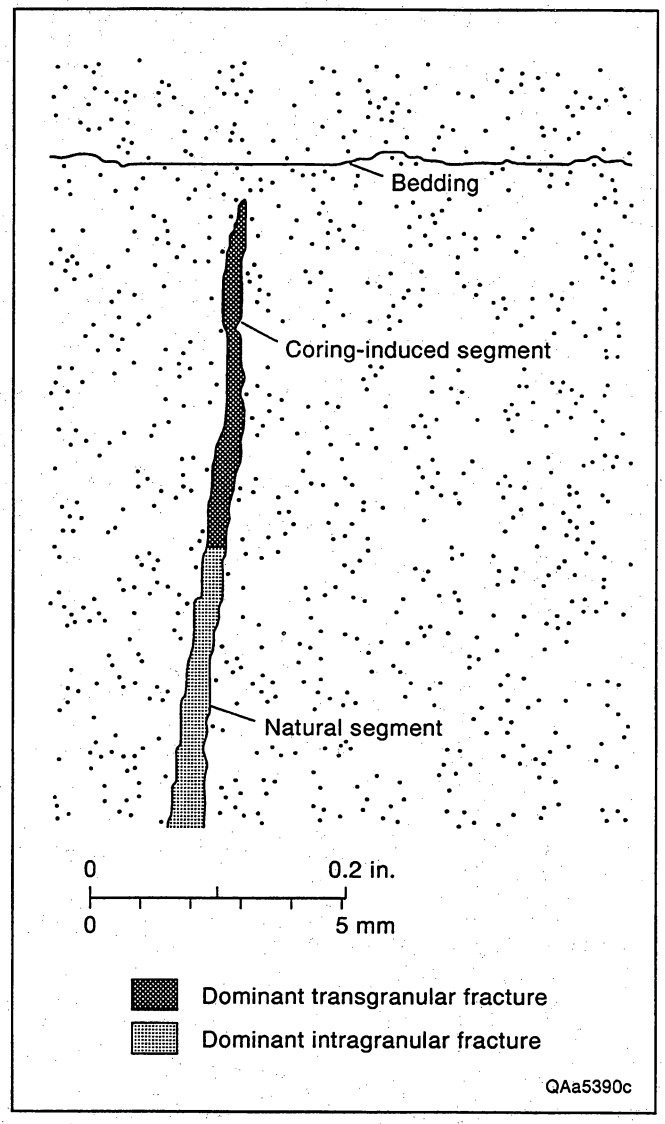

Figure 110. Natural fracture and fracture segment induced by coring operations. Petrographic criteria were used to distinguish different generations of fracture propagation.

reactivated and grew by a small amount (length increases of less than 10 percent of their original length). From this we infer that under typical near-wellbore reservoir conditions, natural fractures in rocks having representative fracture toughness values for low-permeability sandstone such as the Canyon sandstones can readily propagate under the influence of fluid pressure perturbations such as those that are likely to obtain during stimulation and probably also as a result of drilling. This is consistent with the large number of coring-induced fractures observed in Canyon core (Laubach and Marin, this volume). Although natural fractures in the Canyon core we studied are all small compared to a fracture created during stimulation, the natural fractures are numerous and each is potentially a nucleus for a larger fracture. Thus multiple fractures may be initiated near the wellbore.

During hydraulic fracture treatments this tendency could make Canyon sandstones prone to a process wherein fracture reactivation and growth in naturally fractured intervals produces multiple interacting fracture strands. This phenomenon has been called on as one cause of the near-wellbore tortuosity that analysis of pressure records has implicated as a cause of some types of high net treatment pressures. This phenomenon has been observed in Canyon fracture treatment pressure records. It is a process that can—if not accounted for in treatment design—have detrimental effects on treatment success.

In summary, natural and induced fractures can be distinguished by contrasts in degree of intragranular fracture pathways. Natural fractures have higher proportions of these. Based on this pattern and the observation that many natural fractures in core have unmineralized segments near their edges that are predominantly transgranular, we conclude that natural fractures are readily reactivated and grow under the influence of perturbations due to drilling activity.

Fracture Toughness as a Guide to Natural Fracture Occurrence

Contrasts in rock properties such as rock stiffness, tensile strength, or fracture toughness may, in some circumstances, be used as guides to areas of preferential natural fracture occurrence. This is not the case for the Canyon Sandstone. Fracture toughness tests on Sonora Canyon sandstone specimens do not clearly distinguish siderite-cemented and non-siderite-cemented sandstones, so contrasts in current values in this parameter cannot account for differences in fracture abundance in Sonora Canyon sandstone core between these two rock types (Laubach and Marin, this volume). These contrasts in fracture abundance are more likely due to sampling bias and contrast in fracture spacing in beds of differing thickness. Contrary to some recently published interpretations (Skopec, 1992), we find that mechanical-property data alone can be misleading if used to rank the natural fracture potential of the formation—even on a relative basis. Moreover, it is certainly true that stress boundary conditions and chemical environments under which natural fractures developed differed from those of experimental fractures.

In sandstones that have experienced a long, involved history of linked diagenesis and fracturing, it seems

unlikely to us that current fracture toughness or any rock property would be a good guide to fracture abundance except where fractures are the result of deformation that occurred after rock properties had been established. This is because compaction and cementation can modify the physical properties, including the fracture characteristics, of rock materials, and diagenetic and mechanical properties contrasts among rock types in a sequence can in principle become more or less pronounced with time as compaction and diagenesis proceed.

For Canyon Sandstones, average fracture toughness values of the sandstones as they exist today probably do not reflect the mechanical property contrast that existed when natural fractures formed. Early siderite cementation locked grains into a rigid framework that permitted fractures to grow, while adjacent sandstones that lacked siderite cement experienced compaction by grain rearrangement and porosity loss. Subsequent quartz and calcite cements and denser grain packing eventually brought these rocks to the point where further deformation was by throughgoing fractures, and this increased their fracture toughness to values comparable to beds that had been cemented earlier with siderite.

Study Summary and Overall Conclusions

Stratigraphy and Depositional Facies

The regional stratigraphic frameworks of Ozona and Sonora Canyon sandstones were mapped and now provide a context for exploration and development in these prolific trends. Depositional facies analysis revealed that most Ozona and Sonora sandstones formed in submarine-fan channel and lobe environments. Fan-channel sandstones are thick-bedded but lenticular, whereas fan-lobe sandstones are thin-bedded but more laterally continuous. Thick and thin beddedness are measures of the abundance of shale laminations and interbeds, which from studies of core were found to have a detrimental effect on Canyon reservoir quality. Net-sandstone, maximum-sandstone, and log-facies maps, when interpreted together, effectively highlighted prospective areas by delineating thick-bedded fan-channel sandstones. Although our data did not permit rigorous verification, we infer that channel sandstones form the best reservoirs. Analysis of limited production data supports this view (fig. 111).

Several field-scale studies showed that the dimensions of individual Sonora sandstones are generally small, fan lobes being a few hundred feet thick and a few miles wide and fan channels less than 100 ft thick and less than 1 mi wide. Both the regional and field-scale stratigraphic findings presented in this report should provide useful starting points for the more focused geologic and engineering analyses that Canyon operators perform when designing exploration and development programs. Our stratigraphic framework will also provide a starting point for effectively applying advanced technology—such as directional drilling or 3-D seismic.

Sandstone Composition

Most Ozona and Sonora Canyon sandstones are fine- to medium-grained litharenites in which much of the original porosity was destroyed by mechanical compaction and by cementation by quartz and carbonate minerals. Siderite cement, however, which apparently occurs only in the Sonora, has the overall effect of preserving porosity and may be the key to good within-sandstone reservoir quality. Because siderite layers are developed preferentially in thick-bedded turbidites (Bouma A divisions), they probably contribute to enhanced reservoir quality in the fan-channel sandstones relative to the fan-lobe sandstones, where thin-bedded turbidites predominate. Although variations in siderite cementation in different facies and areas of the Sonora trend as well as controls on siderite genesis were documented during this study, research based on a more

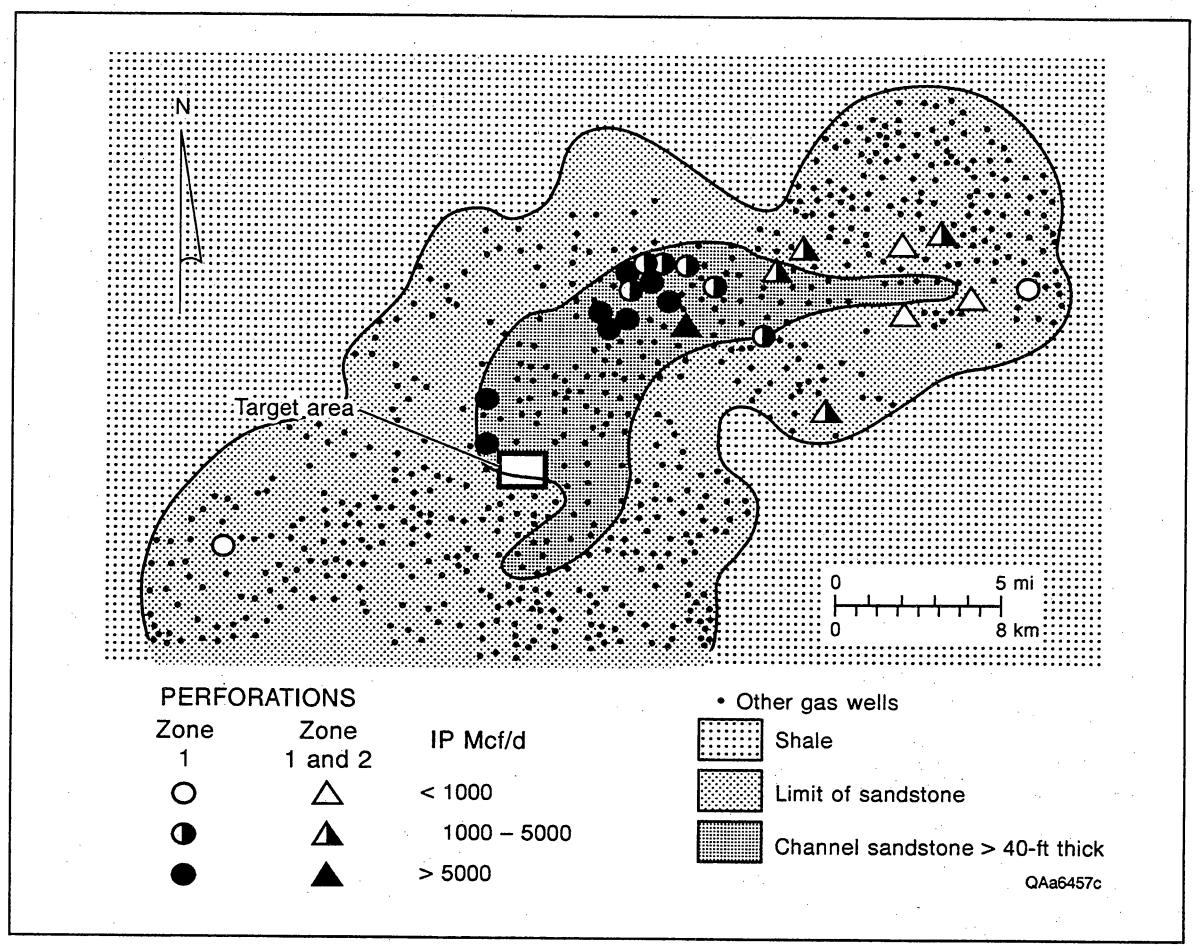

Figure 111. Relationship between depositional facies and productivity—example from the Ozona Canyon.

comprehensive core data base will be required to achieve the level of understanding necessary to predict the occurrence of siderite-enhanced porosity.

Natural Fractures

Natural fractures are widespread in both Sonora and Ozona Canyon sandstones. For the most part these fractures are short (less than 10 inches tall) and this, as well as the closely spaced interbeds in Canyon turbidites that will tend to create vertical permeability barriers and baffles, suggests that successful horizontal drilling to exploit these fractures will be challenging. Clearer understanding of the distribution and orientation of large, through-going natural fractures will probably be necessary for effective application of horizontal drilling technology. Natural fractures play various roles in gas reservoirs, and awareness of their existence and character can help guide reservoir stimulation and management decisions. A method for enhancing natural fracture network conductivity by acid treatment was proposed for testing.

In our study we have used laboratory tests to document fracture toughness of Sonora and Ozona sandstones—values average 1.77 ± 0.46 MN/m$^{1.5}$ to 1.72 ± 0.60 MN/m$^{1.5}$. By developing criteria for recognizing reactivation of natural fractures and by documenting reactivation in Canyon core, this study shows that in rocks with fracture toughness values within the range reported for other tight gas sandstones, fracture reactivation and possibly the growth of multiple fracture strands near the wellbore is possible. These fracture toughness values and insights into possible near-wellbore phenomena can be taken into account in fracture treatment design.

Acknowledgments

This study was funded by the Gas Research Institute under contract no. 5082-211-0708, Larry Brand and John Hansen, Project Managers. We acknowledge Enron Oil and Gas Company and Phillips Petroleum Company for allowing GRI contractors to collect data in the Enron Sawyer 144 "A" No. 5 and Phillips Ward "C" No. 11 cooperative wells. Priscilla P. Nelson, Department of Civil Engineering, provided access to laboratory facilities and discussed rock property testing. Research Assistant Barbara Marin measured the thickness and location of every siderite band or patch in the cores, and research assistant Eugene Kim aided in many aspects of the stratigraphic analysis. Bruce Turbeville performed the isotopic analyses at the Bureau of Economic Geology Mineral Studies Laboratory under the direction of Steven W. Tweedy, Chemist-in-Charge. We appreciate the reviews of this paper by John Hansen, Tucker F. Hentz, and Raymond A. Levey, and editorial comments from Amanda R. Masterson and Jeannette Miether. Word processing was by Susan Lloyd, and design was by Margaret L. Evans. Figures were drafted by Edwin B. Banks, Michele Bailey, and Maria Saenz under the supervision of Richard L. Dillon. David Stephens provided text illustration photography. Publication authorized by the Director, Bureau of Economic Geology, The University of Texas at Austin.

References

Aguilera, Roberto, 1988, Determination of subsurface distance between vertical parallel natural fractures based on core data, AAPG Bulletin, v. 72, no. 7, p. 845–851.

Aviles, C. A., Scholz, C. H., and Boatwright, J., 1987, Fractal analysis applied to characteristic segments of the San Andreas Fault, Journal of Geophysical Research, v. 92, pp. 331–344.

Baek, Hwanjo, 1994, Evaluation of fracture mechanics properties and microstructural observations of rock fractures, Ph.D. dissertation, The University of Texas at Austin, 200 p.

Bahat, D., 1991, Tectonofractography, Springer-Verlag, Berlin, Germany, 354 p.

Barton, N., and Choubey, V., 1977, The shear strength of rock joints in theory and practice: Rock Engineering, v. 10, no. 1, p. 1–54.

Berg, R. R., 1986, Reservoir sandstones: Englewood Cliffs, New Jersey, Prentice-Hall, 481 p.

Berner, R. A., 1971, Principles of Chemical Sedimentology: New York, McGraw-Hill, 240 p.

Berner, R. A.,1981, A new geochemical classification of sedimentary environments: Journal of Sedimentary Petrology, v. 51, p. 359–365.

Berner, R. A., 1985, Sulphate reduction, organic matter decomposition and pyrite formation, *in* Eglinton, G., Curtis, C. D., McKenzie, D. P., and Murchison, D. G., eds., Geochemistry of Buried Sediments: London, The Royal Society, p. 25–38.

Bieniawski, Z. T., and Hawkes, I., 1978, Suggested method for determining tensile strength of rock materials: International Journal of Rock Mechanics and Mining Sciences & Geomechanical Abstracts, v. 15, no. 3, p. 99–103.

Bloomer, R. R., 1977, Depositional environments of a reservoir sandstone in West-Central Texas: American Association of Petroleum Geologists Bulletin, v. 61, p. 344–359.

Bloomer, R. R., 1991, Sandstone systems and reservoirs on the eastern shelves and slopes of the Midland Basin, Texas: American Association of Petroleum Geologists Southwest Section, Abilene Geological Society, 32 p.

Botz, R., and von Rad, U., 1987, Authigenic Fe-Mn carbonates in Cretaceous and Tertiary sediments of the continental rise off eastern North America, Deep Sea Drilling Project Site 603, *in* Van Hinte, J. E., Wise, S. W., Jr., and others, eds., Initial Reports of the Deep Sea Drilling Project, v. 93, p. 1061–1077.

Bouma, A. H., 1962, Sedimentology of some flysch deposits: a graphic approach to facies interpretation: Amsterdam, Elsevier, 168 p.

Brian, Mrs. D. D., Jr., 1955, Miers Field, Sutton County, Texas: San Angelo Geological Society Geological Contributions, p. 59–66.

Brown, L. F., Jr., 1989, Use of sequence stratigraphy to define stratigraphic plays in Upper Pennsylvanian

and Lower Permian lowstand systems tracts, North-Central Texas: Transactions, American Association of Petroleum Geologists Southwest Section, San Angelo, p. 1–21.

Brown, L. F., Jr., and Solis-Iriarte, R. F., and Johns, D. A., 1990, Regional depositional systems tracts, paleogeography, sequence stratigraphy, Upper Pennsylvanian and Lower Permian strata, North- and West-Central Texas: The University of Texas at Austin, Bureau of Economic Geology, Report of Investigations No. 197, 116 p.

Brown, S. R., and Scholz, C. H., 1985, Broad bandwidth study of the topography of natural rock surfaces, Journal of Geophysical Research, v. 90, p. 12,575–12,582.

Carothers, W. W., Adami, L. H., and Rosenbauer, R. J., 1988, Experimental oxygen isotope fractionation between siderite-water and phosphoric acid liberated CO_2-siderite: Geochimica et Cosmochimica Acta, v. 52, p. 2445–2450.

Carpenter, S. J., Erickson, J. M., Lohmann, K. C., and Owen, M. R., 1988, Diagenesis of fossiliferous concretions from the Upper Cretaceous Fox Hills Formation, North Dakota: Journal of Sedimentary Petrology, v. 58, p. 706–723.

CER Corporation, 1991a, Summary of open-hole data acquisition and field operations, Enron Sawyer A-144 No. 5: unnumbered topical report prepared for the Gas Research Institute under Contract No. 5091-221-2130, variously paginated.

CER Corporation, 1991b, Summary of open-hole data acquisition and field operations, Phillips Ward C-11: unnumbered topical report prepared for the Gas Research Institute under Contract No. 5091-221-2130, variously paginated.

Chong, K. P., and Kuruppu, M. D., 1984, New specimen for fracture toughness determination for rock and other materials: International Journal of Fracture, v. 26, no. 2, p. R59–R62.

Claypool, G. E., and Kaplan, I. R., 1974, The origin and distribution of methane in marine sediments, *in* Kaplan, I. R., ed., Natural Gases in Marine Sediments: Marine Science, v. 3, p. 99–140.

Coleman, M. L., 1993, Microbial processes: controls on the shape and composition of carbonate concretions: Marine Geology, v. 113, p. 127–140.

Coleman, M. L., and Raiswell, R., 1993, Microbial mineralization of organic matter: mechanisms of self-organization and inferred rates of precipitation of diagenetic minerals: Philosophical Transactions of the Royal Society of London A, v. 344, p. 69–87.

Collins, E. W., Laubach, S. E., Dutton, S. P., and Hill, R. E., 1992, Depositional environments, petrology and fractures of the Atoka Davis Sandstone: a low-permeability gas-bearing sandstone of the Fort Worth Basin, north-central Texas, Transactions, Southwest Section AAPG, p. 221–230.

Craig, H., 1957, Isotopic standards for carbon and oxygen correction factors for mass-spectrometric analysis of carbon dioxide: Geochimica et Cosmochimica Acta, v. 12, p. 133–149.

Curtis, C. D., 1978, Possible links between sandstone diagenesis and depth-related geochemical reactions occurring in enclosing mudstones: Geological Society of London Journal, v. 135, p. 107–117.

Curtis, C. D., 1986, Mineralogical consequences of organic matter degradation in sediments: inorganic/organic diagenesis, *in* Leggett, J. K., and Zuffa, G. G., eds., Marine Clastic Sedimentology: London, Graham & Trotman, p. 108–123.

Curtis, C. D., and Douglas, I., 1993, Catchment processes and the quantity and composition of sediment delivered to terminal basins: Philosophical Transactions of the Royal Society of London A, v. 344, p. 5–20.

Cys, J. M., and Gibson, W. R., 1988, Pennsylvanian and Permian geology of the Permian Basin region, *in* Sloss, L. L., ed., Sedimentary cover—North American craton, U.S.: Boulder, Colorado, Geological Society of America, The Geology of North America, v. D-2, p. 277–289.

Dutton, S. P., Clift, S. J., Folk, R. L, Hamlin, H. S., and Marin, B. A., 1993, Porosity preservation by early siderite cementation in Sonora Canyon sandstones, Val Verde Basin, southwest Texas (abs.): American Association of Petroleum Geologists 1993 Annual Convention Official Program, p. 95.

Dutton, S. P., Clift, S. J., Hamilton, D. S., Hamlin, H. S., Hentz, T. F., Howard, W. E., Akhter, M. S., and Laubach, S. E., 1993, Major low-permeability-sandstone gas reservoirs in the continental United States: The University of Texas at Austin, Bureau of Economic Geology, Report of Investigations No. 211, 221 p.

Dutton, S. P., and Land, L. S., 1988, Cementation and burial history of a low-permeability quartzarenite, Lower Cretaceous Travis Peak Formation, east Texas: Geological Society of America Bulletin, v. 100, no. 8, p. 1271–1282.

Dutton, S. P., Laubach, S. E., Tye, R. S., Baumgardner, R. W., Jr., and Herrington, K. L., 1991, Geologic characterization of low-permeability gas reservoirs, Travis Peak Formation, East Texas: The University of Texas at Austin, Bureau of Economic Geology Report of Investigations No. 204, 89 p.

Dyke, C. G., 1992a, The detection and characterization of natural fracture permeability whilst drilling,

ISRM Fractured and Jointed Rock Masses, International Society for Rock Mechanics conference preprints, LBL-32379, p. 688–694.

Dyke, C. G., 1992b, How sensitive is natural fracture permeability at depth to variation in effective stress?: ISRM Fractured and Jointed Rock Masses, International Society for Rock Mechanics conference preprints, LBL-32379, p. 88–95.

Ferm, J. B., Ehrlich, R., Kranz, R. L., and Park, W. C., 1990, The relationship between petrographic image analysis data and fracture toughness: Bulletin of the Association of Engineering Geologists, v. 27, no. 3, p. 327–339.

Fix, J. E., Adair, R. G., Fisher, T. W., Mahrer, K. D., Mulcahey, C. C., Myers, B. C., Swanson, J. G., and Worpel, J. C., 1989, Development of microseismic techniques to determine hydraulic fracture dimensions, Gas Research Institute Final Report, Report No. GRI-89/0116, variously paginated.

Folk, R. L., 1974, Petrology of sedimentary rocks: Austin, Hemphill Publishing Company, 182 p.

Folk, R. L., 1993, SEM imaging of bacteria and nannobacteria in carbonate sediments and rocks: Journal of Sedimentary Petrology, v. 63, p. 990–999.

Froelich, P. N., Klinkhammer, G. P., Bender, M. L., Luedtke, N. A., Heath, G. R., Cullen, D., Dauphin, P., Hammond, D., Hartman, B., and Maynard, V., 1979, Early oxidation of organic matter in pelagic sediments of the eastern equatorial Atlantic: suboxic diagenesis: Geochimica et Cosmochimica Acta, v. 43, p. 1075–1090.

Galloway, W. E., and Brown, L. F., Jr., 1972, Depositional systems and shelf-slope relationships in Upper Pennsylvanian rocks, North-Central Texas: The University of Texas at Austin, Bureau of Economic Geology Report of Investigations No. 75, 62 p.

Garrison, R. E., 1981, Pelagic and hemipelagic sedimentation in active margin basins, *in* Douglas, R. G., Colburn, I. P., and Gorsline, D. S., eds., Depositional Systems of Active Continental Margin Basins: Pacific Section Society of Economic Paleontologists and Mineralogists Short Courses Notes, p. 15–38.

Gautier, D. L., and Claypool, G. E., 1984, Interpretation of methanic diagenesis in ancient sediments by analogy with processes in modern diagenetic environments, *in* McDonald, D. A., and Surdam, R. C., eds., Clastic Diagenesis: American Association of Petroleum Geologists Memoir No. 37, p. 111–123.

Hamlin, H. S., Clift, S. J., and Dutton, S. P., 1992a, Stratigraphy and diagenesis of Sonora Canyon deep-water sandstones, Val Verde Basin, southwest Texas: American Association of Petroleum Geologists, Southwest Section Transactions, p. 209–220.

Hamlin, H. S., Miller, W. K., Peterson, R. E., and Wiltgen, N., 1992b, Results of applied research in the Canyon Sands, Val Verde Basin, southwest Texas: In Focus—Tight Gas Sands, v. 8, no. 1, p. 1–32.

Hesse, R., 1986, Early diagenetic pore water/sediment interaction: modern offshore basins, *in* McIlreath, I. A., and Morrow, D. W., eds., Diagenesis: Geoscience Canada Reprint Series 4, p. 277–316.

Hills, J. M., 1968, Gas in Delaware and Val Verde Basins, West Texas and Southeastern New Mexico, *in* Beebe, B. W., ed., Natural gases of North America, v. 2: American Association of Petroleum Geologists Memoir 9, p. 1394–1432.

Hills, J. M., and Galley, J. E., 1988, The Permian Basin region, general introduction, *in* Sloss, L. L., ed., Sedimentary cover—North American craton, U.S.: Geological Society of North America, v. D-2, p. 261–267.

Holmquist, H. J., 1965, Deep pays in Delaware and Val Verde Basins: American Association of Petroleum Geologists Memoir 4, p. 247–279.

Horton, F. R., 1977, Pre-Cretaceous structural history of J-M/Brown-Bassett field area, Crockett, Terrell, Val Verde counties, Texas: Texas Christian University, Master's thesis, 33 p.

Huang, F. F, 1989, Depositional environments, diagenesis and porosity relationships of the Canyon sands, Edwards and Sutton Counties, Texas: Unpublished Ph.D. Dissertation, Texas Tech University, Lubbock, 244 p.

Hugman, R. H., Springer, P. S., and Vidas, E. H., 1993, Tight gas field, reservoir, and completion analysis of the United States, volume 1: project summary: Energy and Environmental Analysis, Arlington, Virginia, topical report no. GRI-92/0226.1, prepared for the Gas Research Institute, variously paginated.

Irwin, H., Curtis, C., and Coleman, M., 1977, Isotopic evidence for source of diagenetic carbonates formed during burial of organic-rich sediments: Nature, v. 269, p. 209–213.

ISRM, 1981, The quantitative description of discontinuities in rock masses *in* Brown, E. T., ed., Rock characterization testing and monitoring: ISRM suggested methods: Pergamon Press, 211 p.

ISRM, 1988, Suggested methods for determining the fracture toughness of rock: International Journal of Rock Mechanics and Mining Sciences & Geomechanical Abstracts, v. 25, no. 2, p. 71–96.

Kaiser, W. R., Swartz, T. E., and Hawkins, G. J., 1991, Hydrology of the Fruitland Formation, San Juan Basin, in Ayers, W.B., Jr. and others, Geologic and

hydrologic controls on the occurrence and producibility of coalbed methane, Fruitland Formation, San Juan Basin: Gas Research Institute, contract no. 5087-214-1544 (GRI-91/0072), p. 195–241.

Kulander, B. R., Dean, S. L., and Ward, B. J., Jr., 1990, Fractured core analysis, AAPG Methods in Exploration Series, No. 8, 88 p.

Lam, T. S. K., and Johnston, I. W., 1985, A scanning device to quantify joint surface roughness: Geotechnical Testing Journal, GTJODJ, v. 8, no. 3, p. 117–124.

Laubach, S. E., 1988, Subsurface fractures and their relationship to stress history in East Texas basin sandstone, Tectonophysics, v. 156, p. 37–49.

Laubach, S. E., 1989a, Fracture analysis of the Travis Peak Formation, western flank of the Sabine Arch, East Texas, The University of Texas Bureau of Economic Geology Report of Investigations No. 185, 55 p.

Laubach, S. E., 1989b, Paleostress directions from the preferred orientation of healed microfractures (fluid-inclusion planes) in sandstone, East Texas basin, U.S.A., Journal of Structural Geology, v. 11, no. 5, p. 603–611.

Laubach, S. E., 1992, Fracture networks in selected Cretaceous sandstones of the Green River and San Juan Basins, Wyoming, New Mexico, and Colorado, *in* Schmoker, J. W., Coalson, E. B., and Brown, C. A., eds., Geological studies relevant to horizontal drilling: examples from western North America: Rocky Mountain Association of Geologists, p. 61–73.

Laubach, S. E., Clift, S. J., Hill, R. E., and Fix, J. E., 1992a, Stress directions in Cretaceous Frontier Formation, Green River Basin, Wyoming, Wyoming Geological Association Field Conference Guidebook, p. 75–86.

Laubach, S. E., Vendeville, B. C., and Reynolds, S. J., 1992b, Patterns in the development of extensional fault-block shapes from comparison of outcrop-scale faults and experimental physical models, *in* Larsen, R. M., Brekke, H., Larsen, B. T., and Talleraas, E., eds., Structural and tectonic modeling and its application to petroleum geology, Norwegian Petroleum Society Special Publication No. 1, p. 231–241.

Lehtonen, Lee R., 1987, Late Paleozoic evolution of the Val Verde Basin, west Texas: Unpublished M.S. Thesis, The University of Texas at El Paso, 164 p.

Mack, L. E., 1984, Petrography and diagenesis of a submarine fan sandstone, Cisco Group (Pennsylvanian), Nolan County, Texas: The University of Texas at Austin, Master's thesis, 254 p.

Marin, B. A., Clift, S. J., Hamlin, H. S., and Laubach, S. E., 1993, Natural fractures in Sonora Canyon sandstones, Sonora and Sawyer fields, Sutton County, Texas: Society of Petroleum Engineers 1993 Joint Rocky Mountain Regional Meeting and Low-Permeability Reservoirs Symposium, SPE Paper 25895, p. 523–531.

Maynard, J. B., 1982, Extension of Berner's "New Geochemical Classification of Sedimentary Environments" to ancient sediments: Journal of Sedimentary Petrology, v. 52, p. 1325–1331.

McWilliams, P. C., Kerkering, J. C., and Miller, S. M., 1990, Fractal characterization of rock fracture toughness for estimating shear strength, *in* Rossmanith, H. P., ed., Mechanics of jointed and faulted rock; Proceedings of the International Conference on Mechanics of Jointed and Faulted Rock, Vienna, p. 331–336.

Meckel, L. D., Jr., Smith, D. G., and Wells, L. A., 1992, Ouachita foredeep basins: Regional paleogeography and habitat of hydrocarbons, *in* Macqueen, R. W., and Leckie, D. A., eds., Foreland basins and fold belts: American Association of Petroleum Geologists Memoir no. 55, p. 427–444.

Meredith, P. G., 1989, Comparative fracture toughness testing of rocks, *in* Mihashi, H., and others, eds., Fracture toughness and fracture energy: test methods for concrete and rock: Proceedings, International Workshop on Fracture Toughness and Fracture Energy, Sendai, Japan, 1988, p. 265–277

Miller, W. K., 1991, Well completion and hydraulic fracture treatment design and analysis of the Canyon Sands (lower interval), Enron Oil & Gas Co. Sawyer A 144 No. 5, Sawyer (Canyon) Field, Sutton County, Texas, NSI Technologies, Inc., topical report prepared for Gas Research Institute, 166 p.

Miller, W. K., Peterson, R. E., Stevens, J. E., Lackey, C. B., and Harrison, C. W., 1991, In-situ stress profiling and prediction of hydraulic fracture azimuth for the Canyon Sands Formation, Sonora and Sawyer fields, Sutton County, Texas, SPE 21848, Proceedings, SPE Rocky Mountain Regional Meeting/Low-Permeability Reservoirs Symposium, p. 445–456.

Missman, R. A., and Jameson, J., 1991, An evolving description of a fractured carbonate reservoir: the Lisburne Field, Prudhoe Bay, Alaska, SPE 22161, Proceedings, SPE Annual Technical Conference and Exhibition, p. 157–166.

Mitchell, M. H., 1975, Depositional environment and facies relationships of the Canyon sandstone, Val Verde Basin, Texas: Unpublished M.S. Thesis, Texas A&M University, College Station, 210 p.

Mozley, P. S., 1989, Relation between depositional environment and the elemental composition of early diagenetic siderite: Geology, v. 17, p. 704–706.

Mozley, P. S., 1992, Isotopic composition of siderite as an indicator of depositional environment: Geology, v. 20, p. 817–820.

Mozley, P. S., and Carothers, W. W., 1992, Elemental and isotopic composition of siderite in the Kuparuk Formation, Alaska: Effect of microbial activity and water/sediment interaction on early pore-water chemistry: Journal of Sedimentary Petrology, v. 62, p. 681–692.

Mozley, P. S., and Wersin, P., 1992, Isotopic composition of siderite as an indicator of depositional environment: Geology, v. 20, p. 817–820.

National Petroleum Council, 1980, Unconventional gas sources: Tight Gas reservoirs, v. 5, part 1, p. 1–222; part II, p. 10-1–19-24; and Executive Summary, 32 p.

Neuberger, D. J., 1987, Swastika (Upper Pennsylvanian) shelf-margin deltas and delta-fed turbidites, Flowers "Canyon sand field" area, Stonewall County, Texas: The University of Texas at Austin, Master's thesis, 170 p.

NSI Technologies, Inc., 1991a, Well completion and hydraulic fracture treatment design and analysis of the Canyon sands (lower interval): topical report no. GRI-91-0165 prepared for the Gas Research Institute under contract no. 5091-221-2130.

NSI Technologies, Inc., 1991b, Well completion and hydraulic fracture treatment design and analysis of the Canyon sands (lower and middle intervals): topical report no. GRI-91/0207 prepared for the Gas Research Institute under contract no. 5091-221-2130, 276 p.

NSI Technologies, Inc., 1991c, Well completion and hydraulic fracture treatment design and analysis of the Canyon sands (middle interval): topical report no. GRI-91-0257 prepared for the Gas Research Institute under contract no. 5091-221-2130, 121 p.

NSI Technologies, Inc., 1991d, Well completion and hydraulic fracture treatment design and analysis of the Canyon sands (upper interval): topical report no. GRI-91-0323 prepared for the Gas Research Institute under contract no. 5091-221-2130, 89 p.

Olszak, W., Kajfasz, S., and Pietrzykowski, J., 1957, Ascertaining tensile strength by crushing cylinders: Concrete Construction Engineering, v. 9, p. 326–328.

Pisciotto, K. A., 1981, Review of secondary carbonates in the Monterey Formation, California, *in* Garrison, R. E., and Douglas, R. G., eds., The Monterey Formation and Related Siliceous Rocks of California: Pacific Section Society of Economic Paleontologists and Mineralogists, p. 273–283.

Pittman, E. D., and Larese, R. E., 1991, Compaction of lithic sands: experimental results and applications: American Association of Petroleum Geologists Bulletin, v. 75, p. 1279–1299.

Posamentier, H. W., Erskine, R. D., and Mitchum, R. M., Jr., 1991, Models for submarine-fan deposition within a sequence-stratigraphic framework, *in* Weimer, P., and Link, M. H., eds., Seismic facies and sedimentary processes of submarine fans and turbidite systems, Springer Verlag, New York, p. 127-136.

Rall, R. W., and Rall, E. P., 1958, Pennsylvanian subsurface geology of Sutton and Schleicher Counties, Texas: American Association of Petroleum Geologists Bulletin, v. 42, no. 4, p. 839–870.

Rosenbaum, J., and Sheppard, S. M. F., 1986, An isotopic study of siderites, dolomites and ankerites at high temperatures: Geochimica et Cosmochimica Acta, v. 50, p. 1147–1150.

Rosenfeld, M. A., 1949, Some aspects of porosity and cementation: Producers Monthly, v. 13, p. 39–42.

Schultz-Ela, D. D., and Yeh, J., 1992, Predicting fracture permeability from bed curvature, Proceedings of the 33rd U.S. Symposium on Rock Mechanics, p. 579–590.

Shanmugam, G., and Moiola, R. J., 1988, Submarine fans: characteristics, models, classification, and reservoir potential: Earth-Science Reviews, v. 24, p. 383–428.

Skopec, R. A., 1992, Evaluating naturally fractured reservoirs, *in* Schmoker, J. W., Coalson, E. B., and Brown, C. A., eds., Geologic studies relevant to horizontal drilling: examples from western North America, p. 37–46.

Szendi-Horvath, G., 1980, Fracture toughness determination of brittle materials using small to extremely small specimens: Engineering Fracture Mechanics, v. 13, no. 4, p. 955–961.

Trabelsi, Ali, 1994, Canyon sand—S.W. Texas example of a low permeability gas reservoir: Oil & Gas Journal, May 9, v. 92, no. 19, p. 83-86.

Tyler, Noel, and Gholston, J. C., 1988, Heterogeneous deep-sea fan reservoirs, Shackelford and Preston waterflood units, Spraberry Trend, west Texas: The University of Texas at Austin, Bureau of Economic Geology Report of Investigations no. 171, 38 p.

Van Siclen, D. C., and Bloomer, R. R., 1988, Eastern shelves subregion, *in* Sloss, L. L., ed., Sedimentary cover—North American craton, U.S.: Boulder, Colorado, Geological Society of America, The Geology of North America, v. D-2, p. 289–295.

Van Wagoner, J. C., Mitchum, R. M., Campion, K. M., and Rahmanian, V. D., 1990, Siliciclastic sequence

stratigraphy in well logs, cores, and outcrops: concepts for high-resolution correlation of time and facies: American Association of Petroleum Geologists, Methods in Exploration Series, No. 7, 55 p.

Walters, L. J., Claypool, G. E., Choquette, P. W., 1972, Reaction rates and $d^{18}O$ variation for the carbonate-phosphoric acid preparation method: Geochimica et Cosmochimica Acta, v. 36, p. 129–140.

Wright, P. J. F., 1955, Comments on an indirect tensile test for concrete: Magazine of Concrete Research, v. 7, no. 20, p. 87–96.

Wright, T. B., Aud, W. W., Cipolla, C., Meehan, D. N., Perry, K. F., and Cleary, M. P., 1993, Identification and comparison of true net fracturing pressures generated by pumping fluids with different rheology in to the same formations: SPE 26153, SPE Gas Technology Symposium, p. 1-14.

Wuellner, D. E., Lehtonen, L. R., and James, W. C., 1986, Sedimentary-tectonic development of the Marathon and Val Verde basins, west Texas, U.S.A.: a Permo-Carboniferous migrating foredeep, *in* Allen, P. A., and Homewood P., eds., Foreland Basins, International Association of Sedimentologists Special Publication No. 8, p. 347–367.

Young, Addison, 1960, Paleozoic history of the Fort Stockton-Del Rio region, West Texas, *in* Conselman, F. B., and others, Aspects of the geology of Texas: a symposium: The University of Texas Publication No. 6017, p. 87–109.

Zoback, M. L., and Zoback, M. D., 1989, Tectonic stress field of the continental United States, in Pakiser, L. C., and Mooney, W. D., eds., Geophysical framework of the continental United States: Boulder, Colorado, Geological Society of America Memoir 172, p. 523–539.

Appendix A. Data acquisition from GRI cooperative wells.

Well	Phillips Petroleum Ward No. C-11 API No. 42-435-33558	Enron Oil and Gas Sawyer A-144 No. 5 API No. 42-435-33579
Location	H.E. & W.T. RR Co. Survey, Block B, Section 109, Sutton County, Texas	H.T. & E. RR Co. Survey, Block C, Section 144, Sutton County, Texas
Conventional core	5515–6422 ft (201 ft, 128 ft oriented), archived at BEG	5275–6580 ft (305 ft, 27.5 ft oriented), archived at BEG
Core analyses	routine petrophysics (ϕ, k, S_w, σ), special (electrical and mechanical properties, relative k), anelastic strain recovery, acoustic anistropy, geologic description, thin-section petrography	routine petrophysics, geologic description, thin section petrography
Open-hole stress tests	5429 ft and 6050 ft, fracture closure pressure data, induced fracture overcored	5957 ft, bottom-hole pressure data, induced fracture overcored
Wireline logs	spectral density, dual spaced neutron, compensated spectral gamma ray, circumferential acoustic scanning, oriented caliper, sequential formation tester, electromagnetic propagation, microlog, dual laterolog, microSFL, digital sonic	spectral density, dual spaced epithermal neutron, sidewall neutron, compensated spectral gamma ray, dual laterolog, microSFL, dual induction, electromagnetic propagation, microlog, formation microscanner, digital array sonic, repeat formation tester, high resolution temperature,
Cased-hole stress tests	bottom-hole pressure data: 6367 ft, 6410 ft, 6519 ft, 6569 ft, 6619 ft, 6709 ft,	bottom-hole pressure data: 6384 ft, 6492 ft, 6594 ft
Well tests	pre-frac/post-frac flow and pressure buildup data: 6260–6651 ft, 6338–6651 ft	pre-frac/post-frac flow and pressure buildup data: 5281–5439 ft, 5921–6212 ft, 6375–6518 ft
Well	Phillips Petroleum Ward No. C-11	Enron Oil and Gas Sawyer A-144 No. 5
Minifrac and main fracture treatment monitoring	time, injection rates, pressures, proppant concentrations for well-test intervals	time, injection rates, pressures, proppant concentrations for well-test intervals
Fracture diagnostics	continuous microseismic radiation survey for fracture height and azimuth, R/A and temperature logging, oriented gamma ray	R/A and temperature logging for fracture height
Injection rate/crossflow experiment	none	relative injection rates in intervals having different stresses, crossflow between perforated intervals (spinner/pressure tool)
Fracture fluids laboratory tests	conductivity, regained permeability, static fluid loss	none
References	CER Corporation (1991b), Hamlin and others (1992b), Miller and others (1991), NSI Technologies, Inc. (1991a,b)	CER Corporation (1991a), Hamlin and others (1992b), Miller (1991), Miller and others (1991), NSI Technologies, Inc. (1991c,d)

Appendix B. Cross section well data.

Ozona Canyon Cross Section F–F′

Map no.	Operator and lease	Correlation horizons (ft)		
		Ozona	Sonora (D)	Penn Limestone
1	Hamilton, White No. 1	2350	4330	14058
556	Shell Oil, Mitchell 1-109	3705	5760	11083
625	Tenneco, Tom Mitchell No. 102-1x	4040	6080	10980
181	Amoco, L. Hoover E. No. 1	5605	7550	11615
185	El Cinco, Hoover Estate No. 1	5500	7300	11200
194	Signal O&G, Henderson No. 2	5690	7080	10410
633	Cities Service Oil, Henderson No. B-1	5840	7340	10529
146	Cities Service Oil, Bean No. 1-B	6048	7496	9810
147	Frio-Tex et al., Suburban Propane Gas et al. No. 6	5890	7285	9202
148	Chambers & Kennedy, Helbing No. 1	5912	7360	9055
643	Amerada Petroleum, M. McDonald No. 1	5610	6930	nd
130	Delta & Pauley, Friend No. 1	5787	7120	8149
127	Dalton Cobb, Hagelstein No.1	6030	7430	8519
83	Cobb, Harrell No. 1	6150	7651	8943

Map no.	Ozona Zone 1			Ozona Zone 2		
	Depth interval (ft)	Net sand (ft)	Max sand (ft)	Depth interval (ft)	Net sand (ft)	Max sand (ft)
1	2350-3060	0	*	3060-3430	trace	*
556	3705-4480	18	*	4480-4825	trace	*
625	4040-4858	0	*	4858-5125	20	*
181	5605-6390	56	*	6390-6710	23	20
185	5500-6164	0	*	6164-6468	43	39
194	5690-6160	40	29	6160-6465	32	35
633	5840-6347	75	44	6347-6660	108	49
146	6048-6525	27	25	6525-6865	18	*
147	5890-6340	17	*	6340-6660	51	23
148	5912-6360	83	43	6360-6745	88	48
643	5610-6060	23	23	6060-6360	62	40
130	5787-6200	trace	*	6200-6530	39	22
127	6030-6450	0	*	6450-6800	57	27
83	6150-6620	0	*	6620-6980	0	*

Appendix B (cont.)

Ozona Canyon Cross Section F–F′

Map no.	Ozona Zone 3			Ozona Zone 4		
	Depth interval (ft)	Net sand (ft)	Max sand (ft)	Depth interval (ft)	Net sand (ft)	Max sand (ft)
1	3430-3700	0	*	3700-4330	153	20
556	4825-5100	48	*	5100-5760	223	58
625	5125-5400	54	*	5400-6080	174	65
181	6710-6966	107	29	6966-7550	68	29
185	6468-6735	37	*	6735-7300	76	23
194	6465-6670	18	*	6670-7181	trace	*
633	6660-6870	53	29	6870-7340	trace	*
146	6865-7055	11	*	7055-7496	trace	*
147	6660-6849	trace	*	6849-7285	trace	*
148	6745-6925	47	39	6925-7360	trace	*
643	6360-6550	12	*	6550-6930	trace	*
130	6530-6715	0	*	6715-7120	0	*
127	6800-6980	trace	*	6980-7430	trace	*
83	6980-7160	0	*	7160-7651	0	*

* Maximum sandstone and/or net sandstone <20 ft.

Appendix B (cont.)

Ozona Canyon Cross Section G–G'

Map no.	Operator and lease	Correlation horizons (ft)		
		Ozona	Sonora (D)	Penn Limestone
138	Resources Investment, Dudley No. 1	6460	7890	9495
139	Standard Oil, Hoover Estate No. 1	5930	7767	10405
177	North American Royalties, Hoover "66" No. 1	5310	7325	10357
181	Amoco, Hoover No. 1-E	5605	7550	11615
496	Ladd Petroleum, Hoover Estate No. 7-13	5362	nd	nd
509	Ladd Petroleum, Warren Foundation No. 5-24	5386	nd	nd
228	Anderson, Clegg No. 13-B	4770	nd	nd
230	E.W. Wiseman, Kincaid No. 1	4180	nd	nd
15	Standard Oil, Alma Unit No. 1	nd	1704	12263

Map no.	Ozona Zone 1			Ozona Zone 2		
	Depth interval (ft)	Net sand (ft)	Max sand (ft)	Depth interval (ft)	Net sand (ft)	Max sand (ft)
138	6460-6780	0	*	6780-7148	0	*
139	5930-6616	16	*	6616-6990	0	*
177	5310-6120	0	*	6120-6490	trace	*
181	5605-6390	56	*	6390-6710	23	20
496	5362-6160	trace	*	6160-6454	73	70
509	5386-6160	55	*	6160-6465	58	42
228	4770-5294	15	*	5294-5515	32	*
230	4180-4510	trace	*	4510-4790	23	20
15	nd	nd	nd	nd	nd	nd

Map no.	Ozona Zone 3			Ozona Zone 4		
	Depth interval (ft)	Net sand (ft)	Max sand (ft)	Depth interval (ft)	Net sand (ft)	Max sand (ft)
138	7148-7328	0	*	7328-7890	0	*
139	6990-7210	103	31	7210-7767	105	60
177	6490-6724	trace	*	6724-7325	105	50
181	6710-6966	107	29	6966-7550	68	29
496	6454-6733	40	20	6733-?	>108	53
509	6465-6722	trace	*	6722-?	>40	*
228	5515-5770	27	20	5770-?	>50	40
230	4790-5050	47	30	5050-?	>62	60
15	nd	nd	nd	1238-1704	94	*

* Maximum sandstone and/or net sandstone <20 ft.

Appendix B (cont.)

Ozona Canyon Cross Section H–H'

Map no.	Operator and lease	Correlation horizons (ft)		
		Ozona	Sonora (D)	Penn Limestone
103	Chambers et al., Perner Ranch No. 1	5689	7104	8560
642	International O&G, Perner No. 31-1	5920	7320	8625
350	Anderson Petroleum, Bud Cox No. 1-23	5920	nd	nd
592	Texas American Oil, S.C. Millsbaugh No. 1	5778	7175	9280
388	Canyon, S.C. Millsbaugh No. 1-2	5712	nd	nd
194	Signal O&G, Henderson No. 2	5690	7181	10410
526	Monitor Natural Gas, J.S. Pierce No. 2-6	5494	nd	nd
199	Texas American O&G, V.I. Pierce No. 1-E	5605	6935	10612
202	Ladd, Childress No. 142-1	5000	6325	nd
576	Union Oil, Marley "A" No. 1	3135	4383	11411

Map no.	Ozona Zone 1			Ozona Zone 2		
	Depth interval (ft)	Net sand (ft)	Max sand (ft)	Depth interval (ft)	Net sand (ft)	Max sand (ft)
103	5689-5975	0	*	5975-6314	0	*
642	5920-6220	0	*	6220-6558	trace	*
350	5920-6343	16	*	6343-6670	0	*
592	5778-6190	31	*	6190-6530	trace	*
388	5712-6205	49	30	6205-6512	trace	*
194	5690-6160	40	29	6160-6465	32	35
526	5494-5960	56	*	5960-6278	90	*
199	5605-6030	0	*	6030-6338	53	*
202	5000-5359	0	*	5359-5655	26	*
576	3135-3630	0	*	3630-3930	48	38

Map no.	Ozona Zone 3			Ozona Zone 4		
	Depth interval (ft)	Net sand (ft)	Max sand (ft)	Depth interval (ft)	Net sand (ft)	Max sand (ft)
103	6314-6535	0	*	6535-7104	0	*
642	6558-6755	16	*	6755-7320	50	*
350	6670-6880	21	*	6880-?	>35	*
592	6530-6728	39	23	6728-7175	49	*
388	6512-6738	125	100	6738-?	trace	*
194	6465-6670	18	24	6670-7181	trace	*
526	6278-6490	23	*	6490-?	0	*
199	6338-6525	trace	*	6525-6935	53	20
202	5655-6915	trace	*	5915-6324	52	*
576	3930-4100	trace	*	4100-4383	0	*

* Maximum sandstone and/or net sandstone <20 ft.

Appendix B (cont.)

Ozona Canyon Cross Section I–I′

Map no.	Operator and lease	Correlation horizons (ft)		
		Ozona	Sonora (D)	Penn Limestone
107	Cities Service, University "CG" No. 1	6150	7631	8530
598	Caroline Hunt Sands, University No. 32-14	5990	7450	8648
647	Delta-Suburban, Couch No. 1	6042	7510	9210
147	Frio-Tex et al., Suburban Propane et al. No. 6	5890	7285	9202
646	Texas O&G, Montgomery "9" No. 1	5750	7065	9850
209	Victor I. Pierce, V.I. Pierce Fee No. 11-6	5390	6690	10340
246	Pan American , Rob Miller "A" No. 1	4760	nd	10060
240	Canyon, Ineez Hudspeth No. 1-74	3648	4875	11551
575	Union Oil of California, Mary "B" No. 1	3356	4593	10925

Map no.	Ozona Zone 1			Ozona Zone 2		
	Depth interval (ft)	Net sand (ft)	Max sand (ft)	Depth interval (ft)	Net sand (ft)	Max sand (ft)
107	6150-6715	0	*	6715-6990	0	*
598	5990-6522	trace	*	6522-6810	0	*
647	6042-6545	93	45	6545-6878	trace	*
147	5890-6340	17	*	6340-6660	51	23
646	5750-6205	11	*	6205-6512	trace	*
209	5390-5845	trace	*	5845-6150	38	*
246	4760-5250	trace	*	5250-5507	36	35
240	3648-4090	0	*	4090-4391	45	*
575	3356-3782	0	*	3782-4058	trace	*

Map no.	Ozona Zone 3			Ozona Zone 4		
	Depth interval (ft)	Net sand (ft)	Max sand (ft)	Depth interval (ft)	Net sand (ft)	Max sand (ft)
107	6990-7175	0	*	7175-7631	0	*
598	6810-6995	23	*	6995-7450	0	*
647	6878-7065	trace	*	7065-7510	0	*
147	6660-6849	trace	*	6849-7285	trace	*
646	6512-6680	trace	*	6680-7065	0	*
209	6150-6328	trace	*	6328-6690	trace	*
246	5507-5688	0	*	5688-?	0	*
240	4391-4600	0	*	4600-4875	0	*
575	4058-4273	0	*	4273-4593	0	*

* Maximum sandstone and/or net sandstone <20 ft.

Appendix B (cont.)

Ozona Canyon Cross Section J–J′

Map no.	Operator and lease	Correlation horizons (ft)		
		Ozona	Sonora (D)	Penn Limestone
644	J.C. Thomson, Thomson Fee No. 21	6021	7272	7700
119	Wilson & Carter, R.R. Henderson No. 1	6050	7450	8340
130	Delta & Pauley, Friend No. 1	5787	7120	8149
278	Texaco, C.E. Davidson NCT-1 No. 1	5795	7140	8505
266	Texaco, A.H. McMullan No. 1	5695	7115	8804
337	American Exploration, H.H. West No. 4-1	5588	7015	8900
168	Sunray, Hudspeth Memorial Hospital No.1	5305	6660	8431

Map no.	Ozona Zone 1			Ozona Zone 2		
	Depth interval (ft)	Net sand (ft)	Max sand (ft)	Depth interval (ft)	Net sand (ft)	Max sand (ft)
644	6021-6421	trace	*	6421-6709	28	*
119	6050-6508	trace	*	6508-6840	54	49
130	5787-6200	trace	*	6200-6530	39	22
278	5795-6230	10	*	6230-6540	38	20
266	5695-6149	0	*	6149-6500	trace	*
337	5588-6040	trace	*	6040-6379	trace	*
168	5305-5740	0	*	5740-6050	trace	*

Map no.	Ozona Zone 3			Ozona Zone 4		
	Depth interval (ft)	Net sand (ft)	Max sand (ft)	Depth interval (ft)	Net sand (ft)	Max sand (ft)
644	6709-6912	13	*	6912-7272	trace	*
119	6840-7015	trace	*	7015-7450	trace	*
130	6530-6715	0	*	6715-7120	0	*
278	6540-6730	trace	*	6730-7140	0	*
266	6500-6700	0	*	6700-7115	0	*
337	6379-6583	0	*	6583-7015	trace	*
168	6050-6268	0	*	6268-6660	0	*

* Maximum sandstone and/or net sandstone <20 ft.

Appendix B (cont.)

Ozona Canyon Cross Section G–G′

Map no.	Operator and lease	Correlation horizons (ft)		
		Ozona	Sonora (D)	Penn Limestone
138	Resources Investment, Dudley No. 1	6460	7890	9495
139	Standard Oil, Hoover Estate No. 1	5930	7767	10405
177	North American Royalties, Hoover "66" No. 1	5310	7325	10357
181	Amoco, Hoover No. 1-E	5605	7550	11615
496	Ladd Petroleum, Hoover Estate No. 7-13	5362	nd	nd
509	Ladd Petroleum, Warren Foundation No. 5-24	5386	nd	nd
228	Anderson, Clegg No. 13-B	4770	nd	nd
230	E.W. Wiseman, Kincaid No. 1	4180	nd	nd
15	Standard Oil, Alma Unit No. 1	nd	1704	12263

Map no.	Ozona Zone 1			Ozona Zone 2		
	Depth interval (ft)	Net sand (ft)	Max sand (ft)	Depth interval (ft)	Net sand (ft)	Max sand (ft)
138	6460-6780	0	*	6780-7148	0	*
139	5930-6616	16	*	6616-6990	0	*
177	5310-6120	0	*	6120-6490	trace	*
181	5605-6390	56	*	6390-6710	23	20
496	5362-6160	trace	*	6160-6454	73	70
509	5386-6160	55	*	6160-6465	58	42
228	4770-5294	15	*	5294-5515	32	*
230	4180-4510	trace	*	4510-4790	23	20
15	nd	nd	nd	nd	nd	nd

Map no.	Ozona Zone 3			Ozona Zone 4		
	Depth interval (ft)	Net sand (ft)	Max sand (ft)	Depth interval (ft)	Net sand (ft)	Max sand (ft)
138	7148-7328	0	*	7328-7890	0	*
139	6990-7210	103	31	7210-7767	105	60
177	6490-6724	trace	*	6724-7325	105	50
181	6710-6966	107	29	6966-7550	68	29
496	6454-6733	40	20	6733-?	>108	53
509	6465-6722	trace	*	6722-?	>40	*
228	5515-5770	27	20	5770-?	>50	40
230	4790-5050	47	30	5050-?	>62	60
15	nd	nd	nd	1238-1704	94	*

* Maximum sandstone and/or net sandstone <20 ft.

Appendix B (cont.)

Sonora Canyon Cross Section A–A'

Map no.	Operator and lease	Correlation horizons (ft) *					
		D	TC	S1	S2	S4	Penn Ls
158	Cosden Petroleum E.G. Baggett "C" No. 2	6754	6910	7170	7467	7820	nd
261	Texam Oil Davidson No. 2	6910	7070	7288	7580	7860	9377
262	SPG Exploration McMullan "18" No. 1	6794	6949	7173	7460	7751	8968
273	American Quasar J.L. Henderson No. 1-2	6800	6958	7166	7480	7800	8770
73	Sonora Southwest Renfro "R" No. 170	6526	6684	6890	7225	7526	8400
409	Amoco Production B.F. Renfro "B" No. 1	6642	6800	6980	7355	7610	nd
422	R.L. Burn Corp. Mayer No. 5-1	6450	6607	6760	7082	7272	nd
9	Tucker Drilling & Henderson Mayer Est. "A" No. 1	6420	6565		7025	7220	7880
17	Amoco Production E.S. Mayer "C" No. 6	6452	6590		7018	7220	nd
401	John Hill E.S. Mayer "B" No. 1	6392	6518		6870	7130	nd
26	HNG Oil Simmons No. 71-1	6322	6447		6775	6980	7539
407	HNG Oil Kirby "184" No. 1	6230			6558	6750	7405
378	HNG Oil Lancaster "154" No. 1	ca. 6050			6336	6520	7280
406	C & K Petroleum Ben Mittel No. 3	ca. 5825			6030	6200	7030
37	Sinclair O&G Christina Mittel No. 1	ca. 5735			5910	6070	6780

	Net sandstone (ft) +		
Map no.	D-S2	S2-S4	S4-base
158	12	26	167
261	12	20	237
262	26	30	134
273	37	30	14
73	50	22	trace
409	102	25	trace
422	110	25	trace
9	134	28	trace
17	165	20	trace
401	127	85	trace
26	97	86	trace
407	112	135	trace
378	34	86	52
406	11	58	trace
37	14	24	0

* Top of Sonora sandstone generally occurs near "D" or "TC" horizons.
+ D-S2 is upper Sonora map unit, S2-S4 is middle Sonora map unit, and S4-base is lower Sonora map unit.

Appendix B (cont.)

Sonora Canyon Cross Section B–B'*

Map no.	Operator and lease	Correlation horizons					
		D	TC	S1	S2	S4	Penn Ls
247	Amarex Baggett No. 8-1 Deep	5514	5654	5891	6180		9640
223	Continental Oil Friend No. 1	5389	5521	5765	6066	6353	9319
161	Amoco Production Morris Bros. "F" No. 1	5363	5501	5750	6011	6285	8828
167	Sonora Southwest Morris Ranch "14" No. 102	5444	5575	5800	6053	6332	8565
170	U.S. Smelting, Refining, & Mining, Aldwell No.1	5510	5640	5850	6080	6379	8370
174	Union Oil of California Sawyer No. 1	5596	5677	5920	6135	6445	8170
175	C. L. Norsworthy E. Sawyer No. 1	5553	5681	5870	6061	6420	8310
235	Enron O&G Sawyer "145" No. 3	5309	5410	5505	5700	6085	nd
350	Enron O&G Sawyer 144 "A" No. 5	5100	5195	5276	5445	5815	nd
221	HNG Oil Sawyer "112" No. 2	5172	5258		5535	5860	nd
372	HNG Oil Shurley "95" No. 2	5185			5485	5765	nd
420	HNG Oil Fields "52" No. 1	ca. 5050			5322	5548	nd
110	Ada Oil H. Fields No. 1	ca. 5000			5275	5484	6308
421	HNG Oil Fields "59" No. 1	ca. 5080			5300	5510	6110
117	C.L. Norsworthy Alfred Schwiening No. 1	ca. 4600			4830	5025	5520

Net sandstone (ft) +			
Map no.	D-S2	S2-S4	S4-base
247	4	0	11
223	0	0	20
161	3	0	93
167	36	11	296
170	103	53	392
174	125	138	576
175	106	120	453
235	107	228	557
350	132	149	512
221	52	152	375
372	55	126	216
420	58	56	87
110	0	75	80
421	65	0	10
117	0	0	0

* Top of Sonora sandstone generally occurs near "D" or "TC" horizons.
+ D-S2 is upper Sonora map unit, S2-S4 is middle Sonora map unit, and S4-base is lower Sonora map unit.

Appendix B (cont.)

Sonora Canyon Cross Section C–C'*

Map no.	Operator and lease	Correlation horizons					
		D	TC	S1	S2	S4	Penn Ls
40	HNG Oil Allison No. 11-3	3782	3909	4160	4340	4740	8798
11	Wichita Industries Holeman Ranch No. 1	3778	3897	4159	4331	4710	8495
3	Midwest Oil W.T.O. Holman No. 1	3717	3812	4113	4285	4810	nd
53	North American Royalties Texas A&M "63" No. 2	3773	3878	4160	4310	4618	nd
431	North American Royalties Cox "70" No. 2	3703		4150	4300	4554	nd
328	Harrison Interests Harrison Ranch No. 48	ca. 3750			4190	4543	nd
436	HNG Oil Vanderstucken "80" No. 1	ca. 3635			4100	4448	5710
487	Pennzoil Vanderstucken "A" No. 2	ca. 3320			3760	4104	nd
481	Way & Mills Hicks No. 2	ca. 2960			3402	3718	4170
520	Blackrock Oil Vanderstucken No. 4	ca. 2980			3441	3853	4265
533	Pierce & Dehlinger Wallace No. 1	ca. 2780			3300	3610	4110
510	HNG Oil Wade No. 53-1	ca. 2425			3010	3262	3940

Net sandstone (ft) +			
Map no.	D-S2	S2-S4	S4-base
40	0	0	trace
11	22	30	60
3	54	36	84
53	105	146	238
431	233	116	290
328	228	164	317
436	77	137	161
487	152	190	24.1
481	129	158	38
520	163	184	0
533	91	72	0
510	71	25	3

* Top of Sonora sandstone generally occurs near "D" or "TC" horizons.
+ D-S2 is upper Sonora map unit, S2-S4 is middle Sonora map unit, and S4-base is lower Sonora map unit.

Appendix B (cont.)

Sonora Canyon Cross Section D–D'*

Map no.	Operator and lease	Correlation horizons					
		D	TC	S1	S2	S4	Penn Ls
268	Dan Harrison C.E. Davidson No. 2	7370	7555	7832	ca. 8070		8636
245	Henry Petroleum Henry Petroleum Corp. No. 1	7075	7255	7468	ca. 7750		8550
409	Amoco Production Betty Faye Renfro "B" No. 1	6642	6800	6980	7355	7610	nd
75	Wewoka Exploration Whitehead No. 1	5830	5973	6170	6438	6681	8260
170	U.S. Smelting, Refining, and Mining, Aldwell No.1	5510	5640	5850	6080	6379	8370
173	Shell-Sinclair Aldwell Bros. No. 1	4820	4939	5160	5361	5682	8530
317	Cyclone Exploration Dan C. Cauthorn No. 2-156	4390	4515	4759	4970	5320	nd
3	Midwest Oil W.T.O. Holman No. 1	3717	3812	4113	4285	4810	nd
18	Mitchell Energy Mayfield No. 200-1	2731		3108	3285	3602	nd

Net sandstone (ft) +			
Map no.	D-S2	S2-S4	S4-base
268	20	0	0
245	75	0	0
409	102	25	0
75	27	36	460
170	103	53	392
173	10	23	82
317	32	21	99
3	54	36	84
18	21	28	18

* Top of Sonora sandstone generally occurs near "D" or "TC" horizons.
+ D-S2 is upper Sonora map unit, S2-S4 is middle Sonora map unit, and S4-base is lower Sonora map unit.

Appendix B (cont.)

Sonora Canyon Cross Section E–E'*

Map no.	Operator and lease	Correlation horizons					
		D	TC	S1	S2	S4	Penn Ls
359	Amoco Production D.M. Rousselot "A" No. 2	6792			ca. 7175	ca. 7275	7850
25	Cabot et al. S.O. Byrd No. 1	6534			ca. 6950	ca. 7120	7670
407	HNG Oil Kirby "184" No. 1	6230			6558		7405
359	DiCon Simmons No. A-2	5930			6192	6403	nd
98	Phillips Petroleum Ward "C" No. 11	5380	5495		5700	5935	nd
372	HNG Oil Shurley "95" No. 2	5185			5485	5765	nd
258	Continental Oil Vanderstucken No. 1	4842			5160	5449	6560
263	Pan American Thelma Espy No. 1	ca. 4228			4592	4949	6090
436	HNG Oil Vanderstucken "80" No. 1	ca. 3635			4100	4448	5710
371	Dan Harrison Harrison Ranch No. 27	ca. 2920			3406	3720	5742
49	Lone Star Producing W.L. Miers "B" No.11	ca. 2600			3130	3400	5560

Net sandstone (ft) +			
Map no.	D-S2	S2-S4	S4-base
359	trace	0	0
25	197	trace	0
407	112	135	4
359	145	83	168
98	68	68	426
372	55	126	216
258	73	44	203
263	96	101	246
436	77	137	161
371	162	198	444
49	65	35	553

* Top of Sonora sandstone generally occurs near "D" or "TC" horizons.
+ D-S2 is upper Sonora map unit, S2-S4 is middle Sonora map unit, and S4-base is lower Sonora map unit.

Appendix B (cont.)

Miers Area Cross Section

Map no.	Operator and lease	Correlation horizons				
		29	D	S2	S4	Penn Ls
456	HNG Oil Pfluger "104" No. 6	3520	ca. 3725	4187	4529	nd
464	HNG Oil Pfluger "85" No. 2	3495	ca. 3715	4210	4523	nd
436	HNG Oil Vanderstucken "80" No. 1	3400	ca. 3635	4100	4448	5710
495	HNG Oil Hicks "61" No. 1	3160	ca. 3364	3830	4123	nd
537	Way & Mills Hicks No. 6	2804	ca. 2990			nd
481	Way & Mills Hicks No. 2			3402	3718	nd
502	Way & Mills Hicks No. 3	2770	ca. 2945	3420	3760	nd
486	Western Natural Gas J.M. Vanderstucken No. 2	2785	ca. 2950	3445	3770	4171
540	W.R. Lloyd J.M. Vanderstucken No. 2	2798	ca. 2985	3465	3760	4220
520	Blackrock Oil Vanderstucken No. 4	2745	ca. 2980	3441	3853	4265
335	Ohio Oil Vanderstucken Well No.1	2660	ca. 2860	3360	3770	4194
489	Brown Vanderstucken "67" No. 2	2623	ca. 2820	3400	3765	nd
337	Edward Lawson et al. J.M. Vanderstucken No. 1	2487	ca. 2730	3310	3620	4186

Net sandstone (ft)	
Map no.	Middle Sonora interval
456	140
464	160
436	170
495	175
537	140
481	130
502	90
486	45
540	0
520	trace
335	0
489	30
337	0

Appendix B (cont.)

Sonora Area Cross Section

Map no.	Operator and lease	Correlation horizons					
		D	TC	S1	S2	S4	Penn Ls
350	Enron O&G Sawyer 144 "A" No. 5	5100	5195	5276	5445	5815	nd
349	Delta-Suburban Sawyer No. A-2	5150	5250	5350	5504	5861	nd
103	Lone Star Producing E.E. Sawyer "113" No. 1	5200	5300		5525	5897	nd
218	Enron O&G Sawyer 112 No. 8	6235	5350	5560	5635	5900	nd
101	HNG Oil Shurley 111 No. 7	5260	5342		5570	5888	nd
552	HNG Oil Shurley "111" No. 5	5196	5227		5496	5804	nd
100	HNG Oil Shurley "110" No. 2	5300	5382		5615	5906	nd
99	Amoco Oil Shurley "110" No. 1	5413	5490		5718	5965	nd
198	HNG Oil Shurley "110" No. 5	5380	5450		5670	5950	nd
98	Phillips Petroleum Ward "C" No. 11	5380	5495		5700	5935	nd

Net sandstone				Max sandstone (ft)
Map no.	D-S2	S2-S4	S4-base	S4-base
350	132	149	512	120
349	103	195	482	140
103	102	190	468	110
218	85	118	348	138
101	77	92	368	161
552	105	220	400	135
100	55	33	378	99
99	49	82	374	120
198	70	105	450	130
98	68	68	426	100